On Channel Modelling For Land Mobile Satellite Reception

Dissertation

zur Erlangung des akademischen Grades
Doktoringenieur (Dr.-Ing.)

vorgelegt der Fakultät für Elektrotechnik und Informationstechnik der
Technischen Universität Ilmenau

von Dipl.-Ing. Daniel Arndt
geboren am 28.03.1982 in Dresden

vorgelegt am: 17.10.2014

Gutachter:
1. Prof. Dr.-Ing. Albert Heuberger
2. Univ.-Prof. Dr. rer. nat. Jochen Seitz
3. Prof. Dr. Fernando Pérez-Fontán

Verteidigung am: 14.09.2015

urn:nbn:de:gbv:ilm1-2015000358

Abstract

Modern digital satellite broadcasting systems combine time diversity (i.e. information is spread over a certain time interval) with angle diversity (i.e. information is received from multiple satellites in different orbital positions) to ensure uninterrupted service for mobile receivers over large areas. For assessing propagation effects of the land mobile satellite (LMS) channel and to study the efficacy of diversity, statistical models are required which generate time series of the received fading signal.

In this thesis a narrowband LMS channel model for multi-satellite reception is developed focusing on accurate coverage prediction under consideration of angle- and time diversity. Basis is an existing single-satellite model, which describes large-scale signal variations of the channel by 'good' and 'bad' states, and models slow- and fast signal variations according to a versatile Loo distribution, which parameters are selected randomly when the channel enters a new state.

For dual-satellite state modelling, a *semi-Markov model for correlated state sequences* is developed. It provides an accurate state probability and state duration modelling by considering the statistics of separate channels and their correlation coefficient. For the state modelling with three satellites, a new *Master-Slave* concept is introduced. Therefore, state sequences of slave satellites are conditioned by an existing master state sequence. The great advantage is that Master-Slave makes the parametrisation of a triple-satellite model feasible.

To address slow- and fast variations for multi-satellite reception, the fading interdependence between synchronously received satellite signals is analysed from high-resolution measurement data. Hence additional correlations besides the state correlation are identified and firstly considered in the new multi-satellite LMS model.

The modelling results are compared with the measurements in terms of first- and second order statistics, where improvements in describing diversity become visible when compared to existing models.

Model parameters are derived from large-scale measurement campaigns to enable a time series generation for different environments and various constellations of satellites. The applicability of the new model is finally demonstrated by comparing the performance of different satellite constellations with diversity.

Kurzfassung

In modernen Satellitenrundfunksystemen werden Methoden wie Zeitdiversität (Empfang von zeitlich verteilter Information) und Winkeldiversität (Empfang von mehreren Satelliten mit unterschiedlichen Positionen) angewandt, um die geforderte Dienstequalität für den mobilen Empfang zu gewährleisten. Zur Untersuchung der Ausbreitungseffekte des landmobilen Satellitenkanals sowohl der Wirksamkeit von Diversität werden statistische Modelle benötigt, die den zeitlichen Signalschwund des Empfangssignals nachbilden.

In der vorliegenden Arbeit wird ein Kanalmodell für den Mehrsatellitenempfang entwickelt, welches genaue Versorgungsvorhersagen mit Zeit- und Winkeldiversität erlaubt. Grundlage ist ein Einsatellitenmodell, welches großräumige Schwankungen im Kanal durch die Zustände 'gut' und 'schlecht' definiert, und den langsamen und schnellen Signalschwund gemäß einer variablen Loo-Verteilung beschreibt, deren Parameter nach jedem Zustandswechsel stochastisch bestimmt werden.

Für die Zustandsmodellierung mit zwei Satelliten wird ein 'semi-Markov Modell für korrellierte Zustandssequenzen' erarbeitet. Damit können, unter Berücksichtigung der Statistiken der Einzelkanäle und deren Korrelationskoeffizient, die Zustandswahrscheinlichkeiten und -längen exakt simuliert werden. Für die Zustandsmodellierung mit drei Satelliten wird ein 'Master-Slave'-Ansatz entwickelt. Dabei sind die Zustandssequenzen zweier 'Slaves' bedingt abhängig zur 'Master'-Sequenz. Der 'Master-Slave'-Ansatz ermöglicht die Parametrisierung eines Dreisatellitenmodells.

Zur Beschreibung des langsamen und schnellen Signalschwunds im Mehrsatellitenkanal wird die Wechselbeziehung zwischen synchron gemessenen Satellitensignalen näher untersucht. Es stellt sich heraus dass weitere Signalkorrelationen berücksichtigt werden sollten, die erstmalig im neuen LMS-Kanalmodell implementiert werden.

Die Simulationssergebnisse werden in Statistiken erster und zweiter Ordnung den Messdaten gegenübergestellt. Im Vergleich zu bestehenden Modellen werden Verbesserungen nach Berücksichtigung von Diversität deutlich.

Die Parameter für das Mehrsatellitenkanalmodell wurden aus umfassenden Messkampagnen abgeleitet und gewährleisten die Signalsimulation für verschiedene Umgebungen und Satellitenpositionen. Abschließend wird das Kanalmodell für einen ersten Vergleich verschiedener Satellitenkonfigurationen mit Zeit- und Winkeldiversität angewandt.

Acknowledgements

This dissertation originates from results of my activities within the 'Wireless Distribution Systems / Digital Broadcasting Group' of the Fraunhofer Institute for Integrated Circuits IIS and within the 'Digital Broadcasting Research Laboratory' of the Ilmenau University of Technology.

First of all I wish to thank Prof. Dr.-Ing. Albert Heuberger, head of the Fraunhofer Institute for Integrated Circuits IIS, for giving me the opportunity to study for a doctoral degree and for supervising this work.

I would also like to thank Univ.-Prof. Dr. rer. nat. Jochen Seitz from the Ilmenau University of Technology, and Prof. Dr. Fernando Pérez-Fontán from the University of Vigo, Spain, for accepting to be a reviewer of my work.

A great part of this work originates from results of the ESA-funded research project 'Mobile Satellite Channel with Angle Diversity', which was in progress to the beginning of my activities at the Fraunhofer Institute. Therefore I thank my colleagues from the Fraunhofer Institute for Integrated Circuits IIS from Erlangen for carrying out large-scale measurements of satellite signals in advance of this work. The captured data proved to be a 'veritable gold mine' for this thesis.

The start of this work is due to Dr. Markus Mehnert. He honoured me with his trust and strengthened my will to write a dissertation. Furthermore I thank all colleagues for the smooth beginning of this thesis: in particular Carmen Wagner and Thomas Heyn, who involved me in the research project and thus helped me to get familiar with the topic. Special thanks goes to Ernst Eberlein, who represented an almost inexhaustible source of ideas and visions around satellite broadcasting and gave important impulses for this work.

For valuable contributions in their student works I thank Stefan Häfner, Felix Topf, and in particular my subsequent colleague Jonas König, who always had a keen eye for the scientific mistakes in detail.

I'm eternally grateful to Dr. Alexander Ihlow for his continuous guidance, his support in technical and personal questions, and for his continuous encouragement from the very beginning to the end of this work. Due to his untiring dedication in supporting and reviewing all of my contributions I owe him to 'stand on my own feet' in the scientific field.

For the pleasant working atmosphere throughout this dissertation I thank my colleagues from the 'Wireless Distribution Systems / Digital Broadcasting Group' and from the 'Digital Broadcasting Research Laboratory' led by Prof. Dr.-Ing. Giovanni Del Galdo. The helpfulness of each, the good teamwork, the constructive discussions as well as the excellent equipment at the working place provided a pleasant research environment. Particularly, the daily 'scientific' discussions at lunch and in the cafeteria of the Mensa took big part of the good spirits. Also the weather conditions in Ilmenau contributed to the important motivation, in which it was congenial to sit and work in the warm and dry office.

A huge thanks to my parents for their support in every circumstance. An even bigger thanks to my girlfriend Tina for her unyielding patience and understanding. Especially in the critical phase of this work I wish to thank her and my son Philipp to always provided me different thoughts and served as a source of recreation and new energy.

Contents

1. Introduction

In July 1962, the first television satellite Telstar 1 was launched and it transmitted in the same month a TV program reached by 200 Million subscribers in USA and Europe. It was the beginning of a new era for satellite broadcasting and communications. The transmitter and receiver of these early satellite communication systems were exclusively stationary. [Pun02]

The era for mobile communications started about 20 years later. INMARSAT established in 1982 a system of satellites in a geostationary orbit providing voice, telex, fax and data services to maritime terminals [Inm09]. At the end of the 80's, land mobile satellite reception began in terms of a messaging-service for long-distance road haulage by Qualcomm [AP95].

Today, satellites have a consolidated role in digital communication- and broadcasting systems. Whether they are used as 'back hauling' component between transmitter and cellular network, they are directly linked to the terminal, or they transmit a signal via a terrestrial repeater to the receiver, satellites enable flexible solutions to provide multimedia content (e.g. audio and video streaming) to stationary, portable, and mobile receivers world wide. Besides the ability to meet coverage and high Quality-of-Service (QoS), the use of satellites have economic advantages as they help to minimize the number of terrestrial transmitters and reduce the deployment and operational costs in broadcasting and communication networks [Cou01].

For satellite communication services, a number of frequency bands (UHF, L, S, Ku and Ka bands) ranging from 300 MHz to 30 GHz have been allocated [KP99]. In these frequency bands, satellite signal reception is limited due to shadowing or blocking objects (e.g. buildings, trees, tunnels) in the transmission path. While for stationary receivers (e.g. antennas on buildings) or partly for hand-held terminals a continuous line-of-sight connection to the satellite can be established, this is not realistic for moving terminals. Hence, signal fading can not be avoided. To mitigate fading and to increase the satellite signal availability, a number of active and passive techniques are applied in commercial systems, such as high-elliptical satellite orbits (e.g. Sirius Satellite Radio [Akt08]), increased satellite transmission power, satellite diversity from multiple satellites (e.g. XM Satellite Radio [Mic02]), time interleaving (e.g. WorldSpace [SANS08]). For coverage studies in the planning process of new systems, statistical channel models are frequently used that are able to generate timeseries of the received fading signal. Besides giving statements about expected signal availabilities for mobile terminals, those timeseries are basis to evaluate and select the required modulation and coding techniques for communication or broadcasting systems.

1.1. Land Mobile Satellite Channel Models - Overview and Motivation

Statistical (or generative) channel models for land mobile satellite (LMS) reception describe the fading processes of the received signal: Slow variations of the signal are caused by obstacles between the satellite and the receiver, which induce varying shadowing conditions

of the direct signal component. Fast signal variations are caused by multipath effects due to static or moving scatterers in the vicinity of the mobile terminal. For short time periods these two components (*slow and fast variations*) are usually modelled by a stationary stochastic processes. Distribution functions from Loo [Loo84], Corazza&Vatalaro [CV94], and Suzuki [Suz77] are well known to describe satellite signal propagation. For longer time periods the received signal can not be assumed as stationary. Therefore, different receive states are introduced for statistical LMS modelling to assess the large dynamic range of the received signal. The states correspond to slow varying environmental conditions (lines of trees, buildings, line-of-sight) in the transmission path. The number of states to describe a single satellite path range from two ('good' and 'bad') [LCD+91], three ('line-of-sight', 'shadowed', and 'blocked') [KMM95] to models with higher or variable state number [SAHE]. The temporal sequence of states is usually described by Markov or semi-Markov chains.

While several LMS channel models for single-satellite systems are available and consolidated [LCD+91, PFVCC+01, PCPFB+10], models for multi-satellite propagation are rather rare in literature and thus subject of recent and ongoing research activities.[mil] A crucial element in multi-satellite modelling is the correlation of the fading between different paths. Early multi-satellite studies of camera-based measurements [REE92] show that a high correlation is expected if the angular separation between satellites is low. Especially for azimuth angle separations below 30° a correlation can not be neglected, otherwise a coverage prediction for a multi-satellite system with diversity would be too optimistic. Later contributions report similar satellite correlation studies by emulated satellite signal measurements [JL94] or by theoretical analyses of physical models from the terminals environment [TSE98]. To apply the correlation information into a statistical generative model, a first-order Markov model for correlated channels was developed in 1996 [Lut96] to correlate two satellite sequences consisting of 'good' and 'bad' states. Due to its simplicity this modelling approach is frequently used to this day. However, those first-order Markov chains have limitations in state duration modelling, as their state durations inherently follow an exponential distribution. Authors in [MHEH09] [BT02] found that this condition is not necessarily correct for the LMS channel. Nevertheless, a correct state duration modelling is of high interest for the configuration of physical layer and link layer parameters for modern broadcasting standards with long time interleaving (e.g. for physical layer interleaver size, link layer protection time). Therefore, different concepts to improve the state duration modelling were introduced: semi-Markov chains [BT02] and dynamic Markov chains [MHEH09]. For these approaches some exemplary analyses including model parameters for the single-satellite reception are published. However, a feasible concept for multi-satellite state duration modelling does not exists so far.

A further limitation of available dual- or multi-satellite LMS approaches is the consideration of correlation only for the states between the satellite signals. Since a separation in two or three states is a raw quantisation of the received signal, it is questionable if the actual correlation of the signals is sufficiently described to make an accurate prediction of the joint availability of combined satellite signals.

1.2. Overview of this Work and Own Contributions

The goal of this work is to develop an LMS channel model for multi-satellite reception to provide accurate coverage prediction under consideration of satellite diversity (also denoted as angle diversity) and time diversity.

This target requires

- the development of an appropriate state model for two- and more than two satellites to accurately describe the correlation and state duration.
- the analysis of the correlation between two satellite signals and the development of a suitable model implementation.
- the analysis of measurement data to derive the model parameters for different environments and satellite positions.
- the evaluation of the new model and a comparison with available models.

This work is organised as follows:

Chapter 2 firstly describes propagation effects of the signal from satellite to mobile and stationary receivers. Afterwards, different approaches to characterise the land mobile satellite channel are briefly introduced. Amongst a number of empirical, statistical, or physical models to describe single-satellite reception, also available approaches for multi-satellite reception are presented. Their possible weaknesses in terms of describing correlation effects between satellites and in terms of describing the signals temporal composition are identified.

Chapter 3 deals with a basic element for describing mobile reception: the receive states. Starting with the description of existing Markov models to provide state sequences for single-satellite reception, new state models for dual- and multi-satellite reception are introduced. To assess the performance of existent and new state models, correlation coefficients, state probabilities and state duration statistics are gained from re-simulated state sequences and are compared with measurement data. Further on, the reliability and feasibility of these state models for predicting the mobile reception at different locations and environments from different satellite positions is discussed. To improve the readability of Chapter 3, the major part of mathematics related to the state model analyses are found in **Appendix B**.

For short time intervals the mobile fading signal can be described by a stationary stochastic process, for which the Loo distribution is found as appropriate and commonly used for LMS modelling. In **Chapter 4** correlation effects of such Loo fading processes between two satellites are analysed, and a corresponding implementation of the LMS model is developed. The detailed implementation of the new multi-satellite channel model is presented at the end of Chapter 4.

In **Chapter 5** a comprehensive evaluation of the LMS model output, the complex envelope of the fading signal from multiple paths, is done. For this purpose the re-simulated signals of the proposed LMS model and of alternative approaches developed in this work and from literature are compared with measurement data in terms of first- and second-order statistics. Evaluation criteria are cumulative distribution functions (CDFs), average fade durations (AFD), level crossing rates (LCR), and CDFs under consideration of time interleaving with variable lengths. The model evaluation is done under two aspects:

- A given measurement sequence is parametrised and (immediately) re-simulated by the model. It indicates if the LMS model architecture appropriately describe all important characteristics of fading.
- Exemplary signals from measurements are compared with re-simulated signals based on model parameters from similar receive scenarios, i.e. a combination of environment type, elevation angle, and angular separation. It verifies the representativeness of the model parameter sets to describe fading for multiple environments and satellite constellations.

As a first application for the new multi-satellite LMS model, a coverage study for satellite broadcasting applications under consideration of satellite diversity and time diversity is performed in **Chapter 6**. Starting with a joint analysis of satellite- and time diversity based on measured signals along the U.S. East Coast, the reception of

- a high-power satellite in geostationary orbit,
- a dual-satellite constellation with small azimuth separation, and
- a dual-satellite constellation with large azimuth separation

is compared for selected locations in the USA. Therefore, the required margins for 99% signal availability are derived from the first-order statistics of the channel model output for different types of environments. The results demonstrate the performance of alternative geostationary satellite constellations to serve coverage areas between 30 and 45 degrees latitude and show achievable gains with satellite diversity and time diversity.

Basis for this work are measurement data from existing satellite systems with a quality and resolution that is not previously reported in literature: over a travelled distance of 3700 km the power levels of four satellites were measured synchronously with a sampling rate of 2.1 kHz for a large variety of environments and for different elevation and azimuth angles of the satellites. This data were captured right before this work in 2008 in the context of the project MiLADY [EHH08][HEA+10]. The campaign is described in **Appendix A**. Preprocessing and data analysis of these measurements is an important part of this work.

Appendix C presents tables of parameters for the new multi-satellite channel model. In combination with the implementation guideline in Chapter 4 it allows to generate timeseries of the signal fading in dependency on the environment type an the satellite constellation.

Parts of this thesis were published in 7 international conferences ([AIH+09] [AIH+10] [AIH+11] [AHK+12] [AIHE11b] [AIHE11a] [AHH+12]) and within two journals ([AIHE12][AIH+]).

2. Land Mobile Satellite Channel Characterisation and Modelling

Land mobile satellite (LMS) systems play an essential role in third and fourth generation wireless communication systems. They provide wide area coverage by low operational costs in comparison to terrestrial systems. For LMS communication and broadcasting services, a number of frequency bands have been allocated. Signals are transmitted either in UHF-band (300-1000 MHz) [1] , L-band (1-2 GHz), S-band (2-4 GHz), Ku-band (12-18 GHz) or Ka-band (27-40 GHz) and have each characteristical propagation impairments limiting the signal reception at the receiver.[2] To ensure the QoS for mobile receivers, a sound knowledge of the LMS propagation channel is essential. Therefore, accurate statistical channel models for LMS reception are required.

This chapter focuses on state-of-the-art of LMS channel models. For this purpose, firstly in Section 2.1 the main impairments for radio wave propagation for LMS reception are described. Different methods to mitigate the impairments and to ensure the QoS, such as diversity, are given in Section 2.2. Afterwards, in Section 2.3 and Section 2.4 the fundamentals and the state-of-the-art for LMS channel modelling are introduced incorporating one and multiple satellites, respectively. Finally, in Section 2.5 open aspects in terms of multi-satellite modelling with diversity are identified.

2.1. Propagation Impairments of the Land Mobile Satellite Link

The radio waves transmitted from satellite to the receiver on earth undergo different kinds of propagation impairments: free-space attenuation, atmospheric effects in the ionosphere and the troposphere, and local effects in the near environment of the receiver, as depicted in Figure 2.1.

Effects in Ionosphere
The ionosphere is the greatest part of the atmosphere (from 50 km to 2000 km altitude) including a large quantity on ions and free electrons. Radio waves on the way through the ionosphere activate the free electrons to resonate which causes scintillation, Faraday rotation, propagation delays, and dispersion. *Ionospheric scintillation* are changes in the refraction of radio waves and hence of the signal levels due to rapid variations of the electron density. *Faraday rotation* denotes the rotation of linearly polarised electromagnetic waves, resulting in attenuation losses due to polarisation mismatches between transmit and receive antenna. *Propagation delays* and phase shifts of radio waves are due to the ionospheric refractivity and can cause uncertainties for satellite navigation systems. As propagation delays are frequency dependent, a transmitted impulse arrives the receiver over its bandwidth with a certain *time dispersion*, which limits the possible maximum signal bandwidth. [SAZ07]

[1] The upper bound for UHF is actually 3000 MHz, but in context of satellite communications 1000 MHz are commonly used.
[2] The frequency ranges and frequency bands for telecommunications are found in [ITU00].

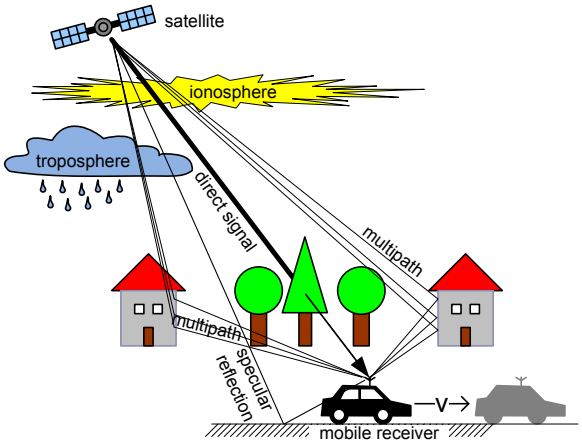

Figure 2.1.: Propagation impairments for land mobile satellite reception.

The intensity of ionospheric effects depend on the path-length through the ionosphere, geomagnetic field strength, electron density and the radio frequency. Most effects - except Faraday rotation - are already negligible in L-Band and can be ignored in Ku- and Ka-bands, as they deteriorate inversely proportional to the radio frequency [ITU03a]. In case of Faraday rotation, polarisation losses can be easily eliminated by employing circular polarisation for the transmitted waves [KP99]. Prediction models and experimental data for ionospheric effects are found in the ITU recommendations [ITU12] and [ITU03a].

Effects in Troposphere

The troposphere is the deepest layer of the atmosphere from ground to 8-15 km height. In this so called 'weather zone', the signal is influenced by clouds, rain, ice particles and atmospheric gases. In general, signal impairments become relevant if the wavelength is in the range of the size of the disturbing structures. Thus, the dominant tropospheric impairment 'rain attenuation' has some impact for frequencies above 10 GHz, i.e. for Ku- and Ka-band, where wavelengths are smaller than few centimetres. Empirical formulas to calculate rain attenuation depending on the path length of radio waves through rain are found in [ITU03a]. For Ku- and Ka-bands it is in the range of several dB per kilometre. Gas attenuation due to water vapour and oxygen is between 0.01 dB and 0.1 dB for frequencies between 10 and 30 GHz (Ku- and Ka-band) and can be neglected [ITU09]. Tropospheric scintillation have major impact above 20 GHz [ITU03a]. For lower frequency bands applied for satellite communications (UHF, S, L), tropospheric impairments can be neglected.[KP99][ITU03b]

Effects in Receiver Environment

For a land mobile receiver, the majority of propagation impairments are found in its local environment. Solid objects like buildings, bridges, and tunnels cause signal blockages, reflection and diffraction of the signal. Vegetation causes shadowing, diffraction, and scattering losses due to different densities of foliage and branches in the transmission path. The degree of these impairments depends on the path length of the signal through the vegetation mass [GV98]. Shadowing and blockage effects are mainly related to the mobile channel. While stationary receivers are typically dimensioned with line-of-sight connection to the satellite (e.g. antennas are mounted on the roof-top of buildings), this can not be ensured for moving receivers (such as vehicular or hand-held terminals).

2.1.1. Features of the Mobile Channel

The received satellite signal can be characterised as a superposition of three components: the direct signal, specular reflected signals, and diffuse multipath [KP99][Dav87].

The **direct signal** may experience shadowing attenuation due to vegetation, may blocked by solid obstacles (buildings, bridges) in the transmission path, or may arrive unshadowed at the receiver in case of line-of-sight. Travelling through zones with those different shadowing conditions leads to large-scale variations of the received signal, as sketched in Figure 2.2. Shadowing effects are particularly frequent in case of low elevation angles of the satellite from the terminals point of view, where a high number of obstructing objects are in the transmission path. For the same reason, the shadowing probability depends on the environment. Thus, in urban areas, for example, more shadowing is expected than on open highways.

Diffuse multipath origins from multiple reflections and scattering of the transmitted signal on surrounding objects and arrive the receive antenna from different directions with different propagation delays and phases. Vehicle movement through regions with constructive and destructive interferences of multipath rays cause fast variations of the received signals' amplitude and phase. The multipath power depends on the distribution of scattering objects in the vicinity of the receiver.

Specular rays are generated by signal reflections from the ground, from car-roofs, or building surfaces, whereat their received power dominate over the diffuse components. In case of vehicular antennas, the contribution of specular reflections from ground is mitigated by the antenna pattern, which is usually directed to the upper hemisphere.

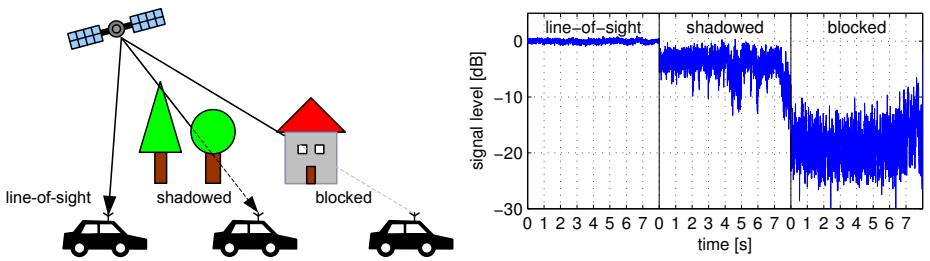

(a) (b)

Figure 2.2.: (a) Different categories of shadowing conditions (states) for the land mobile satellite reception. (b) Received signal samples for different shadowing conditions.

Specular and diffuse components arrive at the receiver with a round-trip detour and a delay with respect to the undisturbed direct signal (**time dispersion**). In case these delays are significantly larger than the symbol duration, the received signal may experience significant distortion such as frequency selectivity or intersymbol interference [SAZ07]. Due to the mobility of the receiver and the satellite, **Doppler phenomena** further affect the channel: Doppler frequency spread is due to the vehicle movement with respect to the scattering objects; satellite movement provides additionally a Doppler shift of the whole received signal spectrum. The dispersion of the received signal in time and frequency domain are subject of next Section 2.1.2. Doppler effects are further discussed in Section 2.3.6.

2.1.2. Characterisation of Time-Variant Multipath Effects

From the previous section it is concluded that the received LMS signal is a superposition of the direct signal, specular reflected rays, and diffuse multipath induced by direct signal and of specular rays illuminating nearby scatterers. All paths sum up at the receive antenna and have different attenuations, phase shifts, and propagation delays with respect to the transmitted signal. These propagation effects are characterised by the **time-variant impulse response**. By assuming a discrete number of paths N, the time-variant impulse response of the channel can be written

$$h(t,\tau) = \sum_{i=1}^{N} a_i(t) e^{j\phi_i(t)} \cdot \delta(t-\tau_i) \tag{2.1}$$

with amplitude $a_i(t)$, phase $\phi_i(t)$, and delay τ_i of the i-th signal component, respectively, and the Dirac delta function $\delta(t)$.

Assuming a transmitted signal after modulation $s_{HF}(t) = \mathrm{Re}\{s(t)e^{j2\pi f_c t}\}$, the received signal $y(t)$ at a time t is found by the convolution of $s_{HF}(t)$ and the channel impulse response (neglecting thermal noise):

$$y(t) = s_{HF}(t) * h(t,\tau) \tag{2.2}$$

The **time-variant transfer function** $T(f,t)$ describes the channel in frequency domain. It is defined by the Fourier transform of the time-variant impulse response with respect to the delay τ:

$$T(f,t) = \mathcal{F}\{h(t,\tau)\} = \int_{\infty}^{\infty} h(t,\tau) e^{-j2\pi f} \mathrm{d}\tau \tag{2.3}$$

The signal spectrum at a time t, $Y(f,t)$, is found by multiplying the signal spectrum with the transfer function.

$$Y(f,t) = S_{HF}(f) T(f,t) \tag{2.4}$$

Both functions, $h(t,\tau)$ and $T(f,t)$, give information about the **time dispersion** of the channel. Time dispersion is due to multipath rays arriving the receiver with different propagation delays which results in a certain spread of a transmitted impulse over time at the receiver. A parameter to describe time dispersion is the **delay spread** T_m. According to [SAZ07], the delay spread can be determined from the power delay profile (PDP), which is calculated from the time-variant impulse response by

$$P(\tau) = \frac{E[|h(t,\tau)|^2]}{2}\,. \tag{2.5}$$

The PDP describes the mean power of the impulse response with respect to the delay τ. The delay spread T_m is then defined as the range of τ over which the PDP is essentially nonzero. As for the LMS channel multipath rays arrive with significant attenuation compared to the direct signal, the more meaningful parameter would by the RMS delay spread τ_{RMS} to appropriately characterise the time dispersion. It takes into account the power and delay of impulses within the PDP and is defined by [SAZ07]

$$\tau_{RMS} = \sqrt{\frac{1}{P_T}\sum_n P_n \tau_n^2 - \tau_0}\,, \tag{2.6}$$

where $P_T = \sum_n P_n$ is the total power of the channel and $\tau_0 = (1/P_T) \sum_n P_n \tau_n$ is the mean delay of the PDP.

If τ_{RMS} is small with respect to the symbol duration, the channel can be assumed as narrowband. Otherwise, if τ_{RMS} is great with respect to the symbol duration, then wideband conditions are assumed.

Large time dispersion of the channel comes along with **frequency selectivity**. It means that the vectorial sum of multipath waves with multiple phases is frequency dependent. Thus, the signal in frequency domain is distorted over its bandwidth. A parameter for frequency selectivity is the **coherence bandwidth** B_c. It describes the frequency separation Δf, for which two components in the channel transfer function have a correlation coefficient of 0.5 for a time separation $\Delta t = 0$. According to [Pro00], the coherence bandwidth depends on the delay spread with

$$B_c \approx 1/T_m \tag{2.7}$$

If the coherence bandwidth B_c is large with respect to the signal bandwidth, then the frequency selectivity can be neglected and narrowband propagation can be assumed.

Due to movement of the terminal or of surrounding objects in the receiver environment, Doppler phenomena affect the channel resulting in **time selectivity** and **frequency dispersion**. Time selectivity occurs if the channel changes its properties whilst the signal is travelling in it. The longer the signal is in the channel (the longer the signal duration), the more probably the channel properties can change. This effect is related to the coherence time T_c, which describes the time over which the channel can be assumed constant. **Frequency dispersion** denotes the positive and negative Doppler frequency shifts of reflected radio waves in the transmitted spectrum. Frequency dispersion is described by the Doppler spread B_d, which is related to the maximum Doppler shift due to vehicle movement (cf. also Section 2.3.6). According to [Pro95], the coherence time and the Doppler spread are related by the expression

$$T_c \approx 1/B_d \tag{2.8}$$

The channel parameters Doppler spread and coherence time can be analysed through the **delay Doppler spread function** $S(\tau, v)$ and the **output Doppler spread function** $H(f, v)$, where v is the Doppler shift. This set of four functions, $h(t, \tau)$, $T(f, t)$, $S(\tau, v)$, and $H(f, v)$ are coupled by Fourier-relationships and were worked out by Bello [Bel63] to closely describe time-variant propagation channels. A comprehensive description of the radio propagation channel is further found in [SAZ07] and [Pro00].

2.1.3. Narrowband and Wideband Propagation

In LMS environments, where the propagation delay spread is small with respect the symbol duration of the system, or equivalently, the coherence bandwidth is larger than the signal bandwidth, then narrowband conditions can be assumed. Within narrowband channels it is considered that the time dependent fading attenuation affects all frequencies in the modulated signal equally. The channel is frequency non-selective or frequency flat and time dispersion is negligible.

Wideband conditions, on the other side, have to be considered if the propagation delays can not be neglected and the signal bandwidth of the LMS system is great with respect to the coherence bandwidth. The time dispersion of the signal results in frequency selectivity, i.e. the channel varies in dependency on frequency and the received signal spectrum is distorted.

Several measurement campaigns have been carried out to characterise wideband effects in the LMS channel. In [PSE97], average RMS delay spreads for the LMS channel in L- and S-bands between 30 and 90 ns were reported. They were estimated for different environments (open, suburban, urban, tree-shadowed) and for different elevation angles. According to Equation (2.7), coherence bandwidths are between 10 and 30 MHz. In [Jah99], delay spreads for L-band between 500 ns and 2 μs are reported for different environments and elevation angles, resulting in coherence bandwidths between 0.5 and 2 MHz.

When comparing the coherence bandwidths mentioned above with typical transmission bandwidths of satellite systems from Table 2.1, it is seen that for a number of satellite communication systems narrowband conditions can be assumed. In literature, narrowband conditions are considered as appropriate even for bandwidths of 5 MHz (e.g. [PCPFB+10] for DVB-SH), although this assumption is not necessarily correct in any LMS environment. For transmission systems with larger bandwidths, however, a wideband characterisation of the channel is required.

Table 2.1.: Examples for mobile satellite transmission systems and their bandwidths.

system	frequency band	carrier bandwidth	reference
Iridium	L-band	31.5 kHz	[Eva97]
Globalstar	L-band	1.25 kHz	[Eva97]
ICO-Global	L-band	25.2 kHz	[Eva97]
XM	S-band	1.84 MHz	[Mic02]
Sirius	S-band	≈4 MHz	[Akt08]
DVB-SH	S-band	subbandwidths can have 1.7 MHz; 5 MHz; 6 MHz; 7 MHz and 8 MHz	[DVB]
S-UMTS	L/S-band	5 MHz	[SUM00]
Inmarsat BGAN system	L-band	630 channels @ 200 kHz	[FHS00]

The goal of this thesis is to contribute for a narrowband channel model for multiple satellite systems with diversity. It is shown that the narrowband condition is an appropriate assumption for a number of existing satellite communication and broadcasting systems. Thus, the description of fading mitigation techniques in next Section 2.2 as well as the state-of-the-art survey for channel models in Section 2.3 will focus on the narrowband case.

2.2. Approaches for Mitigation of Propagation Impairments

Fading due to shadowing and blocking objects in the transmission path causes severe limitation of signal reception for mobile digital satellite services. It results in high bit error rates and temporary link unavailability. To meet quality of service requirements, satellite systems combine different coverage improvement techniques (e.g. the choice of appropriate satellite orbits, usage of active or passive repeaters) with different diversity techniques (e.g. satellite diversity, time diversity, receive antenna diversity) to avoid and mitigate fading,

respectively. Coverage improvement methods are further explained in Section 2.2.1, while diversity techniques are considered in Section 2.2.2.

2.2.1. Coverage Improvement

Satellite orbits and elevation angles
The probability of satellite signal outages due to obstacles in the transmission path highly depends on the satellite elevation. Therefore, the orbit of satellites plays an essential role in system planning aspects:

- Satellites in a geostationary orbit (GEO) are positioned approx. 36000 km above the equator. They are ideal for wide-area broadcasting, as they can cover up to 30% of the earth surface. Due to their high operating distance in comparison to other orbits, long round-trip delays (greater than 250 ms) are indispensable. GEO satellites are therefore less attractive for interactive applications such as telephony or low-delay internet applications. Additionally, the visibility at high latitudes is limited (e.g. elevation angles range from $\approx 20°$ to $50°$ from southern to northern regions of Europe or USA). To meet the coverage requirements for mobile services, a GEO system may require supplementary terrestrial repeaters and/or the use of diversity techniques. Examples for GEO based systems are Inmarsat [Inm09], MSAT [Nor90], and XM Satellite Radio [Mic02].
- Satellites in low and medium earth orbit (LEO, MEO) move 500-2000 km and 10000-12000 km above ground, respectively. They provide a low round-trip delay (e.g. 10-40 ms for LEO) and are therefore feasible for low-latency bi-directional communication applications. By realising a high visibility due to high elevation angle restrictions, the coverage areas are rather small. Therefore, a great number of satellites is necessary which increases the system costs. LEO systems are, e.g. Iridium [Leo91] and Globalstar [Die97], and a MEO system is ICO [Pos98].
- High-elliptical orbits (HEO) allow coverage of entire continents by providing high elevation angles with a small number of satellites. For example, the U.S. broadcaster Sirius Satellite Radio [Akt08] operates three satellites moving in the same high-elliptical orbit, where at least one satellite provides the service from an elevation angle of more than $60°$.

Transmission power
Stationary and mobile terminals require a certain signal-to-noise ratio (SNR) to provide the QoS. Consequently, systems with high link margins admit signal fading up to a certain threshold. To increase the available SNR and to improve coverage, high power geostationary satellites (e.g. Thuraya system, ACeS system [MNG+02]) as well as multiple satellite spot beams providing higher equivalent isotropic radiated power (EIRP) than global beams (e.g. third generation of Inmarsat [Spi94]) are in common use.

Terrestrial gap fillers
In heavy built-up areas, where satellite diversity techniques and other coverage improvement methods fail to provide the required QoS, terrestrial gap fillers are applied to re-transmit the satellite signal to the users. These hybrid networks, i.e. satellites supplemented by a terrestrial repeater network, are used in the Sirius [Akt08], XM [Mic02], MBSAT [SP05], and

the DVB-SH [DVB07] system. In contrast to a satellite signal, the transmit power of terrestrial repeaters is high enough to provide reception without having line-of-sight connection to the receiver. Multiple reflections are utilisable therefore. However, as terrestrial gap fillers need additional power supply by comparably small coverage areas, system planners aim to minimise the number of (uneconomic) gap-fillers by using diversity schemes and optimised satellite orbits.

Passive repeaters
Also passive repeater techniques without power supply are reported in literature for coverage improvement. Those are plane reflectors to guide the satellite signal to shadowed areas [Yan57][SWT92], and back-to-back antennas transmitting the signal without amplification [HYZ04].

2.2.2. Diversity Techniques

In order to ensure high QoS with limited transmit power in the presence of deep fading for mobile satellite reception, different diversity techniques and combinations of it are attractive, such as satellite diversity, receive antenna diversity, and time diversity. The principle of diversity is to increase the service availability by transmitting the information through multiple paths that are subject to statistically independent fading and combining the signals in the receiver [Heu06]. Thus, by taking the random nature of fading effects into account, signal degradations from one of the transmission paths can be compensated by another path.

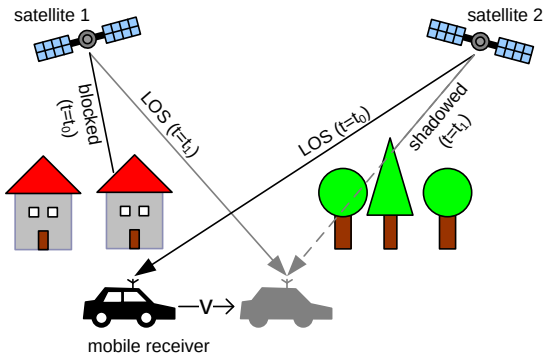

Figure 2.3.: Concept of satellite diversity and time diversity. Multiple transmission paths can be separated in time or in space. If one path is not available, another one is selected.

In the receiver the multiple signals are combined to regain the original information. For this purpose, various diversity combining schemes are available in literature:

- **Switch/selection combining (SC)** selects the link with the highest SNR [Pro95]. It reduces the fading variance of the combined signal, leading to a lower probability of deep fades. A practical implementation is that one link is used until its quality is unacceptable. SC is the simplest form of diversity combining and attractive for mobile antennas, when simplicity of implementation is of primary concern [AS03].
- Within **equal gain combining (EGC)** the received signals are summed after applying a phase-synchronisation. Thus, in contrast to SC, all received signals synchronously

contribute to the output. EGC provide in practice higher gains than SC, i.e. for independently Rayleigh-fading and locally coherent signals with locally incoherent noise and with constant local rms values [Bre59].

- **Maximal ratio combining (MRC)** provides the highest diversity gain and is the most effective combining method for narrowband systems [MSL+09]. It requires perfect channel knowledge at the receiver, as the received signals are summed with phase-synchronisation, and weighted according to their SNR [Pro95]. The additional estimation of the signal strength at the receiver makes MRC much more complicated than EGC. Compared to EGC, MRC maximises SNR instead of signal power.

In case of transmitter diversity, such as satellite diversity, additional space-time coding or space-frequency coding must be applied. It is mandatory to separate the incoming signals from different paths by the receiver. By applying space-time coding techniques an additional coding gain can be achieved. Investigations of coding gains for multi-satellite transmission are found in [Heu08] and [MTTK02].

Satellite diversity

Within satellite diversity (also known as angle diversity), the information is transmitted simultaneously from multiple satellites located at different orbital positions. If one of the satellites is shadowed, there is still some probability that the other satellite has line-of-sight conditions. A high diversity gain is expected when both paths are uncorrelated. This holds for satellites with a certain angular separation in azimuth and elevation from the terminals point of view. In [MPTE98] and [GV98] it is concluded that uncorrelated shadowing of satellite signals can be assumed for azimuth angle separations above 30°. Further details on analyses for multi-satellite correlation are found in Section 2.4.

Satellite diversity is an attractive solution for broadcasting systems such as XM [Mic02], communication systems such as Globalstar [WV93] and ICO [Ber94], and navigations such as GPS [Las75]. It is suitable for low-cost receivers (e.g. in case of selection combining), for time-critical applications and works well under stationary and mobile receive conditions. However, costs for the satellite infrastructure and for reserving different frequency bands have to be taken into account. Performance studies of satellite diversity for LMS reception are found in [Heu08] and [AIH+10].

Time diversity

Time diversity means the spreading of information over time to compensate time-varying or spatial varying signal outages in case of mobility.

A simple method is to repeat the transmitted information with a time delay and to combine the signals at the receiver. This kind of time diversity (**repetition code**) is applied in the Sirius satellite radio system, where two satellites transmit the same signal at different frequencies with four seconds delay [Akt08]. However, repetition coding reduces the power efficiency of the channel and is therefore not the most effective approach.

In case of **time interleaving**, the order of transmitted symbols is rearranged according to a pre-defined pattern. Thus, the information is spread over an interleaver length l_i. Interleaver are proved to be effective if the duration of signal unavailability is below $l_i/2$ [Heu06].

As time diversity relies on the time variability of the transmission channel, it is effective for moving receivers only. Long interleaver sizes of several seconds are especially attractive

for broadcasting applications, which have no real-time requirements. Typical interleaver lengths between 100 ms and 30 s are reported in [DVB] for DVB-SH systems. Time diversity techniques come along with increased costs of the terminals due to increased memory and power requirements.

Receive antenna diversity
Multiple antennas may be applied at the receiver site. Three gains contribute to the overall receive antenna diversity gain.

- **Fading reduction gain**: In contrast to satellite diversity providing a kind of shadowing gain through uncorrelated direct signal paths, a dual-antenna terminal takes advantage from uncorrelated multipath rays. Therefore, a spatial separation of at least one wavelength between the receive antennas is required.
- Linear combining methods, such as MRC and EGC, provide a further **power gain**. In case of MRC, the effective SNR is the sum of the SNR from single pathes.
- Modifications of the received antenna pattern and **beamforming techniques** are possible by phase-synchronised summation of signals incoming from direct path. It improves the available SNR at the receiver.

A detailed overview on multiple-antenna techniques is given in [MSL+09]. Performance studies for multi-antenna systems in context of LMS reception are found in [EAH+10] [AIHE11a] [AIHE11b].

2.3. Statistical Channel Models for Land Mobile-Satellite Communications

For the design and implementation of satellite communication systems an accurate understanding of the radio propagation channel is of paramount importance. Therefore, different types of propagation models are distinguished in literature:

Empirical models are usually given in a form of more or less complex expressions to determine the signal attenuation for a given percentage of locations relating to the satellite elevation angle, the frequency range or other input parameters. These models are derived by fitting mathematical expressions to measurements to find a set of parameters that fits best to the measurements, whereat they fail to give any indication to the physical processes. Empirical channel models are suitable for coverage predictions over large-scale areas with just few input parameters and short calculation time. A comparison between different models for LMS reception is found in [KC96].

Deterministic models describe the composition of the received signal exclusively on pure mathematics for signal and wave propagation. These models are most accurate to describe the signal propagation, but also require a detailed representation of the receive environment, such as a building database. Complex algorithms like ray-tracing or ray-launching techniques are used for signal propagation calculations, such as described in [SM99]. Examples for ray-tracing applied to LMS channels are given in [DJDW01]. The deterministic approach is suitable for propagation studies in urban areas and for indoor reception. However, because of the need for detailed three-dimensional models of the receive environment and the high

calculation time of the wave propagation algorithms, the application of wide-range coverage prediction is limited.

Statistical approaches combine analyses of real propagation data with physical assumptions. For this purpose, several fading processes of the LMS channel are identified: Slow variations of the signal are caused by obstacles between the satellite and the receiver, which induce varying shadowing conditions of the direct signal component. Fast signal variations are caused by multipath effects due to static or moving scatterers in the vicinity of the mobile terminal. Over short time periods of mobile reception these two components (*slow and fast variations*) are usually modelled by a stationary stochastic process. Depending on the interaction and correlation of slow- and fast varying signal components, different so-called *single-state models* are found in literature describing the incoming signal for certain environmental conditions (see also Section 2.3.3). For longer time periods the received signal can not be assumed as stationary. Therefore, advanced LMS channel models consider different receive states (*multi-state models*, Section 2.3.4) to assess the large dynamic range of the received signal. The states correspond to slow varying environmental conditions (e.g. line of trees, buildings, sections with line-of-sight) in the transmission path. Besides information about phase and signal strength of the summation of received signals, statistical LMS models incorporate the temporal composition of the fading signal as well. Thus, time series of the received signal can be generated for various receive conditions in different environment types. Statistical approaches are most favourable for the characterisation and modelling of LMS communication links and are therefore focused in this thesis.

2.3.1. Introduction to Narrowband Channel Modelling

Besides the classification of channel models as summarised above, statistical channel models are further distinguished into narrowband and wideband models. The decision for a corresponding modelling type depends on the duration of multipath propagation delays and the signal bandwidth of the satellite system, as described in Section 2.1.2. By taking LMS propagation delays and coherence bandwidths estimated from several measurements into account, in Section 2.1.3 it was concluded that satellite communication and broadcasting systems up to a bandwidth of approx. 5 MHz are appropriately described with narrowband conditions, which is fulfilled by a number of satellite communication and broadcasting systems in L- and S-bands. Thus, in this work, narrowband channel modelling is in focus and wideband conditions are out of scope.

For a narrowband system, where delay spread is negligible, the channel response can be expressed with

$$h(t) = a(t)e^{-j\phi(t)} \tag{2.9}$$

with $a(t)$ and $\phi(t)$ denote the envelope and phase at time t, respectively.

The received signal $y(t)$, by neglecting thermal noise, is the multiplication of the channel response and the modulated transmitted signal s_{HF}:

$$y(t) = h(t)s_{HF}(t) \tag{2.10}$$

Narrowband channel models target to describe the envelope of the complex fading coefficient $|h(t)|$. Fading of the received signal is a result of reflection, diffraction, and absorption

of radio waves on man-made or natural obstacles in the environment of the receiver. This fading process is traditionally described by a set of statistical distributions, which are subject of the following Sections 2.3.2 and 2.3.3.

2.3.2. Probability Distribution Functions for Different Types of Fading

Various statistical distributions are available in the literature which are suitable to describe fading in different receive environments. In the following, some frequently used distributions are presented to characterise the individual components of the LMS signal: direct signal and multipath. The superposition of these signal components and consequently of the distributions is described by the statistical narrowband LMS models in Section 2.3.3 and 2.3.4.

Rayleigh Distribution

In non-LOS situations and blockages, the received signal of a mobile channel is assumed to be the sum of infinite multipath rays with Gaussian distributed amplitudes, different delays and phase shifts. The phases of multipath components are assumed to be uniformly distributed in the interval $[0; 2\pi)$. The envelope of the received signal $r = |h(t)|$ thus follows a Rayleigh distribution, which probability density function (PDF) can be expressed with

$$P_{\text{Rayleigh}}(r) = \frac{r}{\sigma^2} \exp\left(\frac{-r^2}{2\sigma^2}\right) \qquad r \geq 0\,, \tag{2.11}$$

where σ^2 is the average power of multipath rays. [Jak74]

Rice Distribution

In LMS scenarios with LOS conditions between transmitter and receiver, the received signal is the sum of one dominant direct signal component and a number of uncorrelated multipath components. In addition to the Rayleigh distributed multipath rays, a direct signal with constant amplitude α is assumed. The PDF of the received signals' envelope r has a Rician distribution [Ric48] and is given by

$$P_{\text{Rice}}(r) = \frac{r}{\sigma^2} \exp\left[\frac{-(r^2+\alpha^2)}{2\sigma^2}\right] I_0\left(\frac{r\alpha}{\sigma^2}\right) \qquad r \geq 0\,, \tag{2.12}$$

where σ^2 is the average multipath power, $\alpha^2/2$ is the mean power of the LOS component, and I_0 is the modified Bessel function of first kind and order zero. With $\alpha = 0$, a special case of the Rice distribution is the Rayleigh distribution, assuming no direct path between the transmitter and receiver. A Rice distribution is often expressed by a Rice factor $k = \alpha^2/2\sigma^2$, which is the ratio of the average direct signal power to the average multipath power.

Lognormal Distribution

Vegetation and foliage by trees with irregular pattern of branches and leaves with different densities cause scattering and absorption of radio waves. Consequently, the power of the received direct signal varies about its mean power. In several statistical models the fading of the direct signal component is described by a lognormal distribution. The corresponding PDF is given by

$$P_{\text{logn}}(r) = \frac{1}{r\sigma_{ln}\sqrt{2\pi}} \exp\left[-\frac{(\ln r - \mu)^2}{2\sigma_{ln}^2}\right] . \tag{2.13}$$

μ and σ_{ln} are respectively the mean and standard deviation of the lognormally distributed signal.

Nakagami Distribution

After extensive experiments on long-distance multipath propagation via ionosphere or troposphere, Nakagami [Nak60] proposed the so-called m-distribution to describe the received signal statistics. It covers the condition that two paths have comparable power and are stronger than the others. The PDF of the Nakagami m-distribution is given by:

$$P_{\text{Nakagami}}(r) = \frac{2}{\Gamma(m)} \left(\frac{m}{\Omega}\right)^m r^{2m-1} \exp\left(\frac{-mr^2}{\Omega}\right) \qquad m \geq \frac{1}{2},\, r \geq 0 \tag{2.14}$$

where Ω is the average power of the signal ($\Omega = E(r^2)$), $\Gamma(.)$ represents the Gamma function, and m defines the fade depth. The Nakagami m-distribution contains other distributions as special cases. Depending on m, the distribution is modified: for $m = 1$ a Rayleigh distribution results; $m = 0.5$ results in a one sided Gaussian distribution; for large m a lognormal distribution can be approximated. The Nakagami distribution is proposed in [ALAK03] as alternative for the lognormal distribution, because of its better applicability for closed-form analytical description of fading when combined with other distributions like Rice or Rayleigh.

2.3.3. Single-State Models

Loo Model

Based on LMS propagation measurements (satellite signal was emulated by helicopter) along tree-shadowed rural roads, Loo proposed in 1984 [Loo84] the first statistical LMS model with different behaviour of two signal components: the direct signal (LOS signal) and diffuse multipath. Fading of the LOS component under foliage attenuation is described by a lognormal distribution, whereas diffuse multipath components are described by a Rayleigh distribution conditioned to the LOS power. Between both components a correlation is introduced, following the assumption that foliage not only attenuates but scatters radio waves as well.

The proposed distribution of the received signals' envelope is given by

$$P_{\text{Loo}}(r) = \frac{r}{\sigma^2\sigma_{ln}\sqrt{2\pi}} \int_0^\infty \frac{1}{z} \exp\left[-\frac{(\ln z - \mu)^2}{2\sigma_{ln}^2} - \frac{r^2 + z^2}{2\sigma^2}\right] \cdot I_0\left(\frac{rz}{\sigma^2}\right) \mathrm{d}z\,, \tag{2.15}$$

where σ^2 is the average scattered power due to multipath and μ and σ_{ln} are the mean and standard deviation of the lognormal distribution, respectively. $I_0(.)$ is the modified Bessel function of zeroth order. In limiting cases the values of r are lognormally distributed ($r \gg \sigma$) or Rayleigh distributed ($r \ll \sigma$).

From measurements, the distribution parameters were extracted by curve-fitting. A comparison of first-order statistics (PDF, CDF) and second-order statistics (level crossing rate (LCR) and average fade duration (AFD)) between measurements and model have shown a good agreement [Loo84]. A high correlation ($0.5 < \rho < 0.9$) between the rate of change for multipath and shadowing components has been obtained, which proved the initial assumption.

In some newer LMS models [PFVCC+01][PCPFB+10] (cf. also Section 2.3.4), the Loo distribution is described by three parameters M_A, Σ_A, MP given in dB, denoting the mean and standard deviation of the lognormal distribution, and the multipath power, respectively. The corresponding Loo-PDF was therefore converted into the form

$$P_{\text{Loo}}(r) = \frac{r \cdot 20\log(\mathrm{e})}{\sigma^2 \Sigma_A \sqrt{2\pi}} \int_0^\infty \frac{1}{z} \exp\left[-\frac{(20\log z - M_A)^2}{2\Sigma_A^2} - \frac{r^2 + z^2}{2\sigma^2} \right] \cdot I_0\left(\frac{rz}{\sigma^2}\right) \mathrm{d}z\,, \tag{2.16}$$

with $\sigma = \sqrt{10^{MP/10}/2}$. This notation of Loo parameters will be used for the multi-satellite LMS model developed in this thesis, and continues therefore the notation from the single-satellite model which is taken as basis.

Suzuki Model

Suzuki [Suz77] introduced first a mixture of two distributions to suitable characterise the mobile channel. He proposed a combination of Rayleigh and lognormal processes to describe the terrestrial signal propagation in urban environments. It is assumed that local scattered multipath components around the receiver have Rayleigh characteristic, whereas the signal from transmitter to local area undergo lognormal variations due to refractions. Although this model is designed for terrestrial reception, several multi-state LMS models (cf. Section 2.3.4) use this distribution for shadowed or blocked conditions of the direct signal. The PDF is given by

$$P_{\text{Suzuki}}(r) = \int_0^\infty \frac{r}{\sigma^2} \exp\left(\frac{-r^2}{2\sigma^2}\right) \frac{1}{\sigma\sigma_{ln}\sqrt{2\pi}} \cdot \exp\left(-\frac{(\log\sigma - \mu)^2}{2\sigma_{ln}^2}\right) \mathrm{d}\sigma\,, \tag{2.17}$$

where σ^2 is the average received power of the Rayleigh process, and μ and σ_{ln} are the mean and standard deviation of the lognormal process.

Corazza-Vatalaro Model

Corazza&Vatalaro [CV94] presented in 1994 a further combination of Rice and lognormal distribution to characterise LMS reception. It is assumed that shadowing takes an effect on both, the direct signal and the multipath. For comparison, the Loo model assumes an

influence of shadowing for the direct signal only. The PDF is the product of two independent processes, lognormal and Rice:

$$P_{\mathrm{RLN}}(r) = \int_0^\infty P_{\mathrm{Rice}}(r|s) P_{\mathrm{logn}}(s) \mathrm{d}s \,, \tag{2.18}$$

where $P_{\mathrm{Rice}}(r|s)$ is a Rice PDF conditioned on a certain shadowing s

$$P_{\mathrm{Rice}}(r|s) = 2(k+1)\frac{r}{s^2} \exp\left[-(k+1)\frac{r^2}{s^2} - k\right] I_0\left(2\frac{r}{s}\sqrt{k(k+1)}\right) \qquad r \geq 0 \tag{2.19}$$

with Rice factor k and $P_{\mathrm{logn}}(s)$ is the lognormal PDF of shadowing s. Combining the conditioned Rice distribution and the lognormal distribution, the PDF of the Corazza&Vatalaro model (in literature also known as Rice-lognormal (RLN) model) is given by

$$P_{\mathrm{RLN}}(r) = \frac{2(k+1)r}{h\sigma\sqrt{2\pi}} \int_0^\infty \frac{1}{s^2} \exp\left[-\frac{(\ln s - \mu)^2}{2(h\sigma)^2}\right] \exp\left[-(k+1)\frac{r^2}{s^2} - k\right] I_0\left(2\frac{r}{s}\sqrt{k(k+1)}\right) \mathrm{d}s \tag{2.20}$$

where $h = \ln(10)/20$, μ and $(h\sigma)$ are the mean and standard deviation of the lognormal process, respectively, and Rice factor k.

Corazza&Vatalaro verified their RLN model in [CV94] with measurement data from rural tree-shadowed environment for a wide range of elevation angles. The corresponding set of model parameters (μ, σ, k) are given in [CV94] as well.

Abdi Model

To simplify the analysis of statistical models, Abdi et al. [ALAK03](2003) proposed an alternative to the Loo model. As with the Loo model the multipath component is Rayleigh distributed, but the amplitude of the LOS signal is described by a Nakagami distribution instead of a lognormal distribution. Abdi pointed out that an analytic manipulation of lognormal-based models (incorporating data fitting and parameter extraction) is challenging. Therefore, the Nakagami distribution is proposed as alternative to lognormal distributions, leading to mathematically closed forms for the combined description of direct signal and multipath. The PDF of the Abdi model can be written as

$$P_{\mathrm{Abdi}}(r) = \left(\frac{2\sigma^2 m}{2\sigma^2 m + \Omega}\right)^m \cdot \frac{r}{\sigma^2} \exp\left(-\frac{r^2}{2\sigma^2}\right) \cdot {}_1F_1\left(m, 1, \frac{\Omega r^2}{2\sigma^2(2\sigma^2 m + \Omega)}\right) \qquad r \geq 0 \,, \tag{2.21}$$

where σ^2 is the average power of the multipath component, Ω is the average power of the LOS component, m is the Nakagami parameter, and ${}_1F_1$ is the confluent hypergeometric function.

The Abdi model provides similar fit to Loo model but with less computational effort.

Other Single-State Models

Further, more sophisticated single-state models for LMS reception have been introduced, as seen in Table 2.2. In most cases the primary concepts of additive or multiplicative combination of a lognormal characteristic for the direct signal and a Rice or Rayleigh characteristic for multipath as proposed by Loo and Corazza&Vatalaro are modified or extended.

Paetzold et al. [PKL98] proposed an extension of Suzuki's model by incorporating Doppler phenomena to the fading characteristics. An extension of the Loo model is presented in [HKAW97], where the multipath components are subjected to own lognormal variations which are different from the direct signals variations. An extension of the Corazza&Vatalaro model is given in [Vat95], called generalized Rice-lognormal model. It adds a Rice distributed multipath component with constant power. The model in [XF00] is based on the RLN model, but uses a more general form of the Rice distribution (Beckmann distribution) for multipath based on scattering theory.

Comparitive studies of various single-state models are found in [KP99] and [PFBA+08].

Table 2.2.: Available single-state models for the narrowband LMS channel. (Notation: S corresponds to the direct signal and slow fading processes, R corresponds to the multipath component.)

proposed by	year	complex channel process $r = r_x + jr_y$ (cf. [KP99])	comments
Suzuki [Suz77]	*1977*	$r = RS\exp[j\phi]$ R: Rayleigh S: lognormal ϕ: uniform	*terrestrial propagation*
Loo [Loo84]	1984	$r = R\exp[j\phi_M] + S\exp[j\phi_0]$ R: Rayleigh S: lognormal ϕ_M, ϕ_0: uniform	
Corazza&Vatalaro [CV94]	1994	$r = RS\exp[j\theta]$ R: Rice S: lognormal θ: uniform	also known as RLN model
Vatalaro [Vat95]	1995	$r = RS\exp[j\theta] + x_1 + jy_1$ R: Rice S: lognormal x_1, y_1 : Gaussian	RLN + multipath component with constant power
Hwang et al. [HKAW97]	1997	$r = AS_1\exp[j\phi] + RS_2\exp[j(\theta+\phi)]$ R: Rayleigh A: constant S_1,S_2: lognormal	RLN with extra lognormal fading for multipath components
Pätzold et al. [PKL98]	1998	$r = S\exp[j\theta] + x_1 + jy_1$ S: lognormal x_1, y_1 : Gaussian	Doppler phenomena included
Xie&Fang [XF00]	2000	$r = RS\exp[j\theta]$ R: Beckmann S: lognormal	modification of RLN by general form of Rice distribution
Abdi et al. [ALAK03]	2003	$r = R\exp[j\phi_M] + S\exp[j\phi_0]$ R: Rayleigh S: Nakagami	alternative to Loo's model with simpler mathematics

2.3.4. Multi-State Models

To cope with the large dynamic range of the received signal due to terminal mobility, statistical LMS models describe different states that correspond to slow changes of environmental conditions (e.g. line of trees, buildings, regions with line-of-sight) in the transmission path. The temporal sequence of states can be described by Markov processes. The number of states for such LMS models range from two states to concepts with five and more states. In contrary to single-state models, the distribution of amplitudes within multi-state models are composed by a weighted mixture of single statistical distributions (e.g. Rice, Rayleigh) as well as of certain single-state models itself (e.g. Loo, Nakagami). Different multi-state models are listed in Table 2.3. Selected models are briefly described in this section.

Table 2.3.: Available multi-state models for the narrowband LMS channel.

proposed by	year	structure of the model	comments
Lutz et al. [LCD+91]	1991	Rice + Suzuki	
Wakana [Wak91]	1991	Rice + Rice/Rice	different attenuations for non-LOS states are assumed
Barts&Stutzmann [BS92]	1992	Rice + Loo	
Karasawa et al. [KMM95]	1995	Rice + Loo + Rayleigh	
Akturan&Vogel [AV95]	1995	Rice + Loo + Loo or Rayleigh	photogrammetric approach for state extraction
Perez-Fontan et al. [PFVCB+98]	1997	Loo + Loo + Loo	reference model for DVB-SH [DVB]
Rice&Humpherys [RH97]	1997	Rice/Rice + Suzuki	extension of two-state Lutz model for K-band with two 'line-of-sight' states regarding antenna de-pointing
Mehrnia&Hashemi [MH99]	1999	Rice + Hoyt	
Perez-Fontan et al.[PFSLCn07]	2007	Loo + Loo	enhanced version of earlier three-state model
Ming et al. [MDY+08]	2008	Rice/Rice + Loo + Rayleigh/Rayleigh	

Two-State Models

The first LMS model considering different states was presented by Lutz et al. in 1991 [LCD+91]. It is based on measurement campaigns of satellite signals with a mobile terminal in different European areas for elevation angles between 13° and 43°. As a result of the data analyses an LMS model with two states was developed: 'good' to cover line-of-sight, and 'bad' to cover shadowed areas in the mobile reception. The 'good'-state is characterised by a Rice distribution, which defines a constant power of the direct signal (which is 0 dB in case of LOS), and diffuse Rayleigh distributed multipath components. In 'bad'-state no direct signal is assumed. The multipath components are modelled by a Rayleigh process which mean power underlie slow lognormal distributed variations due to slow changing shadowing conditions in the environment. Both components, Rayleigh and lognormal fading, are

fully correlated and are combined by multiplication (this process was proposed originally by Suzuki [Suz77] for the terrestial reception). The PDF of the envelope of the received signal is described by

$$P_{\text{Lutz}}(r) = (1 - A) \cdot P_{\text{Rice}}(r) + A \int_0^\infty P_{\text{Rayleigh}}\left(\frac{r}{r_0}\right) P_{\text{logn}}(r_0)\mathrm{d}r_0 \,. \tag{2.22}$$

Parameters are Rice factor k, mean μ and standard deviation σ of the lognormal distribution, and time share of shadowing A.

The state transitions between 'good' and 'bad' state are described by a first-order Markov chain (cf. Figure 2.4). Thus, the time share of shadowing A corresponds to the 'bad'-state probability. To allow a time series generation with this Lutz model, state transition probabilities p_{ij} with $i, j \in \{\text{g}, \text{b}\}$ can be estimated by analysing the mean state durations $\bar{D}_\text{g}$ and $\bar{D}_\text{b}$ with:

$$p_{\text{gb}} = \frac{1}{\bar{D}_\text{g}}, \quad p_{\text{gg}} = 1 - p_{\text{gb}}, \quad p_{\text{bg}} = \frac{1}{\bar{D}_\text{b}}, \quad p_{\text{bb}} = 1 - p_{\text{bg}} \tag{2.23}$$

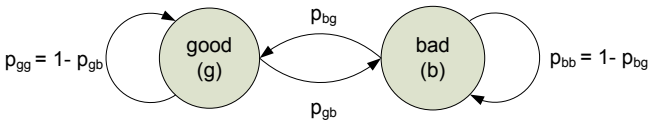

Figure 2.4.: First-order Markov model with two states

Similar models are presented by Barts&Stutzmann [BS92] and later by Mehrnia&Hashemi [MH99]. In contrast to Lutz, the authors in [BS92] characterised the 'bad'-state by a Loo distribution and in [MH99] by a Hoyt (or Nakagami-Q) distribution, which is a special case of the Nakagami m-distribution. Rice&Humpherys [RH97] presented an extension of the Lutz model using two LOS states to cope with antenna de-pointing effects in K-band communications.

Three-State Models

To refine the description of shadowing conditions, enhanced LMS models were developed incorporating three states from Karasawa et al. [KMM95], Perez-Fontan et al. [PFGF+97], Akturan&Vogel [AV97]. These models distinguish line-of-sight and two degrees of shadowing, such as

- **line-of-sight**,
- **moderate shadowing**, which is induced by trees and small obstacles, and
- **heavy shadowing** or **blockage**, which is due to solid object like buidings, bridges, and tunnels.[3]

[3] Please note that the exact vocabulary for state description differs in the literature.

In all models the received signal within the states is composed of a direct signal and diffuse multipath components. Some differences are found in the statistical characterisation of the signal within the states. In [KMM95] as well as in [AV97] the states are described by Rice distribution in LOS state (i.e. direct signal power is constantly 0 dB), Loo for moderate shadowing (i.e. direct signal has lognormal fading) and Rayleigh for blockage conditions (i.e. direct signal is absent).

A greater flexibility is achieved with the model from Perez-Fontan et al., where a Loo distribution (lognormal + Rice) is assumed in each state. Thus, three different rates of fading (very slow, slow, fast) can be described with the LMS model (cf. Figure 2.5). **Fast variations** are due to multipath propagation and are present in each state. They are superimposed by **slow variations** of the direct signal described by lognormal fading, and **very slow variations** of the direct signal described by states. Very slow variations correspond to different gross shadowing conditions due to changing environmental conditions. Slow variations in shadowed states correspond to different degrees of attenuation produced from the same obstacle: e.g. different densities of foliage when passing a group of trees; signal variations behind buildings due to different diffraction zones. In the LOS state, slow variations of the overall signal originate from, e.g. non-uniform receive antenna patterns which affects the direct signal power; specular components reflected from obstacles behind the vehicle affects the overall signal power.

The fading rate of slow variations is described by a correlation distance, which was found to be in the range of 1 m and 2 m for L- and S-bands, respectively. The update rate of states (very slow variations) is defined by a state frame length, for which 3-5 m is assumed. This value corresponds to the minimum state length and is related to the size of obstacles in the transmission path, which induce a state transition. The sequence of three states is generated by a first-order Markov model.

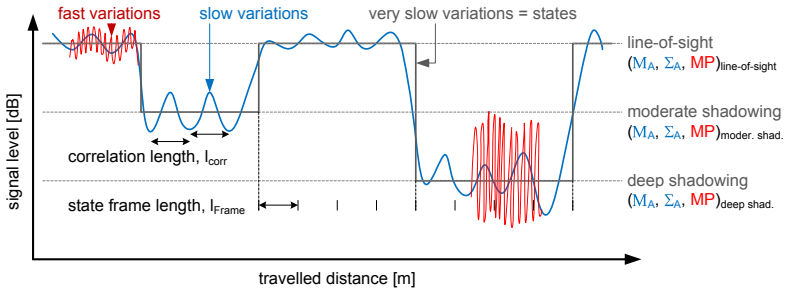

Figure 2.5.: Received signal components with different rates of fading from the three-state LMS model proposed in [PFGF+97].

In [PFVCC+01] the authors presented parameters sets of the Perez-Fontan model for different elevation angles in five different environments estimated from measurements in the UK, Germany, and Austria. Each set include three Loo parameters (M_A, Σ_A, MP, cf. Equation (2.16)) for each state and nine state transition probabilities [4] for the Markov model. Due to its flexibility in terms of received signal dynamics and the availability of parameter sets for various receive scenarios, the three-state model from Perez-Fontan is used as reference model for the DVB-SH standard [DVB].

[4] A first-order Markov model with N states is described by N^2 state transition probabilities.

Besides a time series generation of the received signal amplitudes, the Perez-Fontan model considers also the Doppler effect on direct and multipath signal components. It is separately described in Section 2.3.6.

Further Concepts With Respect to the Number Of States

Narrowband LMS models with five receive states [MDY+08] and six states [DJY+05] are also found in literature. In both contributions the authors analysed a signal of only 150 m length, which is just a scan of an exemplary measurement signal presented in [LCD+91]. The number of states origins from a quantisation of this timeseries in five or six states, for which the state transitions are determined. The conclusions from the authors, a good match with 'measurement data', origins just from an over-trained Markov model. Besides that there is no novelty, both models are not suitable for LMS applications due to the required number of parameters.

In [SAHE] and [ASHE08] a new methodology for the analysis of the LMS channel is proposed. There, in contrast to fixed-state models, no prior assumptions on the number of states is done. The state sequence is estimated by a Reversible Jump Monte Carlo Markov Chain (RJ-MCMC) algorithm, which is an unsupervised process. After detecting N states of Gaussian distributions with variable means, these states are classified by means of a scalable clustering technique according to [WP93]. In this iteratively working algorithm, local clusters (i.e. fading around a certain mean value) are merged together iteration by iteration to greater clusters when they belong to the same cluster centre. The final number of states corresponds to the longest period of iterations where the algorithm have a constant cluster number. State transitions are described by a first-order Markov model. In [ASHE08] the model is validated by urban and highway measurements in the area of Munich and show good agreement with measurement data. Although this approach accurately re-simulates single-satellite signals, from the authors point of view the undefined number of states complicates the applicability of Markov models with multiple satellites.

Advanced Concepts on State Duration Modelling

The state transitions of the previously mentioned multi-state models are described by so called first-order Markov chains. A property of these first-order Markov chains is that state probabilities and mean state durations that are derived from measurements can be re-modelled accurately. Further on, the probability of the time being in the same state always follows an exponential distribution. Results in [ITU03b], [BT02], and [MHEH09] have shown that this behaviour does not accurately model the LMS channel. However, an accurate characterisation of state durations (which affects also the fade durations) is crucial for system planning aspects, such as synchronisation, symbol timing, and framing [BT02].

To improve the state duration modelling, two different concepts where introduced: **semi-Markov** chains are proposed by Braten et al. [BT02], and **dynamic Markov** chains are introduced by Milojevic et al. [MHEH09].

Within semi-Markov models the time of staying in the same state is defined by a certain state duration probability density function (SDPDF). Arbitrary distribution functions and

curves can be defined therefore. To force the duration of each state following its SDPDF, state transitions of a semi-Markov model are only allowed from state i to j with $i \neq j$. The recommended SDPDFs in [BT02] are a power law distribution for LOS states, and a lognormal distribution for non-LOS states (it is the 'bad'-state in two-state models, or 'moderate shadowed' and 'blocked' in three-state models). These results were adapted from fade distribution measurements in [VGH92] and [ITU03b].

In contrast to the semi-Markov model, the update rate for state transitions to the same or another state in the dynamic Markov model is equidistant and equal to first-order Markov chains. The new aspect is that state transition probabilities are described as a function of the current state duration. Depending on the model parametrisation, arbitrary state duration distributions are possible to simulate.

Due to their potential for LMS modelling, dynamic Markov models and semi-Markov models are described, evaluated and compared in detail in Chapter 3.

2.3.5. Versatile Two-State Model

With the development of high link margin systems a more precise description of the received signal became important. Besides uninterupted service availability under LOS conditions, these systems are designed to maintain QoS under partially obstructed links with moderate shadowing conditions. In DVB-SH systems for vehicular reception, for example, the link margins go up to 10-15 dB [DVB]. For the dimensioning of such systems a better understanding of the received signal over the whole dynamic range is essential.

Perez-Fontan et al. [PFSLCn07][PCPFB+10] proposed a new concept which allows a more realistic modelling of the signal than their earlier developed three-state model. The new model is denoted as enhanced or versatile two-state LMS model.

The versatile two-state model distinguishes the states 'good' and 'bad', where this notation doesn't necessarily match LOS and non-LOS conditions such as in [LCD+91], but corresponds to the range of LOS-to-moderate shadowing and moderate-to-deep shadowing. Within each state, a Loo distributed fading signal is assumed, which is described by three Loo parameters M_A, Σ_A, and MP (cf. Equation (2.16)). In contrast to traditional multi-state models, the Loo parameters are randomly generated after each state transition following a certain distribution, as shown in Figure 2.6 and Figure 2.7 (Remember that traditional multi-state models have a fixed assignment of Loo parameters to a state). Thus, the versatile model allows to take different Loo parameters for each new state, which increases the overall dynamic of fading.

The authors propose following Loo parameter distributions:

- The mean of the lognormal fading M_A is generated according to a Gaussian distribution:

$$f(M_A) \sim \mathcal{N}(\mu_1, \sigma_1^2) \tag{2.24}$$

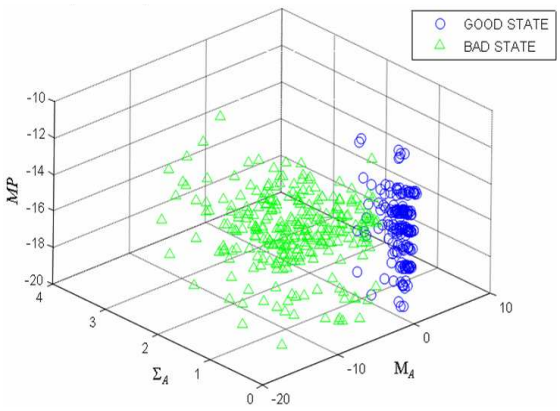

Figure 2.6.: Distribution of Loo parameters assigned to states 'good' and 'bad' for a constant receive environment (image source: [PFSLCn07]).

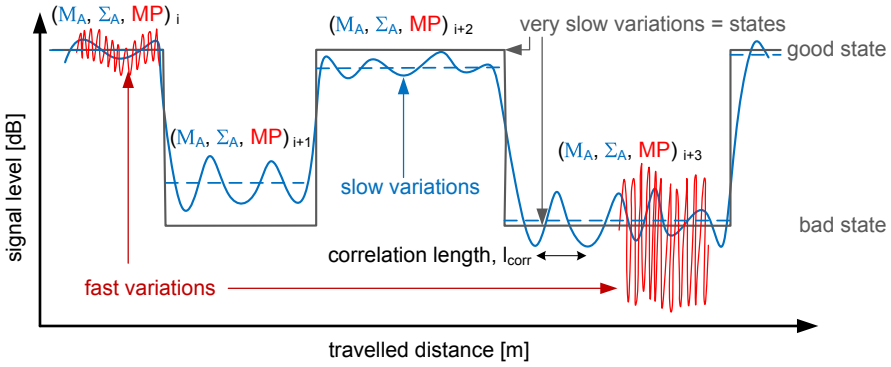

Figure 2.7.: Signal components of the versatile two-state LMS channel model. This model is taken as basis for the new multi-satellite narrowband model developed in this thesis.

- The standard deviation of the lognormal fading Σ_A has a conditional Gaussian distribution to M_A:

$$\begin{aligned} f(\Sigma_A|M_A) &\sim \mathcal{N}(\mu_2, \sigma_2^2) \qquad \text{with} \\ \mu_2 &= a_1 \cdot M_A^2 + a_2 \cdot M_A + a_3 \\ \sigma_2 &= b_1 \cdot M_A^2 + b_2 \cdot M_A + b_3 \end{aligned} \tag{2.25}$$

- The multipath power is Gaussian distributed and independent from the other two values:

$$f(MP) \sim \mathcal{N}(\mu_3, \sigma_3^2) \tag{2.26}$$

To facilitate a realistic fade- and state duration modelling with the versatile two-state model, the semi-Markov concept is proposed for state series generation (cf. previous Section *Advanced Concepts on State Duration Modelling*). Therefore, for both states 'good' and 'bad' the state durations are proposed to be lognormal distributed, which result from analyses of the authors [PFSLCn07].

As for the earlier three-state model, the model parameters sets have to be derived depending on the environment type and the elevation angle. This enhanced two-state model has been validated by using data from L-band and S-band measurements in [PCPFB+10] .

The versatile Loo parameter selection of the newer model allows a more realistic modelling over the full dynamic range of the received signal. Therefore, the two-state model from Perez-Fontan et al. [PFSLCn07] is basis for the new multi-satellite narrowband model developed within this thesis.

2.3.6. Modelling of Doppler Effects

All received signal components, i.e. direct signal and multipath components, are affected by Doppler phenomena due to terminal movement and satellite movement. The combined impairments are separately described in the following.

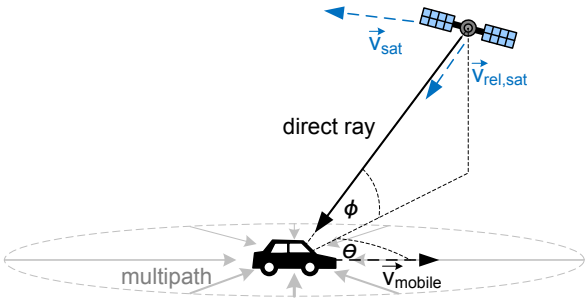

Figure 2.8.: Geometry for Doppler effects.

Multipath components are usually considered to have a uniformly distributed angle of arrival. By vehicle movement the rays incoming from the front have increased frequency, and the rays incoming from the back have decreased frequency with respect to the carrier frequency f_c. Thus, the multipath Doppler spectrum is approximately symmetric to f_c. The maximum Doppler frequency $f_{D\max}$ depends on the mobile speed v_{mobile}:

$$f_{D\max} = v_{\text{mobile}}/\lambda_c, \tag{2.27}$$

with λ_c is the wavelength of the carrier. The Doppler spectrum induced by multipath is independent from the driving direction of the vehicle. Different shapes for the Doppler spectrum are proposed in literature:

1. The Jakes spectrum [J.D00] considers a uniformly distributed angle of arrival between 0 and 2π for multipath components which impinge from zero degree elevation. The Doppler power spectral density (PSD) is described with

$$S_{\text{Doppler}}(f) = \begin{cases} \frac{B}{\sqrt{1-(f/f_{D\max})^2}}, & \text{for } |f| \leq f_{D\max} \\ 0, & \text{for } |f| > f_{D\max} \end{cases} \tag{2.28}$$

   B is a constant to normalise the filter energy equal to one, so that the standard deviation of multipath fading is not changed after filtering.

2. A more realistic case is the assumption that incoming multipath components are distributed in elevation angle as well. This alternative Doppler PSD is described in

[J.D00][KC00]:

$$S_{\text{Doppler}}(f) = \begin{cases} \frac{B}{f_{D\max}} \left\{ \frac{\pi}{2} - \sin^{-1} \left[\frac{2\cos^2\phi_m - 1 - (f/f_{D\max})^2}{1-(f/f_{D\max})^2} \right] \right\}, & |f| \leq f_{D\max}\cos\phi_m \\ \frac{B}{4\sin\phi_m} \left(\frac{1}{f_{D\max}} \right), & f_{D\max}\cos\phi_m \leq |f| \leq f_{D\max} \\ 0, & |f| > f_{D\max} \end{cases} \tag{2.29}$$

where $\pm\phi_m$ describes the maximum and minimum elevation angle of multipath contributions, and B is the normalisation parameter.

3. Also a Butterworth filter is proposed in [PFSLCn07] for the use as Doppler PSD

$$S_{\text{Doppler}}(f) = |H_{\text{Doppler}}(f)|^2 = \frac{B}{\sqrt{1-(f/f_0)^{2k}}} \tag{2.30}$$

with cut-off frequency f_0 which is dimensioned according to $f_{D\max}$, filter order k, and constant B for normalisation. Analyses of LMS measurement data in the context of this thesis confirm the Butterworth filter as appropriate to describe the Doppler PSD in the new LMS model.

The direct signal component experiences a Doppler shift which depends on the relative velocity of the vehicle to the satellite. Considering vehicle movement only while the satellite is stagnant with respect to an earth observation point (which is in the case of geostationary satellites), the Doppler frequency of the direct signal component depends on the vehicle speed v_{mobile}, the elevation angle of the satellite ϕ and the driving direction with respect to the satellite θ:

$$f_{D\text{dir}} = v_{\text{mobile}}/\lambda_c \cdot \cos\phi \cdot \cos\theta \tag{2.31}$$

The overall contribution due to vehicle movement is found in the literature as **Doppler spread** (cf. Figure 2.9) and can be several hundred Hertz wide.

Finally, the satellite movement causes a complete **Doppler shift** of the Doppler spectrum (including direct and multipath components). The important parameter is the relative speed of the satellite $v_{\text{rel,sat}}$ to a fixed observation point in the area of the vehicle, which depends

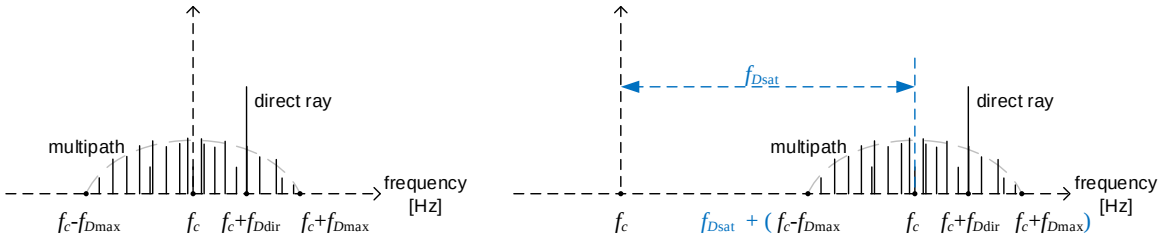

Figure 2.9.: Doppler effect on the mobile channel. Left: The Doppler spread of multipath rays (with equally distributed angle of arrival) origins from terminal movement only. Therefore, the Doppler spectrum is approximately symmetric to the carrier frequency f_c. The Doppler shift of the direct signal $f_{D\text{dir}}$ depends on the mobile speed v_{mobile}, the driving direction θ, and the elevation angle ϕ. Right: In case of satellite movement, a Doppler shift $f_{D\text{sat}}$ of the whole spectrum is present.

on its orbit (LEO, MEO, HEO). The additional Doppler shift due to satellite movement is

$$f_{D\mathrm{sat}} = v_{\mathrm{rel,sat}}/\lambda_c \,. \tag{2.32}$$

For GEO satellites $v_{\mathrm{rel,sat}}$ and consequently $f_{D\mathrm{sat}}$ is zero. The relative speed of LEO satellites is approximately $v_{\mathrm{rel,sat}} \approx 7.4\,\mathrm{km/s}$ [AADH98]. Thus, $f_{D\mathrm{sat}}$ can be in the order tens of thousands or hundreds of thousands Hertz for L-band or K-bands, respectively.

2.3.7. Wideband LMS Channel Modelling

The received LMS signal is characterised by a superposition of the direct signal and multipath rays which are reflected by scatterers in the mobile environment. The incoming rays sum up at the receive antenna and have different attenuations, phase shifts, and propagation delays with respect to the transmitted signal. By assuming a discrete number of paths N, the time-variant impulse response of the channel can be written as

$$h(t,\tau) = \sum_{i=1}^{N} a_i(t) e^{j\phi_i(t)} \cdot \delta(t-\tau_i) \tag{2.33}$$

with amplitude $a_i(t)$, phase $\phi_i(t)$, and delay τ_i of the i-th signal component, respectively, and the Dirac delta function $\delta(t)$.

Wideband channel models are required, when the multipath propagation delays (delay spread) are significantly larger than the symbol duration and the resulting coherence bandwidth is small with respect to the signal bandwidth (cf. Section 2.1.2). Large delay spread results in frequency-selectivity, i.e. the channel varies in dependency on frequency and the received signal spectrum is distorted.

A general approach of wideband models is the implementation of the channel impulse response Equation (2.1) by a filter structure with discrete delay taps, as seen in Figure 2.10. Each tap represents a single beam, which can consist of individual rays or a group of rays with same delay.

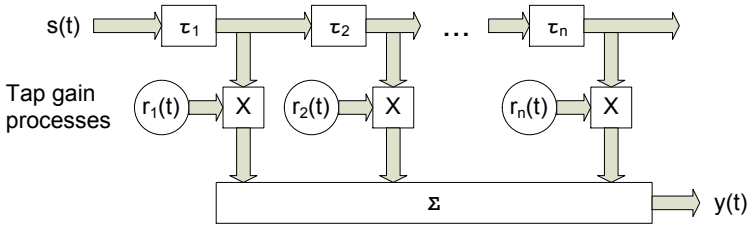

Figure 2.10.: Wideband channel model with n fixed delays.

Such a wideband model for LMS reception was proposed by Jahn et al. [JBH96]. Based on measurement data from L-band, the authors defined a channel impulse response divided into direct path, near echoes (with exponential increasing delay to a maximum of $\tau_e \approx 600\,\mathrm{ns}$), and far echoes (with uniformly distributed delays) as depicted in Figure 2.11.

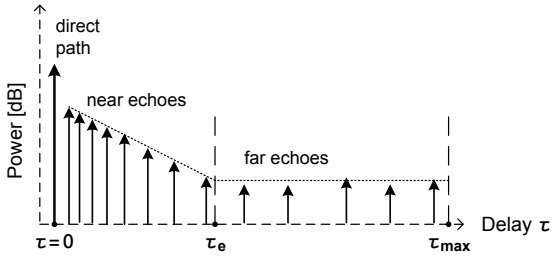

Figure 2.11.: Definition of the echo characteristics for the wideband LMS channel proposed by [JBH96].

2.4. LMS Channel Models with Multiple Satellites

While a number of LMS models for single satellite reception are available and are consolidated for various receive situations, channel models for multi-satellite reception are more or less sporadic and are of ongoing interest. This section gives an overview on contributions for land mobile satellite modelling with at least two satellites in chronological and categorical order.

2.4.1. Empirical Model

Approaches for multi-satellite channel modelling were firstly introduced about 20 years ago. In 1992, Robet et al. [REE92] presented an empirical model for the shadowing probability in dependency on the azimuth angle separation of two satellites.Therefore, images from a camera pointing in driving direction of a vehicle were captured in urban, suburban and countryside areas in the UK.

$$1 - A = b + c\left[1 - \exp\left(\frac{-\Delta\theta}{90b}\right)\right] \tag{2.34}$$

with

$$b = (1 - A_2) + \frac{1}{3}(1 - A_1)(A_1 - A_2) \tag{2.35}$$

and

$$c = \frac{1}{3}(1 - A_1)(4A_2 - A_1) \tag{2.36}$$

A, A_1, A_2 denote the joint shadowing probability, and the single shadowing probability of satellite 1 and 2, respectively. The authors in [REE92] indicated a good agreement of the empirical model with measured curves from urban environment. Amongst others, it has been pointed out that in city environments for azimuth separations $\Delta\theta > 30°$ the diversity gain is close to the maximum.

2.4.2. (Statistical) Markov Model for Correlated State Sequences

Based on his LMS model with two states 'good' and 'bad' [LCD+91], Lutz [Lut96] presented in 1996 a method to calculate joint state transition probabilities for a four-state Markov model to realise correlated state sequences of two satellites. Starting from individual state transition probabilities of two satellites (e.g. p_{gg}, p_{gb}) and only one correlation coefficient, a matrix with combined state transitions (such as $p_{gg \to gg} = p_{11}$) can be calculated (cf. Figure 2.12). With this method, state transition probabilities (and therefore state probabilities and mean state durations) of the individual satellites are not influenced. The advantage is that model parameters are easily to derive and are available in literature, i.e. state transitions of satellites for different elevation angles and environments [PFVCC+01][PCPFB+10], correlation coefficients between two satellites in dependency on the azimuth separation [REE92][TSE98]. The mathematics for this correlated Markov model from Lutz are found in Section B.2.2.

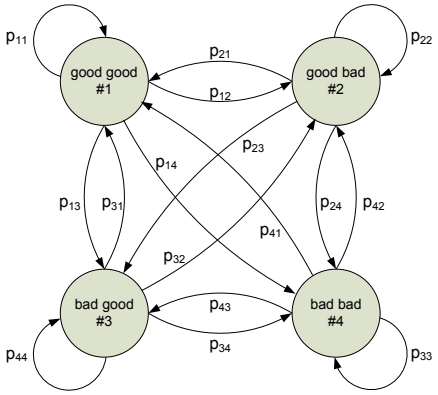

Figure 2.12.: First-order Markov model for two satellites.

2.4.3. Correlation Measurements Combined with Statistical Models

Shortly after the introduction of the correlated Markov model, the straightforward combination of the two-state 'Lutz' model and the correlated Markov model is introduced in 1996 in [BWL96]. It is the generation of two correlated state sequences according to their correlation coefficient, whereas the fading distributions of both satellites depend on their current state, their elevation, and the environment. In [BWL96] this statistical dual-satellite model is used to evaluate the performance of real satellite systems with diversity (Globalstar/LEO and ICO/MEO) for different environments. For this purpose, the correlation coefficients between two satellites were captured from RF measurements with **circular flights** of a plane [JL94]. The correlation coefficients are derived as a function of the azimuth angle separation and the elevation angle separation, as seen in Figure 2.13.

Similar analyses from other authors were carried out in 1998 [MPTE98]. Again, the diversity gain of ICO and Globalstar satellite system was analysed. In this contribution the shadowing statistics as well as correlation coefficients between two satellites are derived from image-based analyses taken by a **fisheye-camera**. It is pointed out that the satellite correlation is significant for azimuth separations below 30°. The results are shadowing probabilities

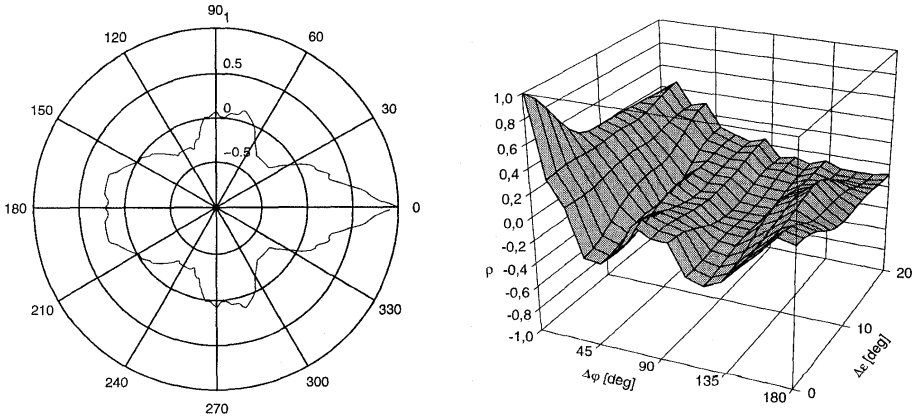

(a) (b)

Figure 2.13.: Correlation coefficients between two satellites in dependency on their azimuth angle separation (left and right) as well as their elevation angle separation (right) in the urban environment. (image source: [JBH96])

in terms of first-order statistics with and without satellite diversity for urban environments in Guildford, Southampton, London (England), Los Angeles (USA). Therefore, the authors merged the two-state 'Lutz' model with the correlated Markov model.

Satellite diversity analyses based on three-state models (LOS/shadowed/blocked) with even more than two satellites are presented in 1997 in Karasawa et al. [KKM97] and Akturan et al. 1997 [AV97]. In the first contribution the satellites are assumed to be uncorrelated. As a result, satellite diversity gains are estimated higher than in reality. In the latter contribution ([AV97]) the correlation is considered by measuring **relevant** joint state probabilities of up to four satellites. These joint probabilities were derived by tracking path angles of multiple satellites within **fish-eye camera images** (cf. Figure 2.14). By using an own model for fade distributions of each satellite, i.e. Rice distribution for clear state, Loo distribution for shadowed and urban blocked state, Rayleigh distribution for non-urban blocked state, the overall fade distribution statistics incorporating satellite diversity with one, two, three, and four satellites are calculated. It should be noted that for such signal availability studies based on first-order statistics it is not relevant which satellite belongs to which state, i.e. the combination 'clear blocked' is the same as 'blocked clear'.

2.4.4. Physical-Statistical Correlation Model

A physical-statistical propagation model for dual-satellite correlation is presented by Tzaras et al. in 1998 [TSE98], which is an extension of a physical-statistical model for single satellite reception in [SE96]. These kind of models are based on computer generated environments, that are constructed by physical parameters such as street widths, distribution of building heights and building widths. By analysing the canonical street canyon geometry, LOS and non-LOS-paths can be determined by placing the satellite at a defined elevation and azimuth angle with respect to the vehicle position. In [TSE98], a simple geometry with constant building heights and street width is assumed, as seen in Figure 2.15. The result is an

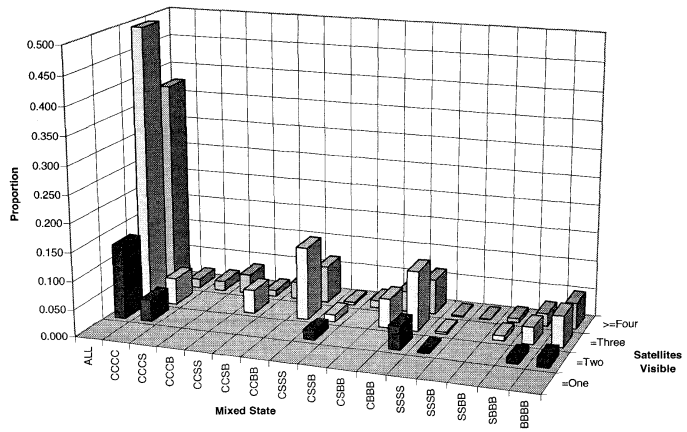

Figure 2.14.: Probabilities of state designations (**C**lear/**S**hadowed/**B**locked) of one, two, three and four satellites derived from fish-eye image analyses in an urban environment (Japan) (image source [AV97]). Correlation effects between the satellites are indirectly considered by analysing these relevant state probabilities. Note that for fade distribution calculations, a complete assignment of satellite to states is not required. Thus, it holds for example CBBB=BBBC.

expression for the correlation coefficient ρ in dependency on $\Delta\theta$ considering two elevation angles (ϕ_1, ϕ_2), the street width w, the building height h_b, receive antenna height h_m, and the distance of the vehicle to the building face d_m. Some exemplary correlation curves are shown in Figure 2.16 according to the implementation in [TSE98].

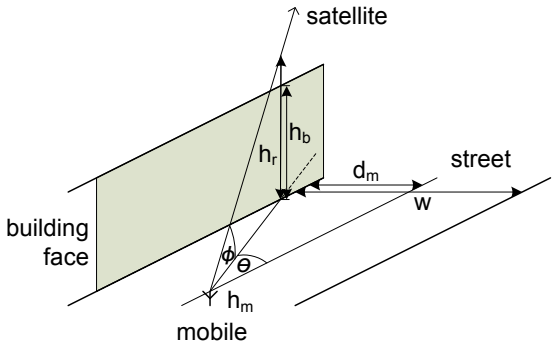

Figure 2.15.: Street geometry for a physical-statistical model. A street canyon with constant building height on both sides is assumed.

A similar model is presented from Vazquez-Castro et al. in 2001 [VCPFISBF01], also based on the street geometry according to Figure 2.15. For analysis, masking angles (MKA) are introduced, which characterise the elevation angles of the top edge of buildings from the terminals point of view. The result is a three-segment model to describe the correlation coefficients in dependency of $\Delta\theta$ within the range $0° \leq \Delta\theta \leq 90°$. Figure 2.16 shows the three-segment model with its four special cases:

- special case 1: both elevation angles are above the MKA for all azimuth angles
- special case 2: only one of the satellites is always above the MKA for all azimuth angles
- special case 3: $\phi_1 = \phi_2$

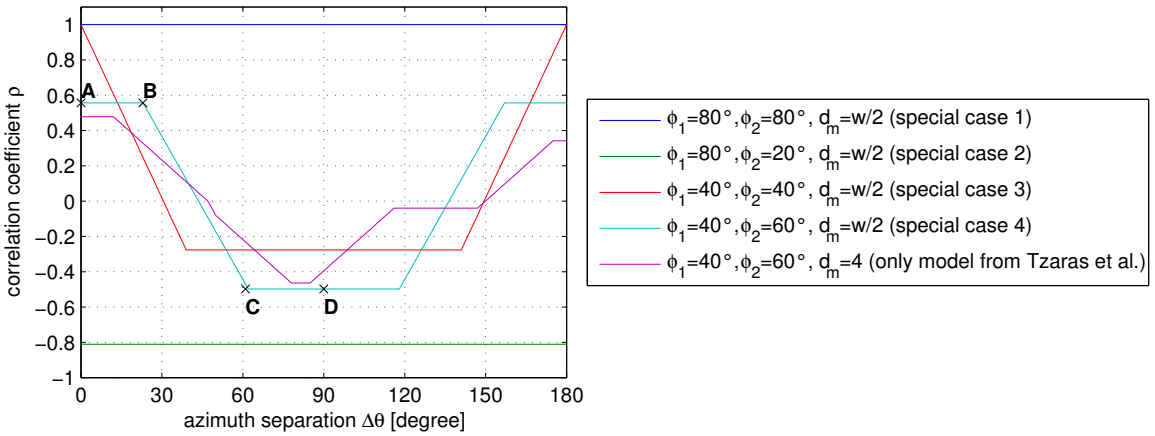

Figure 2.16.: Cross-correlation coefficients ρ in dependency on the azimuth separation $\Delta\theta$ according to a street canyon from Figure 2.15. The parameters are $h_b = 20\,\text{m}, h_m = 2\,\text{m}, w = 14\,\text{m}$. Two physical-statistical models from [TSE98] and [VCPFISBF01] provide equal results in case of $d_m = w/2$. The first model allows additionally the definition of d_m.

- special case 4: $\phi_1 \neq \phi_2$

The three-segment model assumes that the vehicle position is in the middle of the street. Thus, the correlation curves $\rho = f(\Delta\theta)$ are symmetric to 90°. Please note that the three-segment model [VCPFISBF01] and the model from [TSE98] provide equal results for the case $d_m = w/2$. However, the previous model ([TSE98]) allows to define the position of the vehicle on the street (parameter d_m), which is from the authors point of view the more flexible approach.

In 2002, Vazquez-Castro et al. [VCPFS02] extended the physical-statistical correlation model towards 'real' environmental conditions. Therefore, a street canyon is generated with random building heights and building widths on left and right street site following characteristic distributions determined from different cities (London, Guildford, Madrid). Then the street canyon is transformed into skyline masking angles (MKA^s). The result of the MKA^s analysis is a function of the satellite correlation coefficient in dependency of the elevation angles and the azimuth angle separation: $\rho = f(\phi_1, \phi_2, \Delta\theta)$. Multiple correlation coefficient curves for different elevation combinations are further analysed resulting in a mathematical expression for the 'positive correlation coefficient', which corresponds to point **B** from the three-segment model in Figure 2.16. The 'positive correlation coefficient' characterises the mean azimuth separation angle where two satellites become uncorrelated and can be calculated for different cities with parameters given in [VCPFS02]. From the author's point of view, this 'positive correlation coefficient' has an abstract meaning and is itself of limited use for statistical channel modelling. The function $\rho = f(\phi_1, \phi_2, \Delta\theta)$ that was initially derived from MKA^s analysis is of greater importance.

2.4.5. Latest Statistical Approaches on Dual-Satellite Modelling

Milojevic et al. [MHEH09] (2009) presented a novel approach for accurate state duration modelling of a single satellite, namely 'dynamic Markov model' as mentioned in previous

Section 2.3. An extension of this dynamic Markov model for multiple satellites is proposed as well in [MHEH09] by using a multi-state model including all permutations of states from multiple satellites. However, this multi-satellite approach based on the dynamic Markov model is not evaluated by the authors. Nevertheless, in [MHEH09] parameters for a first-order Markov model with two satellites (9 combined states, each with 'LOS/shadowed/blocked') as well as Loo parameters for the individual satellites are presented.

In 2011, Perez-Neira et al. [PNIS+11] presented a dual-satellite model for MIMO applications. For the LMS modelling part, the correlated Markov model by Lutz is combined with the newer 'versatile two-state LMS model' [PFSLCn07][PCPFB+10]. Besides correlated Markov sequences, the authors introduced also fading correlation for lognormal distributed slow variations and fast variations in their calculations for MIMO performance analysis. As the intention of the authors in [PNIS+11] is to compare different MIMO schemes, a detailed validation of these additional fading correlation for a LMS model is not performed.

From the author's point of view, the fading correlation introduced in [PNIS+11] works well for time periods between two state transitions. However, due to a random Loo parameter generation for new states, this fade correlation is expected to be eleminated over longer time periods.

2.5. Open Issues To Be Addressed

Various approaches and contributions are available for LMS channel modelling with multiple satellites. The correlation between two satellite paths is identified thereby as the crucial parameter. As channel models are intended to simulate critical reception cases to optimise fading mitigation, satellite constellations with high correlation of the transmission paths are of closer interest. Therefore, the dependency of the correlation coefficient on the angular separation in azimuth and elevation is described in various ways by empirical formulas, physical-statistical models, and measurements of image- or RF data. However, these correlation coefficients between two satellite signals are mainly considered in terms of only two Markov states: 'good' and 'bad'. As two states are a raw characterisation of the signals dynamic range, correlation of the whole signal is only partly introduced. In this work, the correlation of two satellite signals over the whole dynamic range is therefore analysed and a corresponding implementation for a multi-satellite LMS model is developed (Chapter 4). Furthermore, the required parameters are derived for multiple receive scenarios.

For the study of time diversity techniques (cf. Section 2.2.2) an accurate modelling of the signals temporal composition is crucial. Therefore, advanced concepts for state duration modelling (semi-Markov chains, dynamic Markov chains) are introduced in literature and accepted already for single-satellite LMS modelling. However, existing LMS models for dual-satellite reception rely (only) on the correlated first-order Markov model from Lutz [Lut96], which duration modelling is inaccurate. In this work, new state models for dual-satellite reception are therefore developed incorporating an improved state duration modelling. They are compared with available concepts from literature for a large variability of satellite constellations in Chapter 3.

Besides some suggestions in [Lut96] and [MHEH09] for a model with more than two satellites, a suitable approach for multiple satellites is not available in literature. Hence, state models for more than two satellites are addressed in this thesis in Chapter 3.

3. Statistical Modelling of the LMS Channel, Part I: States

The common statistical approach of generating time series for the LMS propagation channel includes two processes: First, the very slow fading components of the channel due to varying shadowing conditions between the satellite and the receiver are modelled in terms of channel states. In a second process the amplitudes of direct and indirect signal components are generated according to statistical distributions such as Rice, Rayleigh, or lognormal. The corresponding parameters depend on the current state and the receive environment.

In this work, the *versatile two-state model* from Perez-Fontan et al. [PFSLCn07][PCPFB+10] is taken as basis (cf. Section 2.3.5). This model describes two states: a 'good' state (corresponding to line-of-sight/light shadowing), and a 'bad' state (corresponding to heavy shadowing/blockage). Within each state a Loo-distributed fading signal [Loo84] is assumed, which parameters are randomly generated after each state transition. The versatile two-state model allows a realistic modelling of fading over the full dynamic range of the received signal.

This chapter focuses on state sequence modelling for single-, dual-, and multi-satellite systems (Sections 3.1, 3.2, 3.5) assuming the 'good' state and 'bad' state for each satellite. For this purpose, different state modelling methods are compared with measurement data in terms of the state probability, state duration probability, and correlation coefficient between multiple satellites. Moreover the practicability of various state generation methods in terms of generating comprehensive parameter sets, e.g. for different environments and elevation angles, is assessed (Section 3.4). Parts of this chapter are published in [AIH+], [AIHE12] and [AHH+12].

3.1. Channel State Modelling for Single-Satellite Systems

Three types of state modelling approaches to describe the LMS channel are found in the literature:

- First-order Markov model [PFVCC+01]
- Semi-Markov model [BT02]
- Dynamic Markov model [MHEH09]

In the following the main characteristics of these models are described for single-satellite case by focusing on two states. An elaboration of these models for N states including additional mathematical expressions for an analytical evaluation is found in Appendix B.1. A performance comparison between the state models is found in Section 3.3.

3.1.1. First-Order Markov Model

A Markov model is a special random process for generating discrete samples corresponding to channel states s of a predefined sample length. For a first-order Markov model, each state depends only on the previous state. The conditional probabilities of state s_{n+1} given the state s_n are described by state transition probabilities p_{ij} (cf. Figure 3.1). Therefore, the only parameter of the Markov chain is the state transition probability matrix (STPM) $\mathbf{P}_{\text{trans}} \in \mathbb{R}_{0+}^{N\times N}$ with N being the number of states.

$$\mathbf{P}_{\text{trans}} = \begin{bmatrix} p_{11} & \cdots & p_{1N} \\ \vdots & \ddots & \vdots \\ p_{N1} & \cdots & p_{NN} \end{bmatrix} \tag{3.1}$$

The main characteristic of a first-order Markov chain is, that it enables an exact modelling of the state probability and the average state duration. It holds

$$\mathbf{p} \cdot [\mathbf{P}_{\text{trans}} - \mathbf{I}] = \mathbf{0} \tag{3.2}$$

with $\mathbf{p}$ is the row vector of the equilibrium state probabilities, the identity matrix $\mathbf{I}$, and the zero vector $\mathbf{0}$.

The average state duration of state i is calculated as

$$\bar{D}_i = \frac{1}{1-p_{ii}} \cdot \frac{1}{\Delta d}\,, \tag{3.3}$$

where p_{ii} is the state transition probability between two equal states, and Δd denotes the sampling distance (frame length).

The probability that the Markov chain stays in state i for q consecutive samples is given by

$$P_i(D = q\Delta d) = p_{ii}^{q-1} \cdot (1-p_{ii}), \quad n \in \mathbb{N}\,. \tag{3.4}$$

In this thesis the function $P(D)$ will be further denoted as state duration probability density function (SDPDF). The SDPDF of the first-order Markov chain follows an exponential distribution. The first-order Markov model is used in early LMS models [PFVCC+01][LCD+91].

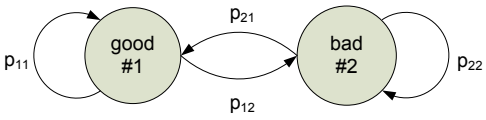

Figure 3.1.: First-order Markov model with two states for single-satellite reception.

3.1.2. Semi-Markov Model

Results in [MHEH09] [BT02] have shown that an exponential SDPDF is not an accurate approximation for the LMS channel. To improve the state duration modelling, semi-Markov chains were proposed in [BT02]. In contrast to the first-order Markov model, the state

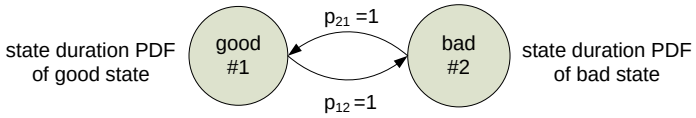

Figure 3.2.: Semi-Markov model for single-satellite reception.

transitions do not occur at concrete time intervals. In fact, the time interval of the model staying in state i depends directly on its SDPDF, as indicated in Figure 3.2.

The semi-Markov model allows some options to describe the SDPDF of each state (cf. Figure 3.3):

- *no fit*: The measured state duration statistic is used without any approximation for re-modelling, i.e. the state duration is a random realisation of the measured SDPDF.

$$P(D) = P(D_{\text{measured}}) \tag{3.5}$$

- *lognormal fit*: The measured SDPDF is approximated with a lognormal distribution, as proposed in [BT02] and [PCPFB+10] individually for the single-satellite states 'good' and 'bad'. The lognormal PDF describing the state duration probability $P(D)$ can be written

$$P(D) = \frac{K}{D\sigma_{\text{Dur}}\sqrt{2\pi}} \exp\left[-\frac{(20\log(D) - \mu_{\text{Dur}})^2}{2\sigma_{\text{Dur}}^2}\right], \tag{3.6}$$

  where σ_{Dur} is the standard deviation of $20\log(D)$ and μ_{Dur} is the mean value of $20\log(D)$ and $K = 20\log\mathrm{e} \approx 8.686$. [1] Only two parameters per state are required to describe the SDPDF. The mean state duration $\bar{D}$ can be calculated with

$$\bar{D} = \exp\left[\frac{\mu_{\text{Dur}}}{K} + 0.5\left(\frac{\sigma_{\text{Dur}}}{K}\right)^2\right]. \tag{3.7}$$

- *piecewise exponential fit*: In [MHEH09] a piecewise exponential curve fit of the SDPDF with four segments is proposed:

$$P(D) = \begin{cases} a_1\,\mathrm{e}^{-b_1 D}, & D_0 \le D \le D_1 \\ a_2\,\mathrm{e}^{-b_2 D}, & D_1 \le D \le D_2 \\ a_3\,\mathrm{e}^{-b_3 D}, & D_2 \le D \le D_3 \\ a_4\,\mathrm{e}^{-b_4 D}, & D_3 \le D \le D_4 \end{cases} \tag{3.8}$$

  Clearly, this requires more parameters than the lognormal curve fit (e.g. 12 parameters for four segments), but it provides a more flexible description of the state duration statistic.

From the SDPDFs, the mean duration of state i can be generally calculated with

$$\bar{D}_i = \int_0^\infty D \cdot P_i(D)\mathrm{d}D\,. \tag{3.9}$$

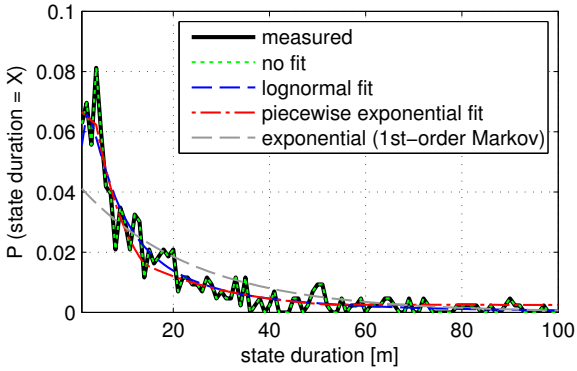

Figure 3.3.: Curve-fits of the state duration PDF for semi-Markov models. For comparison, the exponential SDPDF resulting from a first-order Markov model is shown.

As with the Markov models, the state transitions are described with the state transition probability p_{ij}, but with $i \neq j$. Thus, in any case the diagonal elements (p_{ii}) of the semi-Markov STPM are zero.

$$\mathbf{P}_{\text{trans}}^{semiM} = \begin{bmatrix} 0 & p_{12} & \dots & p_{1N} \\ p_{21} & 0 & \dots & p_{2N} \\ \vdots & & \ddots & \vdots \\ p_{N1} & \dots & & 0 \end{bmatrix} \tag{3.10}$$

In case of a single-satellite model of only two states, the state transition probability is $p_{ij} = 1$ (cf. Figure 3.2). In case the semi-Markov model has more than two states, the state transition probabilities have to be determined from the referenced or measured state sequence, which are independent from the SDPDF approximation.

It is also possible to determine the semi-Markov STPM from the first-order Markov STPM. Assuming p_{ij}^S with $(i \neq j)$ are the transition probabilities of a semi-Markov model and p_{ij}^M are the transition probabilities of a first-order Markov model, it holds

$$p_{ij}^S = \frac{p_{ij}^M}{1 - p_{ii}^M}, \qquad i \neq j\,. \tag{3.11}$$

On SDPDF approximation for semi-Markov chains: An approximation of the state duration PDF possibly changes the mean state duration $\bar{D}$ and consequently the equilibrium probability P of the states. To enable an exact description of $\bar{D}$ and P in accordance to the measurements, a correction of the curve-fit can be implemented. In case of a lognormal fit the parameter μ_{Dur} has to be modified according to

$$\mu_{\text{Dur, corrected}} = K \ln \bar{D}_{\text{measured}} - \frac{1}{2K}\sigma_{\text{Dur}}^2 \tag{3.12}$$

with $K = 20 \log \mathrm{e}$. To best knowledge of the author, this correction is firstly considered in the context of this work and is presented in [AIHE12].

[1] The notation of the lognormal PDF with parameters in dB is used for the LMS model in [PCPFB+10] which is taken as basis in this work.

3.1.3. Dynamic Markov Model

A further method to improve the state duration modelling are dynamic Markov chains introduced in [MHEH09]. For dynamic Markov chains the state transition probability depends on the current state duration q (cf. Figure 3.4)

$$p_{ij} = f(q)\,. \tag{3.13}$$

For this purpose, the two-dimensional STPM is extended to a three-dimensional state transition probability tensor (STPT) $\mathcal{P}_{\text{trans}} \in \mathbb{R}_{0+}^{N\times N\times q_{\max}}$, where $q_{\max}$ corresponds to the maximum state length obtained from the measurements with $D_{\max} = q_{\max}\Delta d$.

$$\mathcal{P}_{\text{trans}} = \begin{bmatrix} p_{11}(q) & \dots & p_{1N}(q) \\ \vdots & \ddots & \vdots \\ p_{N1}(q) & \dots & p_{NN}(q) \end{bmatrix} \qquad q \in \{1, 2, ..., q_{\max}\} \tag{3.14}$$

Using the dynamic Markov model, the probability that the state duration is equal to D is

$$P_i(D = q\Delta d) = (1 - p_{ii}(q\Delta d)) \cdot \prod_{r=1}^{q-1} p_{ii}(r\Delta d), \quad q \in \mathbb{N} \tag{3.15}$$

and the state duration CDF is given by

$$P_i(D \leq q\Delta d) = 1 - \prod_{r=1}^{q-1} p_{ii}(r\Delta d), \quad q \in \mathbb{N}\,. \tag{3.16}$$

If the values for the STPT are directly derived from the measured state sequence (assuming a sampling distance of, e.g. $\Delta d = 1\,\text{m}$), the dynamic Markov model enables an exact reproduction of the state probabilities and also an exact re-modelling of the measured SDPDF. As a disadvantage, a large number of parameters are required to describe the STPT.

In [MHEH09] some model approximations are proposed to reduce the number of required parameters of the STPT:

- partial dynamic Markov model: From Equation (3.15) it is derived that an exact state duration modelling requires only a subset of the STPT. Only the transition coefficients $p_{ii}(q)$ need to be described as a function of the current state duration. For a two-state model the remaining values $p_{ij}(q)$ with $i \neq j$ can be re-calculated easily with $p_{ij}(q) + p_{ii}(q) = 1$. For a multi-state model it is proposed to change the transition probabilities $p_{ij}(q)$ $(i \neq j)$ together with the coefficients $p_{ii}(q)$ by keeping the respective relative ratios S between them constant [MHEH09]. The relative ratios S are derived from $p_{ij}(\Delta d)$, which are the elements of a first-order Markov chain. The relative ratios as described in [MHEH09] are valid only for a model with three states. Thats why a new definition is introduced in this work: The coefficients S_{ij} $(i \neq j)$ are determined from the transition probabilities of a first-order Markov model p_{ij} with $S_{ij} = p_{ij}(1 - p_{ii})^{-1}$ and are therefore equal to the state transition probabilities of a semi-Markov model.

For re-simulation, the calculation of the elements $p_{ij}(q)$ of the STPT is done with

$$p_{ij}(q) = (1 - p_{ii}(q)) \cdot S_{ij} \,. \tag{3.17}$$

The parameters of the partial dynamic Markov model are the diagonal elements of the STPT ($p_{ii}(q)$) and $N(N-1)$ coefficients S_{ij} (with N is the number of states).

- approximated partial dynamic Markov model: For a further reduction of the model parameters, the function $p_{ii}(q)$ can be approximated by a curve fit. In [MHEH09] a piecewise linear approximation of $p_{ii}(q)$ with 7 intervals is proposed. Therefore $p_{ii}(q)$ is estimated at 8 predefined values of q. Taking this assumption, a two-state model would require $8 \cdot 2$ parameters for state sequence generation. A multi-state model would need $8 \cdot N$ parameters to describe the functions $p_{ii}(q)$ (with N is the number of states) and further $N(N-1)$ parameters to describe the coefficients S_{ij}.

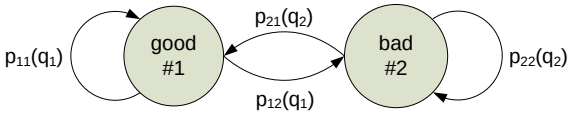

Figure 3.4.: Dynamic Markov model for single-satellite reception.

3.1.4. Relation Between Dynamic Markov Model and Semi-Markov Model

The partial dynamic Markov model provides equal modelling results to the semi-Markov model without SDPDF approximation (*no fit*), which is demonstrated later in Section 3.3. It is indicated since the parameters of the partial dynamic Markov model can be completely estimated from the semi-Markov model parameters and vice versa: According to Equation (3.15) the transition probabilities $p_{ii}(q)$ of $\mathcal{P}_{\text{trans}}$ describe the SDPDF, which is also parameter of the semi-Markov model. The other elements $p_{ij}(q)$ of $\mathcal{P}_{\text{trans}}$ of the partial dynamic Markov model are calculated from the coefficients S_{ij}, that equals the state transition probabilities p_{ij} with $i \neq j$ of the semi-Markov model. The similarity of the algorithms is also confirmed in the modelling process: After the simulation of a state i with duration $D = q\Delta d$, which probability is determined by the SDPDF $P_i(D)$ or by the tensor element $p_{ii}(q)$, the transition probabilities of the semi-Markov model are considered to find the next state j with $(i \neq j)$.

To realise an 'approximated partial dynamic Markov model', Milojevic et al. [MHEH09] proposed a curve-fit of the function $p_{ii}(q)$. By using Equation (3.15), the elements $p_{ii}(q)$ can also be derived from an approximated SDPDF of state i (with lognormal fit or piecewise exponential fit)

It is concluded that parameters of partial dynamic Markov models can be completely estimated from semi-Markov model parameters and vice versa. The selection of a *partial dynamic Markov model* or a *semi-Markov model* for simulation is left to the operator. The 'full' dynamic Markov model, however, provides some additional information if the number of states is greater than two.

3.1.5. Higher Order Markov Model

In the context of the development of the dynamic Markov model, Milojevic et al. verified in [MHEH09] also Markov models of higher order to accurately describe state duration distributions. It was found to be not feasible for LMS modelling. For the sake of completeness, however, it is described here as well.

A Markov model of higher order $N > 1$ works similarly to the first-order Markov model (order $N = 1$): In a Markov model of order $N = 2$, each state s_n depends on the previous state s_{n-1} as well as on its predecessor s_{n-2}. In case of a Markov model of order $N = k$, the state s_n depends on k previous states. Thus, the number of transition coefficients within the STPM for an N-th order Markov model would be M^{N+1}, where M is the number of states. It is seen that the number of parameters grows exponentially with the order N.

In Section 3.1.1 it is stated that a first-order Markov model is able to correctly re-simulate the state transition probability vector and the mean state durations. A Markov model of order N additionally describe accurately the SDPDFs for each state up to a duration of $N-1$ samples. For an exact representation of a SDPDF the order $N = q_{\max}$ should be used, where $q_{\max}$ denotes the maximum state duration in samples. Assuming a sampling length of $\Delta d = 1\,\mathrm{m}$ and a state duration of, e.g. $300\,\mathrm{m}$ (which is obtained for the 'bad'-state in a rural environment in Section 3.3), 2^{301} coefficients are required to accurately re-simulate the SDPDF with the corresponding Markov model. Due to the related computational complexity, a Markov model with such a high number of required parameters is not a feasible solution for LMS state modelling.

3.2. Channel State Modelling for Dual-Satellite Systems

In this section different state modelling concepts are presented focusing on two satellites. Just as for single-satellite case, the dual-satellite models can be assigned to first-order Markov, semi-Markov, or dynamic Markov chains. In addition to state probabilities and state duration statistics, the correlation coefficient between two satellites is the crucial parameter. Besides dual-satellite modelling concepts that are known from literature, new approaches are introduced that are developed in the context of this work.

This section aims to describe different dual-satellite state models and their required parameters. A performance comparison including all models, extensions and subversions from this section is subject of next Section 3.3.

3.2.1. Straightforward Method: Extension to a Multi-State Model

The first-order Markov model, the semi-Markov model, and the dynamic Markov model can be easily extended for dual-satellite modelling. This is by substituting the states 'good' and 'bad' from single-satellite reception by joint states 'good good', 'good bad', 'bad good', and 'bad bad', which result from the combination of the states from two single satellites. Therefore, Figure 3.5 exemplarily shows a semi-Markov model for two satellites. Parameters are a 4×4 semi-Markov STPM and four separate state duration statistics, that have to be

derived from a joint state sequence. Analogously, a dual-satellite first-order Markov model requires a 4×4 STPM. For the dynamic Markov model a $4 \times 4 \times q_{\max}$ STPT is required for the state series simulation. Once the joint state sequence of four states is generated, it can be decomposed to extract two separate single-satellite state sequences.

An obvious problem with this straightforward approach is the exponential growth of the number of parameters with the number of satellites. A multi-satellite model has N^k combined states with N being the number of states per satellite and k being the number of satellites.

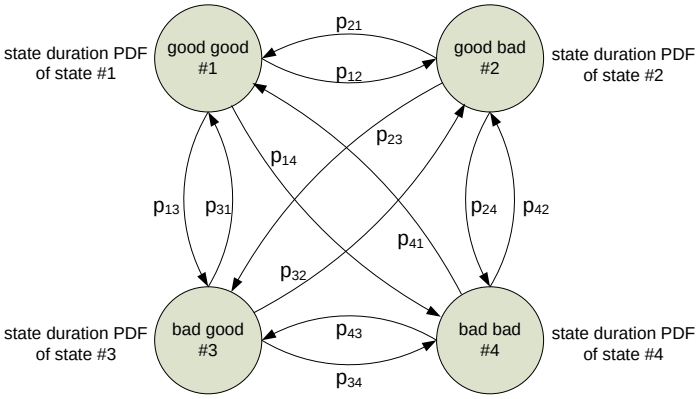

Figure 3.5.: Semi-Markov model for two satellites.

Approximation of joint state duration statistics for semi-Markov chains

The lognormal distribution is accepted for single-satellite state duration modelling in the literature [BT02] [PCPFB+10]. Taking this assumption, the following two examples show expected shapes for a joint SDPDF. In both examples, state series of the single satellites where simulated with a simulation length sufficiently to gain a static SDPDF for the single and joint states.

Example 1: Two satellites are modelled independently. Figure 3.6 (left) shows a lognormal distribution of the 'bad' state from satellite 1 and satellite 2 and the resulting distribution of the combined state 'bad bad'.

Example 2: Assuming two satellites having the same elevation and a marginal azimuth separation. The state sequence from satellite 2 is assumed to be equal to the state sequence from satellite 1, but with a delay of 5 metres. As a result, the joint state duration distribution for 'good bad' or 'bad good' is limited to the range of [0 m; 5 m] and has a peak at 5 metres, as seen in Figure 3.6 (right).

Both examples show that a curve-fit for a joint SDPDF requires some degree of flexibility. A good fit would be a piecewise approximation. Nevertheless, when analysing real measurement data it is obtained that already a (simple) lognormal fit provides a good approximation of state durations (cf. Sections 3.3 and 3.4.2).

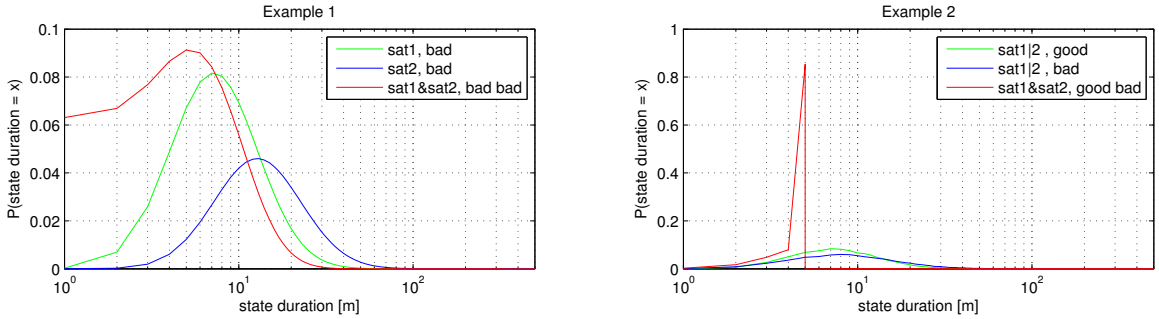

Figure 3.6.: Two examples for the expected distribution of the joint states with the assumption, that single satellite states are lognormal distributed.

3.2.2. Lutz Approach

In [Lut96] an effective method is introduced to calculate a joint STPM for a first-order Markov model with two correlated state sequences. Based on the STPMs of two satellites (each with 2×2 elements) and only one correlation coefficient, a joint STPM (4×4 elements) is calculated without influencing the transition probabilities of the individual satellites. The high flexibility of this algorithm becomes clear, since it requires only single-satellite parameter sets (in form of 2×2 STPMs), that are easy to derive from measurements and are already available in literature for different elevation angles and a number of environments. Databases for correlation coefficients are available as well for different environments, elevation angles, and angular separations of the azimuth and elevation angle [REE92]. In contrast to this Lutz model, the above mentioned 'straightforward methods' (cf. Section 3.2.1) need complete datasets for any combination of elevation angles, azimuth angle separations and environments to achieve the same variability. The Lutz model accurately re-simulates the state probabilities and mean state durations of each single satellite, as well as the probabilities of the combined states. A limitation is that there is no flexibility in describing the state duration distribution. Furthermore, a Lutz approach for more than two satellites and with more than two states per satellite is not available yet. The calculation procedure is given in detail in Appendix B.2.2.

In the context of this work two extensions of the Lutz approach are developed:

1. A modification of the Lutz approach providing correctly the average value of the joint durations.
2. A combination of the Lutz approach (first-order Markov) with a semi-Markov model.

Both approaches are described in the next two subsections 3.2.3 and 3.2.4.

3.2.3. Modification of Lutz Approach for Correct Mean Joint Durations

The Lutz approach as described in [Lut96] provides correct state probabilities of the single satellites of combined states as well as correct mean state durations of both satellites. However, with the only information 'correlation coefficient' the Lutz approach can not correctly predict the mean durations of joint states.

With a modification of the Lutz approach, additional information for joint state durations can be included. The procedure starts with the basic expression of the Lutz approach. It is the addition of a correlation matrix to a joint STPM of two uncorrelated channels:

$$\mathbf{P}_{\text{trans}}^{joint} = \mathbf{P}_{\text{trans}}^{joint,uncorrelated} + \begin{bmatrix} x & -x & -x & x \\ y & -y & -y & y \\ v & -v & -v & v \\ w & -w & -w & w \end{bmatrix} \tag{3.18}$$

The calculation of $\mathbf{P}_{\text{trans}}^{joint,uncorrelated}$ is given in Equation (B.29) in Appendix B.2.2.

According to Equation (3.3), the mean durations of the joint states depend on the diagonal elements of $\mathbf{P}_{\text{trans}}^{joint}$. Thus, taking the mean joint durations $\bar{D}_i$ ($i \in \{1,2,3,4\}$, denoting 'good good', 'good bad', 'bad good', 'bad bad') as parameter, the elements of the correlation matrix from Equation (3.18) would be:

$$\begin{array}{rcl} x_D &=& (1-1/\bar{D}_1) - p'_{11} \\ y_D &=& (-1+1/\bar{D}_2) + p'_{22} \\ v_D &=& (-1+1/\bar{D}_3) + p'_{33} \\ w_D &=& (1-1/\bar{D}_4) - p'_{44} \end{array} \tag{3.19}$$

where p'_{ij} ($i,j \in \{1,2,3,4\}$) are the joint state transitions of $\mathbf{P}_{\text{trans}}^{joint,uncorrelated}$.

If all values x, y, v, w are calculated according to the previous terms, i.e. $x = x_D$, $y = y_D$, $v = v_D$, $w = w_D$, then a certain correlation coefficient could not be provided with $\mathbf{P}_{\text{trans}}^{joint}$.

To consider a certain correlation coefficient in the correlation matrix, the following expression (derived from Equation (3.2)) must be solved

$$P_4 = P_1(p'_{14} + x) + P_2(p'_{24} + y) + P_3(p'_{34} + v) + P_4(p'_{44} + w) \tag{3.20}$$

where P_i ($i, \in \{1,2,3,4\}$) are the joint state probabilities of the correlated channel. They are to calculate with Equation (B.26) from Appendix B. Knowing P_1, P_2, P_3, and P_4, Equation (3.20) has four variables x, y, v, w.

case 1: considering three joint durations $x = x_D$, $y = y_D$, and $w = w_D$
In 'best' case, the Lutz approach can be modified such that the correlation coefficient and three of four mean durations are correctly provided. Assuming $x = x_D$, $y = y_D$, and $w = w_D$, we got from Equation (3.20):

$$v = -\{P_1(p'_{14} + x_D) + P_2(p'_{24} + y_D) + P_3 p'_{34} + P_4(p'_{44} + w_D - 1)\}/P_3 \tag{3.21}$$

Knowing v, it may happen that the resulting elements of $\mathbf{P}_{\text{trans}}^{joint}$ (cf. Equation (3.19)) are negative and this modification is not possible. As there are some restrictions for x, y, v, w for non-negative elements of $\mathbf{P}_{\text{trans}}^{joint}$ (cf. Appendix B.2.2, Equation (B.31)), we propose to focus only the states with high priority, 'bad bad' and 'good good', which is described in *case 2*.

case 2: considering two joint durations $x = x_D$, and $w = w_D$
With $w = w_D$ (related to 'bad bad') and $x = x_D$ (related to 'good good') Equation (3.20) can be written:

$$\begin{array}{rcll} v &=& Ay + B & \text{, with} \\ A &=& -P_2/P_3 & \\ B &=& -\{P_1(p'_{14} + x_D) + P_2 p'_{24} + P_3 p'_{34} + P_4(p'_{44} + w_D - 1)\}/P_3 & \end{array} \tag{3.22}$$

A solution by considering the restrictions $y_{\min} \leq y \leq y_{\max}$ and $v_{\min} \leq v \leq v_{\max}$ is to calculate the intersection point between the straight line from Equation (3.22) and a straight line s going through points $(y_{\min}, v_{\min})^T$ and $(y_{\max}, v_{\max})^T$ as drafted in Figure 3.7.

The straight line s is given by:

$$s : v = \left(\frac{v_{\max} - v_{\min}}{y_{\max} - y_{\min}}\right) y + \left(\frac{v_{\min} y_{\max} - v_{\max} y_{\min}}{y_{\max} - y_{\min}}\right) \tag{3.23}$$

For the intersection point P_I results

$$\begin{pmatrix} y \\ v \end{pmatrix} = \begin{pmatrix} \frac{v_{\min} y_{\max} - v_{\max} y_{\min} - B(y_{\max} - y_{\min})}{v_{\min} - v_{\max} + A(y_{\max} - y_{\min})} \\ \frac{A(v_{\min} y_{\max} - v_{\max} y_{\min}) + B(v_{\min} - v_{\max})}{v_{\min} - v_{\max} + A(y_{\max} - y_{\min})} \end{pmatrix} \tag{3.24}$$

where A and B are given in Equation (3.22). If the calculated values v and y are outside of their limits (e.g. if $y_{\min} \leq y \leq y_{\max}$ is false), then a realisation of *case 2* with $x = x_D$ and $w = w_D$ is not possible.

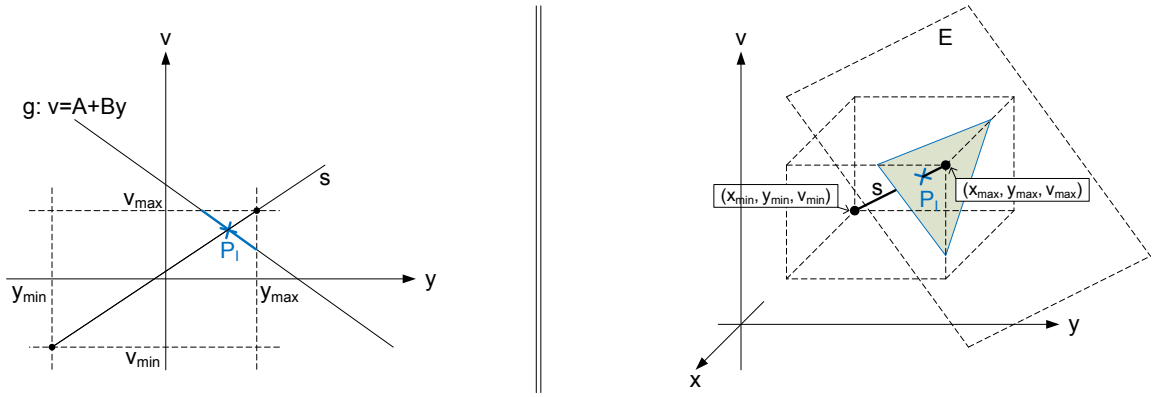

Figure 3.7.: Left: Sketch for modified Lutz approach, case 2. The marked section on straight line g are valid parameters of v and y to calculate the Lutz matrix with non-negative elements. A recommended solution is the intersection point P_I between g and s. If P_I is outside of the parameter range, then *case 2* is not viable. Right: Sketch for modified Lutz approach, case 3. Possible solutions for x, v, and y are found within the marked intersecting plane. A recommended solution is the intersection point P_I of plane E and line s.

case 3: considering one joint duration $w = w_D$

If *case 2* fails, the modification of 'bad bad' only is of interest. Assuming $w = w_D$, Equation (3.20) is:

$$\begin{aligned} K &= P_1 x + P_2 y + P_3 v \quad \text{, with} \\ K &= -\{P_1 p'_{14} + P_2 p'_{24} + P_3 p'_{34} + P_4 (p'_{44} + w_D - 1)\} \end{aligned} \tag{3.25}$$

With variables x, y, and w, Equation (3.25) represents a plane E in a three-dimensional coordinate system (Figure 3.7). Analogously to *case 2*, to find a solution for $x_{\min} \leq x \leq x_{\max}$, $y_{\min} \leq y \leq y_{\max}$, and $v_{\min} \leq v \leq v_{\max}$, it is appropriate to calculate the intersection point of that plane with a straight line s going through points $(x_{\min}, y_{\min}, v_{\min})^T$ and $(x_{\max}, y_{\max}, v_{\max})^T$:

$$s: \begin{pmatrix} x \\ y \\ v \end{pmatrix} = \begin{pmatrix} x_{\min} \\ y_{\min} \\ v_{\min} \end{pmatrix} + t \cdot \begin{pmatrix} x_{\max} - x_{\min} \\ y_{\max} - y_{\min} \\ v_{\max} - v_{\min} \end{pmatrix} \tag{3.26}$$

The intersection of E and s is found at

$$t = \frac{K - P_1 x_{\min} - P_2 y_{\min} - P_3 v_{\min}}{P_1(x_{\max} - x_{\min}) + P_2(y_{\max} - y_{\min}) + P_3(v_{\max} - v_{\min})} \tag{3.27}$$

3.2.4. Lutz Approach Combined With a Semi-Markov Model

Knowing that the Lutz approach can be modified such, that the mean value of a joint state duration can be correctly described, then it could be possible to include complete joint SDPDFs as a parameter in the model.

It is mentioned that the Lutz approach is based on a first-order Markov model, which has limitations in modelling of state duration distributions. Semi-Markov models are on the contrary efficient for correct state duration modelling. However, the parametrisation of a semi-Markov model for two satellites is quite challenging. Problems occur especially when different satellite constellations are compared, e.g. for the evaluation of the diversity gain in dependency on the azimuth angle separation (cf. Section 3.4.2).

A solution would be the combination of a semi-Markov model with the Lutz approach. The approach is as follows:

1. First of all, the joint STPM from the Lutz approach $\mathbf{P}_{\text{trans}}^{Lutz}$ considering the single satellite parameters and the correlation coefficient (cf. Appendix B.2.2) has to be calculated. $\mathbf{P}_{\text{trans}}^{Lutz}$ describes correctly the state probabilities of single and combined satellites, the mean durations of single satellites and, by using the modified Lutz version, the mean durations of 'bad bad' and 'good good'.

2. Further on, the SDPDFs of the combined states are derived from measurement data and are approximated with, e.g. a lognormal fit.

3. It should be noted that the mean state duration after SDPDF curve-fitting doesn't match the mean state duration given by $\mathbf{P}_{\text{trans}}^{Lutz}$. The solution is to modify the SDPDF curve-fits such, that their mean durations equal the mean durations according to $\mathbf{P}_{\text{trans}}^{Lutz}$. A modification of the lognormal fit is given in Equation (3.12).
   For the special case that the Lutz approach is prepared for correct mean duration modelling of 'bad bad' and 'good good' as shown in previous section, there is no need to additionally modify the corresponding SDPDFs. Thus, also SDPFDs of 'bad bad' and 'good good' without approximation can be used. Only the mixed states 'good bad' and 'bad good' need to be adapted.

4. Finally, the diagonal elements of $\mathbf{P}_{\text{trans}}^{Lutz}$ are set to zero and the STPM is normalised thereafter. The results are the semi-Markov transitions $\mathbf{P}_{\text{trans}}^{semiM}$.

The simulation is done by a semi-Markov model using the modified joint SDPDFs and $\mathbf{P}_{\text{trans}}^{semiM}$.

3.2.5. Master-Slave Concept

Various state models for a single satellite are found in literature which model parameters are consolidated for a number of receive situations. The Master-Slave concept (first proposed in [EHH08]) follows the idea, that a multi-satellite model is realised by extending these consolidated single-satellite models. Thus, the master sequence and its channel characteristics are not influenced, when an additional slave satellite is modelled. In contrast, the 'traditional' concepts (straightforward approach, Lutz approach) simulate multiple sequences jointly.

The challenge within Master-Slave is the generation of a slave state sequence by providing certain characteristics of the combined system, such as the correlation coefficient between the satellites. For this purpose, the conditional state transition probabilities of the slave in dependency on the master behaviour, e.g, the current state or state transition, have to be analysed. Various realisations of Master-Slave are possible. Thus, the term 'Master-Slave' describes a concept – not a concrete implementation.

In the context of this work the first Master-Slave realisations for LMS modelling are developed and evaluated. In the following, two Master-Slave realisations are described, namely the *Conditional Assembling Method* (Section 3.2.6) and *Adaptive Slave Transition Matrix based on Master State Transitions* (Section 3.2.7). The former method is also described and evaluated in [AIHE12].

Master-Slave has some advantages for multi-satellite modelling, i.e. with more than two satellites. An elaboration on this topic is subject of Section 3.5.

3.2.6. Master-Slave with Conditional Assembling Method

One possible realisation of Master-Slave we define as **Conditional Assembling Method** (cf. Figure 3.8). For parametrisation, the principle of the Conditional Assembling Method is first to concatenate all parts of the slave state sequence for which the master is in 'good' state. Afterwards, this state sequence is parametrised following an arbitrary Markov model (e.g. first-order Markov, semi-Markov). The same procedure is followed for the slave state sequence in case the master is in 'bad' state.

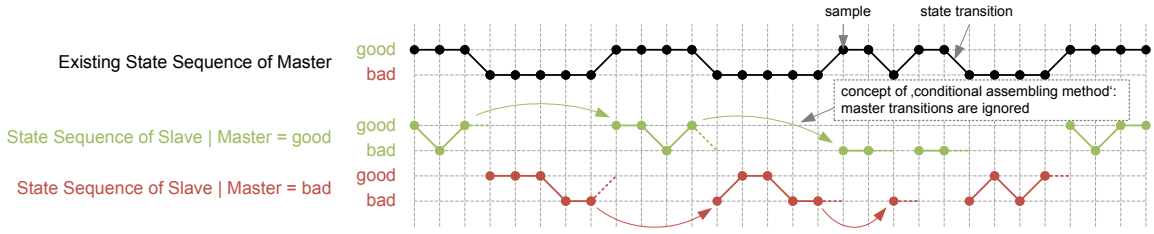

Figure 3.8.: Realisation of Master-Slave with the **Conditional Assembling Method**: Given a master sequence, two independent conditional slave sequences are generated for the cases 'master is good' and 'master is bad'. Different state models (1st-order Markov, semi-Markov, etc.) can be chosen individually therefore. Finally, the slave sequence is composed by piecewise assembling the two conditional sequences according to the master sequence. In this way the correlation coefficient between master and slave, the individual state probabilities, and the combined state probabilities can be accurately described.

The simulation is done in reverse order: First, the master state sequence is modelled. Second, two conditional slave state sequences with respect to the master state are generated independently (i.e. the conditional slave sequence for master is 'good', and the conditional slave sequence for master is 'bad'). For master and conditional slave states an arbitrary Markov model can be used. The final state sequence of the slave is composed of parts from both conditional sequences according to the current master state.

The Conditional Assembling Method provides

- accurate modelling of state probabilities of the master and of the slave, and
- accurate modelling of joint state probabilities and consequently the correlation coefficient between the satellites.

Both results are under the condition that the chosen Markov model accurately describes the state probabilities of the master as well as the conditional state probabilities of the slave in case of a constant master state.

Furthermore, the state durations of the master sequence can be modelled with high accuracy (by, e.g. taking a complex model such as dynamic Markov). However, the Conditional Assembling Method has some limitations in state duration modelling of the combined states ('good good', 'good bad' etc.) and of the slave states. This will be further investigated in Section 3.3.

3.2.7. Master-Slave with Adaptive Slave Transition Matrix based on Master Transitions

Master-Slave implementations can be generally described by means of an adaptive state transition probability matrix of the slave (further denoted as *adaptive slave transition matrix – ASTM*) with respect to a certain master characteristic. Different variants are possible where the slave is modelled as a Markov chain and its state transition probabilities are a function of, e.g. the master state, the master state transition, or the current state length of the master.

The previously described Conditional Assembling Method could be understood as a realisation of an ASTM being a function of the master state s_M:

$$\mathbf{P}_{\text{trans}}^{Slave} = f(s_M) \tag{3.28}$$

As the state sequence generation for the slave is interrupted in case of a master transition, the Conditional Assembling Method offers no control on the state lengths of the slave as well as on the state lengths of the joint states.

To improve the state duration description, an ASTM which is a function of the master state transitions is addressed in this section:

$$\mathbf{P}_{\text{trans}}^{Slave} = f(p_{ij}^{Master}), \qquad i,j \in \{\text{g},\text{b}\} \tag{3.29}$$

For further use this concept is referred to as **adaptive slave transition matrix based on master transitions** (ASTM-MT).

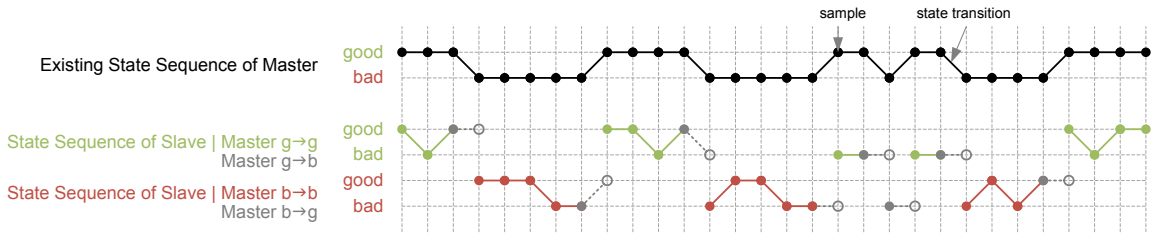

Figure 3.9.: Master-Slave approach with **adaptive slave transition matrix based on master transitions** (ASTM-MT). The state transitions of the slave depend on the current state transition of the master $\mathbf{P}_{\text{trans}}^{Slave} = f(p_{ij}^{Master})$.

Figure 3.9 shows a sample-by-sample simulation of an ASTM-MT. Depending on the current master state transition, a corresponding slave STPM is selected to find the next slave state. Assuming 'good' and 'bad' states, four STPMs of the slave with each four transitions are required (=16 parameters).

Special attention has to be paid on the parametrisation for Master-Slave approaches. While for traditional discrete state models (first-order Markov, dynamic Markov) a sample-by-sample parametrisation by counting and normalising of state transitions is possible, it fails for Master-Slave concepts. In fact, to introduce model characteristics such as state probabilities or mean state durations, the Master-Slave parameters have to be calculated, which complicates the parametrisation.

For the concept ASTM-MT the joint state characteristics depend on the applied state model of the master. If the master satellite is simulated according to a **first-order Markov model**, then the joint state transition probabilities of master and slave are the product of the master transition probabilities with the corresponding ASTM. It holds

$$\mathbf{P}_{\text{trans}}^{joint} = \begin{bmatrix} p_{\text{gg}}^{Master} \cdot \mathbf{P}_{\text{trans}}^{Slave|\text{gg}} & p_{\text{gb}}^{Master} \cdot \mathbf{P}_{\text{trans}}^{Slave|\text{gb}} \\ p_{\text{bg}}^{Master} \cdot \mathbf{P}_{\text{trans}}^{Slave|\text{bg}} & p_{\text{bb}}^{Master} \cdot \mathbf{P}_{\text{trans}}^{Slave|\text{bb}} \end{bmatrix} \tag{3.30}$$

Two options are identified to calculate the state transition probabilities of the slave:

- **Option 1: Calculation of $\mathbf{P}_{\text{trans}}^{Slave}$ by considering the mean joint state durations.** It enables an accurate re-simulation of
  - joint state probabilities,
  - single satellite state probabilities,
  - and mean durations of the combined states.

  For this version, the diagonal elements p_{ii} ($i \in \{1,2,3,4\}$) of $\mathbf{P}_{\text{trans}}^{joint}$ are calculated first by taking the mean joint durations as parameter following Equation (3.3). Then, the transitions p_{ii} and p_{ij} from $\mathbf{P}_{\text{trans}}^{Slave|\text{gg}}$ and $\mathbf{P}_{\text{trans}}^{Slave|\text{bb}}$ are found with

$$\begin{aligned} p_{ii}^{Slave|kk} &= p_{ki\rightarrow ki}^{joint} / p_{kk}^{Master} \\ p_{ij}^{Slave|kk} &= 1 - p_{ii}^{Slave|kk} \end{aligned} \tag{3.31}$$

with $i, j, k \in \{\mathrm{g}, \mathrm{b}\}$.

With knowledge of $\mathbf{P}_{\mathrm{trans}}^{Slave|\mathrm{gg}}$, $\mathbf{P}_{\mathrm{trans}}^{Slave|\mathrm{bb}}$, and the joint state probabilities, the missing elements of $\mathbf{P}_{\mathrm{trans}}^{joint}$ and finally the slave ASTMs can be calculated.

- **Option 2: Calculation of $\mathbf{P}_{\mathrm{trans}}^{Slave}$ by using the Lutz approach.** The simulation results are identical to the original Lutz approach [Lut96] (Section 3.2.2), but with Master-Slave functionality. It enables an accurate re-simulation of
  - joint state probabilities,
  - single satellite state probabilities,
  - mean state durations of the single satellites.
  - mean durations of the joint states 'good good' and 'bad bad', if the modification of the Lutz model from Section 3.2.3 is applied.

  The model parameters are determined as follows: First, the correlated Lutz-STPM ($\mathbf{P}_{\mathrm{trans}}^{joint}$) is estimated by considering the individual state transition probabilities of master and slave and a correlation coefficient. Second, the ASTMs are estimated by dividing the joint transition probabilities with the master transition probabilities according to Equation (3.30). For example, the ASTM $\mathbf{P}_{\mathrm{trans}}^{Slave|\mathrm{gg}}$ is found with:

$$\mathbf{P}_{\mathrm{trans}}^{Slave|\mathrm{gg}} = \begin{bmatrix} p_{11}/p_{\mathrm{gg}}^{Master} & p_{12}/p_{\mathrm{gg}}^{Master} \\ p_{21}/p_{\mathrm{gg}}^{Master} & p_{22}/p_{\mathrm{gg}}^{Master} \end{bmatrix} \tag{3.32}$$

  where p_{ij} (with $i, j \in \{1, 2\} = \{\mathrm{gg}, \mathrm{gb}\}$) are elements of the Lutz correlation matrix. The rows of the Slave ASTMs are already normalised ($\sum = 1$). It is due to an important characteristic of the correlated Lutz-STPM:

$$\begin{aligned} p_{11} + p_{12} &= p_{21} + p_{22} \\ p_{13} + p_{14} &= p_{23} + p_{24} \\ p_{31} + p_{32} &= p_{41} + p_{42} \\ p_{33} + p_{34} &= p_{43} + p_{44} \end{aligned} \tag{3.33}$$

When the Master is modelled by a semi-Markov or dynamic Markov algorithm, then Equation (3.30) is only approximately valid. By applying ASTMs from the parametrisation above with a semi-Markov or dynamic Markov master sequence, an accurate re-simulation of the joint probabilities as well as the correlation coefficient between the satellites is nevertheless possible.

3.2.8. Master-Slave with Adaptive Slave Transition Matrices based on State Durations

The concept Master-Slave for dual-satellite state modelling and a possible realisation was first drafted in [EHH08]. The initial idea is to implement the master chain with a dynamic Markov model, and to describe the transition probabilities of the slave as a function of the master state s_M, the current state length of the master q_M, and the current state length of the slave q_S:

$$\mathbf{P}_{\mathrm{trans}}^{Slave} = f(s_M, q_M, q_S) \tag{3.34}$$

As already stated for the concept ASTM-MT, a sample-by-sample parametrisation by simply counting and normalising the slave transitions is not an option to find appropriate parameters. The required expression for this concept *ASTM based on state durations* to calculate state probabilities and correlation coefficients, from which the model parameters are derived, is not determined in the context of this thesis. This complex task could be topic of activities beyond this work.

3.3. Comparison of State Models on a Dual-Satellite Scenario

In this section the different dual-satellite state models from previous Section 3.2 are compared considering a realistic scenario with two geostationary satellites. Specificially, a measurement sample from a mixed rural environment from the SDARS campaign (cf. Appendix A for details) of 23 km length is chosen. The satellites are seen at elevations $\phi_1 = 23°$ and $\phi_2 = 38°$ and have an azimuth angle separation of $\Delta\theta = 34°$.

17 different approaches are applied to re-simulate this scenario, including versions of first-order Markov models, semi-Markov models, dynamic Markov models and Master-Slave approaches. Before starting the comparison, the evaluation criteria are described.

3.3.1. Evaluation Criteria

To evaluate state algorithms for dual-satellite reception, the following criteria are chosen:

- **probabilities of single satellite states and joint states (P_{single}, P_{joint}).** The probability of the single-satellite states influences the overall fading probability statistics at the output of the LMS model. It weights the contribution of the signal from 'good' and 'bad' state to the overall signal.

  The probability of the joint states is directly coupled to the correlation coefficient between two satellite signals (see also Equation (B.25) in Appendix B.2.1). An inaccurately described correlation coefficient can lead to false performance predictions for a satellite diversity system.

- **mean durations of single- and combined states ($\bar{D}_{single}, \bar{D}_{joint}$).** An analysis of mean state durations indicate as a first approximation, if the time variability of the channel is correctly simulated. They affect also the average fade durations of simulated LMS timeseries.

- **number of parameters**. The number of parameters of state models ranges from four to tens of thousands. Although a model with a high number of parameters is no problem for the simulation process and storage, it is rather challenging to find appropriate model parameter sets.

- **state duration statistics ($P(D)_{single}, P(D)_{joint}$).** The state durations are analysed in terms of complementary cumulative distribution functions (CDF). Figure 3.10 (left) shows exemplarily a statistic of the 'bad' state from one satellite. The ordinate describes the probability of the state exceeding a certain length. A quality measure for the performance of state models is the mean squared error (MSE) between measured

and re-simulated state duration PDF, not its CDF. It is due to the fact that state duration distributions are captured from SDPDFs (e.g. the lognormal distribution). The MSE between simulated SDPDF $P_{sim}(D)$ and referenced or measured SDPDF $P_{ref}(D)$ is calculated:

$$MSE = \frac{1}{k}\sum_{q=1}^{k}(P_{sim}(D_q) - P_{ref}(D_q))^2\,, \tag{3.35}$$

where $P(D_q)$ is the probability of the duration D equals q samples, and k is the maximum state duration for the comparison. In this thesis, the SDPDFs are compared to a fixed length of 500 m, with a sample length of 1 m ($k = 500$). This limitation seems appropriate, since the SDPDFs of first-order Markov and semi-Markov models are unlimited in theory.

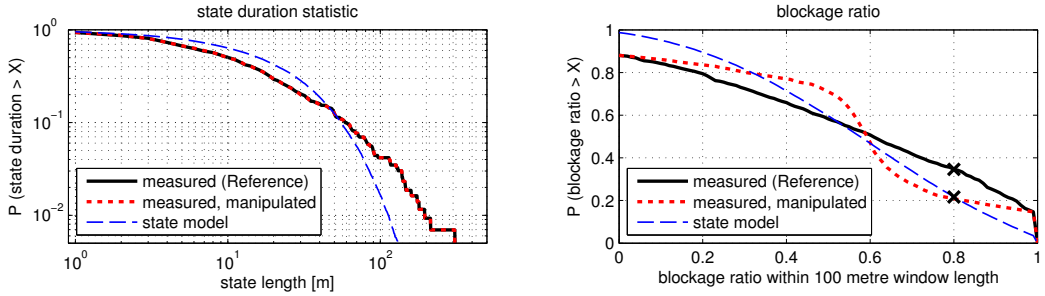

Figure 3.10.: Evaluation methods of the temporal composition of state sequences. Left: Complementary state duration CDF of the 'bad' state. Right: complementary CDF of the blockage ratio over 100 metre window length. The figures show corresponding curves from a measured state sequence, from a re-simulated sequence with a state model, and from a manipulated state sequence to demonstrate the purpose of the new proposed blockage ratio statistic.

- **blockage ratio statistic**. This evaluation criteria is gathered in the context of this thesis for LMS modelling and is therefore described in a separate passage below.

Blockage Ratio Statistic

To describe the behaviour of the state sequence over time, the state duration statistic is well accepted in literature as evaluation criterion. Indeed, the SDPDF gives information about state-length probabilities, but not about the time-based correlation of these lengths within the entire sequence. For an extended evaluation of the signal's time composition, the blockage ratio statistic over a certain window is introduced in this thesis.

The difference between state duration statistic and blockage ratio statistic is demonstrated by two curves in Figure 3.10: the statistics from a *measured* state sequence and a *manipulated sequence*. In the latter case the measured sequence is reconstructed such, that all state durations are sorted with increasing length. Although the state duration distribution of both sequences is equal (Figure 3.10 left), significant differences of the signals are detected within the blockage ratio statistic (Figure 3.10 right). It shows that a state model that is optimised in terms of state duration modelling may still have limitations in describing the

signals composition over time, which affects the analysis of fading mitigation techniques such as time interleaving (cf. Section 2.2.2).

Two values are exemplarily derived from the curves in Figure 3.10 and can be interpreted as follows: The measurements indicate, that in 40% of the obtained 100-metre intervals the blockage ratio exceeds 80%. The state model, however, predicts a blockage ratio above 80% in only 20% of observations. For critical receive conditions, the state model prediction would be more optimistic than the reality (measurements).

3.3.2. Comparison of State Models on a Dual-Satellite Scenario: Results

17 different state models are applied to re-simulate a measured scenario as described at the beginning of this Section 3.3. A full list of algorithms is given in Table 3.1, including each the re-simulation performance in terms of joint and single satellite state probabilities, mean durations, duration statistics as well as the required number of parameters.

Figure 3.11 shows the state duration statistics for the combined 'bad bad'-state and the 'bad'-states of the individual satellites derived from the measurements and after re-simulation with different algorithms. Due to better visibility the 17 algorithms are arranged in four groups (and therefore four figures) according to their modelling process: first-order Markov, semi-Markov, dynamic Markov, Master-Slave. The MSE between measured and re-simulated SDPDF from Figure 3.11 are given for selected states in Table 3.1.

The blockage ratio statistics within 100 metre window length from measurements and after re-simulation are presented in Figure 3.12. They are depicted for the combined satellites (ratio of 'bad bad') as well as for the individual satellites.

The following results are obtained from Table 3.1, Figure 3.11, and Figure 3.12:

First-order Markov models

- The probabilities of single- and combined states are accurately re-modelled with all first-order Markov algorithms.
- The multi-state first-order Markov model (according to *straightforward method*) accurately re-simulates the mean durations of single and combined states. The 'first-order Markov & Lutz' approach, on the contrary, has no information about the mean joint durations. An exact re-simulation is not possible therefore. However, with additional information, the Lutz approach can be modified such that mean durations of 'good good' and 'bad bad' are generated correctly ('first-order Markov & Lutz modified').
- The SDPDF of first-order Markov models follows an exponential distribution. It deviates highly from the measured duration statistics as obtained in Figure 3.11. The MSE of the SDPDF is high when compared with other algorithms. The limited performance of first-order Markov models for temporal aspects is also reflected by the blockage ratio statistic.

Semi-Markov models

- Semi-Markov models offer an accurate modelling of the state duration statistic. Their re-modelling accuracy depend on the applied curve-fit. If the full SDPDF of the joint states is parametrised (no fit), then the joint SDPDFs are accurately re-modelled. A good approximation of the joint SDPDF is provided with a lognormal fit or a piecewise exponential fit.
- A curve fit of the SDPDF may change slightly the mean state duration. The changed mean state duration affects further the state probabilities. Therefore, in case of 'semi-Markov, logn. fit' and 'semi-Markov, piecewise exponential fit' the mean durations and the state probabilities are well, but not accurately, re-modelled.
- A correction of the curve-fit with respect to a correct mean duration of joint states ('semi-Markov, logn. fit (corrected)') provides an accurate re-simulation of state probabilities as well as the mean durations of the individual satellites.
- The semi-Markov model can be combined with the Lutz approach ('semi-Markov, logn. fit & Lutz modified'). Although it provides less good performance than the algorithm 'semi-Markov, logn. fit (corrected)', this algorithm has great advantages in terms of the LMS model parametrisation (cf. Section 3.4.2).
- The re-simulation of the measured blockage ratio statistic with semi-Markov models is significantly better than with first-order Markov models. For critical receive scenarios, it is when the blockage ratio is high, the semi-Markov models are still too optimistic. The difference between 'semi-Markov, no fit' and 'semi-Markov, *approximated*' in terms of blockage ratio is marginal.

Dynamic Markov models

- The full dynamic Markov model (i.e. no approximation) accurately re-simulates the state probabilities and mean durations of the combined states and the single satellite states, and the joint SDPDFs. However, the SDPDF of the single satellites is only approximately re-simulated. Despite the full dynamic Markov model has more information and requires a multiple of parameters than the 'partial dynamic Markov model', the performance is quite similar.
- The 'partial dynamic Markov' model provides exactly the same results as 'semi-Markov, no fit'. Despite different algorithms, the decision processes during simulation are equal (cf. Section 3.1.4).
- The 'approximated partial dynamic Markov' model provides similar results as semi-Markov models with approximated SDPDFs. The relation between these algorithms is described in Section 3.1.4.
- Similarities between semi-Markov and dynamic Markov models are also seen in the blockage ratio statistics.

Nth-order Markov model

- The best re-simulation performance is provided by the Nth-order Markov model. It allows to accurately re-simulate the duration statistics of joint states AND from single satellite states as well as the blockage ratio. However, in terms of LMS modelling this approach is highly impractical due to the high number of parameters. Nevertheless,

re-simulation results of a 25th-order Markov model are presented in Figure 3.11 and Figure 3.12. In comparison to the other models, the better performance in terms of blockage ratio and state duration statistics (up to 25 m) is clearly seen.

Master-Slave models

- The Conditional Assembling Method provides an accurate description of the probabilities of combined states and single satellite states. Further on the duration statistics of the master satellite can be accurately re-modelled. However, the Conditional Assembling Method offers no control on the state duration statistics for slave and for combined channel.
- The Master-Slave method with 'adaptive slave transition matrix based on master transitions (ASTM-MT)' enables an accurate re-modelling of mean state durations. As this approach is similar to a first-order Markov model, it has limitations in modelling the SDPDFs and the blockage ratio.
- The approach 'ASTM-MT, option 1: Lutz' is the original Lutz model re-used for Master-Slave functionality. In case the master is generated with first-order Markov, the results are exactly the same.

Note that the 're-simulation' results of the LMS models in terms of state probabilities and mean state durations (Table 3.1) and state duration statistics (Figure 3.11) are all analytically derived. It represents a simulation of state series with infinity length. Corresponding mathematical expressions are partly developed in this work and are found in Appendix B. For the blockage ratio statistics, a state series simulation over 1000 km is performed to minimise a statistical spread of results.

Table 3.1.: Performance comparison of dual-satellite state models. Notation: the characteristics from measurement data are *accurately* re-modelled (✓), *approximated* by the model (O) or *not applicable* by the model (X). These attributes are universally valid and are quantified on multiple LMS scenarios in next Section 3.4. Exemplary state duration statistics are found in Figure 3.11.

algorithm	**described in**	**state probability**		**mean state duration**		**state duration PDF**		**parameters**
		P_{joint}	P_{single}	$\bar{D}_{joint}$	$\bar{D}_{single}$	$P(D)_{joint}$ [1]	$P(D)_{single}$	
multi-state approaches								
1st-order Markov	Sec. 3.1.1	✓	✓	✓	✓	X (1.7)	X	16
1st-order Markov & Lutz	Sec. 3.2.2	✓	✓	X	✓	X (1.8)	X	9
1st-order Markov & Lutz modified	Sec. 3.2.3	✓	✓	(✓)[2]	✓	X (1.6)	X	11
semi-Markov, no fit	Sec. 3.1.2	✓	✓	✓	✓	✓	O	2792
semi-Markov, lognormal fit	Sec. 3.1.2	O	O	O	O	O (0.4)	O	20
semi-Markov, piecewise exponential fit	Sec. 3.1.2	O	O	O	O	O (0.4)	O	64
semi-Markov, lognormal fit (corrected)	Sec. 3.1.2	✓	✓	✓	✓	O (0.4)	O	20
semi-Markov, lognormal fit & Lutz modified	Sec. 3.2.4	✓	✓	(✓)[2]	✓	(O)[2] (0.4)	O	20
dynamic Markov	Sec. 3.1.3	✓	✓	✓	✓	✓	O	11120
partial dynamic Markov	Sec. 3.1.3	✓	✓	✓	✓	✓	O	2792
approximated partial dynamic Markov	Sec. 3.1.3	O	O	O	O	O (0.4)	O	20
Nth-order Markov	Sec. 3.1.5	✓	✓	✓	✓	✓	✓	4^{N+1}

algorithm	**described in**	**state probability**			**mean state duration**			**state duration PDF**			**parameters**
		P_{joint}	P_M	P_S	$\bar{D}_{joint}$	$\bar{D}_M$	$\bar{D}_S$	$P(D)_{joint}$ [1]	$P(D)_M$	$P(D)_S$	<M>+<S>
Master-Slave: Conditional Assembling Method											
Master: 1st-order M., Slave: 1st-order M.	Sec. 3.2.6	✓	✓	✓	X	✓	X	X (1.3)	X	X	4+8
Master: dyn. Markov, Slave: 1st-order M.	Sec. 3.2.6	✓	✓	✓	X	✓	X	X (0.7)	✓	X	1000+8
Master-Slave: Adaptive Slave Transition Matrix based on Master Transitions (ASTM-MT)											
option 1: mean joint dur., Master: 1st-order M.	Sec. 3.2.7	✓	✓	✓	✓	✓	X	X (1.6)	X	X	4+16
option 2: Lutz , Master: 1st-order M.	Sec. 3.2.7	✓	✓	✓	X	✓	✓	X (1.8)	X	X	4+7
option 2: Lutz , Master: dyn. Markov	Sec. 3.2.7	O	✓	O	X	✓	O	X (1.4)	✓	X	1000+5

[1] The values in brackets are the mean squared errors (MSE) in $[10^{-5}]$ between measured and re-simulated SDPDF for 'bad bad'. They are valid for the exemplarily selected dual-satellite scenario of this Section 3.3. In case of 'accurate' re-simulation, the MSE is zero.

[2] This result holds only for combined states 'good good' and 'bad bad'.

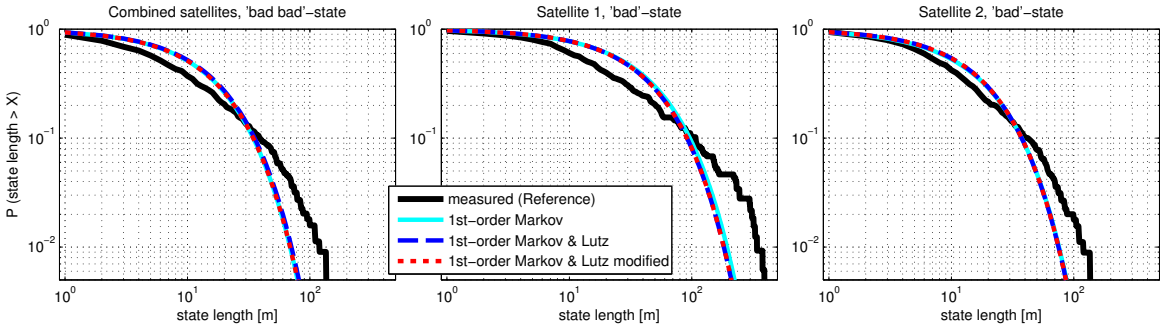

(a) First-order Markov models.

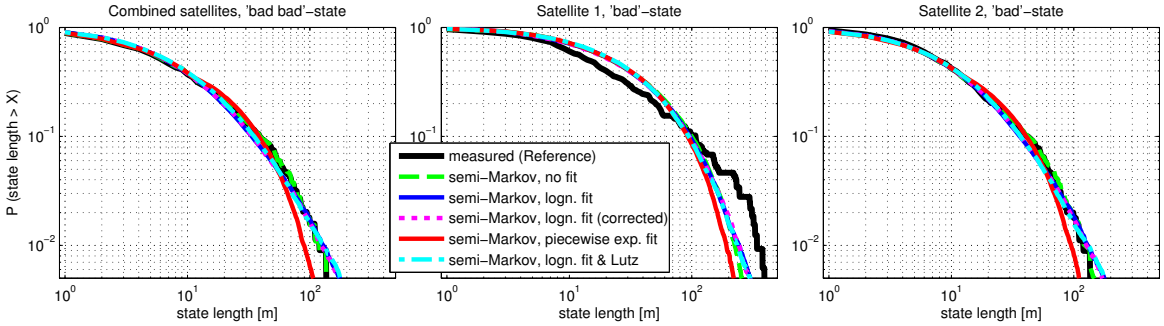

(b) Semi-Markov models.

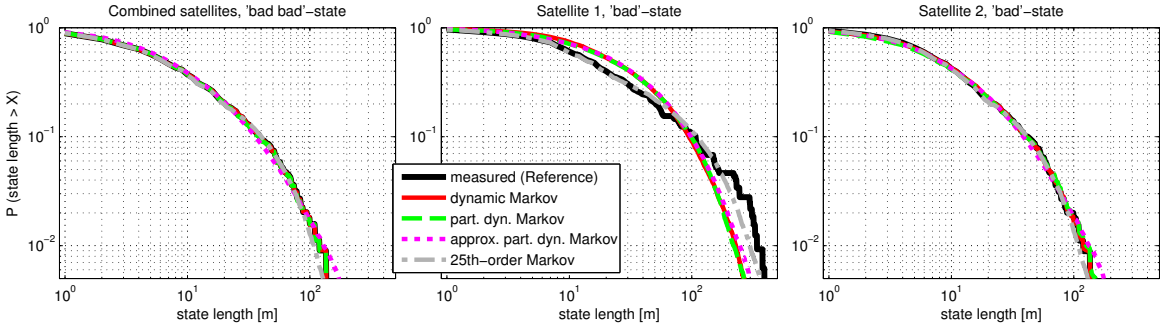

(c) Dynamic Markov models and higher order Markov model.

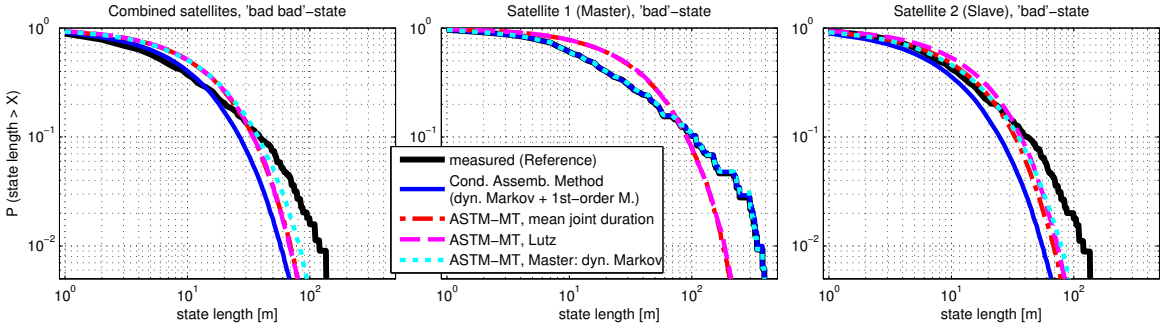

(d) Master-Slave approaches.

Figure 3.11.: State duration statistics of the combined 'bad bad'-state (left) and single satellite 'bad'-states (center, right) derived from the measurements and re-simulated with different modelling approaches.

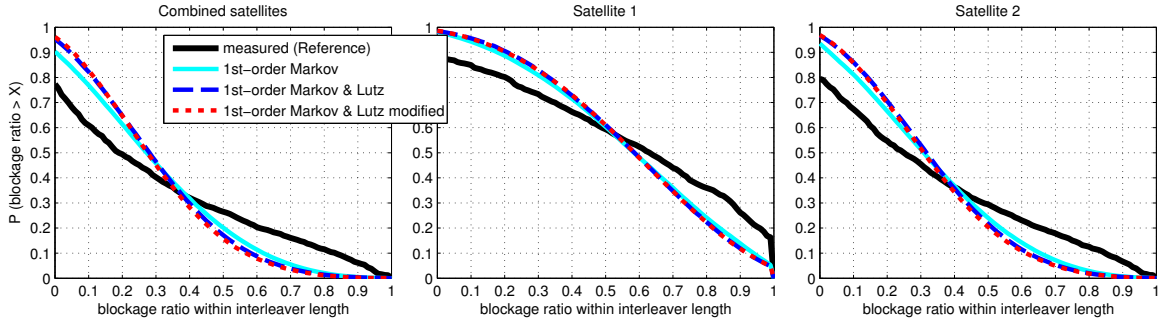

(a) First-order Markov models.

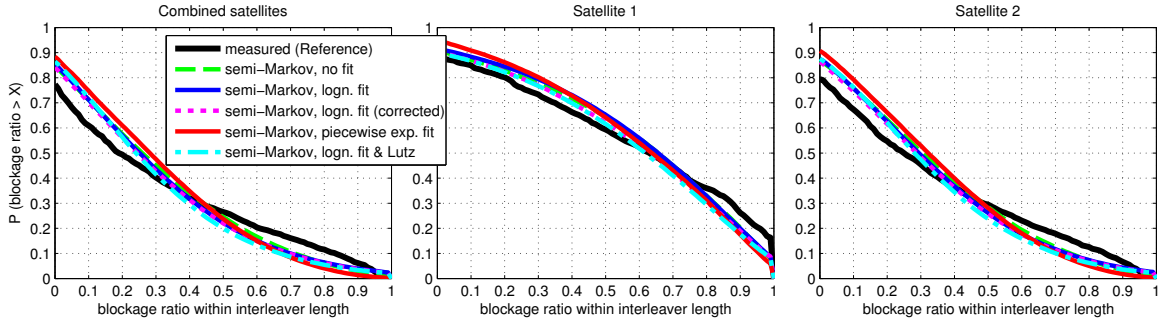

(b) Semi-Markov models.

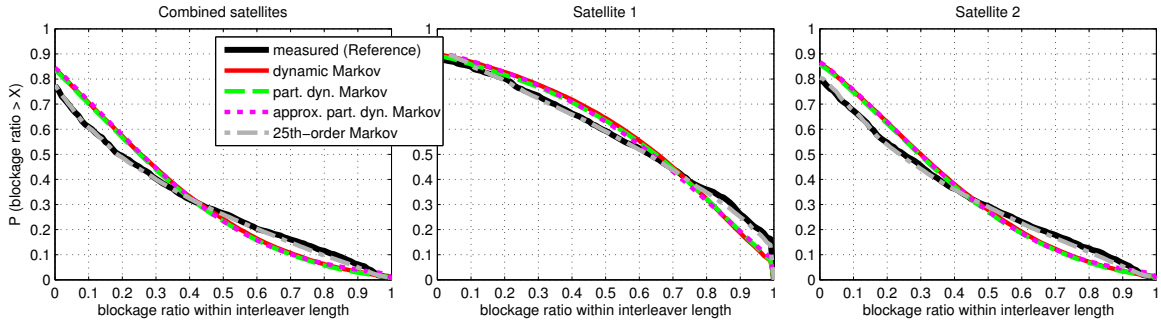

(c) Dynamic Markov models and higher order Markov model.

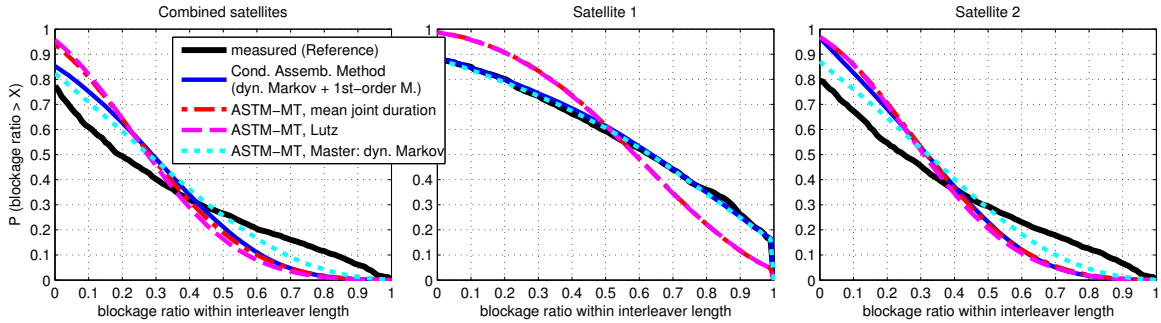

(d) Master-Slave approaches.

Figure 3.12.: Complementary CDF of the blockage ratio over 100 m window length of the combined 'bad bad'-state (left) and single satellite 'bad'-states (center, right) derived from the measurements and re-simulated with different modelling approaches.

3.3.3. Conclusions for Dual-Satellite Models

The best re-modelling performance in terms of state probabilities and state duration statistics is provided with the algorithms **Nth-order Markov model**, **dynamic Markov model**, **partial dynamic Markov model**, and **semi-Markov model, no fit**. However, due to their required number of parameters, they are not feasible to generate a dual-satellite model database representing arbitrary receive situations.

Models based on **first-order Markov** have limitations in terms of describing the state duration distribution and therefore the temporal composition of the channel. Although they are easy to parametrise, especially in combination with the Lutz approach, these models would not provide an accurate channel representation for optimising physical layer and link layer parameters of satellite broadcasting systems with high quality-of-service requirements.

The **semi-Markov models with approximated SDPDF** as well as the **approximated partial dynamic Markov** model achieve good modelling results of the state duration statistics and of the blockage ratio by using an acceptable number of parameters. By small modifications, they enable an accurate description of state probabilities and mean durations as well. In order to decide for an appropriate state model for the final LMS channel emulator, in Section 3.4 these state models are compared on a large number of receive scenarios.

All of the presented **Master-Slave** algorithms are accurate in terms of state probability modelling, but have limitations in terms the time-based description of the channel. Of course the general concept 'Master-Slave' may have potential for accurate state duration modelling as well. However, due to the mathematical complexity only a limited set of Master-Slave realisations are developed within this thesis providing an acceptable performance. It can be concluded that in terms of dual-satellite modelling the given Master-Slave approaches have a minor role, since other concepts (e.g. semi-Markov) provide better performance. However, for multi-satellite systems with more than two satellites the Master-Slave concept has some advantages. The preferred Master-Slave algorithm for dual- and multi-satellite modelling would be the *ASTM-MT with Lutz parametrisation*. It combines the performance and flexibility of a 'first-order Markov & Lutz' model with the Master-Slave functionality.

3.4. Measurement Results and State Modelling Statistics for Single- and Dual-Satellite Reception

The LMS channel presents significant differences depending on the kind of the environment the mobile traverses. Several environmental categories have been used in the planning of satellite transmission systems, including urban, suburban, rural, forest, and open. Furthermore, the orbital position of the satellite has an impact on the LMS channel. In case of single-satellite reception, the dominant parameters to describe the channel are thus the environment type env, the elevation angle of the satellite ϕ, and the azimuth of the satellite relative to the driving direction θ. The dual-satellite (and multi-satellite) reception additionally depends on the angular separation in azimuth $\Delta\theta$ and elevation $\Delta\phi$ between the satellites, which affects the correlation of the received signals.

In this section results of measurement analyses are presented in terms of state probabilities and state duration statistics for different environments and orbital positions of the satellites. Data from two campaigns are analysed therefore: SDARS measurements and GNSS measurements (cf. Appendix A). In the following two subsections the characteristics for single-satellite reception and dual-satellite reception are addressed. Furthermore, the parameters for different state models are derived to compare the re-modelling results with the measurements. On this basis, an appropriate state modelling approach is identified and recommended for the final LMS model.

3.4.1. Results for the Single-Satellite Channel

The single-satellite LMS channel depends on the kind of the environment, the elevation angle of the satellite ϕ, and the azimuth of the satellite relative to the driving direction θ. For a detailed analysis of the single-satellite state characteristics, the SDARS- and GNSS measurement data are divided into

- five environment types 'Urban', 'Suburban', 'Forest', 'Commercial', 'Open'.
- different elevation angles from 10° to 90° in segments of 10°. The mean elevation angles represented by these datasets are therefore 15°, 25°, ... , 85°, respectively.
- four classes of driving directions (for GNSS data, only) with the intervals [0°, 10°], [10°, 30°], [30°, 60°], and [60°, 90°]. [2]

The available amount of measurement data for the different segments (further denoted as *receive scenarios*) is given in Appendix A.6.

For the defined receive scenarios, Figure 3.13 shows the probabilities of the 'bad'-state (P_b), and Figure 3.14 shows the mean durations of the 'bad'-state ($\bar{D}_\mathrm{b}$) for single-satellite reception. The corresponding 'good'-state results are calculated with $P_\mathrm{g} = 1 - P_\mathrm{b}$ and $\bar{D}_\mathrm{g} = P_\mathrm{g}/P_\mathrm{b} \cdot \bar{D}_\mathrm{b}$, respectively. The following observations are made in Figure 3.13 and 3.14:

- In general, P_b and $\bar{D}_\mathrm{b}$ decrease with increasing satellite elevation. The slope of the curves depends on the driving direction.
- P_b and $\bar{D}_\mathrm{b}$ increase with increasing angle between satellite azimuth and driving direction θ within the interval $[0°, 90°]$. Except, for high elevation angles ($\phi > 70°$) the influence of the driving direction is low. For system planning and the study of effective fading mitigation techniques it is important to consider the worst case ($\theta \approx 90°$).
- Comparing different environments, the 'bad'-state probability in urban and forest areas is on average higher than in other environments. Also the discrepancy between the worst ($\theta = 90°$) and best ($\theta = 0°$) reception case is higher than in suburban, commercial and forest.

[2] By analysing the driving direction it is assumed that the vehicle moves in the middle of the street. Thus, the reception is symmetric in four quartals within $[0, 2\pi)$ (e.g. $\theta_{0°} = \theta_{180°}$; $\theta_{90°} = \theta_{270°}$; $\theta_{30°} = \theta_{150°} = \theta_{210°} = \theta_{330°}$). This assumption is made due to the limited amount on RF measurement data. To analyse the influence of driving directions in detail, camera based measurement data would be an convenient basis.

- In case of GNSS, for elevation angles above 70° the 'bad'-state probability in urban environments is lower than in suburban and forest environments. A reason could be shadowing from trees reaching above the streets in suburban environments and forests, which is minor probable in urban areas.

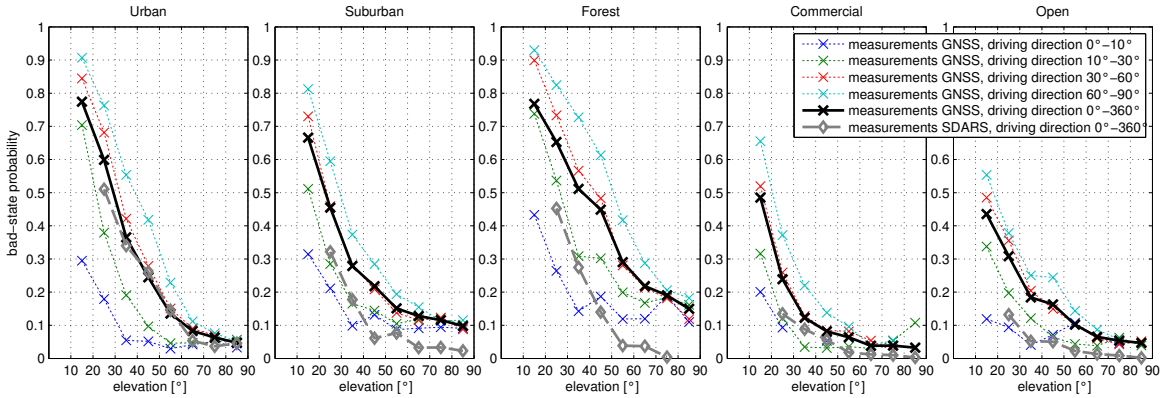

Figure 3.13.: 'bad'-state probabilities derived from the GNSS and SDARS measurements for single-satellite reception as a function of the elevation angle and the azimuth angle relative to the driving direction.

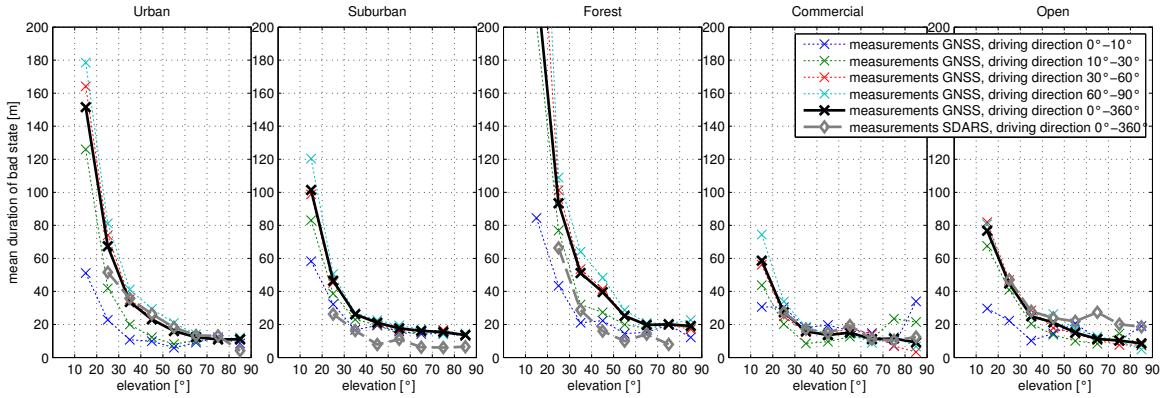

Figure 3.14.: Mean durations of the 'bad' state derived from the GNSS and SDARS measurements for single-satellite reception as a function of the elevation angle and the azimuth angle relative to the driving direction.

By comparing SDARS and GNSS measurements, similar results are obtained for urban areas only.[3] In suburban, forest, commercial, and open environments, the probabilities and durations of the 'bad' state obtained from SDARS are significantly lower than from GNSS. A reason could be mainly wider streets in the U.S. than in Europe. Furthermore, the driving direction may affect the SDARS results, which cannot be considered in any case as equally distributed between 0° and 360°. Please note that also different methods of environment classification may have an influence to the results.

Nevertheless, similar tendencies of P_b and $\bar{D}_\mathrm{b}$ in dependency on the satellites' elevation are obtained. Therefore, it can be concluded that differences of P_b and $\bar{D}_\mathrm{b}$ between SDARS

[3] A basis for comparison between SDARS and GNSS measurements are the values for $\theta \in [0°, 360°]$.

and GNSS originate mainly from differences within the environment classes. It may be worth noting that the definition of environment classes is highly subjective due to manual annotation. An objective environment classification, e.g. based on image data, would be a very interesting field of research. However, it is out of scope of this thesis.

Different state modelling approaches, including the recommended state model for the new LMS channel model, accurately re-simulate the measured state probabilities and state durations. Thus, the graphs from Figure 3.13 and 3.14 represent the channel model output as well. The representativeness of the channel model parameters consequently depend on the quality of the measurements. It is concluded that due to the available amount of SDARS- and GNSS measurement data (cf. Appendix A), both campaigns allow to derive reliable model parameter sets for realistic single-satellite receive scenarios. Therefore, two model parameter sets for single satellite reception are represented by the results in Figure 3.13 and 3.14:

- The **MiLADY SDARS state parameter set** allows a state sequence generation for five different environments and seven elevation angles ($\phi \in [20°, 90°]$ in intervals of 10°). The parameters are found in Table C.2 in Appendix C.
- The **MiLADY GNSS state parameter set** allows a state sequence generation for five different environments, eight elevation angles ($\phi \in [10°, 90°]$), and four driving directions. The parameters are found in Table C.3.

3.4.2. Results for the Dual-Satellite Channel

The dual-satellite (and multi-satellite) LMS channel depends on the kind of the environment, the elevation angle of each satellite (ϕ), and the azimuth of each satellite relative to the driving direction (θ). Especially the angular separation of the satellites of elevation ($\Delta\phi$) and azimuth ($\Delta\theta$) is crucial, since it affects the correlation of the received signals. To investigate this in detail, dual-satellite parameters are derived for 5 different environments, the combination of 8 different elevation angles from two satellites, and 7 intervals of the azimuth angle separation between the satellites (cf. Appendix A). A total of $5 \cdot 8 \cdot 8 \cdot 7 = 2240$ segments of measurement data are defined.[4] Due to limited measurement data, a further division into driving directions is omitted. Displaying the results of dual-satellite modelling is much more complex than in the single-satellite case. Therefore, in this section only the urban results are presented for only a subset of receive scenarios which are obtained from GNSS measurements. Additionally, the parameters for different state modelling approaches are derived from GNSS data. The re-simulation results are compared with the measurements in terms of correlation coefficients, state probabilities and state duration statistics.

The Correlation Coefficient Between Two Satellites

Figure 3.15 shows the correlation coefficient between the states ρ_{states} of two satellites in dependency on the azimuth separation $\Delta\theta$ derived from the measurements and after re-simulation with dual-satellite state models for the urban environment. Each subplot shows

[4] For single-satellite analysis only 160 segments (8 elevation angles, 5 environments and 4 driving directions) are required.

a certain combination of two elevation angles. As this matrix of subplots is symmetric, only the lower triangle is shown. For a better visibility, only the elevation angles $\phi < 50°$ are shown to focus on the critical receive scenarios.

Additionally the results from an empirical model from Robet et al. [REE92] are shown in Figure 3.15. This empirical model allows to calculate the *shadowing probability* in dependency on the azimuth separation and the *shadowing probabilities* of the individual satellites (cf. Chapter 2.4.1). By taking the 'bad'-state probabilities (P_{b1}, P_{b2}) from the single-satellite GNSS measurement database (Figure 3.13) as parameter, the correlation coefficient ρ_{states} can be calculated from the resulting joint state probability (P_{bb}) according to Equation (B.26) from Appendix B.2.1.

The following observations can be made in Figure 3.15:

- In case of small azimuth separations, both state sequences are highly correlated (up to $\rho_{states} = 0.9$). (Note: For two exactly co-located satellites $\rho_{states} = 1$ is expected, this special case is not covered in the results.) The correlation has a minimum within the range $60° < \Delta\theta < 120°$. It can reach values $\rho_{states} < 0$. Towards 180° azimuth separation, ρ_{states} slightly increases.

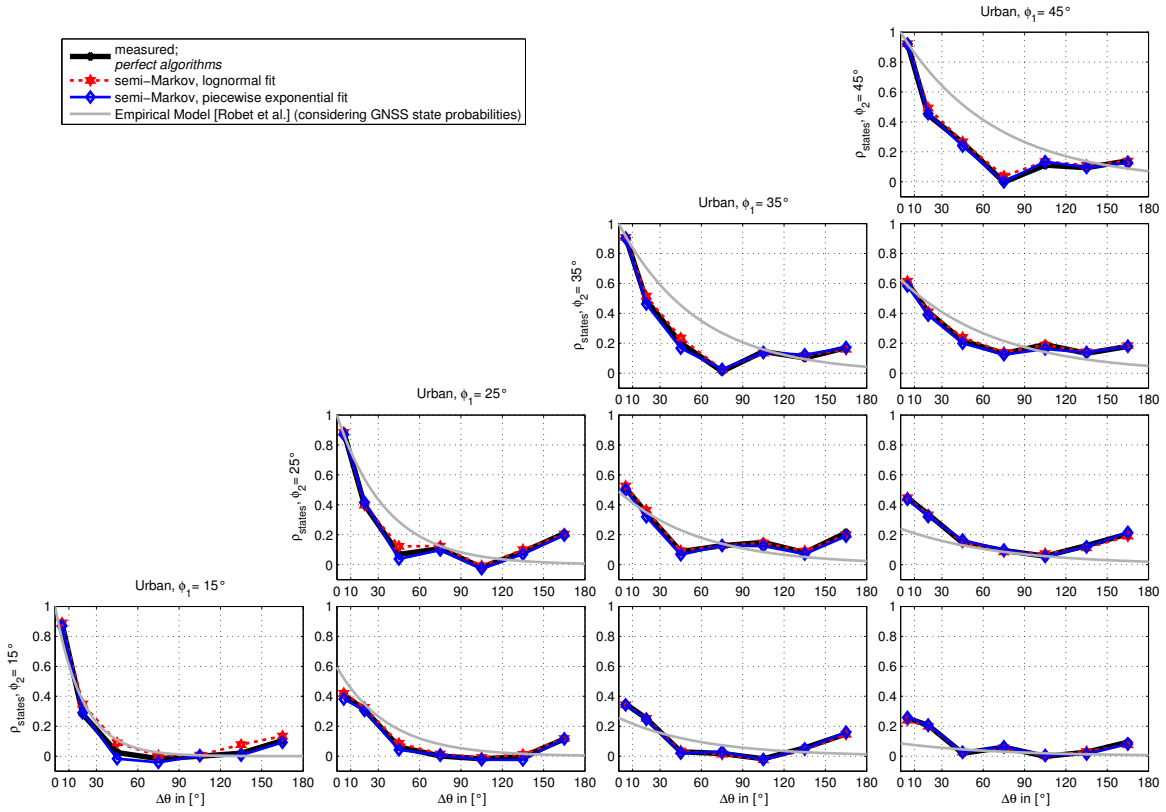

Figure 3.15.: Correlation coefficients of the state sequences from two satellites (ρ_{states}) in dependency on the azimuth separation ($\Delta\theta$) and for different elevation angle combinations (ϕ_1, ϕ_2) derived from the measurements and re-calculated with different channel models.

- In case of small azimuth separation, the correlation coefficient further depends on the elevation angle separation between two satellites.
- The correlation coefficient is accurately re-simulated by algorithms which provide accurate state probability modelling (cf. Table 3.1: algorithms with accurately re-modelled P_{joint}). These are: *1st-order Markov*, *semi-Markov, no-fit* and *semi-Markov, logn. fit (corrected)*, *dynamic* and *partial dynamic Markov*, *Nth-order Markov*, *Conditional Assembling Method*, *ASTM-MT* when Master is modelled as 1st-order Markov. Due to visibility, these algorithms are denoted with 'perfect algorithms' in Figure 3.15.
- A good fit of the correlation coefficients is also achieved with the semi-Markov approaches assuming a lognormal fit or a piecewise exponential fit of the SDPDF. For only a small number of receive scenarios the correlation coefficient deviates by ± 0.1 from the measurements. This is acceptable, as the variation of the correlation coefficients between different elevation angles and azimuth separations is much higher.
- After a modification of the lognormal fit according to Equation (3.12), the coefficients ρ_{states} generated with the semi-Markov model are equal to the measured values (represented by 'perfect algorithms').
- Comparing the empirical model from Robet et al. [REE92] with the GNSS results, a good agreement of the correlation coefficient is obtained for $\phi_1 = \phi_2 = 15°$, only. For other elevation angle combinations, the slope of curves $\rho_{\text{states}} = f(\Delta\theta)$ from GNSS measurements is greater than from the empirical model.

State Probabilities for Dual-Satellite Reception

The 'bad bad'-state is the critical system state and requires special attention for LMS modelling. Therefore, Figure 3.16 shows exemplarily the probabilities of the 'bad bad'-state (P_{bb}) as well as the 'bad'-state probabilities of the single satellites ($P_{\text{b1}}, P_{\text{b2}}$) in dependency on the azimuth angle separation ($\Delta\theta$) in the urban environment.

For each receive scenario, i.e. a combination of $\Delta\theta$, ϕ_1, and ϕ_2, GNSS data is taken from different parts of the measurement route. As a consequence, from measurements different values of P_{b1} and P_{b2} are obtained for different values of $\Delta\theta$, although $\Delta\theta$ should have no influence to P_{b1} and P_{b2}. This fact is the main problem of estimating adequate parameter sets for dual- and multi-satellite state models according to the straightforward method (cf. Section 3.2.1). Whether a dynamic Markov, semi-Markov, or first-order Markov model with four combined states is used, they all re-simulate accurately the measured state probabilities of the current dual-satellite receive scenario (represented by 'straightforward models' in Figure 3.16). A challenge with these models would be, e.g. a comparison of the dual-satellite gain for different satellite constellations: the fluctuations of single satellite state probabilities may have a higher influence to the satellite diversity gain than $\Delta\theta$. Although a large amount of RF measurement data is analysed, it has limitations to generate consistent state parameter sets for dual-satellite reception. A promising solution would be the analysis of image-based data, e.g. from fish-eye cameras [IAT+11], or the analysis of three-dimensional environmental databases.

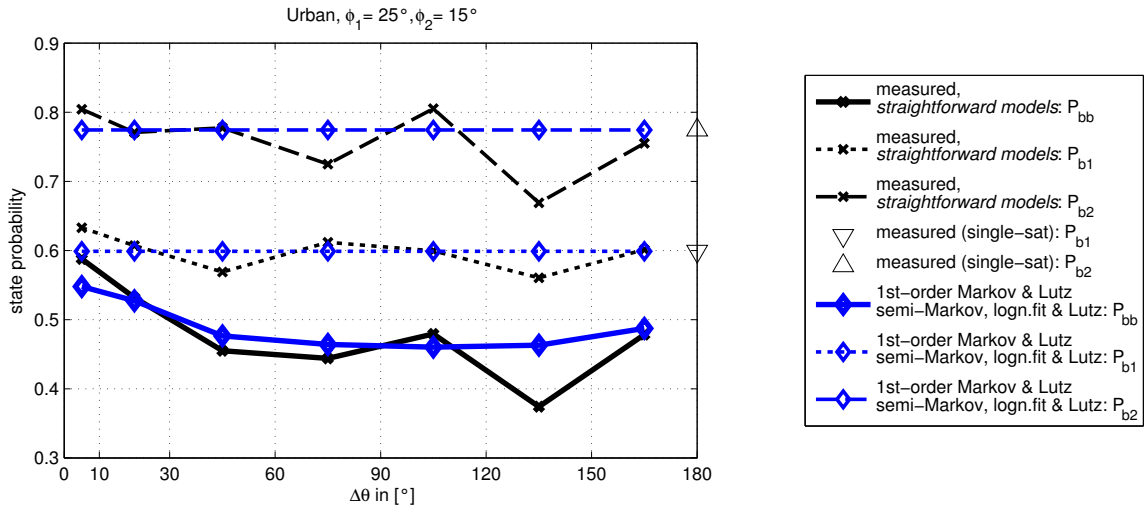

Figure 3.16.: Probabilities of the combined state 'bad bad' (P_{bb}) and of the single satellites' state 'bad' (P_{b1}, P_{b2}) in dependency on the azimuth separation ($\Delta\theta$) derived from the measurements and re-calculated with different channel models. For comparison, the state probabilities derived from the single-satellite measurement database are given (*measured (single-sat)*). For better visibility they are shown in the corner at $\Delta\theta = 180°$.

Another alternative to gain consistent LMS parameter sets is the use of the Lutz approach for parametrisation (Section 3.2.2). The principle is to derive the probability and mean duration of the combined states from single satellite parameters and the correlation coefficient between the satellites. The Lutz approach presented in [Lut96] parametrises a first-order Markov model for two satellites (cf. Figure 3.16, '1st-order Markov & Lutz'). In this work, a method is introduced to derive also dual-satellite parameters for a semi-Markov model with the Lutz approach. Firstly, a joint STPM is calculated by using single-satellite parameters and a correlation coefficient.[5] Next, the semi-Markov parameters are adjusted to provide the mean durations, which are given in the joint STPM (cf. Section 3.2.4). As a result, the dual-satellite parameter sets for the semi-Markov model represent the characteristics of the single satellite parameter sets (Section 3.4.1) and include additional information obtained in dual-satellite case. Consequently, no fluctuations of single satellite state probabilities are obtained for different values of $\Delta\theta$ in Figure 3.16 ('semi-Markov, logn.fit & Lutz').

To analyse a greater number of receive scenarios, Figure 3.17 shows the probabilities of combined and single satellite states (P_{bb}, $P_{\mathrm{b1}}, P_{\mathrm{b2}}$) in dependency on the azimuth separation ($\Delta\theta$) and for different elevation angle combinations (ϕ_1, ϕ_2) in the urban environment. The layout of elevation angles and azimuth separations is equal to Figure 3.15. Since different state models provide equal results in terms of state probabilities, Figure 3.17 shows two groups: the measurement results of dual-satellite scenarios (also representing the straightforward models) and the re-simulation results of Lutz-based models. The following observations can be made from Figure 3.17:

- The 'bad bad'-state probability (*measured*) strongly depends on the elevation angles

[5] As the driving direction is not analysed for dual-satellite reception, the dual-satellite parameters are derived from single-satellite parameters with driving direction $\theta \in [0°, 360°]$.

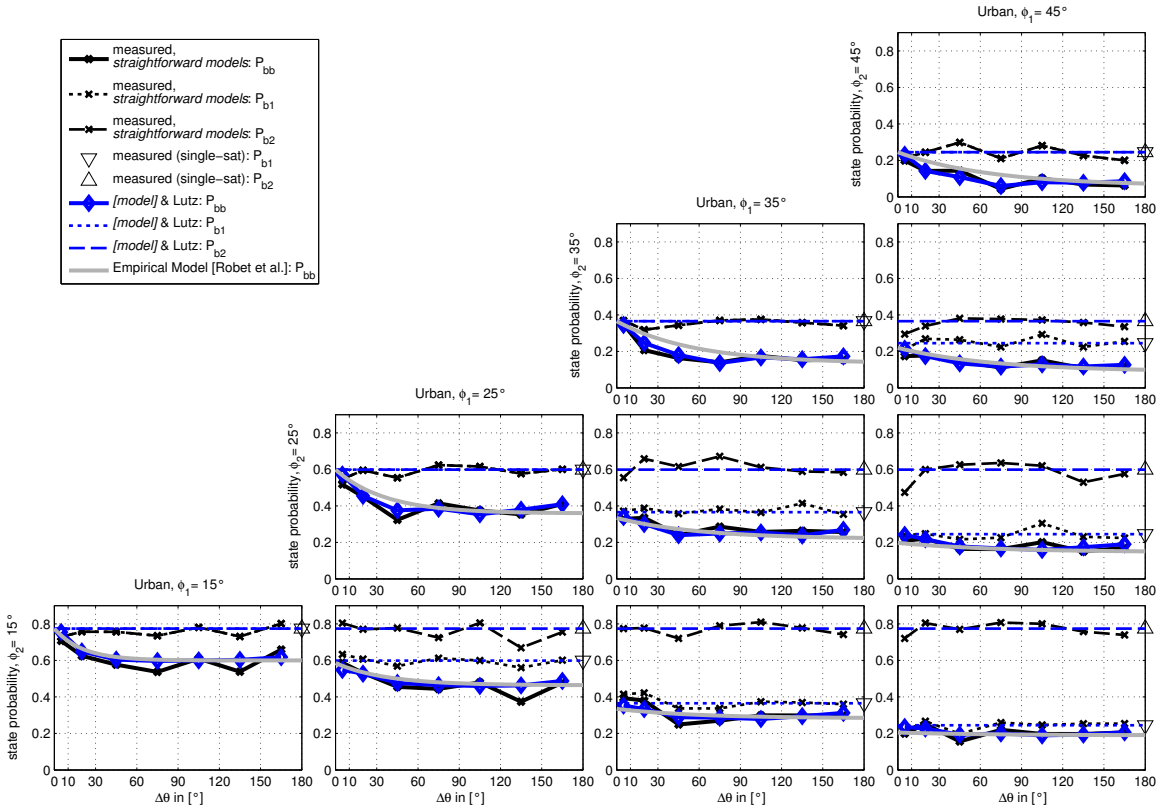

Figure 3.17.: Probabilities of the combined state 'bad bad' (P_{bb}) and of the single satellites' state 'bad' ($P_{\mathrm{b1}}, P_{\mathrm{b2}}$) in dependency on the azimuth separation for different elevation angle combinations derived from the measurements and re-calculated with different channel models. For comparison, the state probabilities derived from the single-satellite measurements are given (*measured (single-sat)*, cf. Figure 3.16). Note: in case of $\phi_1 = \phi_2$, the single-satellite results are overlaid.

ϕ of the single satellites (cf. Figure 3.13). Assuming small elevations $\phi_1 = \phi_2 = 15°$, P_{bb} is between 0.6 and 0.8 with respect to the azimuth angle separation. For the combination $\phi_1 = 45°$ and $\phi_2 = 15°$, P_{bb} is between 0.20 and 0.25. When both satellites have 45° elevation, P_{bb} is only between 0.05 and 0.20.

- P_{bb} further depends on the azimuth angle separation $\Delta\theta$. It is related to the state correlation coefficient ρ_{states} between the satellites (cf. Figure 3.15), whereas a low correlation coefficient results in a low 'bad bad'-state probability and provides therefore a high signal availability.

- A large variance of P_{bb} due to $\Delta\theta$ is seen when the elevation angle separation $\Delta\phi$ is small. In case $\Delta\phi = 0$ (both satellites have same elevation), between $\Delta\theta = 5°$ and $\Delta\theta \approx 90°$ a reduction of P_{bb} of 20% is obtained. In contrast, for $\phi_1 = 45°$ and $\phi_2 = 15°$ only a reduction of 5% is obtained from $\Delta\theta = 5°$ to $\Delta\theta \approx 90°$.

- Although for each dual-satellite receive scenario approximately 30 km measurement data is analysed, the single satellite probabilities P_{b1} and P_{b2} at a constant elevation angle have high variations of ± 0.1. On the contrary, the Lutz method provides stable results for P_{b1} and P_{b2}. A further fact, that becomes visible for the Lutz models at

constant elevation angles, is that P_{bb} is proportional to ρ_{states} (cf. Equation (B.26) from Appendix B.2.1).

- The empirical model from Robet et al. [REE92] provide plausible results as well. Due to the relation $P_{\mathrm{bb}} \sim \rho_{\mathrm{states}}$, the ratio between P_{bb} of the Lutz-based model and of the empirical model is analogue to the ratio between the measured values of ρ_{states} and of the empirical model from Figure 3.15: A high agreement is obtained for the constellation $\phi_1 = \phi_2 = 15°$. For constellations $\phi_1 = \phi_2 = 25°$ or $\phi_1 = \phi_2 = 35°$ with $\Delta\theta \approx 45°$, the probability P_{bb} of the empirical model is up to 0.1 greater than from the Lutz model and the measurements. Considering constant elevations, the empirical model provides the minimal value of P_{bb} at $\Delta\theta = 180°$, whereas from the GNSS data the minimum is found around $\Delta\theta = 90°$.

  Of course, the empirical model does not accurately represent the characteristics of the GNSS data, since it was dimensioned with data from other environments. However, the parametrisation of an LMS model for a large variety of satellite positions usually makes a merge of parameters from different measurements and/or from different environments necessary (cf. Chapter 5.3; Appendix A.3). Thus, the correlation coefficients of the empirical model are a feasible alternative to the correlation coefficients derived from GNSS measurements.

Mean State Durations for Dual-Satellite Reception

The mean durations of the state 'bad bad' ($\bar{D}_{\mathrm{bb}}$) as well as the mean 'bad' durations of the individual satellites ($\bar{D}_{\mathrm{b1}}, \bar{D}_{\mathrm{b2}}$) are depicted in Figure 3.18. Similar to Figure 3.17, measurement results for dual-satellite scenarios (representing also results of straightforward algorithms) as well as results for Lutz-based algorithms are presented. Additionally, the results of the modified Lutz approach (cf. Section 3.2.3) are shown. It allows an accurate re-simulation of the measured mean durations for the combined state 'bad bad', whereas the characteristics of the single satellite states are unchanged. The modified Lutz approach is not applicable for each receive scenario (cf. Section 3.2.3, *case 1*, *case 2*, *case 3*), which leads to gaps in Figure 3.18.

The mean duration of the single satellites for Lutz-approaches in Figure 3.18 equals in all cases the mean durations from Figure 3.14 for GNSS data with driving direction 0°- 360°.

The results show that for small azimuth separations the mean duration of 'bad bad' is close to the mean duration of 'bad' from the single satellite with the higher elevation. In worst case (15° elevation, small azimuth separation) the 'bad bad' duration is about 150 metres in urban environments. If only one of the satellites has a higher elevation, the mean duration of 'bad bad' is significantly lower. Values are $\bar{D}_{\mathrm{bb}} \approx 50\,\mathrm{m}$, $\bar{D}_{\mathrm{bb}} \approx 40\,\mathrm{m}$, and $\bar{D}_{\mathrm{bb}} \approx 20\,\mathrm{m}$ for elevations 25°, 35°, and 45°, respectively.

A conspicuous fluctuation is seen for the measured single satellite durations $\bar{D}_{\mathrm{b2}}$ at $\phi_2 = 15°$. The reason is on the one hand less available measurement data for the 'bad' state due to longer state lengths. On the other hand the great influence of driving directions to the mean duration at low elevation angles may affects the results. Please remember that the dual-satellite measurements include data from driving directions between 0° and 360°. However,

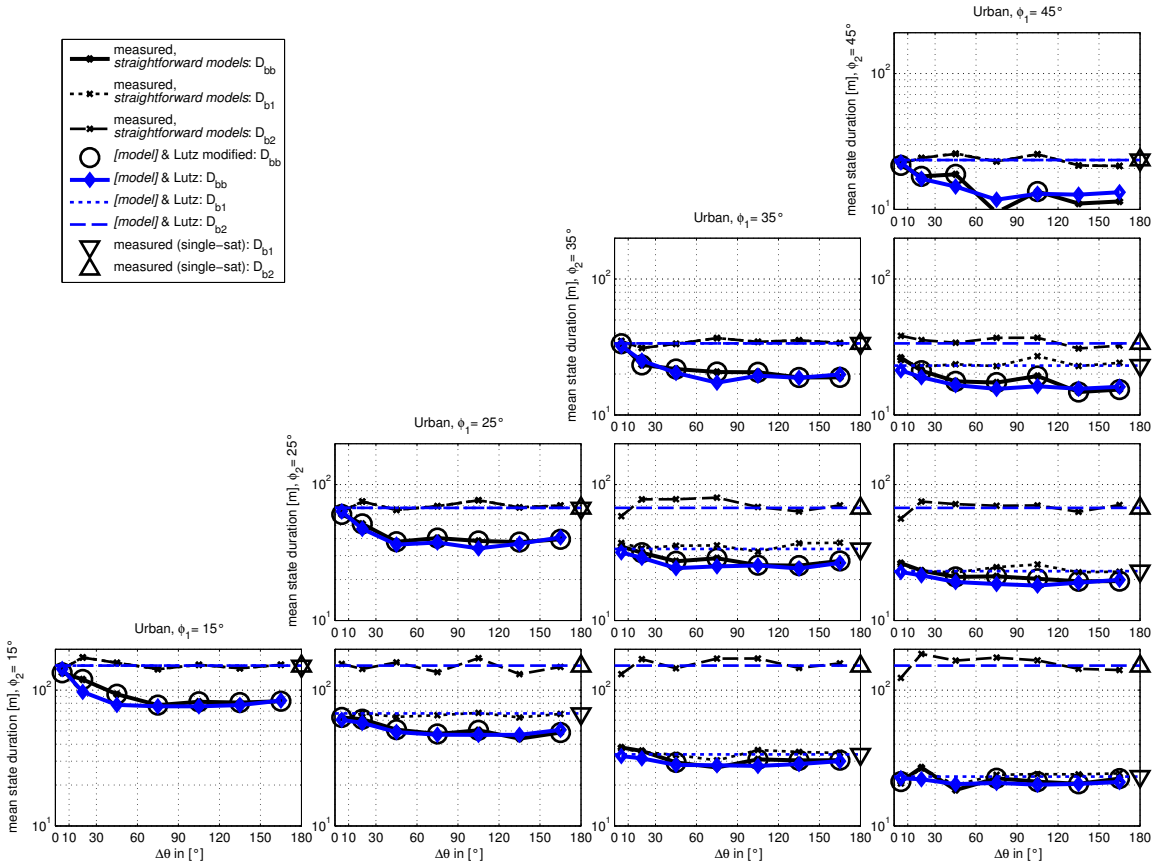

Figure 3.18.: Mean durations of the combined state 'bad bad' ($\bar{D}_{\mathrm{bb}}$) and of the single satellites' state 'bad' ($\bar{D}_{\mathrm{b1}}, \bar{D}_{\mathrm{b2}}$) in dependency on the azimuth separation for different elevation angle combinations derived from the measurements and re-calculated with different channel models. For comparison, the mean 'bad'-state probabilities from the single-satellite measurement database are depicted at position $\Delta\theta = 180°$. In case of $\phi_1 = \phi_2$, the single-satellite results are overlaid.

the actual driving direction within the receive scenarios could not be considered as equally distributed in that range.

The empirical model from Robet et al. [REE92] is not further regarded in Figure 3.18 and in subsequent state duration analyses, since it provides no information about state durations.

Evaluation of State Duration Modelling for Dual-Satellite Reception

While several state models provide equal results in terms of state probabilities and mean state durations (e.g. they re-simulate exactly the measurements), their performance in terms of state duration modelling is quite different. Therefore, an evaluation of state duration modelling is performed for dual-satellite and single-satellite reception by using the following algorithms:

- first-order Markov & Lutz
- semi-Markov, logn. fit

- semi-Markov, logn. fit (corrected)
- semi-Markov, logn. fit & Lutz modified
- **semi-Markov, logn. fit & Lutz, empirical:** Based on the availability of measurement data for numerous dual-satellite constellations, an empirical add-on is developed for the model *semi-Markov, logn. fit & Lutz*. A detailed description is found in next Section 3.4.3.
- semi-Markov, piecewise exponential fit
- semi-Markov, no fit (represents also the results of *partial dynamic Markov*)

First of all, the state duration evaluation is exemplarily demonstrated in Figure 3.19 for one receive scenario. It shows the duration statistics of the 'bad bad'-state (left) and of the 'bad'-state (right) from measurements and after re-simulation with a four-state semi-Markov model (lognormal fit) for dual-satellite reception. For comparison, the 'bad'-state duration is re-simulated with a two-state semi-Markov model (lognormal fit) for single-satellite reception. It is obtained that the dual-satellite algorithm (using four states) and the single-satellite algorithm (using two states) provide different statistics for the 'bad'-state. A quality measure of the state models performance is the MSE between the measured and re-modelled SDPDF (cf. Equation (3.35)). Clearly, the MSE of the 'bad'-state is smaller after re-simulation with the single-satellite model, as the curve-fit is directly applied on the 'bad'-state statistic. The only state model which is able to accurately re-simulate the SDPDF of the 'bad bad'-state and the SDPDF of the 'bad'-state with one state series simulation is the Nth-order Markov model (with $N \approx 500$). An accurate composition of state lengths over time is required therefore. It demonstrates that the quality of the duration modelling from dual-satellite algorithms can be evaluated also on their capability to re-simulate the single-satellite duration statistics. Thus, the evaluation based on the blockage ratio statistic (cf. Section 3.3.1) is not necessarily required.

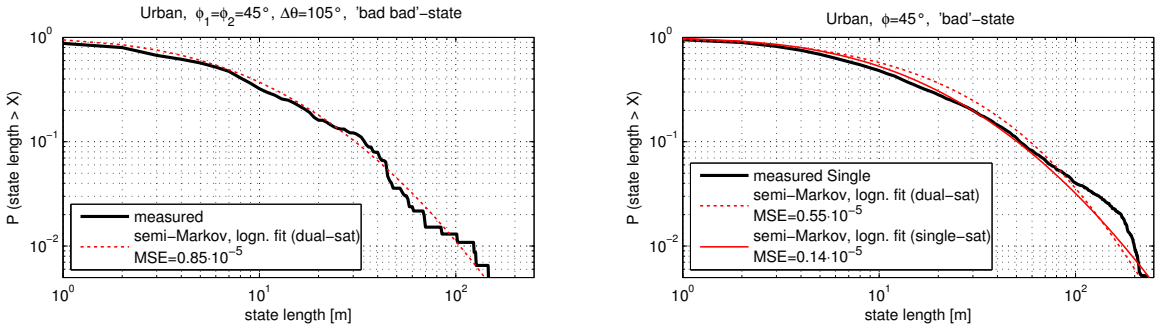

Figure 3.19.: Evaluation of state duration modelling: Left: 'bad bad'-state duration statistics (complementary CDF) of the measurements and after re-simulation with a semi-Markov model for dual-satellite reception. Right: 'bad'-state duration statistics of the measurements and after re-simulation with a semi-Markov model for dual-satellite reception as well as for single-satellite reception. Data is taken from: urban environment, elevation $\phi_1 = \phi_2 = 45°$, azimuth separation $\Delta\theta = 105°$. The quality measure of the curve-fits is the MSE between measured and re-simulated state duration statistic. Results for different state models are given in Figure 3.20 and 3.21.

Figure 3.20 shows the MSE for the 'bad bad'-state re-simulated with dual-satellite algorithms for different satellite constellations ($\Delta\theta$, ϕ_1, ϕ_2) in the urban environment. Figure 3.21 depicts their performance for the single-satellite case.

Starting with the evaluation of 'bad bad'-modelling, the following is obtained from Figure 3.20:

- State durations simulated with first-order Markov chains follow an exponential distribution. Already in Figure 3.11 it is seen that the exponential distribution doesn't fit the measured state durations in an accurate manner. Therefore, the MSEs for single- and for dual-satellite case are large when compared with other algorithms.

- Semi-Markov chains have high flexibility in state duration modelling. The MSEs in Figure 3.20 indicate that the piecewise exponential fit as well as the lognormal fit well approximate the measured state durations.

- Although a piecewise exponential function has higher flexibility in curve-fitting, the lognormal fit provides similar results. Due to the less number of lognormal parameters per SDPDF (2 lognormal parameters instead of 11 parameters for piecewise exp. fit with 4 segments, cf. Equation (3.8)), the lognormal fit is suggested as the preferred semi-Markov approximation.

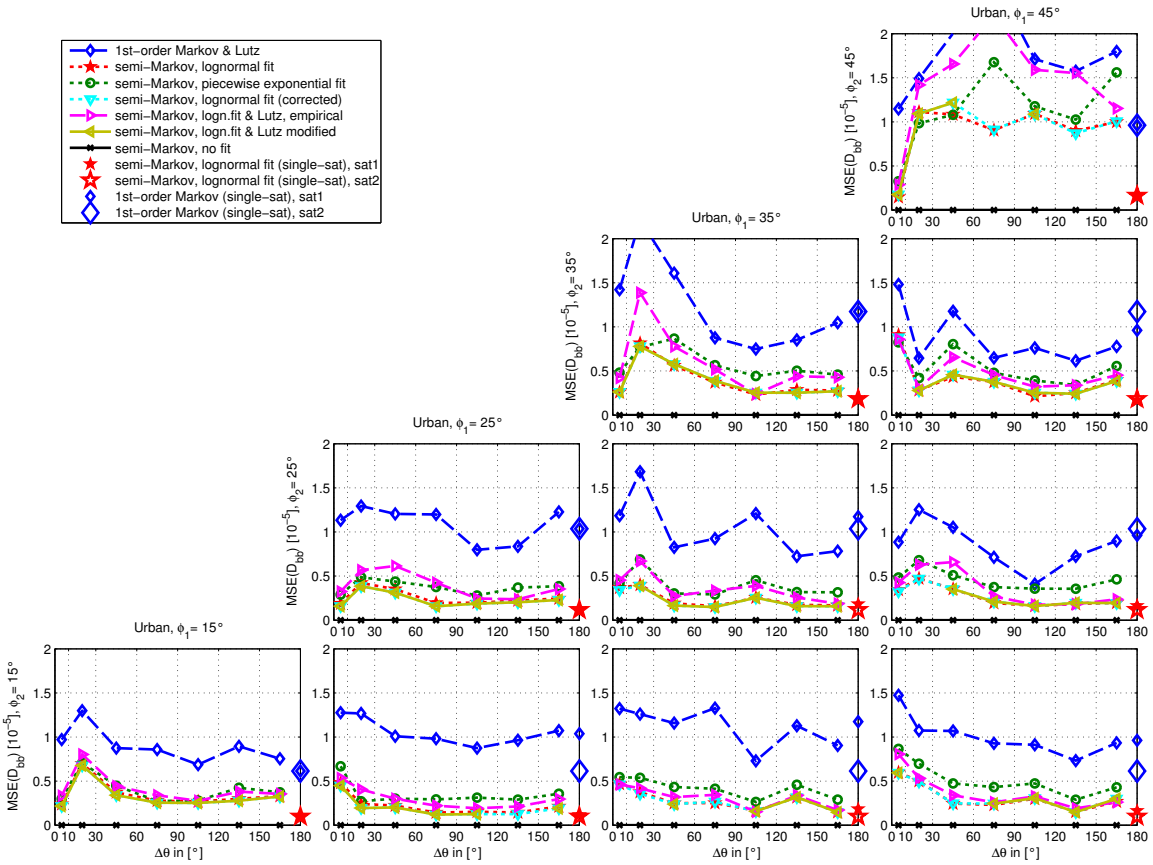

Figure 3.20.: Evaluation of the state duration fit for the 'bad bad'-state: The MSE of the state duration PDF is calculated for seven different dual-satellite state modelling approaches. For comparison, the MSEs of the 'bad'-state statistic of satellite 1 and satellite 2 are calculated for two different single-satellite models and are depicted at position $\Delta\theta = 180°$.

- The lognormal parameters are modified for the semi-Markov algorithms: '...logn. fit (corrected)', '...logn. fit & Lutz, empirical', '...logn. fit & Lutz modified'. In terms of the state 'bad bad', this correction of lognormal parameters has no noticable influence on the quality of the SDPDF curve-fit, when compared with to the original lognormal fit ('semi-Markov, lognormal fit').

- Comparing dual-satellite with single-satellite results in Figure 3.20, a lognormal fit approximates the 'bad' state better than the 'bad bad' state. Nevertheless, a curve-fit with more flexibility and a higher number of parameters is minor feasible for dual-satellite scenarios.

The evaluation of the 'bad'-state duration modelling of a single satellite with a dual-satellite state algorithm (Figure 3.21) leads to following conclusions:

- For semi-Markov models, the MSEs for the 'bad'-state vary for different azimuth separations. It is due to the fact that the re-simulated 'bad'-duration statistic of a satellite with elevation ϕ changes with the azimuth angle separation to a second satellite. In contrast, the model 'first-order Markov & Lutz' provides always the same duration

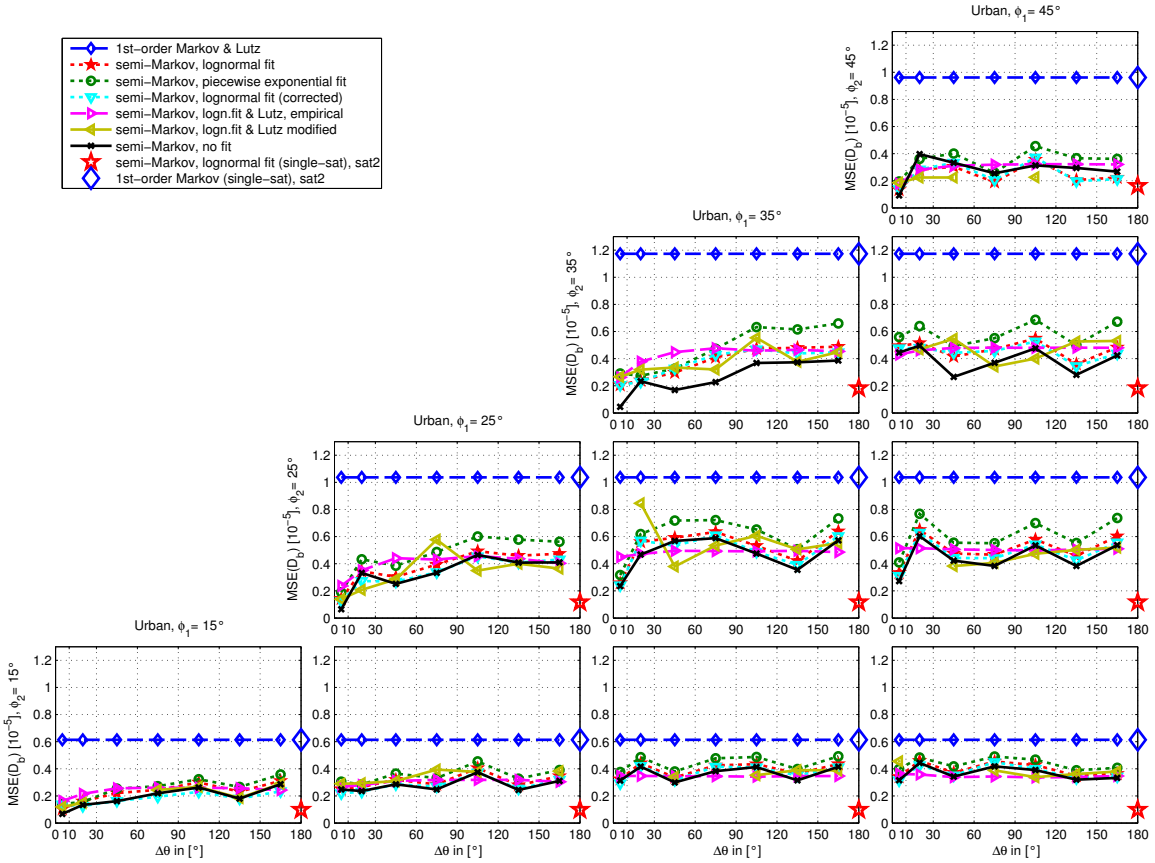

Figure 3.21.: Evaluation of the state duration fit for the 'bad'-state: The MSE of the state duration PDF for satellite 2 is calculated with seven dual-satellite algorithms. For comparison, the MSEs for two single-satellite algorithms are depicted at position $\Delta\theta = 180°$.

statistic for a satellite at a constant elevation. However, this state duration statistic is not realistic.

- In general, a semi-Markov model dimensioned for single-satellite reception re-simulates the 'bad'-state statistic more accurate than a semi-Markov model dimensioned for two satellites (Same holds for dynamic Markov models). It is independent from the curve-fit.

- The dual-satellite model 'semi-Markov, no fit' has similar performance as 'semi-Markov, logn. fit' in terms of single-satellite state duration modelling. Certainly it is true that 'semi-Markov, no fit' describes accurately the duration statistics of combined states, but the composition of the combined states in time is not better described than from approximated models.

- Semi-Markov models combined with Lutz have similar performance as 'semi-Markov, logn. fit' (dual-sat. model) for single-satellite case. It indicates, that a combination with the Lutz approach can be applied without performance deficits. Further on, a correction of mean joint durations (*semi-Markov, logn. fit & Lutz modified*) doesn't improve the state duration modelling for single-satellite case.

3.4.3. Empirical Analysis of Lognormal Parameters

Previous results show, that a dual-satellite semi-Markov model with lognormal fit well approximates the combined and single satellite SDPDFs. Therefore, two parameters (μ_{Dur} and σ_{Dur}) per joint state duration statistic are required. However, to gain model parameter sets for different environments and satellite constellations, thousands of state duration statistics have to be analysed.

To avoid a lognormal parameter extraction for that amount of dual-satellite receive scenarios, an alternative is the estimation of lognormal parameters for combined states from single-satellite parameters. For this purpose, the Lutz approach provides information about the combined state probabilities P_{joint} and makes an estimation of mean state durations $\bar{D}_{\mathrm{joint}}$ for dual-satellite reception. To estimate the lognormal parameters for joint state durations, Figure 3.22 shows the dependency of μ_{Dur} on the mean state duration, as derived from all obtained joint states and dual-satellite receive scenarios from GNSS measurements.

It is seen that the relation between μ_{Dur} and $\bar{D}$ can be well approximated by a logarithmic function:

$$\mu_{\mathrm{Dur}} = r_1 \cdot \ln(\bar{D}) + r_0 \tag{3.36}$$

with $r_1 = 6.48$ and $r_0 = 0.75$.

The great advantage becomes clear as all required parameters for a dual-satellite semi-Markov model can be estimated from single-satellite parameter set and a correlation coefficient. Of course this parameter extraction is already possible with the Lutz approach in combination with first-order Markov model. However, results in Figure 3.20 and Figure 3.21 show that the duration modelling is significantly improved by the new algorithm *'semi-Markov, logn. fit & Lutz, empirical'*.

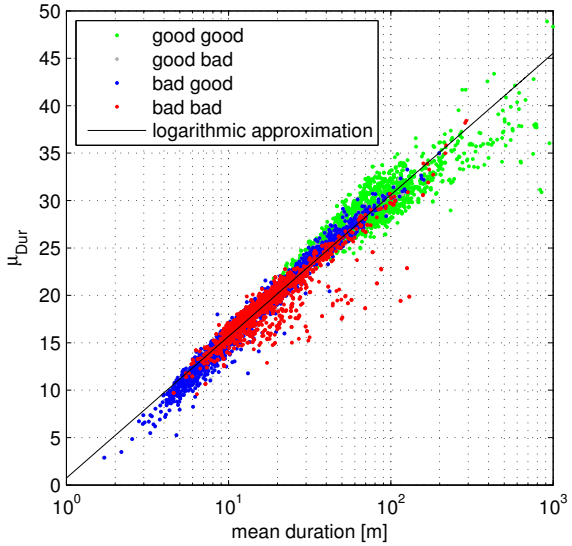

Figure 3.22.: Dependency of lognormal parameter μ_{Dur} to the mean joint state duration $\bar{D}$. These lognormal parameters are derived for all states from various dual-satellite receive scenarios (environment, ϕ_1, ϕ_2, $\Delta\theta$) from GNSS measurements. The dependency between μ_{Dur} and $\bar{D}$ can be well approximated by a logarithmic expression.

The parameters for this *'semi-Markov, logn. fit & Lutz, empirical'* model can be extracted with following procedure:

1. The STPM for a single satellite is given by:

$$\mathbf{P}_{\mathrm{trans}}^{sat} = \begin{bmatrix} 1-(1/\bar{D}_{\mathrm{g}}) & 1/\bar{D}_{\mathrm{g}} \\ 1/\bar{D}_{\mathrm{b}} & 1-(1/\bar{D}_{\mathrm{b}}) \end{bmatrix} \tag{3.37}$$

   The mean durations for 'good' and 'bad' state can be derived from the single satellite parameter sets with $\bar{D} = \exp[\mu_{\mathrm{Dur}}/K + 0.5(\sigma_{\mathrm{Dur}}/K)^2]$, where $K = 20\log\mathrm{e}$ and $\{\mu_{\mathrm{Dur,g}}, \sigma_{\mathrm{Dur,g}}, \mu_{\mathrm{Dur,b}}, \sigma_{\mathrm{Dur,b}}\} = f(env, \phi, \theta)$ (env denotes the environment type). These parameter sets are given in Table C.2 and Table C.3 in Appendix C.

2. A correlation coefficient between two satellites is found in the dual-satellite parameter sets (Table C.4) in the form $\rho_{\mathrm{states}} = f(env, \phi_1, \phi_2, \Delta\theta)$.

3. Considering two satellites with $\mathbf{P}_{\mathrm{trans}}^{sat1}$, $\mathbf{P}_{\mathrm{trans}}^{sat2}$ and correlation coefficient ρ_{states}, the correlation matrix $\mathbf{P}_{\mathrm{trans}}^{Lutz}$ is calculated according to the Lutz approach (Appendix B.2.2).

4. From $\mathbf{P}_{\mathrm{trans}}^{Lutz}$ the mean durations of state i are estimated with

$$\bar{D}_i = \frac{1}{1-p_{ii}} \qquad i \in \{\mathrm{gg}, \mathrm{gb}, \mathrm{bg}, \mathrm{bb}\} \tag{3.38}$$

5. The lognormal parameter $\mu_{\mathrm{Dur},i}$ of state i is calculated with the empirical expression:

$$\mu_{\mathrm{Dur,i}} = 6.48 \cdot \ln(\bar{D}_i) + 0.75 \tag{3.39}$$

6. After calculating $\sigma_{\mathrm{Dur},i}$ by taking the relation

$$\sigma_{\mathrm{Dur},i} = \sqrt{2K(K \ln \bar{D}_i - \mu_{\mathrm{Dur},i})}\,, \tag{3.40}$$

   with $K = 20 \log \mathrm{e}$, the lognormal parameters for all joint states are available.

7. Finally, the diagonal elements of $\mathbf{P}_{\mathrm{trans}}^{Lutz}$ are set to zero and the STPM is normalised such that the sum of each row equals 1. So we get the semi-Markov transitions $\mathbf{P}_{\mathrm{trans}}^{semiM}$.

The resulting parameter set is valid for a certain constellation of $[env, \phi_1, \phi_2, \theta_1, \theta_2]$, where the driving direction of the vehicle is included as well.

To get dual-satellite parameters independent from the vehicles driving direction, the driving direction θ must be ensured to be uniformly distributed within $[0, 2\pi)$ while extracting the single-satellite parameters $f(env, \phi, \theta)$.

3.4.4. Interpolation of State Model Parameters

For single-satellite reception, state model parameters (μ_{Dur}, σ_{Dur}) are derived from five environment types for different elevation intervals with centre values $\phi \in \{15, 25, 35, 45, 55, 65, 75, 85\}^\circ$ from GNSS measurement data. To consider dual-satellite reception, the *'semi-Markov, logn. fit & Lutz, empirical'* model requires a correlation coefficient ρ_{states} which is available for five environments, for combinations of elevations ϕ_1 and ϕ_2 with $\phi_1, \phi_2 \in \{15, 25, 35, 45, 55, 65, 75, 85\}^\circ$, and for different intervals of the azimuth angle separation $\Delta\theta$ with centre values $\Delta\theta \in \{5, 20, 45, 75, 105, 135, 165\}^\circ$. For some applications of the LMS model, such as the performance comparison between different multi-satellite constellations in Chapter 6, it would be useful to have model parameters for a finer gradation of satellite positions. This can be facilitated by interpolation.

In case of a single-satellite model, a parameter interpolation over the elevation ϕ is suitable. Important characteristics for a single-satellite state model are the probability P and the mean duration $\bar{D}$ of 'good' and 'bad' state. The mean state duration is related to the lognormal parameters by (cf. Equation (3.7))

$$\ln \bar{D} = \frac{1}{8.686}\mu_{\mathrm{Dur}} + \frac{1}{150.889}\sigma_{\mathrm{Dur}}^2\,. \tag{3.41}$$

It is seen that $\ln \bar{D}$ is proportial to μ_{Dur} and σ_{Dur}^2. Thus, to achieve smoothed curves of characteristics P and $\bar{D}$ in dependency on ϕ, a linear interpolation of μ_{Dur} and σ_{Dur}^2 over ϕ is found to be appropriate. It results in an exponentially interpolated mean duration $\bar{D}$ (i.e. a linear interpolation of $\ln \bar{D}$), as indicated in Figure 3.23 for the urban environment.

The parameters μ_{Dur} and σ_{Dur}^2 at elevation ϕ are determined with

$$\mu_{\mathrm{Dur}}(\phi) = \mu_{\mathrm{Dur},\phi_m} + \frac{\mu_{\mathrm{Dur},\phi_n} - \mu_{\mathrm{Dur},\phi_m}}{\phi_n - \phi_m}(\phi - \phi_m) \tag{3.42}$$

$$\sigma_{\mathrm{Dur}}^2(\phi) = \sigma_{\mathrm{Dur},\phi_m}^2 + \frac{\sigma_{\mathrm{Dur},\phi_n}^2 - \sigma_{\mathrm{Dur},\phi_m}^2}{\phi_n - \phi_m}(\phi - \phi_m)\,, \tag{3.43}$$

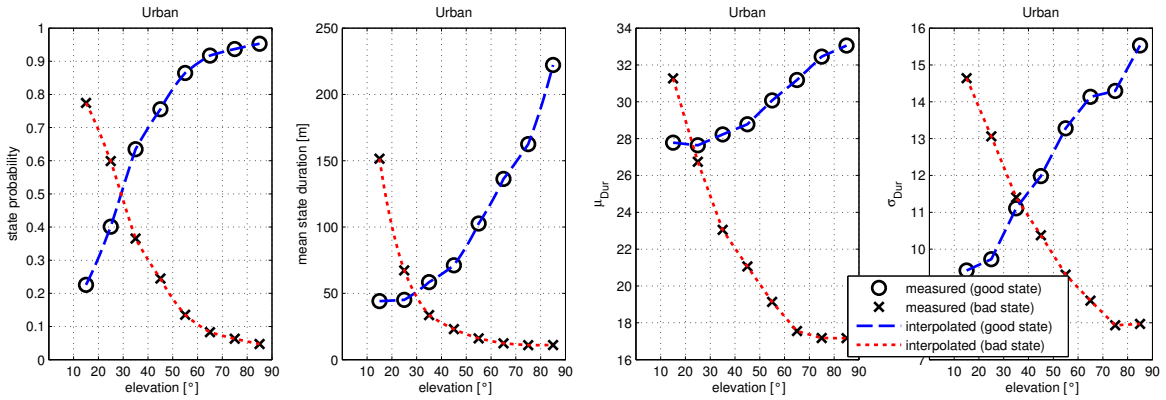

Figure 3.23.: To refine the state model parameter set with respect to the elevation ϕ, a linear interpolation of the lognormal parameters μ_{Dur} and σ^2_{Dur} over ϕ is proposed. It results in an exponential interpolation of the mean state duration $\bar{D}$. The state probabilities P depend on $\bar{D}$.

where $\mu_{\mathrm{Dur},\phi_m}$, $\sigma_{\mathrm{Dur},\phi_m}$ and $\mu_{\mathrm{Dur},\phi_n}$, $\sigma_{\mathrm{Dur},\phi_n}$ are estimated from measurements at elevations ϕ_m and ϕ_n, respectively. After calculating $\bar{D}_{\mathrm{g}}$ and $\bar{D}_{\mathrm{b}}$ from interpolated parameters, the state probabilities for 'good' and 'bad' are determined finally with

$$P_{\mathrm{g,b}} = \frac{\bar{D}_{\mathrm{g,b}}}{\bar{D}_{\mathrm{g}} + \bar{D}_{\mathrm{b}}} \,. \tag{3.44}$$

To refine the model parameters for dual-satellite reception, a joint linear interpolation of the state correlation coefficient ρ_{states} over three dimensions ϕ_1, ϕ_2, and $\Delta\theta$ is proposed (=trilinear interpolation). It is demonstrated exemplarily in Figure 3.24 for the constellation $\phi_1 = 35°$, $\phi_2 = 32°$, and $\Delta\theta = 35°$ in the urban environment.

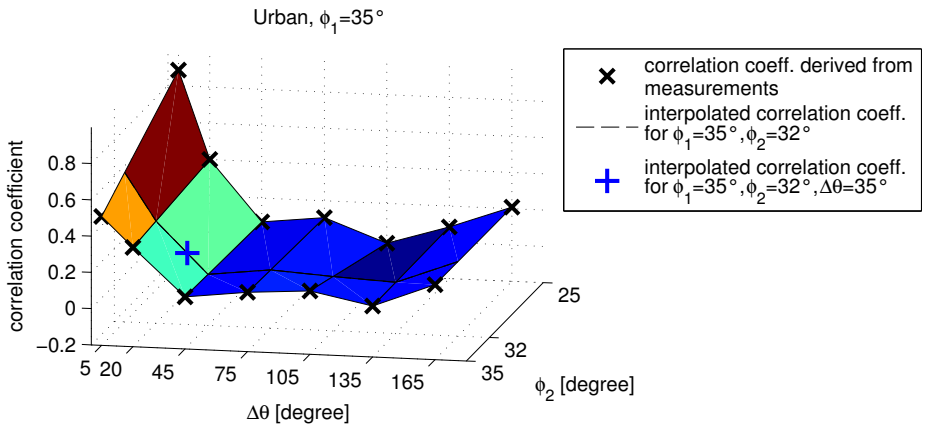

Figure 3.24.: A trilinear interpolation of the state correlation coefficient ρ_{states} over the dimensions ϕ_1, ϕ_2, and $\Delta\theta$ is used to determine ρ_{states} for the constellation $\phi_1 = 35°$, $\phi_2 = 32°$, and $\Delta\theta = 35°$. For better visualisation, this interpolation is only bilinear and ϕ_1 is constant.

3.4.5. Conclusions on Dual-Satellite State Modelling

Dual-satellite reception depends on the kind of the environment (env), the elevation angle of each satellite (ϕ_1, ϕ_2), and the azimuth of each satellite relative to the driving direction (θ_1, θ_2). In this section different state models are compared to cope with the high number of dual-satellite scenarios.

A widely accepted approach is the Lutz model which is based on first-order Markov chains. The Lutz model accurately describes state probabilities and mean durations of two individual satellites, as well as the correlation coefficient between them. Due to the low complexity, it is easy to parametrise for different combinations of env, ϕ_1, ϕ_2, and $\Delta\theta$. However, a weakness of the Lutz model is the capability of correct state duration modelling. For the optimisation of physical layer and link layer parameters for satellite broadcasting systems with high QoS requirements it has some limitations, as it describes system blockage lengths or line-of-sight durations with insufficient accuracy.

Semi-Markov models and dynamic Markov models accurately describe the state durations of the LMS propagation channel. Due to the large number of parameters, such models without any approximation are not feasible for the application for dual-satellite receive scenarios. To reduce the complexity, two variants of SDPDF approximations are analysed: a piecewise exponential fit and a lognormal fit. It has been shown that both approximations describe well the state duration distributions. Further on, the curve-fits can be modified such that measured state probabilities and mean durations of single and combined states are accurately re-simulated. Due to the smaller number of required parameters, the lognormal distribution is the preferred curve-fit for the joint SDPDFs.

It has been shown that measurement data from different dual-satellite scenarios can not provide stable results for single-satellite reception. In order to provide consistent model parameters, a combination of a semi-Markov model with the Lutz approach is introduced. Parameters for dual-satellite reception are derived from single-satellite parameters, a correlation coefficient for dual-satellite scenarios, and an empirical expression. The result is denoted **semi-Markov, logn. fit & Lutz, empirical** model, which accurately re-simulates the state probabilities and mean durations of the single satellites, the correlation coefficient between the satellites, and approximates well the state duration distribution of single satellite states and of combined states.

3.5. On Channel State Modelling for Multi-Satellite Systems

The straightforward method to realise a multi-satellite model is to parametrise a multi-state model including all permutations of single satellite states, such as 'good good good', 'good good bad', 'bad bad bad' (cf. Section 3.2.1). Assuming two states per satellite, a three-satellite constellation is thus described by eight joint states. The performance of a 'straightforward' state model for three satellites is analogue to the dual-satellite case: a first-order Markov model accurately describes the state probabilities and mean state durations of single and joint states; a dynamic Markov model additionally describes accurately the joint SDPDFs (cf. Table 3.1). However, the parameters for a three-satellite model according to the straightforward method can only be derived, if a corresponding joint state sequence with eight states is available. As the state parameters depend on the environment type, the elevation angle of each satellite and the azimuth separation between the satellites, a straightforward parametrisation of a three-satellite model from RF measurement data including a suitable set of satellite positions on the hemisphere is not feasible in practice.

A solution for that parametrisation problem is to use the *Master-Slave* concept for multi-satellite modelling. Within Master-Slave it is assumed that each slave satellite depends only on a master satellite, whereas the correlation between the slaves is not described. Possible implementations for the concept Master-Slave with two satellites, i.e. one master and one slave, are described in Section 3.2.5. A Master-Slave constellation with three satellites is shown in Figure 3.25. It is built of two independent dual-satellite channels, which parameters are available in the dual-satellite state database. Thus, Master-Slave allows a state series generation for arbitrary constellations of three satellites.

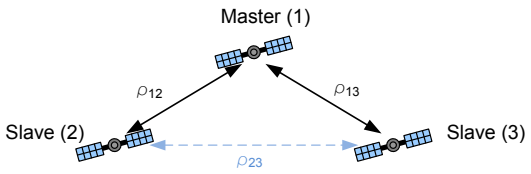

Figure 3.25.: Master-Slave concept for three-satellite modelling. The slave satellites are modelled according to the correlation to one master satellite, while neglecting the correlation between the slave satellites. The Master-Slave concept has advantages in terms of model parametrisation compared to the conventional approach, where each individual correlation is described.

It is not surprising that ignoring the correlation between the slaves could be a reduction of relevant information in case of multi-satellite modelling. Therefore, this section focuses on a performance analysis of Master-Slave with three satellites.

3.5.1. Exemplary Evaluation of Master-Slave With Three Satellites

Figure 3.26 shows an exemplary constellation of three satellites including correlation coefficients as obtained during SDARS measurements from the project MiLADY (cf. Appendix A). Since the Master-Slave concept only considers the correlations between the master and slaves, the simulation results depend highly on the definition of the master satellite. For this purpose, two mappings (Mapping 1 and Mapping 2, as shown in Figure 3.26) are defined with

different positions of master and slave satellites. For these two mappings Figure 3.27 shows re-simulation results of a Master-Slave approach in terms of correlation coefficients, state probabilities and mean state durations. The approach 'ASTM-MT with Lutz parametrisation' is selected as Master-Slave realisation (cf. Section 3.2.7). For comparison, the results of a first-order Markov model (using a 8×8 STPM for 8 joint states) are also presented in Figure 3.27.

It is obtained that the first-order Markov model allows an accurate description of correlation coefficients between all satellites, of state probabilities, and of mean state durations for single satellites states and combined states. The Master-Slave algorithm ASTM-MT is based on the first-order Markov model as well (i.e. the conditional transition probabilities of the slaves are modelled with first-order Markov chains). The result is that for Mapping 1 and Mapping 2 the state probabilities of the individual satellites, the correlation coefficients between master and slaves, and the mean state durations of the individual satellites are modelled accurately.

Slaves are modelled independently within Master-Slave. The correlation coefficient between the slaves ρ_{slaves} depends on the individual correlation coefficients between master and slaves (cf. Equation (B.74) in Appendix B.3) and minor on the applied Master-Slave realisation.

Mapping 1 is defined such that the correlation between the slaves is low (with $\rho_{\text{slaves}} = \rho_{23} = 0.06$). The larger correlation coefficients between master and slaves ($\rho_{12} = 0.15$ and $\rho_{13} = 0.40$) provide some correlation of the slaves as well. Thus, in Mapping 1 the correlation ρ_{slaves}, and consequently the joint state probabilities ('good good good',...,'bad bad bad') are remodelled with high accuracy.

In Mapping 2 the correlation between the slaves is high (with $\rho_{\text{slaves}} = \rho_{13} = 0.40$). Due to small correlation coefficients between the master and the slaves ($\rho_{12} = 0.15$, $\rho_{23} = 0.06$), ρ_{slaves} after remodelling is approx. zero and deviates strongly from the measurements. For the application of system planning it should be noted that in case of describing an insufficient correlation a higher diversity gain for the multi-satellite constellation will be predicted. Hence, Mapping 2 suggests a lower probability of the combined state 'bad bad bad' than obtained from measurements. The corresponding probability error is $\Delta P_{\text{bbb}} = 0.0247$ in this example, which falsifies the signal statistics of satellite diversity by several dB (cf. also Chapter 5.2). Such a modelling error should be avoided. A solution to minimise the Master-Slave error is an appropriate definition of master and slave satellites, which is focused in Section 3.5.2 and Section 3.5.3.

The mean duration of the single satellites are accurately re-modelled with the selected Master-Slave approach 'ASTM-MT with Lutz parametrisation'. It holds for both mappings. For the mean durations of the joint states some deviations are seen with respect to the measurements for Mapping 1 and Mapping 2. The advantage of the appropriate mapping (Mapping 1) is not seen for mean joint durations. As the Master-Slave implementation already does not accurately describe the mean joint durations of a dual-satellite constellation (it is due to the Lutz approach, cf. Section 3.3), it does not work for three satellites.

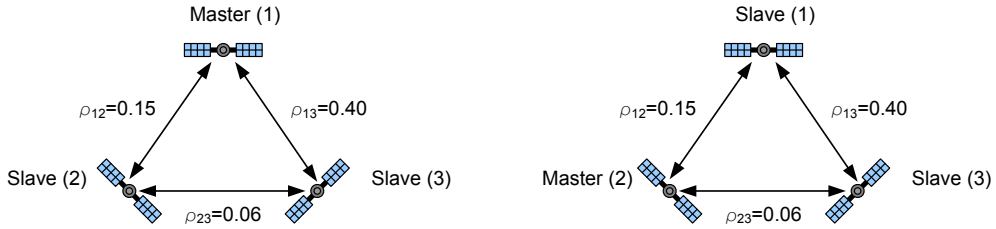

Figure 3.26.: Left: Appropriate mapping of a three-satellite constellation for the Master-Slave approach (Mapping 1: master is on satellite position 1) – the correlation between the slaves is low. Right: Inappropriate mapping of the three-satellite constellation (Mapping 2: master is on satellite position 2) – the correlation between the slaves is high.

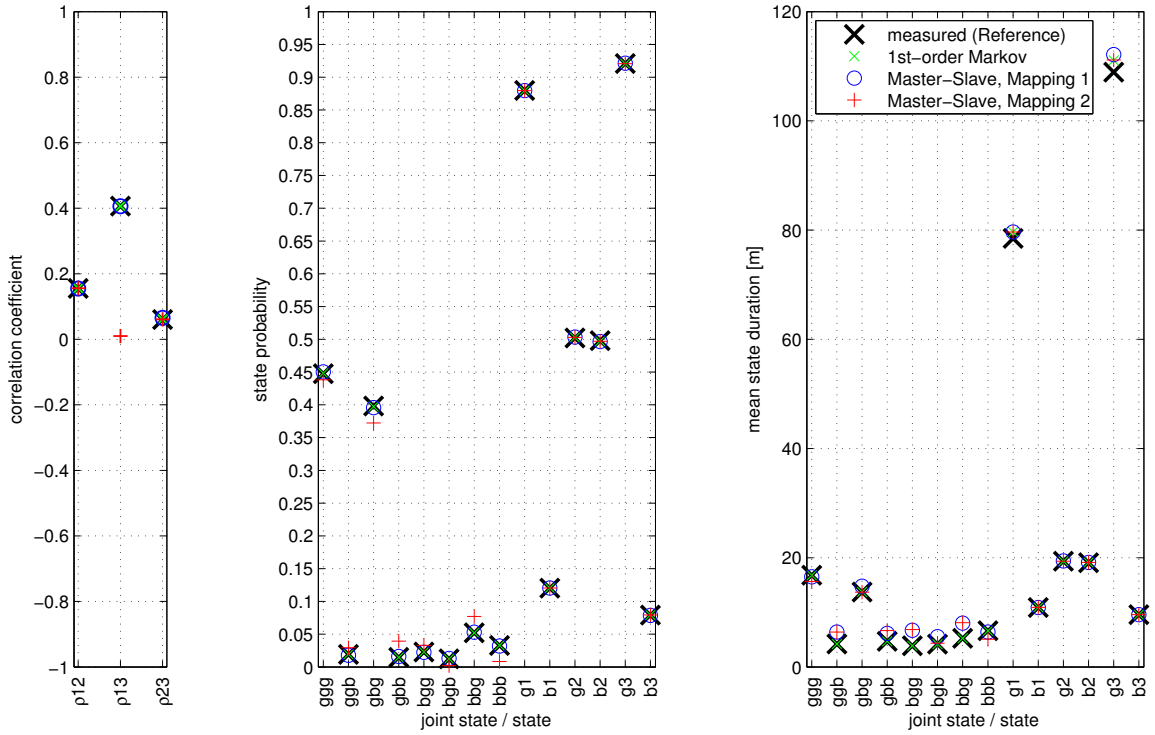

Figure 3.27.: Correlation coefficient (left), state probability (middle), and mean state duration (right) for the three-satellite constellation mappings (Mapping 1 and Mapping 2) from Figure 3.26. Data is taken from measurements of 5.4 km length in a suburban environment. Re-simulation with Master-Slave gives the following results: Clearly, the resulting correlation coefficient between the slave satellites deviates for Mapping 2. The joint state probability is modelled accurately in case of Mapping 1, while Mapping 2 shows deviations. The mean state duration shows deviations for all joint states. (notation of states: g...'good', b...'bad', ggg ... 'good good good', etc.)

3.5.2. State Probability Analysis of a Three-Satellite System

This section focuses on the performance of the Master-Slave approach for three satellites. Quality criterion is the deviation of the joint 'bad' state probability (ΔP_{bbb}), depending on the azimuth- and elevation constellation. Basis of the analysis is a three-satellite constellation according to Figure 3.28. In the sequel, the master satellite is always referred to as index 1, while indices 2 and 3 refer to the slaves. The constellation (and the mapping) is described by the elevation angles ϕ_1, ϕ_2, and ϕ_3 and the azimuth angle separations $\Delta\theta_{12}$, $\Delta\theta_{13}$, and $\Delta\theta_{23}$. According to the Master-Slave approach, only the correlations between master and slave are described (ρ_{12} and ρ_{13}), while the correlation between the slaves (ρ_{23}) is neglected. In the following, the consequences of neglecting the correlation ρ_{23} are investigated.

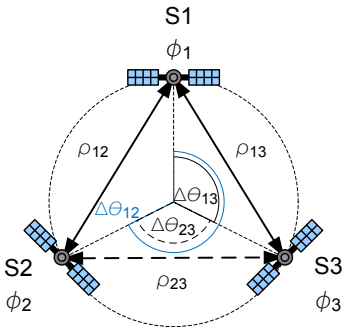

Figure 3.28.: Three-satellite constellation for the Master-Slave analysis with elevation angles ϕ, azimuth angle separations $\Delta\theta$, and correlation coefficients ρ.

Influence of the Azimuth Angle Separation

Figure 3.29 shows the state correlation coefficient ρ_{states} between **two** satellites in dependency on their azimuth angle separation $\Delta\theta$ in the urban environment with elevation angles $\phi_1 = \phi_2 = 15°$. For the subsequent analysis, the measured ρ_{states} known from dual-satellite analysis (Section 3.4.2) are extrapolated to the interval $0° \leq \Delta\theta \leq 180°$ and are extended to $\Delta\theta \leq 360°$ due to a symmetry at $\Delta\theta = 0°$ and $\Delta\theta = 180°$. This extension is appropriate as the driving direction can be assumed as equally distributed between 0° and 360°. In Figure 3.29 it is indicated that the Master-Slave approaches *Conditional Assembling Method* and *ASTM-MT* accurately re-simulate the correlation coefficients for the two-satellite constellation master & slave. This result for dual-satellite reception is basis for the three-satellite analysis of Master-Slave.

Figure 3.30 shows the correlation coefficient ρ_{23} from measurements and from Master-Slave in dependency on the azimuth angle separations $\Delta\theta_{12}$, $\Delta\theta_{13}$, and $\Delta\theta_{23}$. The calculation of the slave correlation coefficient $\rho_{\mathrm{slaves}} = \rho_{23}$ with ASTM-MT is given in Equation (B.73) in Appendix B.3.2. The correlation error is given by $\rho_{\mathrm{slaves}} = |\rho_{23,\mathrm{measured}} - \rho_{23,\mathrm{Master\text{-}Slave}}|$. Clearly, this correlation error is large when the two slaves come close to each other ($\Delta\theta_{12} \approx \Delta\theta_{13}$) – except one slave is close to the master.

Besides the state correlation, for designing mobile satellite communication systems an important parameter is the probability of all satellites being in 'bad' state, that is P_{bbb}. It char-

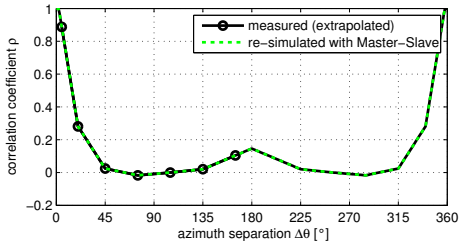

Figure 3.29.: State correlation coefficient ρ_{states} between two satellites in dependency on the azimuth angle separation $\Delta\theta$ derived from measurements and re-calculated with Master-Slave for the urban environment with $\phi_1 = \phi_2 = 15°$. The Master-Slave implementations *Conditional Assembling Method* as well as the *ASTM-MT* approach accurately re-simulate the correlation coefficients for the two-satellite constellation master & slave.

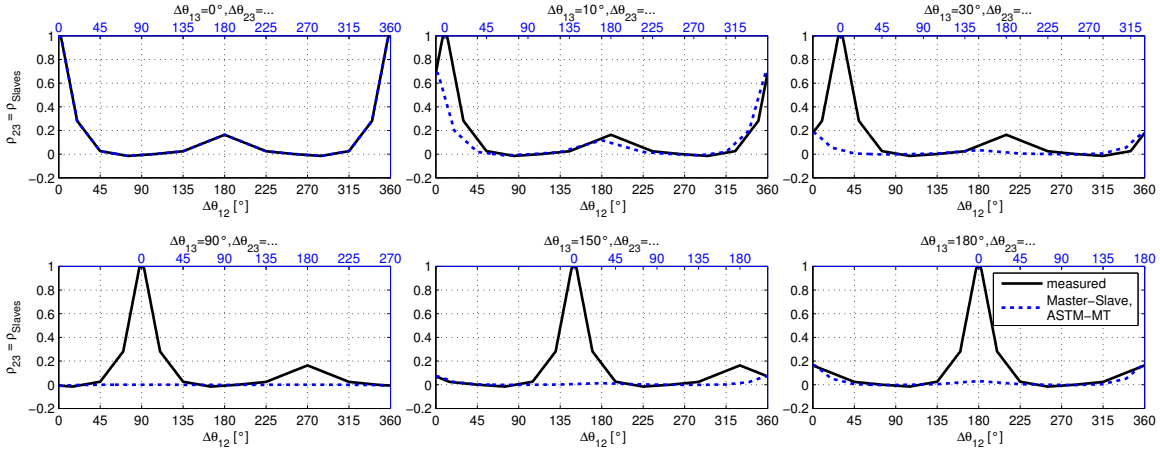

Figure 3.30.: Correlation coefficients between the slaves (ρ_{23}) in dependency on the azimuth angle separations $\Delta\theta_{12}$, $\Delta\theta_{13}$, and $\Delta\theta_{23}$ from measurements and re-calculated with Master-Slave. $\Delta\theta_{13}$ is kept constant in each subfigure. The elevation angles are $\phi_1 = \phi_2 = \phi_3 = 15°$.

acterises the probability of service unavailability for the entire system and requires special attention, therefore. In contrast to the reference value for the slave correlation $\rho_{23,\text{measured}}$, which is available in the dual-satellite measurement database, the probability $P_{\text{bbb, measured}}$ can only be analytically estimated for various satellite constellations. In Appendix B.3.3 the reference joint probability $P_{\text{bbb, reference}}$ is calculated such, that the individual state probabilities of three satellites and the correlation coefficients ρ_{12}, ρ_{13}, and ρ_{23} are fulfilled. The result is a small range of valid joint probabilities $P_{\text{bbb, min}} \leq P_{\text{bbb, reference}} \leq P_{\text{bbb, max}}$. As final reference probability $P_{\text{bbb, reference}}$ the average of minimum and maximum is selected. A quality measure of the three-satellite analysis with Master-Slave is the probability error $\Delta P_{\text{bbb}} = |P_{\text{bbb, reference}} - P_{\text{bbb, Master-Slave}}|$, where the calculation of $P_{\text{bbb, Master-Slave}}$ is given in Appendix B.3.2.

The reference probabilities and re-simulated probabilities P_{bbb} in dependency on the azimuth separation are given in Figure 3.31 for the urban environment. Additionally the minimum and maximum curves of the reference probabilities are shown. The uncertainty of the $P_{\text{bbb, reference}}$ is up to ≈ 0.05. It is seen a reference joint probability of $P_{\text{bbb}} \approx 0.8$ if all three satellites are co-located (i.e. $\Delta\theta = 0°$, $\Delta\phi = 0°$) and $P_{\text{bbb}} \approx 0.6$ if two of the three

satellites are co-located. Using the Master-Slave approach, the highest probability error of $\Delta P_{\mathrm{bbb}} \approx 0.15$ is obtained when the azimuth separation between the slaves is zero.

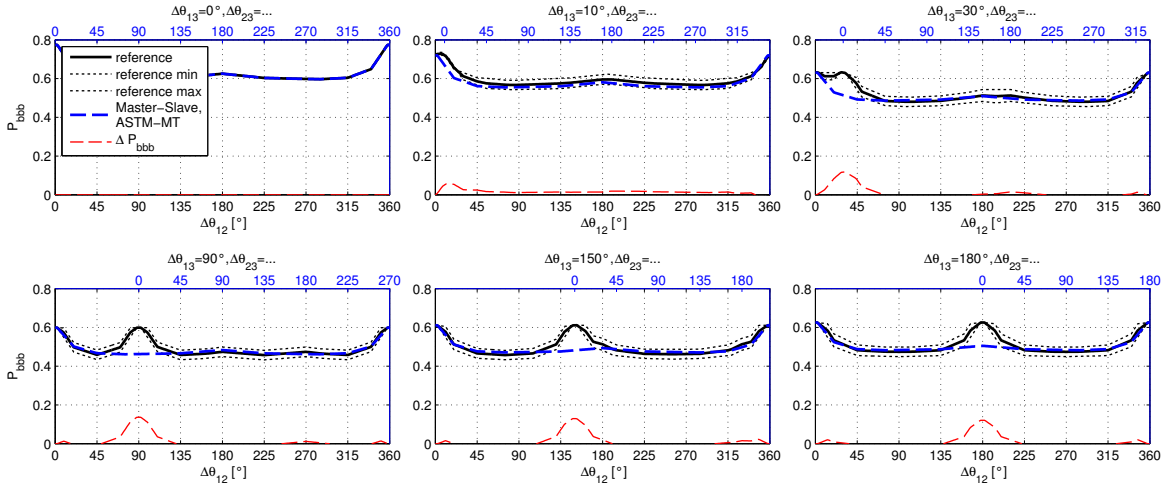

Figure 3.31.: 'bad bad bad'-state probabilities (P_{bbb}) of three satellites for different azimuth angle separations $\Delta\theta$ derived from theoretical analysis and re-modelled with Master-Slave. The elevation angles are $\phi_1 = \phi_2 = \phi_3 = 15°$, where the 'bad'-state state probability of each individual satellite is $P_{\mathrm{b}} = 0.77$ (cf. Figure 3.13, urban, measurements GNSS).

Influence of the Elevation Angles

Figure 3.32 shows the probability error ΔP_{bbb} with Master-Slave in dependency on the azimuth separations $\Delta\theta_{12}$ and $\Delta\theta_{13}$ in the urban environment for three selected elevation angle combinations of master, slave satellite 2 and slave satellite 3:

- The elevation angles of master and slaves are equal.
- The elevation angles of the three satellites are different, whereas the master is at the lowest elevation.
- The elevation angles of the three satellites are different, whereas the master is at the highest elevation.

For one elevation angle combination (one subfigure in Figure 3.32) all possible azimuth separations of a three-satellite system are displayed. The following observations are made:

- Assuming constant elevation angles (represented by one subfigure), the error ΔP_{bbb} is maximal for a low azimuth separation between the slaves, while some azimuth separation to the master exists. If the elevation angles of three satellites are equal, this error can be avoided by redefinition of the system such that the low azimuth separation is between the master and one of the slaves.
- A great performance difference is seen between the constellations $\phi_1 = 15°, \phi_2 = 25°, \phi_3 = 35°$ and $\phi_1 = 45°, \phi_2 = 45°, \phi_3 = 15°$. Although the elevation angles are equal, for the second Master-Slave elevation mapping the probability errors are significantly smaller with respect to the azimuth angle constellations. It is concluded that a high elevation of the master is beneficial.

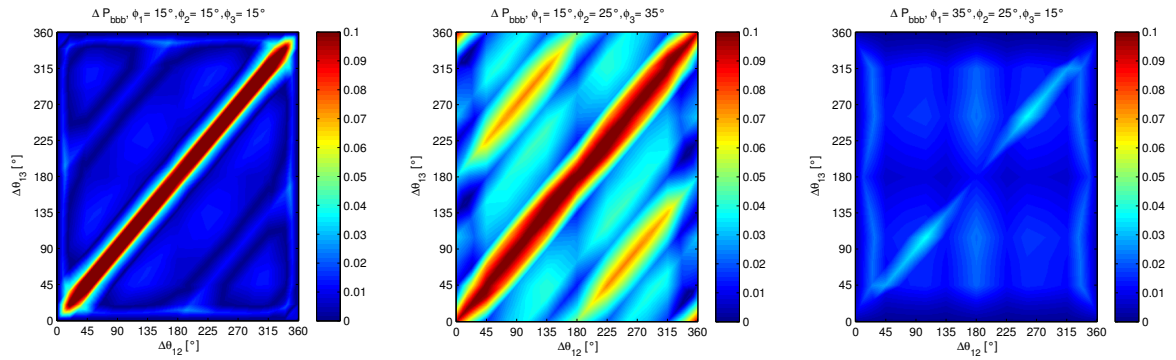

Figure 3.32.: Difference between measured and resimulated 'bad bad bad'-state probability (ΔP_{bbb}) for different elevation angles (ϕ_1, ϕ_2, ϕ_3) and azimuth angle separations ($\Delta\theta_{12}$, $\Delta\theta_{13}$). The master is satellite 1.

3.5.3. Optimal Mapping of Three-Satellite Constellations for Master-Slave

Based on the previous results, in this section a strategy is derived to find an optimal mapping of master and slave satellites. It is found that constellations are appropriate when:

- there is a small azimuth separation between master and one of the slaves ($\Delta\theta \lessapprox 10°$).
- a small azimuth separation between the slaves is avoided ($\Delta\theta \gtrapprox 30°$).
- the master has a higher elevation than the slaves.

An optimal Master-Slave mapping targets the definition of the master. The definition of the slave-order has no effect. Given the three-satellite constellation from Figure 3.28, three options to define the optimal master are relevant:

1. The optimal master is found by maximising the azimuth separation between the slaves $\Delta\theta_{\mathrm{slaves}}$ within the range $[0°; 180°]$:

$$\max_x \{\Delta\theta_{\mathrm{slaves}}(master = Sx)\} \tag{3.45}$$

with

$$\Delta\theta_{\mathrm{slaves}} = \begin{cases} \Delta\theta_{23}\,, & master = S1 \\ \Delta\theta_{13}\,, & master = S2 \\ \Delta\theta_{12}\,, & master = S3 \end{cases} \tag{3.46}$$

This method allows a fast decision if all satellites have similar elevation. However, if the satellites have some noticeable elevation separation, this mapping criterion fails.

2. The optimal master is found by detecting the constellation with lowest probability error ΔP_{bbb}.

$$\min_x \{\Delta P_{\mathrm{bbb}}(master = Sx)\} \tag{3.47}$$

3. The optimal master is found by the constellation providing the minimal correlation error between the slaves $\Delta\rho_{\mathrm{slaves}}$:

$$\min_x \{\Delta\rho_{\mathrm{slaves}}(master = Sx)\} \tag{3.48}$$

with

$$\Delta\rho_{\text{slaves}} = \begin{cases} \rho_{23} - \rho_{23,MasterSlave}\,, & master = S1 \\ \rho_{13} - \rho_{13,MasterSlave}\,, & master = S2 \\ \rho_{12} - \rho_{12,MasterSlave}\,, & master = S3 \end{cases} \tag{3.49}$$

For the two latter mapping criteria the probability error ΔP_{bbb} is analysed for different azimuth and elevation angle combinations in Figure 3.33. Using the mapping with minimised ΔP_{bbb}, it is seen that still constellations exist with a probability error of $\Delta P_{\text{bbb}} \approx 0.035$. For a great number of constellations the error is $\Delta P_{\text{bbb}} \leq 0.015$. If the correlation error is minimised, the probability errors are generally greater. There are constellations with errors $\Delta P_{\text{bbb}} \approx 0.04$ and a great part of constellations with error $\Delta P_{\text{bbb}} \approx 0.02$.

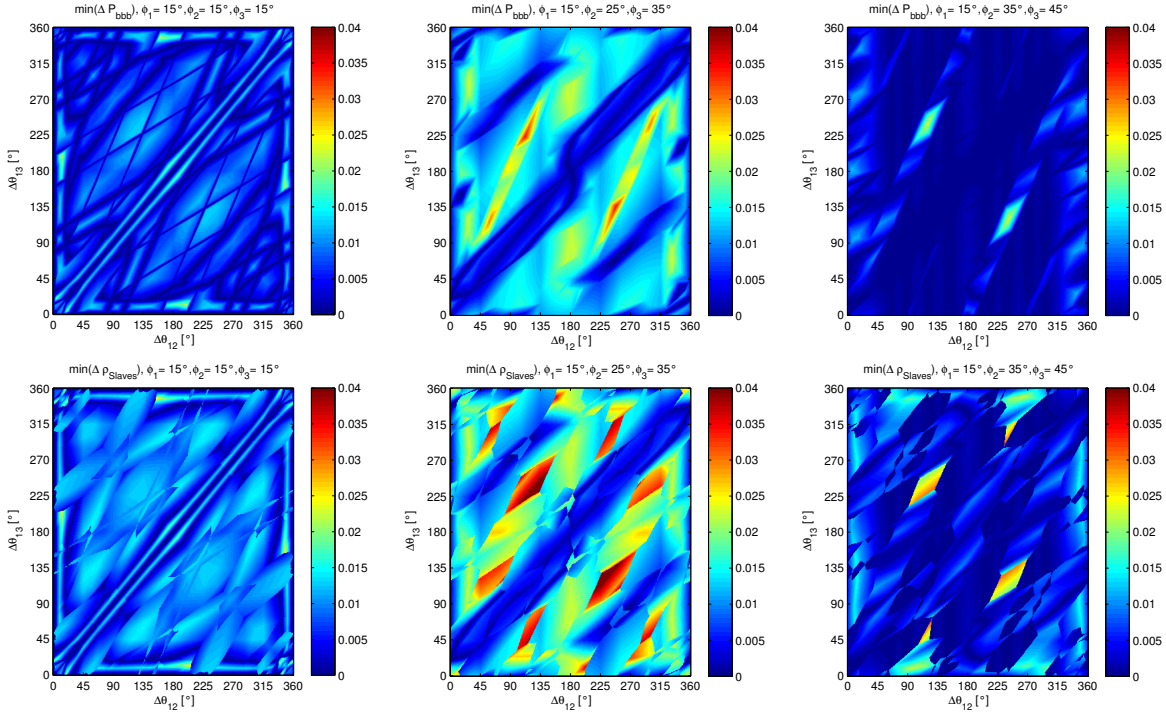

Figure 3.33.: ΔP_{bbb} from Master-Slave with optimised mapping for a three-satellite constellation in dependency on the azimuth separations $\Delta\theta_{12}$ and $\Delta\theta_{13}$ for different elevation combinations. An optimal mapping of the Master-Slave constellation is found by either minimising ΔP_{bbb} (top), or minimising $\Delta\rho_{\text{slaves}}$ (bottom). For a comparison with Figure 3.32 (results without optimised mapping), note that the color scaling is different and a further elevation combination is added.

It is not surprising that the mapping criterion 'minimum of ΔP_{bbb}' provide the lowest probability error after optimised mapping. However, the Master-Slave mapping with lowest probability error ΔP_{bbb} does not necessarily provide the minimal probability error for other joint states, such as P_{ggg} – all satellites are in 'good' state. When the correlation error $\Delta\rho_{\text{slaves}}$ is minimised, then it is ensured that the error of all (eight) joint probabilities are jointly reduced. For this purpose, the minimisation of $\Delta\rho_{\text{slaves}}$ is the more robust and therefore preferred method for the Master-Slave mapping with three satellites.

Also with optimised mapping it is noteworthy that the error with Master-Slave is not zero. To assess the consequence of the Master-Slave error in context of an LMS model implementation,

the fading statistics of a three-satellite model using Master-Slave are analysed in Chapter 5.2. The author recommends to interpret the results for three-satellite diversity with caution, if the probability error ΔP_{bbb} is greater than the regarded signal unavailability. To analyse, for example, a signal availability of 99%, the probability error should be $\Delta P_{\mathrm{bbb}} < 0.01$.

3.5.4. State duration modelling with Master-Slave

Two implementations are developed and described in Section 3.2.5, the *Conditional Assembling Method* and the method *ASTM-MT*. The main difference is found with respect to the state duration modelling. For two satellites, the recommended Master-Slave approach is *ASTM-MT, option Lutz* (cf. Section 3.2.5). It allows an accurate description of the mean state durations of the single satellites. If the master is modelled by a semi-Markov chain, also accurate state duration statistics of the master are provided. In this section the state duration modelling of *ASTM-MT, option Lutz* for three satellites is addressed.

Figure 3.34 shows the state duration statistics of the joint states 'good good good' and 'bad bad bad' and of the single satellites' 'bad'-states derived from measurements and re-simulated with different state algorithms. Measurement data is taken from a mixed rural environment of 23 km length with satellite positions $\phi_1 = 38°$, $\phi_2 = 23°$, $\phi_3 = 62°$, $\Delta\theta_{12} = 34°$, $\Delta\theta_{13} = 132°$. (Satellite 1 and satellite 2 are equal to Section 3.3).

Two variants of a three-satellite model with Master-Slave are proposed to re-simulate this scenario:

- *2 x Master-Slave*: After an appropriate Master-Slave mapping, the master satellite it is modelled by a first-order Markov chain. Two slaves are modelled independently using ASTM-MT (option: Lutz).
- *Dual-Sat & Master-Slave*: The state series of two satellites are jointly modelled by the recommended dual-satellite approach 'semi-Markov, lognormal fit & Lutz, empirical'. Therefore, it must be ensured that one of the satellites is the optimal master. The second satellite can be arbitrarily chosen. The remaining satellite (slave) is modelled with respect to the master using the approach ASTM-MT.

The optimal master in Figure 3.34 is satellite 1 and found by minimising the correlation error. For comparison, the results of the *straightforward* first-order Markov model are presented as well.

The following results are gained from Figure 3.34:

- Since the variant *2 x Master-Slave* uses a first-order Markov model for master and for the conditional slave transitions, the state duration statistics of the single satellites from *2 x Master-Slave* are in high agreement with the statistics of the *straightforward* first-order Markov model. Also the joint duration statistics for 'good good good' and 'bad bad bad' are similar between *2 x Master-Slave* and the first-order Markov model.
- With the variant *Dual-Sat & Master-Slave* two satellites are modelled by a semi-Markov chain which provides a well-approximated description of the single-satellite state duration statistics. This is obtained for satellite 1 (master) and satellite 3 (exemplarily selected) in Figure 3.34. The duration statistics of the remaining satellite 2, it is the slave, are similar to the first-order Markov model due to similar implementation.

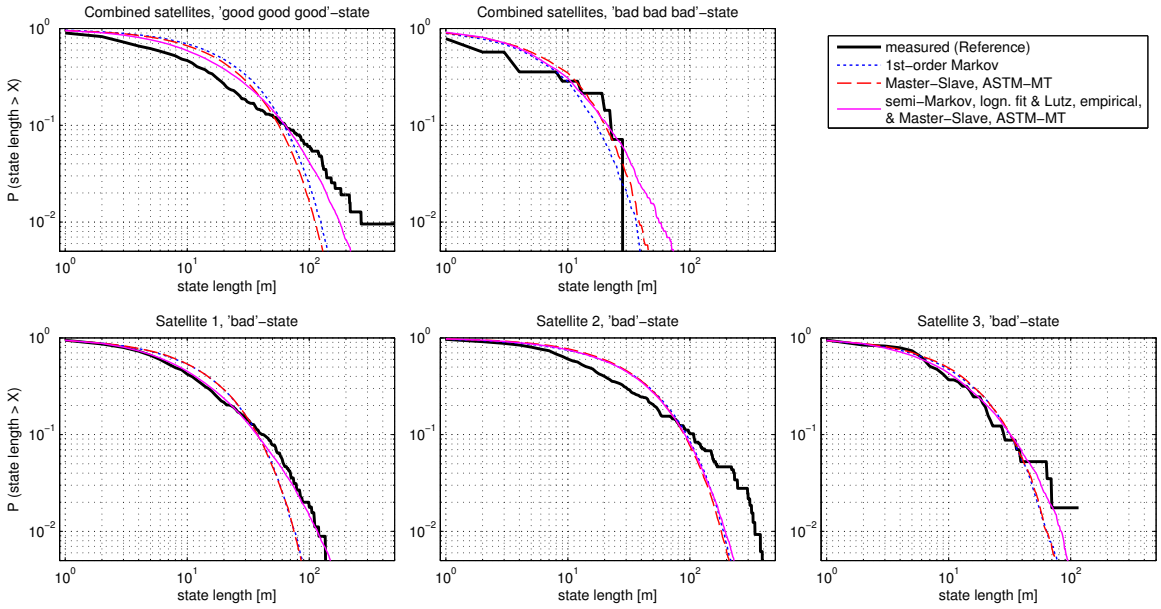

Figure 3.34.: State duration statistics of the joint 'good good good' and 'bad bad bad'-state and the single satellite 'bad'-states derived from the measurements and re-simulated with different modelling approaches.

- The dual-satellite semi-Markov model provides an accurate re-simulation of the joint duration statistics of two satellites, satellite 1 and satellite 3 (not depicted in Figure 3.34). This changes the joint state duration statistics of three satellites as well. It is obtained that the constellation *Dual-Sat & Master-Slave* is able to simulate longer joint state durations than the first-order Markov model. For the joint state 'good good good' the variant *Dual-Sat & Master-Slave* provide therefore a better approximation of the SDPDF than the approach *2 x Master-Slave*. However, both simulation variants of Master-Slave are not able to accurately describe the joint duration statistics of three satellites.

Analogue to the dual-satellite case, the most accurate model in terms of state duration modelling is the straightforward dynamic Markov model. However, due to challenges in terms of LMS model parametrisation, alternatives to the straightforward methods are required. For dual-satellite modelling, alternative approaches based on the Lutz method are found. For state series generation of three satellites, the only available alternative to the straightforward methods is Master-Slave.

An accurate state duration modelling becomes relevant, amongst others, if time diversity of a satellite system is analysed. A corresponding evaluation of Master-Slave in context of the complete LMS model considering different interleaver lengths is presented in Chapter 5.2.

3.5.5. Conclusions on Multi-Satellite State Modelling

In this Section 3.5 a performance evaluation of Master-Slave for a three-satellite system is carried out with a focus on state probability modelling. Therefore, measured correlation coefficients between the satellites are compared with re-calculated correlation coefficients from Master-Slave in dependency on the elevation angles and the azimuth angle separations of the three-satellite system. The difference between the measured and re-simulated correlation coefficient between the slaves is defined as correlation error. Furthermore, the probability of the state 'bad bad bad' (P_{bbb}) resulting from Master-Slave is compared with a theoretic estimation of P_{bbb} from measurements. The difference of P_{bbb} from Master-Slave and from measurements is defined as probability error.

It is obtained that Master-Slave has a high probability error in case of a low azimuth separation and therefore a high correlation between the slave satellites. Furthermore, a master satellite with a high elevation provides a lower probability error compared to a master with low elevation. The probability error with Master-Slave can be mitigated by an appropriate definition (mapping) of master and slave satellites. To find the master, it is proposed to select the mapping with the lowest correlation error between the slaves.

Master-Slave is a generic name for a modelling concept, for which different realisations can be applied. Two implementations are developed and described in Section 3.2.5, the *Conditional Assembling Method* and the method *ASTM-MT*. Based on a dual-satellite scenario, it is concluded in Section 3.3 that these Master-Slave implementations are indeed accurate in terms of state probability modelling, but are less accurate in terms of state duration modelling than other dual-satellite algorithms. Therefore, to improve the state duration modelling it is beneficial to use Master-Slave in combination with another state algorithm:

- First, one of three satellites are selected to be master (by considering the mapping guidelines).
- Second, state series of two satellites are generated with the recommended dual-satellite model 'semi-Markov, lognormal fit & Lutz, empirical', whereas one of the satellites is the master.
- Third, the remaining slave satellite is generated with a Master-Slave approach. The recommended algorithm is ASTM-MT, which provides correct state probabilities and correct mean durations for the slave satellite.

The combination of 'dual-satellite & Master-Slave' has the advantage, that the duration statistics from at least two of three satellites are accurately modelled. However, the joint duration statistics are only roughly estimated, and an accurate description of joint duration statistics is not possible.

The necessity of the Master-Slave approach depends on the purpose of the LMS model. For an accurate re-simulation of synchronously measured signals of three satellites, the straightforward dynamic Markov model is the recommended state model. For coverage studies of three-satellite diversity systems for satellite positions and environments, where measurement data is not available, the Master-Slave approach is required. To the best knowledge of the author, there is no other three-satellite model available for this task.

4. Statistical Modelling of the LMS Channel, Part II: Slow- and Fast Variations and Model Implementation

For a new multi-satellite channel model the versatile two-state model from [PFSLCn07] [PCPFB+10] is taken as a baseline (cf. Figure 2.7, Chapter 2.3.5). It describes two states 'good' and 'bad' to assess the large-scale environmental features in the transmission path, which is focused in the previous Chapter 3, and Loo distributed fading to describe the slow- and fast signal variations within the states.

In this chapter the Loo distributed fading within the states is addressed. It includes a slow fading component (lognormal fading) due to varying shadowing conditions of the direct signal, and a fast fading component (Rice fading) due to multipath effects. The Loo model is described by three parameters M_A, Σ_A, and MP (Equation (2.16)), denoting the mean and standard deviation of the lognormal component (on a dB scale) and the multipath power, respectively. Following the versatile two-state model, after each state transition a random Loo parameter triplet is generated. The statistical distribution of Loo parameter triplets depends on the current state and the receive environment of the terminal.

In the first part of this chapter, a verification of the basic LMS model architecture for single satellite reception (i.e. the versatile two-state model) is performed based on the satellite propagation data which is available for this work. In the second part, dependencies of slow- and fast variations between two satellites are identified. Finally, a model structure and a generator implementation for multi-satellite reception is proposed.

4.1. Analysis of Slow- and Fast Signal Variations for a Single Satellite

When the channel model enters a new state, a new Loo parameter triplet (M_A, Σ_A, and MP) is generated following a statistical process. For this purpose, Loo parameters are estimated from measurement data by curve-fitting within intervals of a state duration (cf. Appendix A.5). Figure 4.1 shows the distribution of the Loo parameters for an exemplary scenario. In general the modelling approach as observed in [PCPFB+10] can be confirmed:

- The distribution of M_A can be approximated by a normal distribution with mean μ_1 and standard deviation σ_1:

$$M_A \sim \mathcal{N}(\mu_1, \sigma_1^2) \tag{4.1}$$

- Σ_A has a conditional normal distribution with respect to parameter M_A:

$$\begin{aligned} \Sigma_A | M_A &\sim \mathcal{N}(\mu_2, \sigma_2^2) \qquad \text{with} \\ \mu_2 &= a_1 \cdot M_A^2 + a_2 \cdot M_A + a_3 \\ \sigma_2 &= b_1 \cdot M_A^2 + b_2 \cdot M_A + b_3 \end{aligned} \tag{4.2}$$

- The distribution of MP can be approximated by a normal distribution and is independent from M_A and Σ_A:

$$MP \sim \mathcal{N}(\mu_3, \sigma_3^2) \tag{4.3}$$

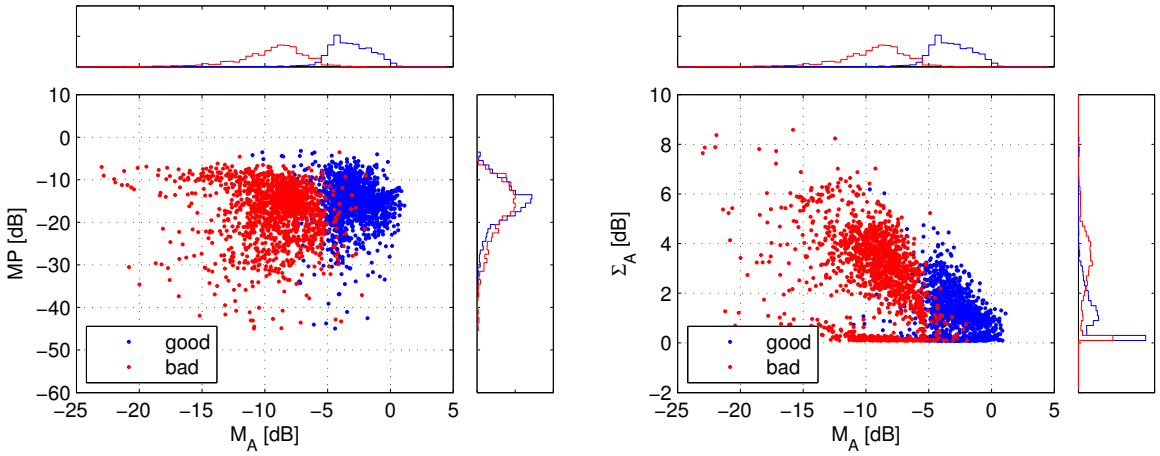

Figure 4.1.: Joint distributions and marginal distributions of Loo parameters. MP versus M_A (left). Σ_A versus M_A (right).

4.1.1. Dependency of Loo Parameters on the State Length

For the description of the signals temporal evolution, the dependency of Loo parameters on the current state duration is analysed. Exemplary, but representative results for multiple receive scenarios are shown in the Figures 4.2, 4.3, 4.4.

It is obtained that the spreading of parameters M_A, Σ_A, and MP is greater for short state durations than for long state durations. As long events dominate the overall signal statistic, it is found to be effective to capture the distribution for M_A, Σ_A, and MP by considering the weight of the current state duration. Thus, it makes firstly no difference if Loo parameters are estimated within equidistant intervals or intervals with variable length. Secondly, statistical outliers resulting from the Loo-fitting are compensated.

For the mean of the lognormal fading M_A a dependency on the current state length D_{state} is obtained in Figure 4.2 for 'good' as well as for the 'bad' state. For the 'bad'-state a long state length has a deeper fading than short shadowing events. This effect is expected due to the terminal being deeper in the diffraction zone behind large objects. Short shadowing events on the other hand due to foliage and trees lead to only light shadowing. As a threshold (5 dB below LOS, cf. Appendix A.4) is defined to separate 'good' from 'bad' states, it is rather random if short and light shadowing events are assigned to 'good' or 'bad'. To include this state duration dependency for short events into the model, the following modification for the Loo parameter generation is proposed (cf. Figure 4.5):

$$\begin{aligned} f(M_A) &\sim \mathcal{N}(\mu_1', \sigma_1^2) \quad \text{with} \\ \mu_1' &= a_0 + b_0 \cdot c_0^{-D_{\text{state}}} \end{aligned} \tag{4.4}$$

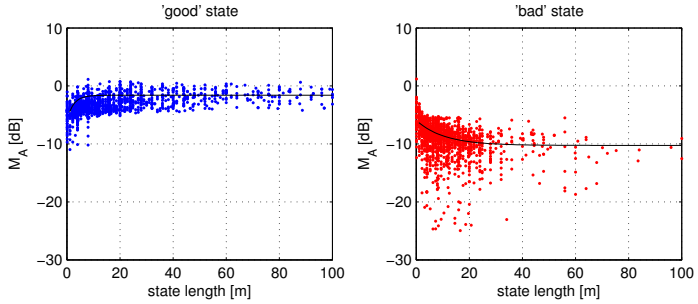

Figure 4.2.: Loo parameter M_A versus state length for the 'good' and 'bad' state.

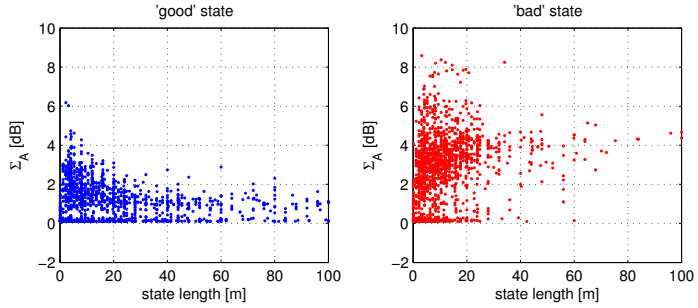

Figure 4.3.: Loo parameter Σ_A versus state length for the 'good' and 'bad' state.

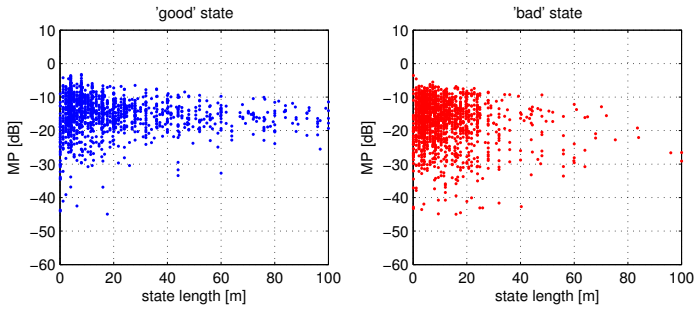

Figure 4.4.: Loo parameter MP versus state length for the 'good' and 'bad' state.

To reduce the number of additional parameters, it is proposed to set $a_0 = \mu_1$ according to Equation (4.1), $(a_0 + b_0)$ is the mean value of $\mu_{1,\mathrm{g}}$ and $\mu_{1,\mathrm{b}}$, and c_0 is globally defined and valid for all receive scenarios. ($c_{0,\mathrm{g}} = 2.0$ and $c_{0,\mathrm{b}} = 1.1$ are found to be appropriate)

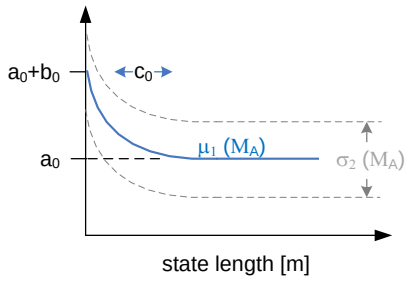

Figure 4.5.: Dependency of M_A on the state length: Modelling approach.

As those effects, observed for M_A, are minor significant for Σ_A and MP (Figure 4.3, Figure 4.4), no further dependencies to the state duration are considered.

4.1.2. Analysis and Implementation of Doppler Phenomena

In the project MIMOSA [EBW+11] that ran parallel to this work, measurements were carried out in the area of Erlangen (Germany) to capture channel impulse responses in S-Band (2.2 GHz) from a geostationary satellite located at 10° East. Goal of these measurements was to characterise the dual-polarised MIMO LMS channel. Amongst others, Doppler spectra were analysed and are provided for this work.

Figure 4.6 shows exemplarily the power spectral density of the measured series and the Doppler spectrum after normalisation to the direct signal. The latter case represents the spectrum for constant mobile speed and driving direction. The normalised spectrum is the interesting one, since the mobile speed and the driving direction are intended to be parameters of the LMS model. The following conclusions for the implementation of Doppler phenomena in the LMS model can be drawn:

- Multipath components, that arrive the receive antenna equally distributed between 0 and 2π, experience a Doppler spread in case of vehicle movement. This Doppler spread can be appropriately described by using a Butterworth filter, whose bandwidth depends on the vehicle speed. It is proposed in [PCPFB+10] and also confirmed by the measurement results in Figure 4.6.
- The location of the direct signal component within the Doppler spectrum depends on the driving direction relative to the satellite θ, the satellite elevation ϕ, and the vehicle speed v_{mobile}. It holds

$$f_{D\text{dir}} = v_{\text{mobile}} \cdot f_c/c \cdot \cos\phi \cdot \cos\theta \tag{4.5}$$

  with carrier frequency f_c, and speed of light c. This fact was already described from Fontan et al. in [PFBA+08]. However, the implementation of the direct signal's Doppler shift is missing in the proposed model generators in [PFSLCn07] and [PCPFB+10].
- A joint Doppler shift of all signal components is induced by satellite movement. In this case, the speed of the satellite relative to a fixed earth observation point in the area of the vehicle is important.

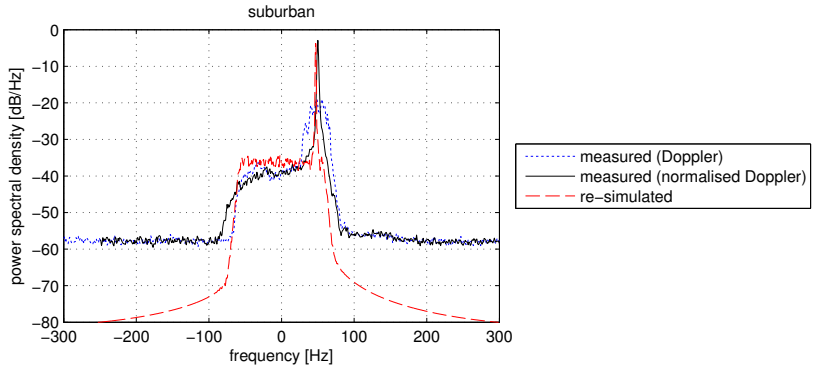

Figure 4.6.: Power spectral density of measured and re-simulated signals for a suburban environment. The Doppler shift of the direct signal component within the spectrum depends on the driving direction with respect to the satellite (θ). A Butterworth filter is used for multipath Doppler spread. Parameters are $\phi \approx 35°$, $\theta \approx 12°$, $v_{\text{mobile}} \approx 7.5\,\text{m/s}$, $f_c = 2.2\,\text{GHz}$.

4.2. Single-Satellite Model Implementation

To generate timeseries of the complex envelope of the received signal, Figure 4.7 shows an implementation diagram of the narrowband LMS channel model for single satellite reception proposed from this work. A separation into three generator types is found to be appropriate:

1. The **state sequence generator (SSG)** simulates series of 'good' and 'bad' states by using a semi-Markov model [BT02]. This approach provides an accurate modelling of the state duration and the state probabilities. In the context of this work it has been shown that a lognormal distribution is a good approximation to describe the state duration distributions for both states. A detailed comparison for different state modelling approaches in terms of LMS modelling is done in Chapter 3.

   Parameters for the SSG are mean and standard deviation of the lognormal state duration distribution μ_{Dur} and σ_{Dur} for 'good' and 'bad' state. A momentary output of the SSG is a state i ($i \in \{\text{g}, \text{b}\}$) of a certain duration D_i.

2. The **propagation parameter generator (PPG)** generates random Loo triplets (M_A, Σ_A, and MP) after each state transition according to Equations (4.1)-(4.4). For M_A a statistical dependency on state durations is proposed. This modification with respect to the initial literature model [PCPFB+10] is indicated in Figure 4.7. An evaluation of the overall signal output with respect to this modification is done in next Chapter 5.

3. In the **small-scale fading generator (SSFG)** Loo distributed timeseries including Doppler shaping are generated. Two modifications with respect to the Loo generator implementation in the literature [PFSLCn07][PCPFB+10] are found to be necessary: Firstly, the interpolation of the normally distributed samples (block 'Rate conversion & interpolation') is done **before** a conversion into lognormal distributed samples (block '$10^{A/20}$') is performed. Thus, a lognormal distribution for the slow signal variations is ensured after interpolation as well. Secondly, an additional Doppler shift of the

lognormal varying direct signal is included, which is related to the vehicle speed and depends on the driving direction of the vehicle. After summation of lognormal fading and Rice fading, a Doppler shift due to satellite movement is done.

Figure 4.8 shows the simulation chain including the SSG, PPG and SSFG. Output of this generator is the complex envelope of the received signal. It follows a stationary Loo distribution for the time of a state length and switches to another Loo distribution after a state transition. To avoid sharp changes of the signal between 'good' and 'bad' states, a smooth state transition is implemented allowing a maximum slope of 5 dB/m for the lognormal signal, as proposed in [PCPFB+10]. An overview on required parameters for a single-satellite model is given in Table 4.1.

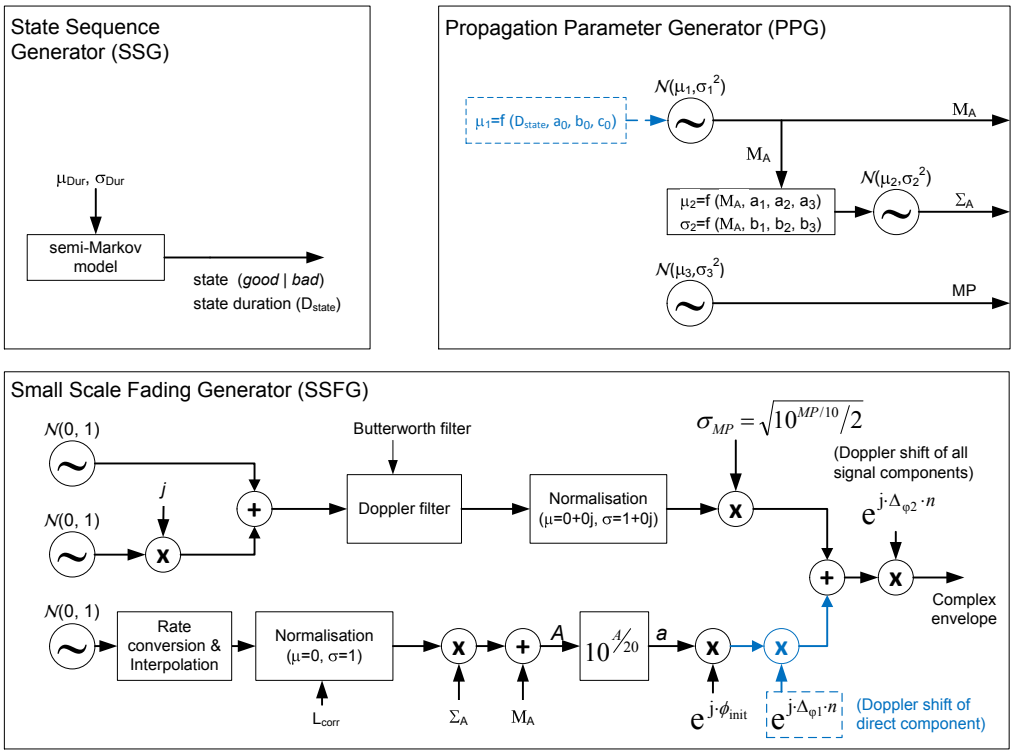

Figure 4.7.: Implementation of State Sequence Generator, Propagation Parameter Generator, and Small-Scale Fading Generator for LMS timeseries generation. Modifications with respect to the existing two-state literature model are indicated in blue.

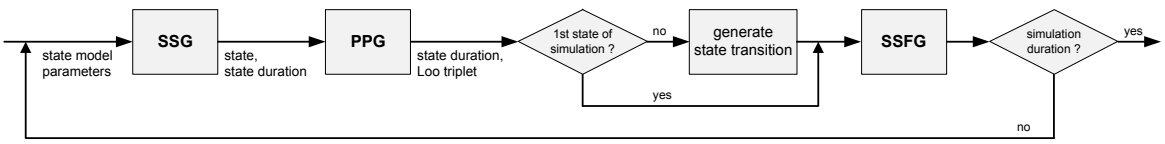

Figure 4.8.: Simulator block diagram.

Table 4.1.: Model parameters for single satellite narrowband LMS model. (adapted from [PFSLCn07][PCPFB+10]). Bold printed values are to be estimated from measurement data and accordingly are required for simulation. Other parameters are calculated.

parameter (in SSFG)	secondary parameter	description	values
M_A	$\boldsymbol{\mu_1}, \boldsymbol{\sigma_1}$ or $\boldsymbol{a_0}, \boldsymbol{b_0}, \boldsymbol{c_0}, \boldsymbol{\sigma_1}$ (Eq.4.4)	mean of lognormal fading and distribution parameters	Table C.1,
Σ_A	$\boldsymbol{a_1}, \boldsymbol{a_2}, \boldsymbol{a_3}, \boldsymbol{b_1}, \boldsymbol{b_2}, \boldsymbol{b_3}$	standard deviation of lognormal fading and distribution parameters	Table C.1
MP	$\boldsymbol{\mu_3}, \boldsymbol{\sigma_3}$	multipath power and distribution parameters	Table C.1
D	$\boldsymbol{\mu_{Dur}}, \boldsymbol{\sigma_{Dur}}$	state duration and distribution parameters	Table C.2 or Table C.3
$\boldsymbol{D_{min}}$		a minimum state duration of 1 m is assumed in this work	1 m
$\boldsymbol{f_c}$,$\boldsymbol{\lambda_c}$		carrier frequency, carrier wave length	
$\boldsymbol{v}_{\text{mobile}}$		constant mobile speed	
f_0	$v_{\text{mobile}}, \lambda_c$	minimum sampling rate	$8v_{\text{mobile}}/\lambda_c$
$\boldsymbol{L_{corr}}$		correlation distance = lognormal fading sampling period	2 m for S-band
$f_{D\text{dir}}$	$\boldsymbol{\phi}, \boldsymbol{\theta}, \boldsymbol{v}_{\text{mobile}}, \boldsymbol{f_c}$	Doppler shift of direct signal	
$f_{D\text{max}}$	v_{mobile}, f_c	maximum Doppler shift	
Doppler spread filter		Butterworth filter with a maximum ripple of 3 dB up to $0.9v_{\text{mobile}}/\lambda_c$ and an attenuation of 100 dB at $3v_{\text{mobile}}/\lambda_c$ [PCPFB+10]	

4.3. Correlation of Fast- and Slow Variations Between Two Satellites

Correlation between two satellite signals is not only expected in terms of LOS and non-LOS conditions (states), but also for the specific attenuation of the direct signal or the amount of multipath propagation in the local area. Therefore, with respect to the given LMS model architecture, the interdependency between Loo parameters of two satellite signals has been analysed and presented in [KAIH12]. They are derived from synchronous and equidistant intervals of 30 λ_c length (≈ 3.8 m) from two measured satellite signals.

Figure 4.9 shows exemplarily the conditional dependency of the Loo parameters M_A, Σ_A, and MP between two satellites for an urban environment. For comparison the mean power for same statistical intervals is given. Measurement data from two geostationary satellites with $\phi_1 \approx 37°$, $\phi_2 \approx 24°$, and $\Delta\theta \approx 34°$ have been analysed. To assess additional correlation effects besides the state correlation, a separation into four joint states is performed. In case of M_A as well as for the signals mean power, for the joint state 'bad bad' a correlation between two satellite signals is obvious in Figure 4.9. For this purpose, correlation coefficients for the Loo parameters have been derived in [KAIH12] for all joint states and three different environment types. Results are depicted in Figure 4.10. In urban and highway environments, the correlation coefficients of M_A and MP for state 'bad bad' go up to ≈ 0.75 and ≈ 0.5, respectively. Hence, for LMS modelling the correlation for M_A and MP can not be neglected. Also for mixed states ('bad good', 'good bad') correlation coefficients above 0.25 are obtained in Figure 4.10. Since the signals have different shadowing conditions (states), a correlation for mixed states is not expected and a statistical significance has to be checked therefore.

Correlation coefficients for Σ_A are rather low with $\rho < 0.2$ and need not to be considered. As Σ_A is modelled by conditional distribution to parameter M_A, a dependency between $\Sigma_{A,sat1}$ and $\Sigma_{A,sat2}$ is indirectly provided in case of introducing a correlation of M_A.

For a dual-/multi-satellite LMS model, the relation between Loo parameters of two satellites can be introduced by either defining conditional distributions, or in terms of correlation coefficients. The latter approach is recommended, as only one additional parameter is required.

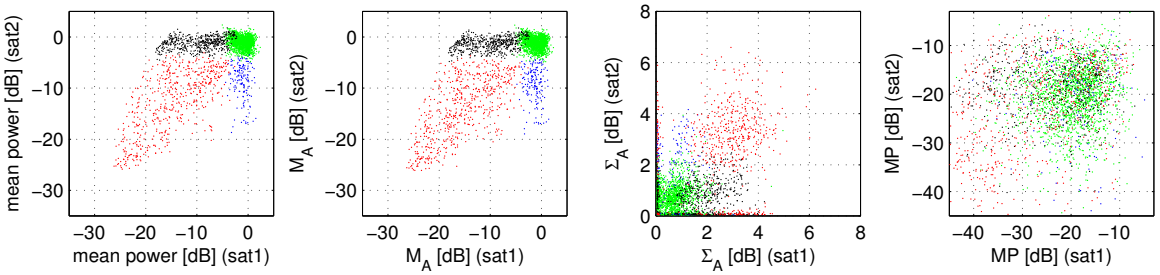

Figure 4.9.: Joint distribution of statistical parameters (from left to right: mean normalised power, M_A, Σ_A, MP) between two satellites for an urban environment. Joint states are indicated by different colours: 'good good', 'good bad', 'bad good', 'bad bad'.

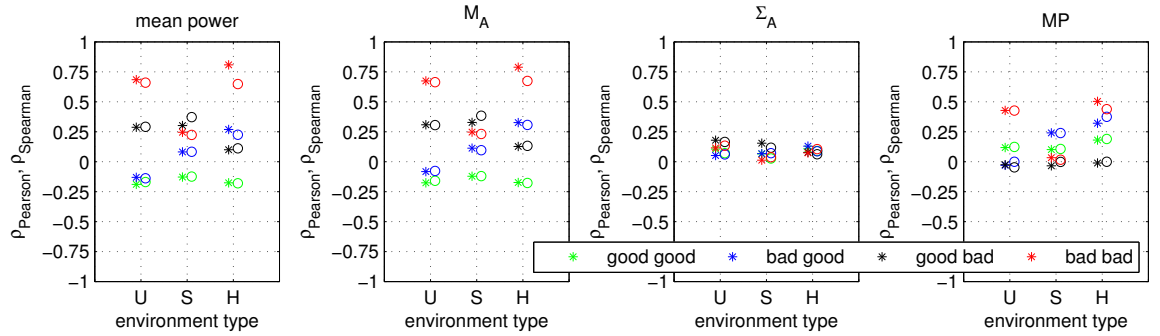

Figure 4.10.: Correlation coefficients according to Pearson (*) and Spearman (o) for mean power and Loo parameters for different environment types urban (U), suburban (S), and highway (H) separated into four joint states. The Spearman's coefficient is more robust against statistical outliers and proposed for further analyses.

On Extraction of Loo Parameter Correlation Coefficients From Measurement Data

In [KAIH12] and [ALAK03] it was stated that the Loo parameter estimation from measurement data is a complicated process. As a separation of a slow and fast varying signal component, e.g. by filtering, is not possible from field strength data, the curve fitting procedure is found as the only reliable approach. However, different triplets of Loo parameters provide very similar statistical distributions [KAIH12], which avoids a precise estimation of M_A, Σ_A, and MP.

Nevertheless, Loo parameters are commonly used to describe the single satellite reception. As indicated above, for multi-satellite reception a correlation coefficient for M_A between

two satellite signals needs to be derived. Results in [KAIH12] indicate, that the mean values of the overall signals provide similar correlation coefficients as the Loo parameters M_A (see also Figure 4.10), although their absolute values are different. Consequently, ρ_{M_A} can be estimated alternatively by using $\rho_{\text{mean signal}}$ and makes a complicated Loo parameter estimation for the parametrisation of numerous dual-satellite receive scenarios unnecessary. In practice, an estimation of ρ_{M_A} is also possible with measurement data of low resolution and dynamic range (such as GNSS signals, cf. Appendix A), where multipath fading is not obtained and a Loo parameter estimation is not possible.

Figure 4.11 shows the correlation coefficients of the mean signal power in dependency on the azimuth angle separation and for selected elevation angle combinations derived from GNSS data. It is obtained that high correlation coefficients with $\rho \approx 0.9$ occur for states 'good good'

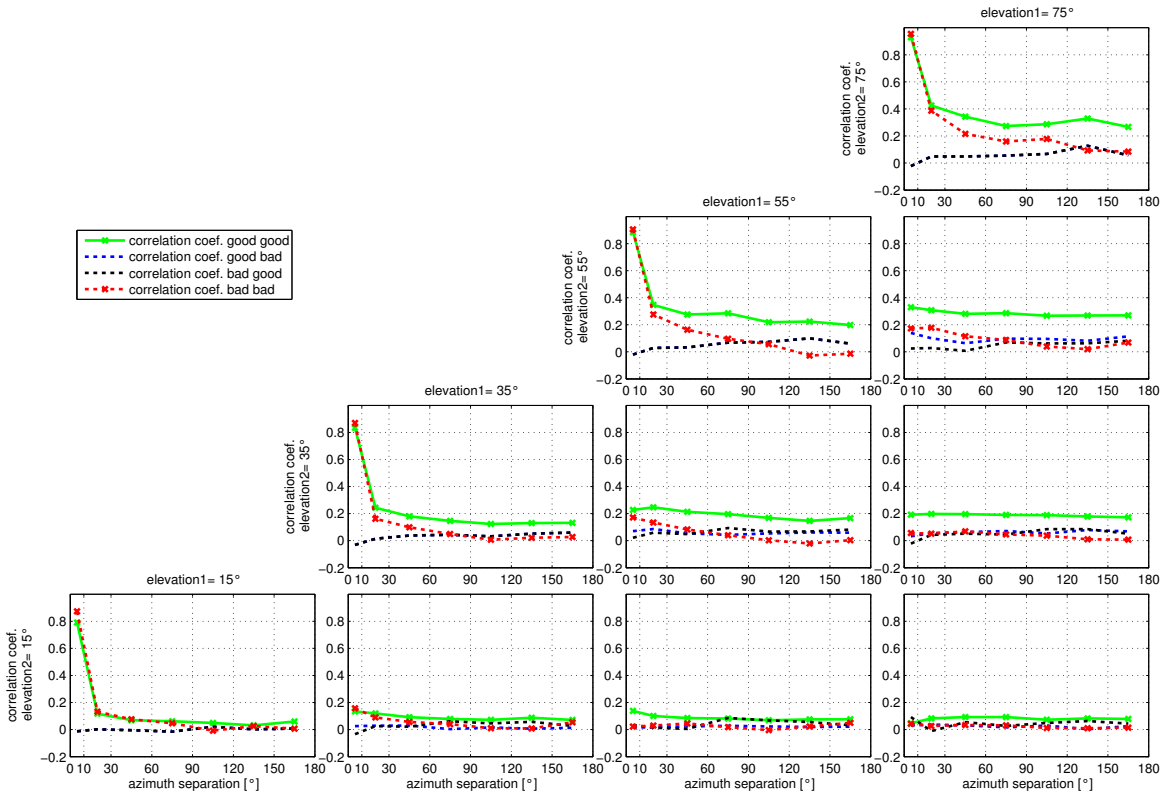

Figure 4.11.: Correlation coefficients of mean C/N values from two satellites within the joint states in dependency on the azimuth separation and for different elevation angle combinations derived from GNSS measurements.

and 'bad bad' in case of low angular separation in azimuth and elevation ($\Delta\theta, \Delta\phi < 10°$). For azimuth separations above 10° these values fall rapidly to $\rho \leq 0.4$. At high elevations it is noticeable that ρ_{gg} has a constant high level. The reason could be that the dynamic range of the signal at high elevations is rather small, whereas short shadowing events, e.g. from a bridge or a foliage over the street influence both signals synchronously. A further fact is that the effective angular separation for, e.g. $\phi_1 = \phi_2 = 75°$ is significantly lower than for $\phi_1 = \phi_2 = 15°$ for constant $\Delta\theta$. The statistical parameters for mixed states 'good bad' and 'bad good' are uncorrelated for all constellations and need not to be considered for LMS

modelling.

By deriving these values from GNSS data, it is found that the correlation coefficients ρ_{M_A} are similar for different environment types. To consolidate the parameters with respect to the satellite constellations, it is appropriate to omit a separation into different environments at this point. Thus, the given values in Figure 4.11 are valid for all environment types. A complete list for correlation coefficients ρ_{M_A} is given in Appendix C, Table C.5.

4.4. Introduction of Correlation Effects in the LMS Model

Signal correlation can be introduced at several stages in a dual-satellite LMS model:

- *Correlation of states in the SSG*: A correlation of state sequences is defined by combined state probabilities and can be introduced by a state transition matrix of a Markov model. This part of an LMS model is explicitly analysed in Chapter 3.
- *Correlation of Loo parameters in the PPG*: The versatile two-state model assumes random Loo parameters after a state transition. As a multiple of that triplets are generated over the entire simulation distance following a statistical distribution, a correlation of Loo parameters can be implemented.
- *Correlation of lognormal samples in the SSFG*: Slow lognormal variations of the direct signal and of the multipath components over several meters (defined by correlation distance l_{corr}) are modelled in the SSFG. It corresponds to fading variations under quasi-stationary conditions. A correlation of lognormal distributed samples between two satellites can be realised before rate conversion as seen in Figure 4.7.

4.4.1. Implementation of Dual-Satellite SSG and PPG

An implementation of the SSG and the PPG for dual-satellite reception is shown in Figure 4.12.

In the SSG, a semi-Markov model generates a sequence of four joint states: 'good good', 'good bad', 'bad good', and 'bad bad'. Required parameters are the lognormal distribution parameters $(\mu_{\mathrm{Dur}}, \sigma_{\mathrm{Dur}})$ of four joint states, and a state transition probability matrix. The joint state sequence is decomposed into two state sequences to trigger the PPG of the individual satellites.

Resulting from the analysis in previous Section 4.3, a correlation of Loo parameters M_A and MP between two satellites is task of the PPG. As this Loo parameter generation must be time synchronous for both satellites, a Master-Slave configuration is proposed. In case of the master, the single-satellite LMS implementation from Figure 4.7 is used without any modifications. It means, Loo parameter updates are done after state transitions between 'good' and 'bad'. For the slave, a new Loo parameter triplet is generated after a joint state transition of master and slave, as indicated in Figure 4.13. In an additional **correlator** block within the slave-PPG, the normal distributed values of $(M_A)_{\mathrm{slave}}$ and $(MP)_{\mathrm{slave}}$ are forced to be correlated to normal distributed values of $(M_A)_{\mathrm{master}}$ and $(MP)_{\mathrm{master}}$, respectively, without changing their statistical mean and standard deviations (cf. Figure 4.12 and explanation below).

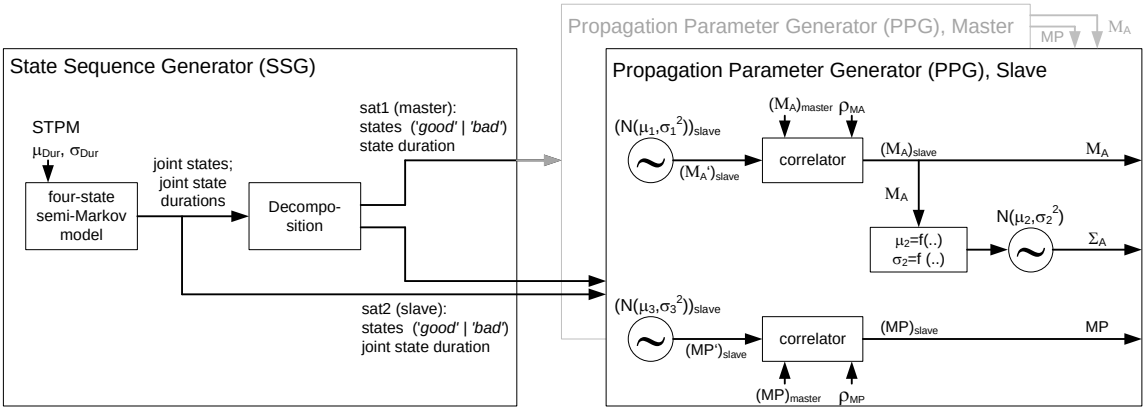

Figure 4.12.: Implementation of SSG and PPG for dual-satellite time series generation. A Master-Slave configuration is used for the PPG.

Task of the Correlator

Assuming X_1 and X_2 are two sequences of uncorrelated normal distributed numbers with $X_1 \sim \mathcal{N}(\mu_1, \sigma_1^2)$ and $X_2 \sim \mathcal{N}(\mu_2, \sigma_2^2)$. A new sequence Y_2 calculated with

$$Y_2 = \sigma_2 \cdot \left[\rho \cdot \left(\frac{X_1 - \mu_1}{\sigma_1} \right) + \sqrt{1 - \rho^2} \cdot \left(\frac{X_2 - \mu_2}{\sigma_2} \right) \right] + \mu_2, \tag{4.6}$$

consists of normal distributed numbers with mean μ_2 and standard deviation σ_2 and have a correlation coefficient ρ to sequence X_1.

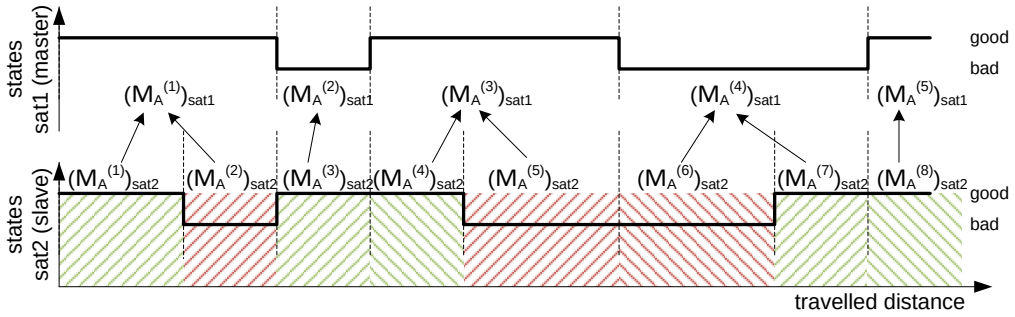

Figure 4.13.: Realisation of a Loo parameter correlation between two satellites using a Master-Slave configuration. The Loo parameters (here exemplarily only M_A) of the master are updated with its state transitions, whereas Loo parameters of a slave are updated with joint state transitions of master and slave. Each random slave value after a state change is correlated to the current master value.

4.4.2. Implementation of Dual-Satellite SSFG

In the SSFG a correlation of the lognormal variations between two satellites is introduced over the time interval between two state transitions, where the individual fading mean and standard deviations are constant. Assuming a Master-Slave configuration, a **correlator** in

the slow-fading branch of the slave-SSFG realises a target correlation coefficient between normal distributed master- and slave-samples (Figure 4.14). The conversion into lognormal distributed samples as well as the sampling rate conversion is done afterwards.

It should be noted that the correlation coefficient between two lognormal series ρ_{logn} is different from the correlation coefficient of the corresponding normal series ρ_{normal} before normal-to-lognormal conversion. The calculation $\rho_{\text{logn}} = f(\rho_{\text{normal}})$ is described below.

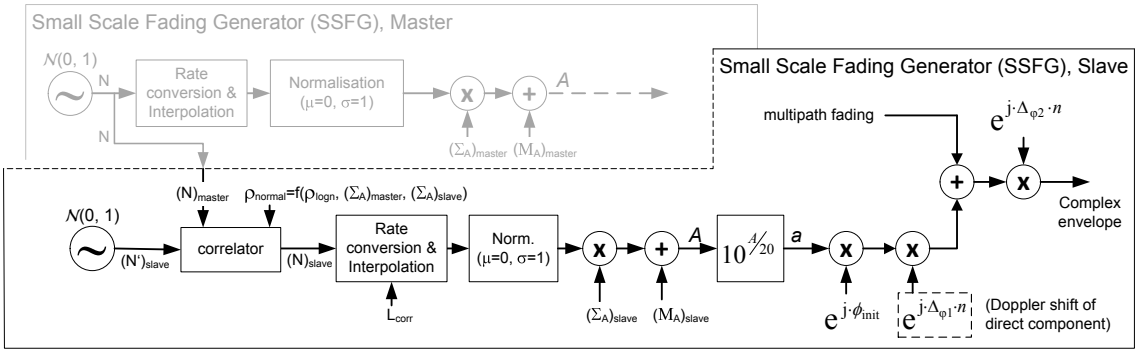

Figure 4.14.: Implementation of slave-SSFG (only slow-fading branch) for dual-satellite time series generation. Lognormal samples of the slave are correlated with lognormal samples of the master.

Conversion of Correlation Coefficient Between Lognormal and Normal Series

Assuming two normal distributed series $X_1 \sim \mathcal{N}(M_1, \Sigma_1^2)$ and $X_2 \sim \mathcal{N}(M_2, \Sigma_2^2)$ and the corresponding lognormal series $x_1 = 10^{(X_1/20)}$ and $x_2 = 10^{(X_2/20)}$. To realise a certain correlation coefficient between the lognormal series (ρ_{x_1,x_2}), the following correlation coefficient for the normal series (ρ_{X_1,X_2}) is required:

$$\rho_{X_1,X_2} = \frac{\ln\left(\rho_{x_1,x_2} \cdot \sqrt{(\exp(\sigma_1^2)-1)\cdot(\exp(\sigma_2^2)-1)} + 1\right)}{\sigma_1 \sigma_2} \tag{4.7}$$

with

$$\sigma_1 = (\Sigma_1/20)\cdot\ln(10), \qquad \sigma_2 = (\Sigma_2/20)\cdot\ln(10) \tag{4.8}$$

4.4.3. Dual-satellite LMS Model Parameters

Previous analyses result in the parameters in Table 4.2 required for a dual-satellite LMS model. They are valid for the 'versatile LMS model' and are to be applied in combination with the parameters for single-satellite reception from Table 4.1.

4.4.4. Modelling Results for Different Types of Signal Correlation

To demonstrate the necessity of Loo parameter correlation and lognormal sample correlation on top of state correlation, simulation results with five LMS model configurations are

Table 4.2.: Required LMS model parameters in addition to Table 4.1 for the simulation of multiple satellite signals.

parameter	description	values
ρ_{states}	correlation coefficient for state sequences	Table C.4
$\rho_{M_A,\text{gg}}$; $\rho_{M_A,\text{bb}}$	correlation coefficients for Loo parameter M_A in case of joint state 'good good' and 'bad bad'	Table C.5, denoted with ρ_{gg} and ρ_{bb}
$\rho_{MP,\text{gg}}$; $\rho_{MP,\text{bb}}$	correlation coefficients for Loo parameter MP in case of joint state 'good good' and 'bad bad'	*not available*
$\rho_{\text{logn,gg}}$; $\rho_{\text{logn,bb}}$	correlation coefficients for lognormal fading samples for the time of a state duration	Table C.5, denoted with ρ_{gg} and ρ_{bb} (same values as for ρ_{M_A} are used)

presented and analysed in this section. The following correlation configurations are considered:

1. *independent*: Two satellite signals are modelled independently.
2. *corr. states*: The state sequences – with 'good' and 'bad' states – of two satellites are correlated (parameter ρ_{states}). The state correlation (only) is used in almost every of the dual-satellite channel models found in literature. For this purpose, the correlated Markov model from Lutz is combined with independently modelled fade distributions for 'good' and 'bad' state.
3. *corr.states&*M_A: This configuration denotes the correlation of states as well as the correlation of the Loo parameter M_A (parameter ρ_{M_A}). Therefore, correlated normal distributions of the parameter M_A for both satellites are generated in case of 'good good' and 'bad bad'. It can be realised only if the state transitions of both satellites are synchronised, e.g. by a Master-Slave configuration (cf. Figure 4.13). This configuration considers the fact that satellite signals with a small azimuth separation undergo same large-scale shadowing conditions due to similar or identical obstacles in the transmission path.
4. *corr. states&*M_A*&logn.*: This configuration denotes the correlation of states, the correlation of Loo parameter M_A, and the correlation of lognormal distributed samples (parameter ρ_{logn}). Such a full correlation has to be considered for very small angular separations, where the direct signal from both satellites is not only attenuated by the same obstacles, rather the direct signal undergo synchronously same small-scale variations of the same obstacle.
5. *corr. states&*M_A*&MP&logn.*: Additionally to configuration 4, a correlation of the Loo parameter MP (parameter ρ_{MP}) is considered.

Figure 4.15 shows the CDF of the channel model output (C/N normalised to LOS-level) of two single satellite channels simulated with equal model parameters (i.e. they have same elevation) and of a maximal-ratio combined (MRC) signal such as in case of satellite diversity after considering the five correlation configurations. From Figure 4.15 it is seen that the highest diversity gain is achieved if both satellite signals are modelled independently. The diversity gain is the difference between the CDFs of single satellites and the CDF of the MRC signal at a constant ordinate. A state correlation (*corr. states*) reduces the satellite diversity

gain. Obviously this gain reduction is smaller for deep fades ($(C/N)_{MRC} < -10\,\mathrm{dB}$) than for medium fades ($-10\,\mathrm{dB} < (C/N)_{MRC} < -3\,\mathrm{dB}$). For deep fades ($(C/N)_{MRC} < -10\,\mathrm{dB}$) a remarkable reduction of the diversity gain is obtained when states and Loo parameters are jointly correlated in comparison to 'state correlation only'. A further diversity gain reduction is achieved with additional lognormal fading correlation (*corr. states&M_A&logn.*). The additional multipath correlation (*corr. states&M_A&MP&logn.*), however, minor influences the first-order statistic of the MRC signal and can be neglected. Amongst others it has the advantage that the complicated *MP* estimation, and consequently the ρ_{MP} estimation, for multiple dual-satellite environments is not necessarily required.

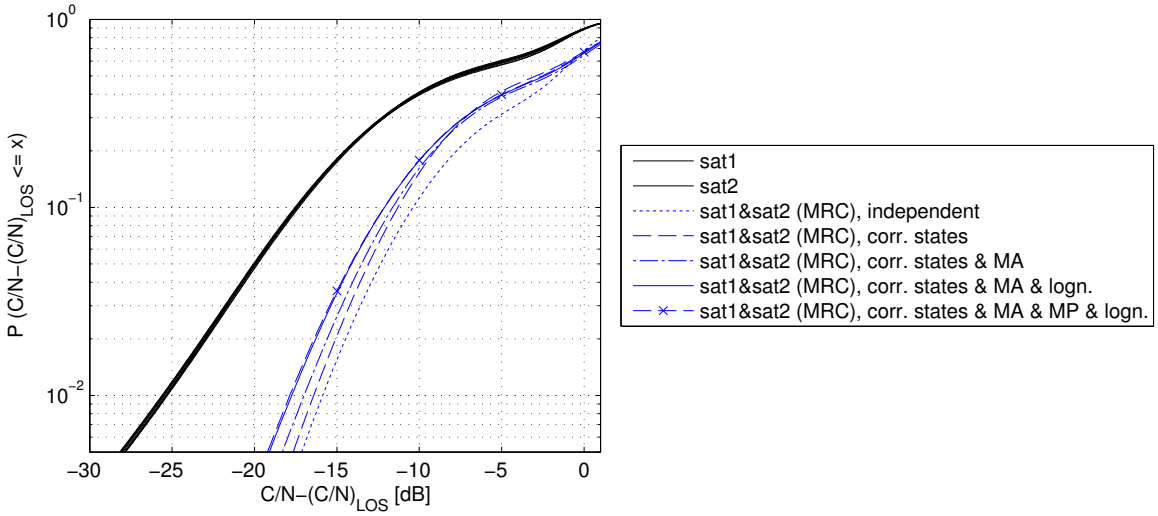

Figure 4.15.: CDF of the channel model output including satellite diversity. An urban environment with two satellites at 25° elevation is assumed. The correlation of signals is introduced at several stages in the generator. To evaluate the contribution of different types of correlation, the correlation coefficients are all set to $\rho = 0.5$ (i.e. $\rho_{\mathrm{states}} = \rho_{M_A} = \rho_{\mathrm{logn}}$). The dual-satellite simulations does not influence the single-satellite statistics, as verified by the overlaid curves for sat1 and sat2.

The results indicate that a correlation of two satellite signals, as in case of small azimuth separation, not only have to be considered in terms of states, but also in other parts of the model. The additional contribution of Loo parameter and lognormal samples correlation is as high as a state correlation in comparison to independent signals. By ignoring these characteristics, a satellite diversity gain would be predicted too optimistic.

5. Simulation Results and Model Validation

This chapter targets to compare the performance of the new multi-satellite model with other LMS models from literature. A comparison is done in two categories:

- Evaluation of the model architecture: Parameters for the proposed LMS model and for other LMS models are derived from an exemplary measurement sequence. The re-simulated signals of these LMS models are compared with the measurement sequence in terms of first- and second-order statistics.
- Validation of model parameter sets: For some LMS models in literature comprehensive parameter sets are given for different receive scenarios (environments, elevation angles, etc.). A 'channel model & parameters' comparison gives statements on the representativeness of the model. Furthermore, the feasibility and consistency of model parameter sets are verified by, e.g. obtaining the model output for different elevation angles.

5.1. Evaluation of Model Architecture

In Chapter 2 different generative multi-state LMS models from literature have been presented. The structure of each can be composed of a state modelling part (e.g. Markov model, semi-Markov model) and a fading modelling part (e.g. Rice, Loo, Suzuki with constant or variable parameters). Considering a certain combination of state and fade modelling concept, four architectures are compared in this section:

- *3-state model & constant Loo parameters*: This architecture represents the three-state model from Perez-Fontan et al. [PFVCC+01], which is used as reference for DVB-SH analyses. The three states describe line-of-sight, moderate shadowing and heavy shadowing conditions, whereas the fading in each state is characterised by a constant set of Loo parameters.
- *2-state model & constant Loo parameters*: Two-state approaches (with 'good' and 'bad' states) are commonly used for multi-satellite case [MPTE98] [BWL96] [PNIS+11]. Different distributions are proposed to characterise the fading within the states (Loo, Rice, Suzuki). For the subsequent comparison, a model architecture with constant Loo parameters for both states is assumed, equivalent to the three-state Fontan model above.
- *2-state model & variable Loo parameters*: This model architecture is proposed in [PFSLCn07] and [PCPFB+10] and is taken as basis for the LMS model in this work. It assumes a random generation of Loo parameters after a state transition.
- *2-state model & variable Loo parameters considering state duration*: In this work a dependency of the Loo parameter M_A on the current state duration is found (cf. Section 4.1.1), which is evaluated in this section.

The four models are intended to re-simulate two dual-satellite scenarios that are exemplarily derived from SDARS measurements (cf. Appendix A), which are

- an urban route with 10 km length in Portland (Maine). Signals are taken from two geostationary satellites with elevations $\phi_1 \approx 24°, \phi_2 \approx 37°$ and azimuth separation $\Delta\theta \approx 34°$. In this section the short notation *sat1* and *sat2* is used for the two satellites.
- a suburban route with 8.9 km length in Portland. Satellite positions are same as for urban.

Output of the channel models are time series of the carrier-to-noise ratio (C/N) at the mobile terminal, which are compared with measured C/N data in terms of first- and second-order statistics.

5.1.1. Model Parameters

The SDARS measurements are preprocessed to have LOS-normalised C/N series with a spatial resolution of 1 cm per sample. The states are derived by thresholding of the low-pass filtered series by using a sliding window of 5 m length (cf. also Appendix A.4). Thresholds are 5 dB below LOS for the two-state models and 3 dB and 10 dB for the three-state model, respectively. Similar values have been used in the literature in [BT02] and [PFVCB+98].

In case of the *'3-state-'* and *'2-state model with constant Loo parameters'*, global Loo triplets are derived once for each state by fitting theoretical Loo distribution functions to the measured signal distribution. Parameters for two satellites for the selected urban and suburban route are given in Table 5.1 for the three-state model and in Table 5.2 for the two-state model.

Table 5.1.: Parameters of the *'3-state model & constant Loo parameters'* (in dB) for the urban route (left) and the suburban route (right).

env	ϕ [°]	State	M_A	Σ_A	*MP*
U	23°	1	-1.25	0.79	-15.13
		2	-5.53	0.22	-11.16
		3	-16.59	5.37	-46.00
U	37°	1	-1.20	0.65	-13.83
		2	-6.67	1.61	-10.00
		3	-16.78	5.59	-46.00

env	ϕ [°]	State	M_A	Σ_A	*MP*
S	23°	1	-1.06	0.52	-14.22
		2	-6.51	0.13	-10.96
		3	-13.89	3.78	-33.18
S	37°	1	-1.39	0.54	-13.64
		2	-6.80	2.18	-10.00
		3	-13.19	4.36	-20.32

Table 5.2.: Parameters of the *'2-state model & constant Loo parameters'* (in dB) for the urban route (left) and the suburban route (right).

env	ϕ [°]	State	M_A	Σ_A	*MP*
U	23°	1	-1.78	0.76	-12.74
		2	-15.03	6.26	-46.00
U	37°	1	-1.54	0.61	-12.36
		2	-13.96	6.93	-46.00

env	ϕ [°]	State	M_A	Σ_A	*MP*
S	23°	1	-1.92	0.64	-11.32
		2	-10.89	5.25	-46.00
S	37°	1	-1.73	0.68	-12.69
		2	-13.17	3.80	-10.00

In case of the models with variable Loo parameters, curve-fitting is applied within intervals of a state duration to get multiple Loo-triplets for the 'good' and the 'bad' state. Finally, the statistical distribution of M_A, Σ_A, and *MP* for the *'2-state model & variable Loo parameters'* is parametrised according to Section 4.1. For the *'2-state model & variable Loo parameters*

Table 5.3.: Parameters of the *'2-state model & variable Loo parameters'* and the *'2-state model & variable Loo parameters considering state duration'* for the urban route (top) and the suburban route (bottom). The models differs in the description of parameter M_A. The former model uses parameters μ_1 and σ_1, whereas the latter model uses a_0, b_0, c_0 and σ_1 instead. Additionally the correlation coefficients for Loo parameter M_A (ρ_{M_A}) and for the lognormal fading (ρ_{logn}) are given for combined states 'good good' and 'bad bad'.

env		M_A				$\Sigma_A(\mu_2)$			$\Sigma_A(\sigma_2)$			*MP*	
=U	s	$\mu_1 = a_0$	b_0	c_0	σ_1	a_1	a_2	a_3	b_1	b_2	b_3	μ_3	σ_3
$\phi_1 =$	1	-1.75	-6.82	2.00	1.10	-0.01	-0.21	0.65	0.02	0.03	0.30	-18.72	5.91
23°	2	-15.39	6.82	1.10	4.52	-0.02	-0.61	-0.99	-0.00	0.06	2.00	-37.50	10.47
$\phi_2 =$	1	-1.58	-6.56	2.00	1.03	0.02	-0.22	0.59	0.02	-0.02	0.29	-16.94	4.35
37°	2	-14.71	6.56	1.10	4.50	-0.03	-0.82	-2.30	-0.00	0.04	1.81	-31.75	12.59
		$\rho_{M_A,\text{gg}} = \rho_{\text{logn,gg}} = -0.21$ $\rho_{M_A,\text{bb}} = \rho_{\text{logn,bb}} = 0.52$											

env		M_A				$\Sigma_A(\mu_2)$			$\Sigma_A(\sigma_2)$			*MP*	
=S	s	$\mu_1 = a_0$	b_0	c_0	σ_1	a_1	a_2	a_3	b_1	b_2	b_3	μ_3	σ_3
$\phi_1 =$	1	-1.84	-4.81	2.00	1.39	-0.02	-0.21	0.62	-0.04	-0.29	0.07	-19.43	7.57
23°	2	-11.46	4.81	1.10	2.89	-0.06	-1.63	-6.37	0.00	0.15	1.88	-30.18	12.49
$\phi_2 =$	1	-1.78	-4.64	2.00	1.08	0.03	-0.15	0.58	0.02	-0.09	0.18	-18.51	6.87
37°	2	-11.06	4.64	1.10	2.39	-0.05	-1.23	-4.16	0.01	0.27	2.46	-19.43	12.15
		$\rho_{M_A,\text{gg}} = \rho_{\text{logn,gg}} = -0.08$ $\rho_{M_A,\text{bb}} = \rho_{\text{logn,bb}} = 0.19$											

considering state duration', the distribution parameters for M_A are estimated according to Section 4.1.1. Parameters of both approaches are given in Table 5.3 for the selected routes.

State parameters for a semi-Markov model and a first-order Markov model and the corresponding correlation coefficient are given in Table 5.4. They allow to generate dual-satellite state series according to the *'first-order Markov & Lutz'* model (cf. Section 3.2.2) or the *'semi-Markov, logn. fit & Lutz, empirical'* model (cf. Section 3.4.3).

Further on, the correlation coefficients for the Loo parameters M_A between two satellites (ρ_{M_A}) are derived in case of joint states 'good good' and 'bad bad' and are given in Table 5.3. They are used again to correlate the lognormal distributed samples (ρ_{logn}) within the duration of a joint state.

Table 5.4.: First-order Markov parameters, semi-Markov parameters, and the state correlation coefficient for the urban route (left) and the suburban route (right). The semi-Markov parameters are given in dB (cf. Equation (3.6)). For the first-order Markov model, a state frame length of $\Delta d = 1\,\text{m}$ is assumed.

env=U	$\mu_{\text{Dur},1}$ $\mu_{\text{Dur},2}$	$\sigma_{\text{Dur},1}$ $\sigma_{\text{Dur},2}$	p_{11} p_{21}	p_{12} p_{22}
$\phi_1 = 23°$	24.4924	12.9135	0.9803	0.0197
	25.6407	11.1681	0.0228	0.9772
$\phi_2 = 37°$	24.3232	12.0637	0.9768	0.0232
	21.6651	10.2973	0.0408	0.9592
	$\rho_{\text{states}} = 0.3316$			

env=S	$\mu_{\text{Dur},1}$ $\mu_{\text{Dur},2}$	$\sigma_{\text{Dur},1}$ $\sigma_{\text{Dur},2}$	p_{11} p_{21}	p_{12} p_{22}
$\phi_1 = 23°$	21.2042	11.3314	0.9629	0.0371
	21.0838	11.6360	0.0360	0.9640
$\phi_2 = 37°$	24.4033	11.8197	0.9762	0.0238
	18.5592	8.8108	0.0706	0.9294
	$\rho_{\text{states}} = 0.2885$			

5.1.2. Model Validation in Terms of First-Order Statistics

Figure 5.1 shows the CDF of the line-of-sight-normalised C/N of two satellites from measurements and from the re-simulated signal by applying four modelling concepts. To evaluate satellite diversity, maximal-ratio combining (MRC) of the satellite signals is assumed. Therefore, the C/Ns from both satellites are added. The MRC gain depends on the correlation of the satellite signals, where a high correlation leads to a small MRC gain.

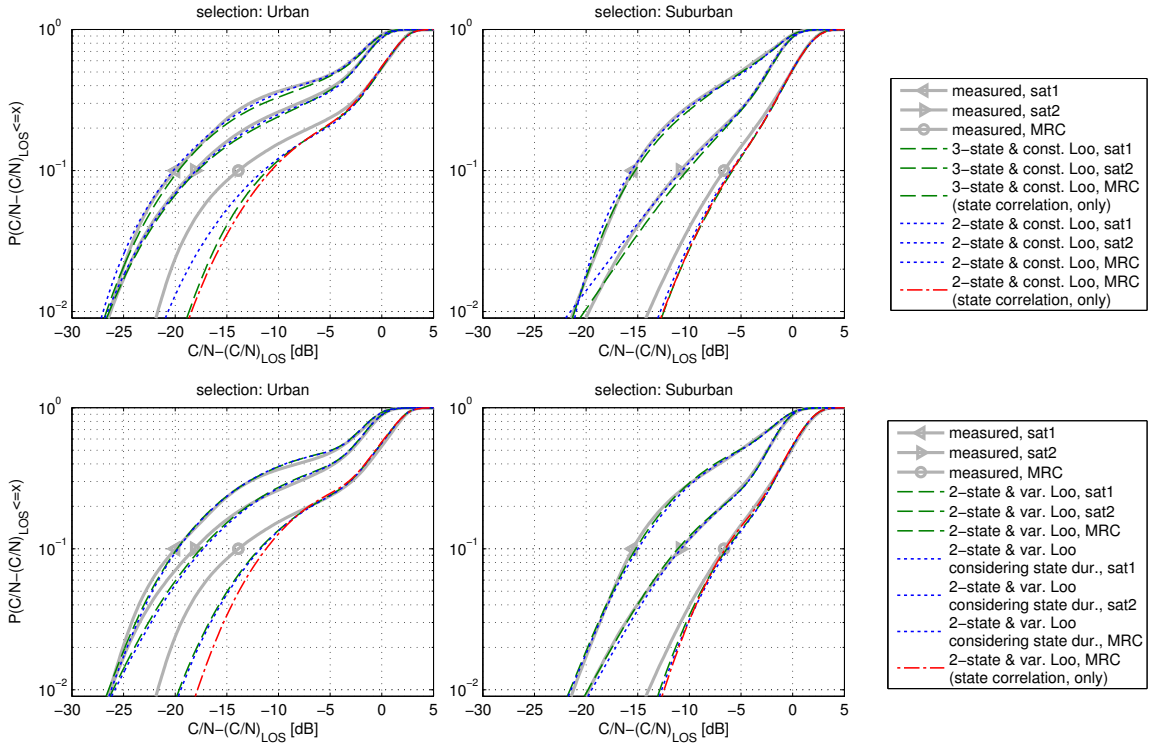

Figure 5.1.: CDFs of measured and re-simulated normalised C/N from two satellites ($\phi_1 \approx 24°$, $\phi_2 \approx 37°$, $\Delta\theta \approx 34°$) and of the combined signal using MRC. Measurement data is taken from an urban and suburban environment. Four LMS models are intended to re-simulate these dual-satellite scenarios. For better visibility, the four models are split to the upper and lower figure.

Comparing the statistics for single satellites in Figure 5.1, the measurements are accurately re-simulated by all three- or two-state models with constant or variable Loo parameter sets. Deviations are below ±1 dB over almost the complete dynamic range for the urban and the suburban test scenario.

For multi-satellite case, available LMS models assume a state correlation only. However, simulation results with models *'2-state / 3-state & constant Loo'* and *'2-state & variable Loo'* in Figure 5.1 demonstrate that the MRC gain is still too high when only state correlation is considered. In the context of this work it has been found that also fading correlation within the joint states 'good good' and 'bad bad' exists (cf. Section 4.3). It holds also for the selected urban route, where a non-negligible fading correlation coefficient in 'bad bad'-state of $\rho_{\mathrm{bb}} \approx 0.52$ is derived (cf. Table 5.3).

In models with variable Loo parameters an additional fading correlation is introduced for

Loo parameter M_A and for the lognormal samples as described in Section 4.4. In case of algorithms with constant Loo parameters, this additional correlation is introduced while generating the lognormal distributed samples. The improvement of the additional correlation it is clearly seen in Figure 5.1, as the MRC curves for *'2-state & const. Loo'* and *'2-state & var. Loo'* are clearly closer to the measurement results than the corresponding curves considering 'state correlation only'.

Although the new multi-satellite LMS model has an improved description of fading correlation, the re-simulated MRC signal in the selected urban scenario has still deviations from the measurements. A possible reason is that correlation of multipath-fading exists, which is not considered in the current model. Even though a correlation coefficient of the multipath power (Loo parameter MP) is considered, the multipath (Rayleigh) fading generators of two satellites are independent. A detailed analysis of such a multipath correlation requires a clear separation of multipath fading, the fading of the direct signal component and the thermal noise, which is very limited from the available field strength data and therefore out of scope of this work. A further improvement for the MRC re-simulation in the urban scenario may be achieved if more variability of the fading correlation between two satellite signals is considered. The developed LMS model considers one average correlation coefficient between the fading signals in case of the state 'bad bad'. In the reality, however, there may be 'bad bad'-state sections of the route with high fading correlation (e.g. in case of two completely blocked signals in tunnels) and sections with lower fading correlation (e.g, tree-shadowing). The advanced modelling of the signal correlation requires further modifications of the LMS model implementation and is task of future activities.

It can be concluded that the correlation of further signal elements in the LMS model besides the states is essential to describe satellite diversity. Furthermore, all given models provide similar performance in terms of first-order statistics and there is no preference. Differences are expected by analysing the signals in time-domain (second-order statistics).

State Model and First-Order Statistics

The results in Figure 5.1 are independent from the selected state model, whether a first-order Markov model, semi-Markov model, or dynamic Markov model is selected. In fact, the PDF (and CDF) of the simulated signal depends on the state probabilities P and the PDF of the signal $P(r)$ within the states:

$$P_{\text{Model}}(r) = P_{\text{state1}} \cdot P(r)_{\text{state1}} + P_{\text{state2}} \cdot P(r)_{\text{state2}} + ... + P_{\text{state}N} \cdot P(r)_{\text{state}N} \tag{5.1}$$

In Chapter 3 it has been shown that different state models provide to re-simulate exactly the state probabilities for single satellites or combined satellites. With

$$P_{\text{state, Markov}} = P_{\text{state, semi-Markov}} = P_{\text{state, dynamic Markov}} \tag{5.2}$$

follows

$$P_{\text{Model, Markov}}(r) = P_{\text{Model, semi-Markov}}(r) = P_{\text{Model, dynamic Markov}}(r)\,. \tag{5.3}$$

5.1.3. Model Validation in Terms of Second-Order Statistics

Average Fade Duration and Level Crossing Rate

The LCR and the AFD are common methods to statistically evaluate the signals development over time, for which the term 'second-order statistics' is equivalently used. They are shown for the measurements and the re-simulated signals with four LMS models in Figure 5.2 and Figure 5.3.

For urban and suburban test scenarios it is obtained that models with variable Loo parameter generation more accurately re-simulate the LCR and the AFD of experimental data from

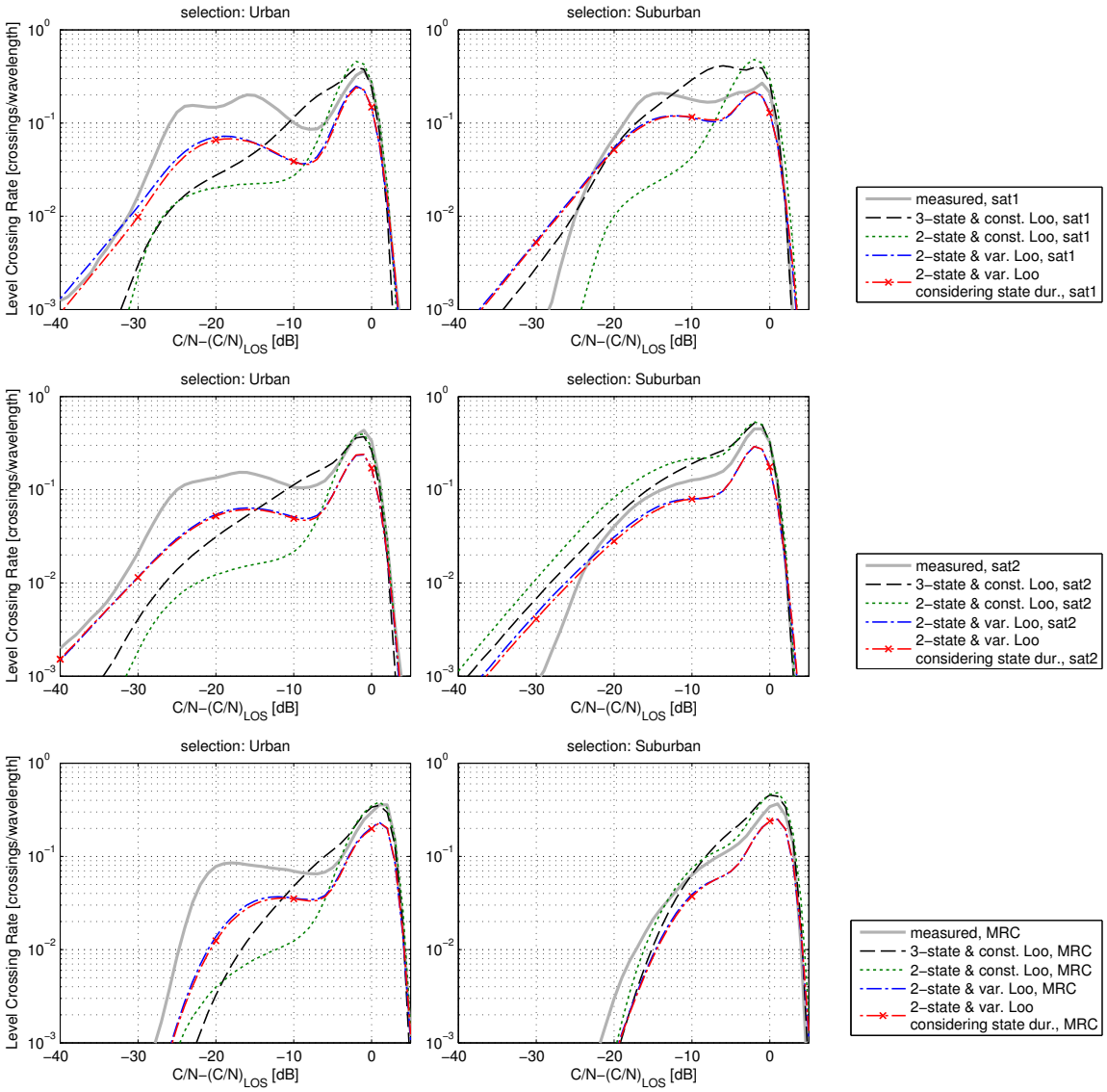

Figure 5.2.: Level crossing rate from measurement data and from different LMS models for satellite 1, satellite 2, and from the MRC signal of two satellites in an urban and suburban environment.

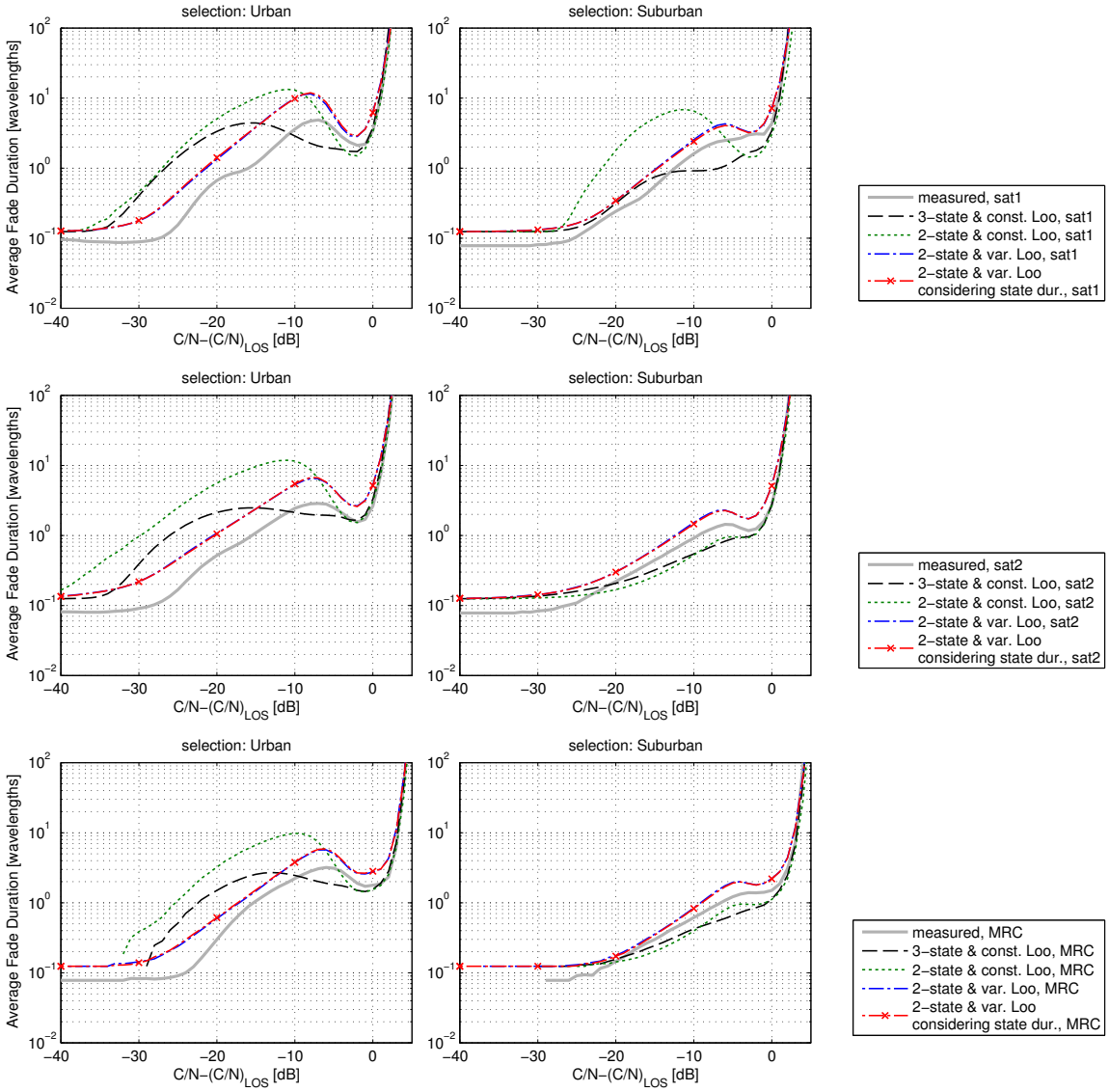

Figure 5.3.: Average fade durations from measurement data and from different LMS models for satellite 1, satellite 2, and from the MRC signal of two satellites in an urban and suburban environment.

a single satellite than constant Loo models. This better fit is also true for the combined satellite signals.

The reason for greater second-order deviations for 'constant Loo parameters' is possibly caused by parameter estimation. A curve-fit alone may not be the best option for Loo parameter estimation, as it does not consider the ratio of the statistical variation for slow and fast fading components. As a consequence, a good Loo distribution curve-fit does not necessarily lead to a good representation of the fading in time domain. In case of parameter estimation for 'variable Loo models' multiple curve-fits are applied. Thus, inappropriate Loo parameter triplets (which cause mismatches for second-order statistics) are only a part of the Loo parameter space and are possibly statistical outliers. In consequence, besides better

performance for second-order statistics, 'variable Loo models' are more robust in terms of parameter extraction than the constant Loo models.

From the proposed model with *'variable Loo parameters considering state duration'* no remarkable enhancement to the earlier *'2-state model & variable Loo parameters'* is gained for AFD and LCR statistics.

For the results in Figure 5.2 and Figure 5.3 the first-order Markov approach is selected as state model. As the first-order Markov approach as well as other state models (e.g. semi-Markov, dynamic Markov) accurately re-simulate the average state duration, similar AFD and LCR statistics are expected by applying different state models. Nevertheless, the influence of the state model becomes apparent when time interleaving is evaluated.

Validation of Time Interleaving and Influence of the State Model

Besides the AFD and LCR, the temporal composition of the signal can be effectively validated by obtaining the CDFs when considering time interleaving. It is realised by a low-pass filter (moving average) of the measured and/or simulated signal with a certain window size.

By evaluating the LMS models in time domain, performance differences between different state models (providing a characteristic state duration distribution) are expected. The following three state models are of closer interest:

1. The semi-Markov model in combination with the Lutz approach (notation: *semi-Markov, lognormal fit & Lutz, empirical*), as it is developed in the context of this work and proposed for accurate state probability and state duration modelling and feasible for multiple dual-satellite scenarios (cf. Chapter 3.4.3).
2. The Lutz approach (notation: *first-order Markov & Lutz*), as it is widely used in literature and the current reference for dual-satellite models.
3. The *dynamic Markov model*, as it is the algorithm with best possible state duration accuracy for dual-satellite modelling. For a comparison with other state models it is adequate to take the dynamic Markov model as reference, as it accurately re-simulates the state probabilities and joint duration statistics of the measurements. In Section 3.3 it is shown that the *Nth-order Markov* model (Chapter 3.1.5) provides better performance in theory. However, it is highly impracticable due to the related computational complexity.

The three state models are applied with the *'2-state model & variable Loo parameters'* which provided best fits for CDFs, LCRs and AFDs. Figure 5.4 shows the CDFs of the effective normalised C/N from measurements and after re-simulation with three different state models after time de-interleaving with different interleaver lengths.

It should be noted that, without interleaving, the state models provide **equal** CDFs for single and combined satellites. These results are given in Figure 5.1 (represented by *2-state & variable Loo*).

By considering a short time interleaver of 10 m length, a performance difference between different state models is still negligible, as seen in Figure 5.4. The suburban scenario is well

re-simulated by the LMS models, whereas their CDFs deviate by up to 1 dB. However, for the urban scenario significant differences between the measured and re-simulated statistics are obtained for 10 m interleaving.

As this deviation holds for all applied state models (same effect has been obtained with a 25th-order Markov model), an inaccurate modelling of a state sequence can be excluded as possible cause. The difference between measurements and re-simulation is already present for the single-satellite channel. To cope with that problem, the consideration of a correlation between Loo parameters, or the inclusion of further state length dependencies on the Loo parameters might be a solution. In this thesis an existent single-satellite LMS model is taken as basis for multi-satellite modelling. Fundamental changes of its architecture are out of scope of this work. The short interleaver demonstrate that the urban scenario is still challenging for LMS modelling.

By considering interleaver lengths of 25 m and 100 m, the re-simulated statistics vary with respect to the state model, as seen in Figure 5.4. The interleaver gains achieved with the *first-order Markov & Lutz* model are generally greater than the interleaver gains from the *semi-Markov* and *dynamic Markov* model, whereat the *semi-Markov* and *dynamic Markov* model are closer to the measurements. A reason is that first-order Markov models not accurately describe long state durations, i.e. the probability of modelling long blockages is lower than from semi-Markov or dynamic Markov models (cf. also Figure 3.11 in Chapter 3.3). Thus, a greater percentage of signal blockages due to a first-order Markov chain are compensated by an interleaver. The lognormal SDPDF approximation of the semi-Markov model has the opposite effect in the current urban example: state durations are described and re-simulated, which are longer than the measured durations. Thats why the interleaver gains are smaller in comparison to the dynamic Markov model.

Significant differences between the state models are obtained for 100 m interleaving in Figure 5.4. Due to the limited length of the measured sections, the CDFs from measurements after 100 m interleaving are bumpy curves, which complicates a comparison between measurements and re-simulation. For the urban scenario, the *dynamic Markov* model (which is the reference model) most likely matches the measurements. With respect to the *dynamic Markov* model, the interleaver gains from *first-order Markov & Lutz* model are greater and the gains from *semi-Markov, logn.fit & Lutz, empirical* are smaller. For example, the interleaver gains with MRC are +3 dB for Lutz and -2 dB for semi-Markov at 99% signal availability with respect to the dynamic Markov model. For the suburban scenario the differences between the CDFs for the three state models are smaller with ≈1 dB. In both environments, the MRC statistics of the *semi-Markov, logn.fit & Lutz, empirical* model are closer to the dynamic Markov model and the measurements than *first-order Markov & Lutz* anyway.

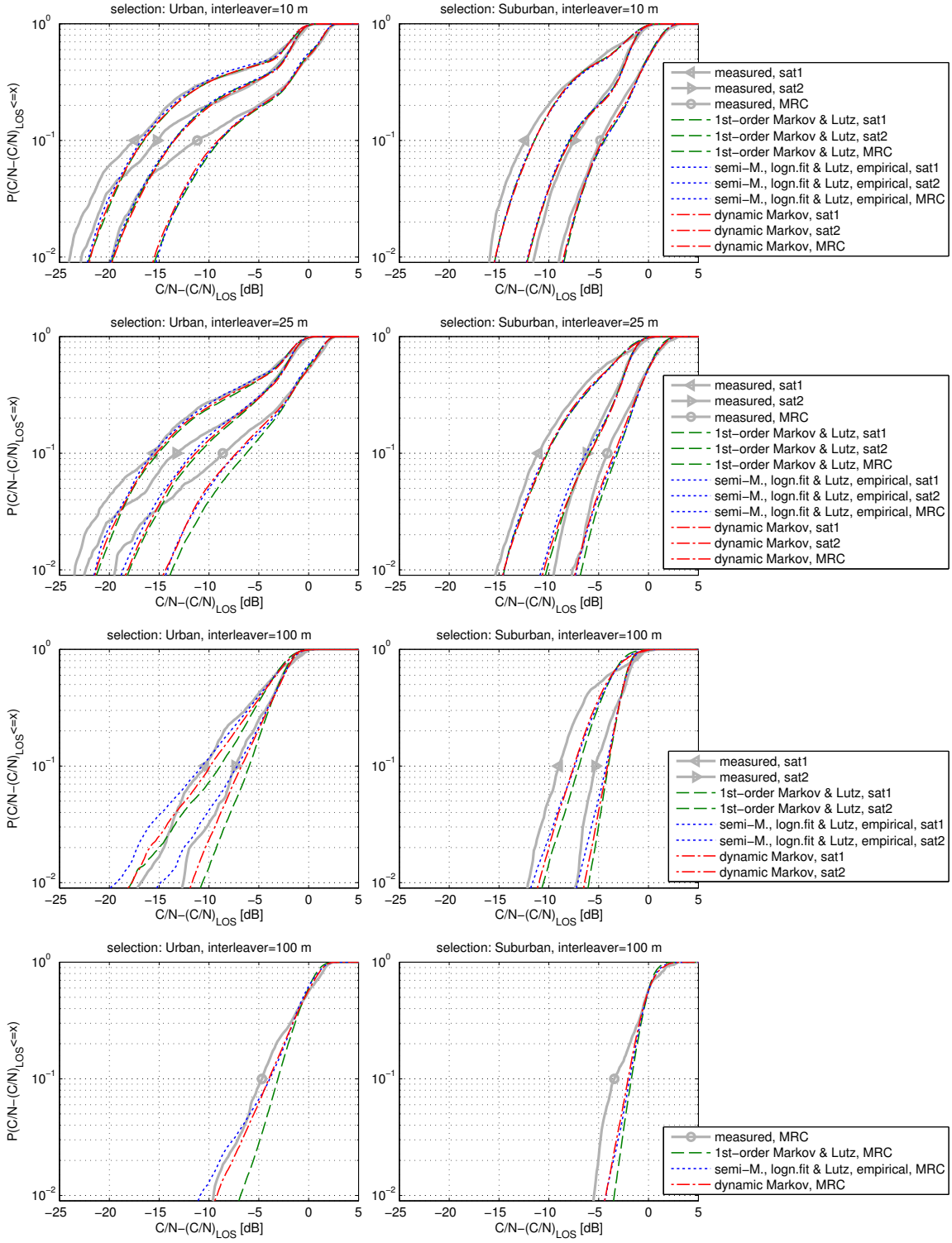

Figure 5.4.: Effective CDFs after time de-interleaving for measured and re-simulated signals of two satellites and the MRC signal. For re-simulation, different state models are combined with the versatile Loo model. Interleaver lengths are 10 m, 25 m, and 100 m. The re-simulation results without interleaving for the given state models are identical and are represented by *'2-state & var. Loo'* in Figure 5.1.

5.1.4. Conclusions on Model Architecture

In Chapter 4 a channel model implementation for dual-satellite reception has been developed based on observations from experimental data. It consists of a 'four-state semi-Markov model' to generate state sequences, and a 'variable Loo model' to generate the fading signal within the states. Signal correlation is introduced for states and for slow fading components as well. In this section this new channel model architecture is compared with measurement data and with other reference LMS modelling concepts in terms of first- and second-order statistics.

It following conclusions are drawn:

- The new dual-satellite model more accurately describes satellite diversity than existent multi-satellite models from literature. It is due to the additional correlation of slow fading when both satellites are in same state. In contrast, existing models provide state correlation only. However, the model validation on an urban scenario demonstrates that the current implementation need further to be optimised for challenging scenarios.
- The first-order statistics of the individual satellites are accurately described with the proposed model. Same holds for other existing single-satellite LMS models.
- The AFD and LCR statistics indicate the improvement of a model using 'variable Loo parameters' with respect to models using 'constant Loo parameters'. It is already stated in [PCPFB+10] for single-satellite reception and confirmed in this section for single- and dual-satellite reception as well.
- The model extension 'variable Loo parameters considering state duration' has no enhancement to 'variable Loo'. Thus, with respect to the number of parameters, the earlier 'variable Loo' model is recommended for the single-satellite channel. It is extended for dual-satellite reception in this work.
- By considering time interleaving there are still challenges for LMS modelling. The re-simulation of an urban environment with a short time interleaver (of, e.g. 10 m) has shown differences between measurements and re-simulated signals already for the single-satellite case. This result is independent of the chosen state model. For a possible correction the fading model or the corresponding model parameters within the states have to be adapted.
- By considering long time interleaving, it is shown that a semi-Markov model have performance benefits for dual-satellite modelling over the state-of-the-art approach, the Lutz approach based on first-order Markov chains. In the context of this work, the semi-Markov model is modified to make it feasible for parameter extraction for multiple dual-satellite constellations. This *semi-Markov, lognormal fit & Lutz, empirical* approach is successfully evaluated in this section.
  Nevertheless, the best performance with long time-interleaving is provided by using the dynamic Markov model without any approximation of parameters. For re-modelling sporadic scenarios, where timeseries of fading satellite signals are available, the dynamic Markov model is thus the recommended selection. However, the dynamic Markov model has strong limitations for the parametrisation of an LMS model able to compare mobile reception from different satellite positions or between different coverage areas.

5.2. Evaluation of Three-Satellite Modelling with Master-Slave

Analogue to the dual-satellite model, the challenge of LMS modelling with three satellites is to find model parameters for satellite constellations, for which measurement data is not available. A solution is the Master-Slave approach, where parameters of a three-satellite constellation are completely derived from dual-satellite parameters. Thus, timeseries for arbitrary constellations of three satellites can be generated with Master-Slave. Within a three-satellite constellation, two slaves depend on one master. Since the correlation coefficient between the slaves is not considered, a certain correlation error and a probability error of the combined signal of three satellites have to be taken into account with Master-Slave. Although these errors are minimised by an appropriate definition of the master satellite (cf. Section 3.5.3), they are not zero.

In this section the state approach 'Master-Slave' is evaluated in the context of the complete LMS model implementation. The modelling results are compared with measurement data and with results of a reference state model for three-satellite reception in terms of first- and second-order statistics. The reference is the straightforward dynamic Markov model, which accurately describes the correlation coefficients between three satellites as well as the state duration distributions. By comparing the Master-Slave approach with the reference model, the influence of the correlation error of the Master-Slave approach (considering an appropriate mapping) is visible. For improved state duration modelling, the three-satellite Master-Slave model is implemented by a combination of the dual-satellite *semi-Markov, logn.fit & Lutz, empirical* model and the Master-Slave approach ASTM-MT (cf. Chapter 3.5.4 for details). In the following, a three-satellite Master-Slave-constellation with a small correlation error and a constellation with a great correlation error is presented.

Master-Slave with Small Correlation Error

Two LMS models with different state approaches are intended to re-simulate satellite signals obtained within the urban and suburban scenario known from previous Section 5.1. The measured statistics of satellite 1 (short notation: *sat1*) and satellite 2 (*sat2*) are equal to Figure 5.1. Now a third satellite (*sat3*) is considered, which is located at $\phi_3 \approx 65°$ for the urban scenario. The azimuth angle separations are $\Delta\theta_{12} \approx 34°$, $\Delta\theta_{13} \approx 99°$, and $\Delta\theta_{23} \approx 133°$. For the suburban scenario the positions are $\phi_3 \approx 69°$, $\Delta\theta_{12} \approx 34°$, $\Delta\theta_{13} \approx 4°$, and $\Delta\theta_{23} \approx 30°$. The different positions of *sat3* between urban and suburban are due to the high-elliptical orbit of the satellite and the ordering of the constellation for small- and great correlation error.

The CDFs of the measurements and after re-simulation considering Master-Slave and the dynamic Markov model are compared in Figure 5.5. Results without interleaving are presented as well as results with interleaver lengths of 25 m and 100 m for *sat1*, *sat2*, *sat3* and for MRC of the three satellites. After an optimised Master-Slave mapping, in which master is *sat2*, the remaining correlation error for the urban scenario is $\Delta\rho = 0.0477$ and the probability error of 'bad bad bad' is $\Delta P_{\mathrm{bbb}} = 0.0023$. For suburban it is $\Delta\rho = 0.0628$ and $\Delta P_{\mathrm{bbb}} = 0.0036$.

The following results are obtained in Figure 5.5:

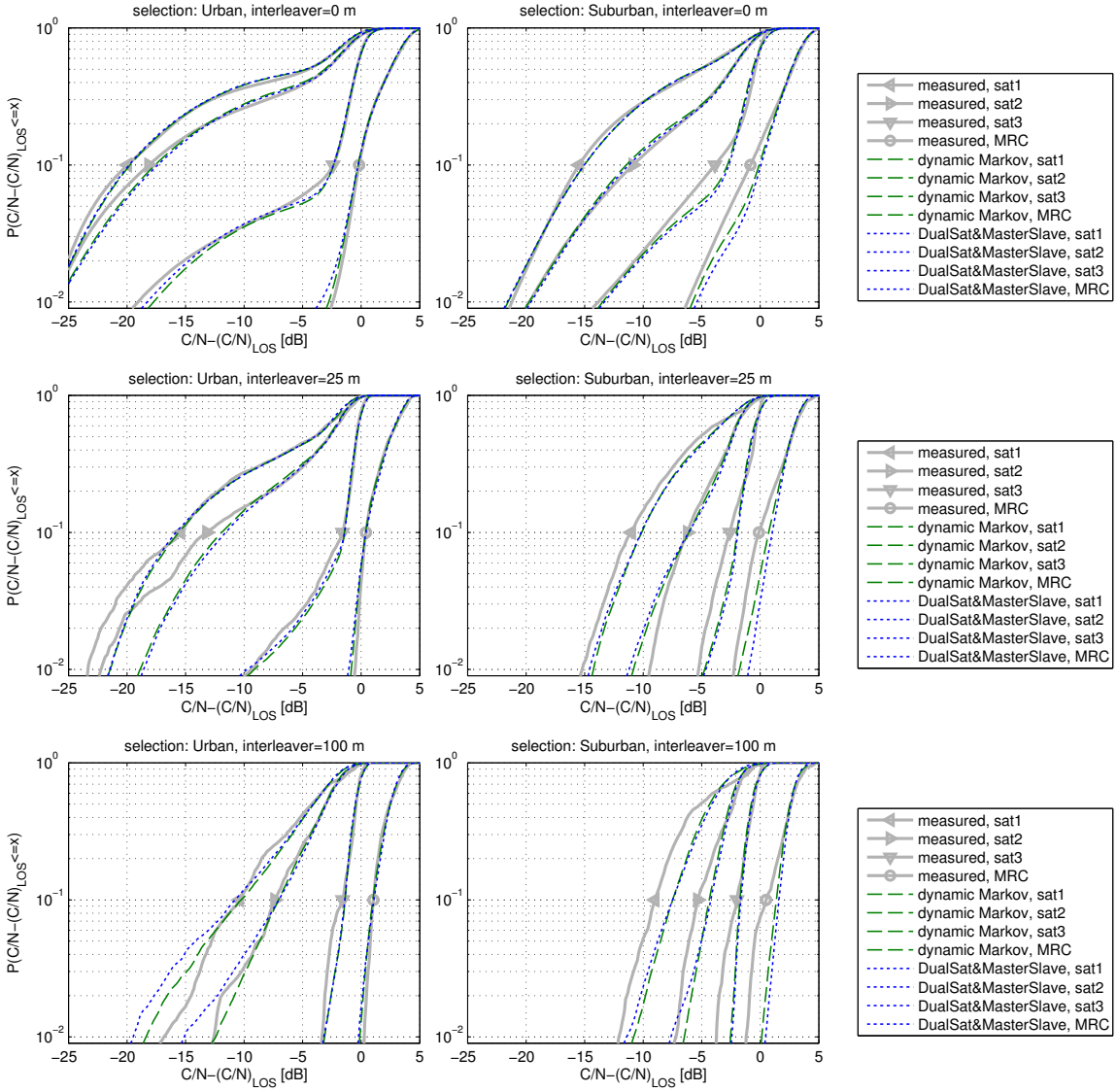

Figure 5.5.: Effective CDFs without interleaving and after time de-interleaving for measured and re-simulated signals of three satellites and the MRC signal in an urban and suburban environment. For re-simulation, the versatile Loo model is combined with two different state models: a dynamic Markov model, and the Master-Slave approach ASTM-MT. Interleaver lengths are 25 m, and 100 m.

- Without time interleaving, the simulation results of the Master-Slave approach are close to the results of the reference state model. It holds for the single-satellite channels as well as for the MRC signal in the urban and the suburban scenario. Both models accurately re-simulate the measurements.

- Considering time interleaving of 25 m, the LMS simulation of *sat1* and *sat2* in the urban environment have some deviations to the measurements. It holds for both state models and is already discussed in previous Section 5.1.3. For *sat3*, the re-simulated statistics have a high agreement with the measured statistics. As *sat3* dominates the reception and mainly contributes to the MRC signal, the good re-simulation of *sat3*

leads to a good re-simulation of the combined signal. The differences between the state models are small with ≤ 1 dB.

- With 100 m interleaving, the statistics of the Master-Slave approach diverge from the dynamic Markov model in the urban environment. *Sat1* and *sat2* are generated with the dual-satellite *semi-Markov, logn.fit & Lutz, empirical* model, which partly considers too long state durations. The results for *sat1* and *sat2* are already discussed in Section 5.1.3. The results for *sat3* as well as the MRC signal re-simulated with Master-Slave is in a high agreement with the dynamic Markov model as well as with the measurements. Also in the suburban environment the Master-Slave model provide similar results as the reference dynamic Markov model at 100 m interleaving. However, the time diversity gains are up to 2 dB greater than from the measurements.

Master-Slave with Great Correlation Error

For certain satellite constellations Master-Slave provide a high error even with optimised mapping, as shown in Section 3.5.3. For the subsequent analysis a third satellite in urban is considered with elevation $\phi_3 \approx 57°$, and azimuth separations $\Delta\theta_{12} \approx 34°$, $\Delta\theta_{13} \approx 47°$, and $\Delta\theta_{23} \approx 13°$. For the suburban scenario the positions are $\phi_3 \approx 70°$, $\Delta\theta_{12} \approx 34°$, $\Delta\theta_{13} \approx 85°$, and $\Delta\theta_{23} \approx 119°$.

The CDFs of the measurements after re-simulation with Master-Slave and with a reference state model are shown in Figure 5.6. Time interleaving of 0 m (no interleaving), 25 m, and 100 m is considered. After Master-Slave mapping, the correlation- and probability errors are $\Delta\rho = 0.1138$ and $\Delta P_{\text{bbb}} = 0.0198$ for the urban scenario, and $\Delta\rho = 0.128$ and $\Delta P_{\text{bbb}} = 0.0064$ for the suburban scenario, respectively.

The following observations are done in Figure 5.6:

- The Master-Slave approach accurately describes the state probabilities of the single-satellite channels. Without interleaving, there is no difference between Master-Slave and another state model therefore.
- The probability error of Master-Slave influences the MRC signal. Without interleaving it is seen that the MRC gain with Master-Slave is greater than with a reference state model, which accurately describes the joint state probabilities. It is due to the smaller state correlation considered with Master-Slave. However, accurate modelling of joint probabilities does not necessarily result in an accurate modelling of the satellite diversity signal, as obtained for the urban environment and discussed in Section 5.1.2.
- For 25 m time interleaving, the resulting CDFs of Master-Slave and the reference state model are similar for the single satellite channels in urban and suburban. For the MRC signal, the deviation between Master-Slave and the reference model is increased due to the probability error.
- Assuming 100 m time interleaving, in the suburban scenario the performance of Master-Slave is similar to the dynamic Markov model. In the urban scenario, the dual-satellite semi-Markov model provide the deviation of *sat1* and *sat2* in comparison to dynamic Markov. Also the slave satellite *sat3* modelled with ASTM-MT has more signal attenuation than the reference model, although it is modelled by a first-order Markov algorithm. Obviously this result is influenced by the master *sat2*. The correlation

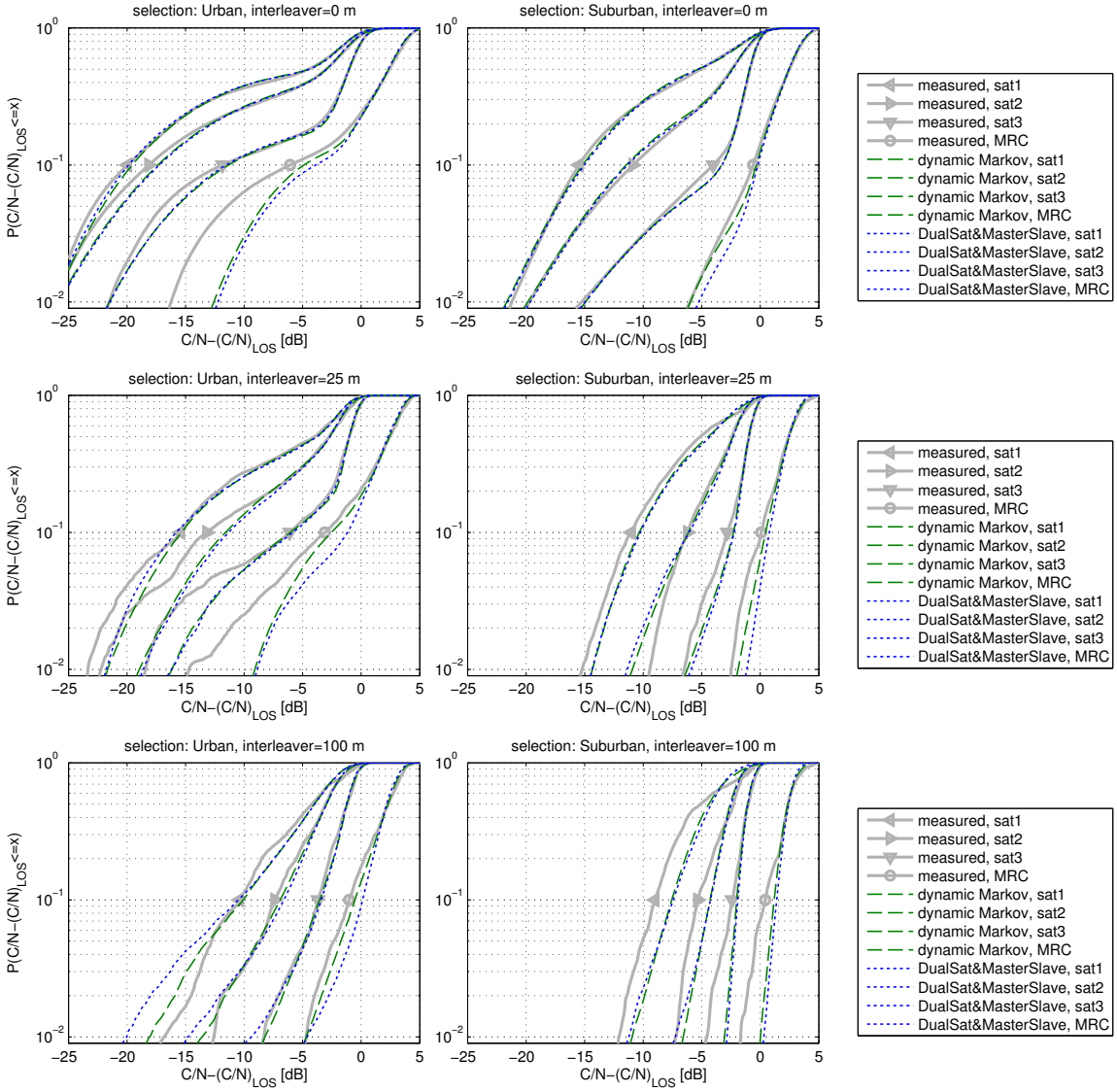

Figure 5.6.: Effective CDFs without interleaving and after time de-interleaving for measured and re-simulated signals of three satellites and the MRC signal in an urban and suburban environment. For re-simulation, the versatile Loo model is combined with two different state models: a dynamic Markov model, and the Master-Slave approach ASTM-MT. Interleaver lengths are 25 m, and 100 m. Note that satellite 3 is different than in Figure 5.5.

error and probability error of Master-Slave is indicated again with the MRC signal: Although the single satellites have more signal attenuation than the reference, the MRC signal has less attenuation anyway.

The results in Figure 5.5 and in Chapter 3.5.3 demonstrate, that Master-Slave is an appropriate state model to generate timeseries for three-satellite reception and feasible for a great variability of satellite positions. However, also different satellite constellations exist where the Master-Slave approach provides a state probability error which leads to inaccurate predictions of satellite diversity with three satellites. As the Master-Slave error can be

calculated, critical satellite constellations can be identified and the Master-Slave results can be properly handled.

5.3. Validation of Model Parameter Sets

In the context of this work parameters sets have been derived for a **single-satellite LMS model** and a new **dual-satellite LMS model**, describing the fading for

- five different environments: Urban, Suburban, Forest, Commercial and Open
- different elevation angles for each satellite between 20° and 90° , that are interpolated from elevation segments of 10° range
- different azimuth angle separations interpolated from intervals: 0-10°, 10-30°, 30-60°, 60-90°, 90-120°, 120-150°, 150-180° (for dual-satellite case)
- different driving directions with intervals: 0-10°, 10-30°, 30-60°, 60-90°

To achieve this variability, models parameters are jointly derived from two measurement campaigns:

- State parameters and correlation coefficients are derived from GNSS measurements (L-band at 1.6 GHz), which provide a high variability of satellite constellations.
- Loo parameters are derived from SDARS measurements (S-band at 2.3 GHz), which have the required signal resolution in time and amplitude to obtain fast and slow fading parameters. From SDARS measurements, also state parameters can be derived for single-satellite case.

Details of the measurements are found in Appendix A.

In this section the channel model parameter sets are validated by comparing SDARS measurement data with the channel model output. For the model implementation, state parameters are derived either from GNSS measurements (L-band) or from SDARS measurements (S-band), and the Loo parameters from SDARS measurements (S-band). Hence, two parameter sets are available from the project MiLADY:

1. *MiLADY SDARS parameter set.* (Parameters are found in Table C.1 and Table C.2.)
2. *MiLADY SDARS Loo- & GNSS state parameter set.* (Parameters are found in Table C.1 and Table C.3.)

For dual-satellite case, correlation coefficients are exclusively derived from GNSS measurements. This additional *GNSS correlation parameter set* is found in Table C.4 and Table C.5.

As the frequency band mainly affects the fast fading characteristics, which parameters are derived from the SDARS (S-band) measurements, the simulation results are all valid for S-band. An influence of the frequency difference between L-band and S-band onto the state parameters can be neglected. Output of the channel model is a timeseries of the LOS-normalised C/N at the mobile terminal, which is compared with measured C/N data.

5.3.1. Validation of Model Parameter Sets in Terms of First-Order Statistics

In Figure 5.7 the CDFs of the new LMS model output for single-satellite reception are compared with the SDARS measurement data and with the three-state model from Fontan et al. ([PFVCC+01], S-band parameters) for a suburban environment. For first-order statistics, it should be mentioned that the output of the single-satellite models equals the outputs of the corresponding dual-satellite model. The following results are obtained:

- Taking the state parameters from SDARS, a high agreement between (SDARS) measurements and modelling results is seen. This indicates a correct model parameter estimation for slow- and fast variations and states. However, the amount of SDARS measurement data is too small for conclusions about different driving directions.

- The GNSS state parameters allow a simulation of four sections of driving directions for single-satellite reception. The statistic considering all driving directions (0°-360°) has a similar characteristic as 30°-60° driving direction. The worst case is obtained when the satellite azimuth is approximately 90° to the street orientation.

- The *MiLADY SDARS parameter set* simulates less signal attenuation than the *MiLADY SDARS Loo & GNSS state parameter set*. It is already indicated by the 'bad'-state probabilities in Figure 3.13 from Chapter 3.4.1. A reason could be typically smaller streets in European environments and therefore a higher shadowing probability than in U.S. environments.

- The DVB-SH reference model at $\phi = 40°$ is similar to the SDARS measurements at $\phi = 35°$ in the suburban environment. The deviation between the CDFs is below 2 dB. At $\phi = 60°$ the DVB-SH reference model is more optimistic than the SDARS measurement statistics and our modelling results. The SDARS measurements at $\phi = 75°$ are in turn more optimistic than the DVB-SH reference at $\phi = 80°$.

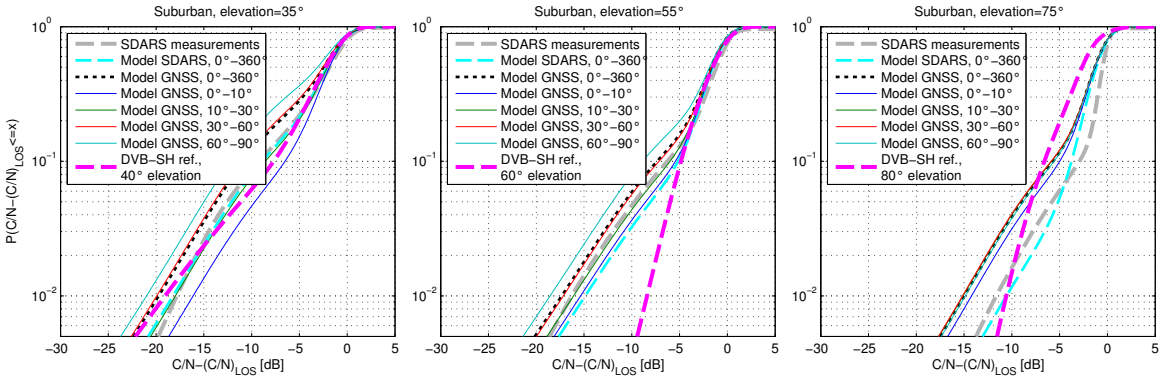

Figure 5.7.: Comparison of first-order statistics between the channel model simulation, the SDARS measurements, and the DVB-SH reference model (3-state model from Fontan et al. [PFVCC+01]) for three elevation angles in the suburban environment. For simulation, the Loo parameters from SDARS measurements are combined with the state parameters from GNSS (Model GNSS) or from SDARS measurements (Model SDARS). The GNSS state parameters provide to distinguish four driving directions, which are denoted in the legend.

For a comprehensive analysis of modelling results for multiple receive scenarios, the required margins for 90% and 99% signal availability are derived from the CDFs. It is the difference between the C/N at LOS (0 dB) and the C/N, which is exceeded in 90% or 99% of driven distance, respectively. Figure 5.8 shows the required margins for different environments and elevation angles after simulation. A good agreement between SDARS measurements and the model simulation with the *MiLADY SDARS parameter set* is seen (with most deviations below 2 dB), which indicate that the parameter set well represents the SDARS measurements. By using the merged *MiLADY SDARS Loo & GNSS state parameter set* an LMS timeseries simulation of more challenging scenarios can be performed, since the required margins for Suburban, Forest, Commercial and Open are larger in comparison to the SDARS measurements. Both parameter sets provide plausible simulation results with respect to the environment type, the elevation angle, and the driving direction.

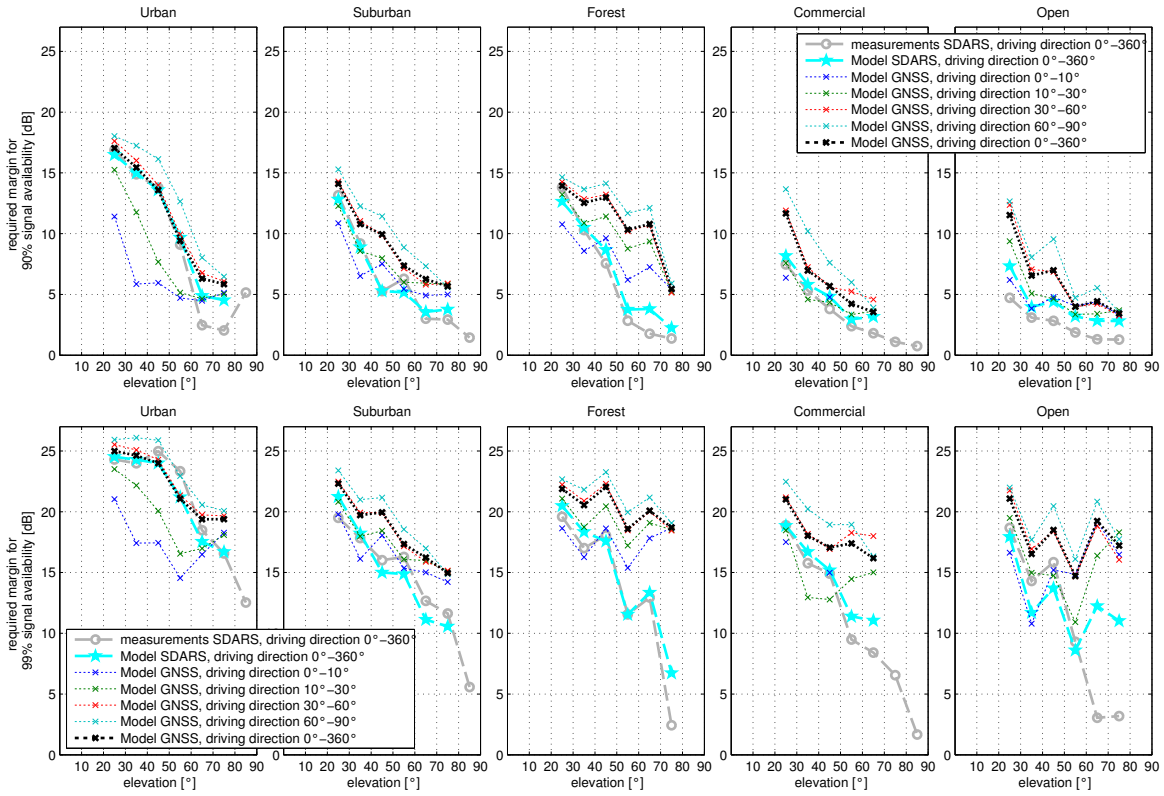

Figure 5.8.: Required margins for 90% signal availability (top) and 99% signal availability (bottom) from SDARS measurements and after simulation using the *MiLADY SDARS parameter set* (Model SDARS) or the *MiLADY SDARS Loo- & GNSS state parameter set* (Model GNSS). The parameter sets are found in Table C.1, Table C.2, and Table C.3.

5.3.2. Re-modelling of Satellite Diversity

For dual-satellite reception the correlation between the satellites needs to be considered. Correlation coefficients for states (ρ_{states}) are derived from GNSS measurements for different azimuth separations $\Delta\theta$ and for pairs of elevations ϕ_1 and ϕ_2 in a certain environment. By applying the correlation coefficients with further parameters of the proposed *semi-Markov,*

logn. fit & Lutz, empirical model, simulation results in terms of state probabilities and state duration statistics are presented in Chapter 3 for various satellite constellations in the urban environment.

Additional correlation effects between two satellites are found for fading within the states. Therefore, correlation coefficients are derived for signals within the combined states 'good good' (ρ_{gg}) and 'bad bad' (ρ_{bb}) in Chapter 4 for same satellite constellations as with the states. They are applied to the slow lognormal variations twice for the versatile Loo parameter generation and for the lognormal samples generation in the proposed model.

In the following the dependency of the dual-satellite fading on the correlation of two satellite signals is demonstrated. Figure 5.9 shows the signal correlation coefficients in dependency on the azimuth angle separation $\Delta\theta$ of the satellites in the suburban environment. These values are parameters of the dual-satellite LMS model and are found in the *GNSS correlation parameter set*. Based on these correlation coefficients, Figure 5.10 shows CDFs of two satellites and the MRC signal for different values of $\Delta\theta$ from the LMS model output. The driving direction of the vehicle is assumed to be equally distributed. Each subfigure include statistics resulting from seven dual-satellite model simulations (due to seven different values of $\Delta\theta$) with constant parameters of the single satellites due to same elevation angle. The

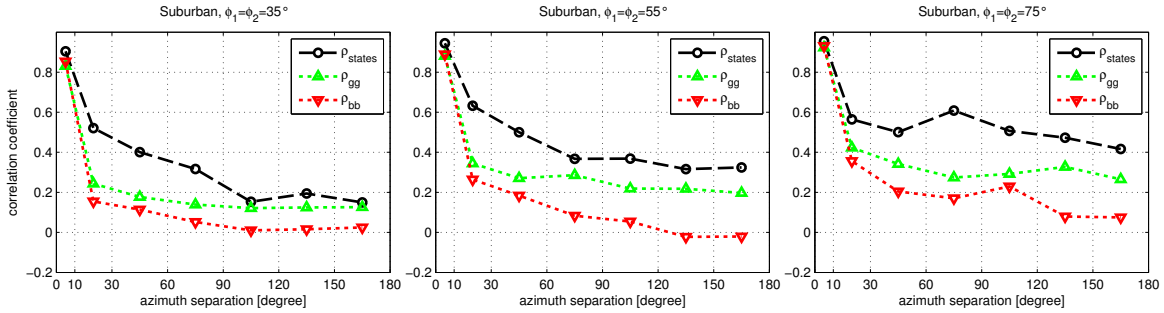

Figure 5.9.: Correlation coefficients from the *GNSS correlation parameter set* for three elevations ϕ_1 and ϕ_2 and different azimuth separations $\Delta\theta$.

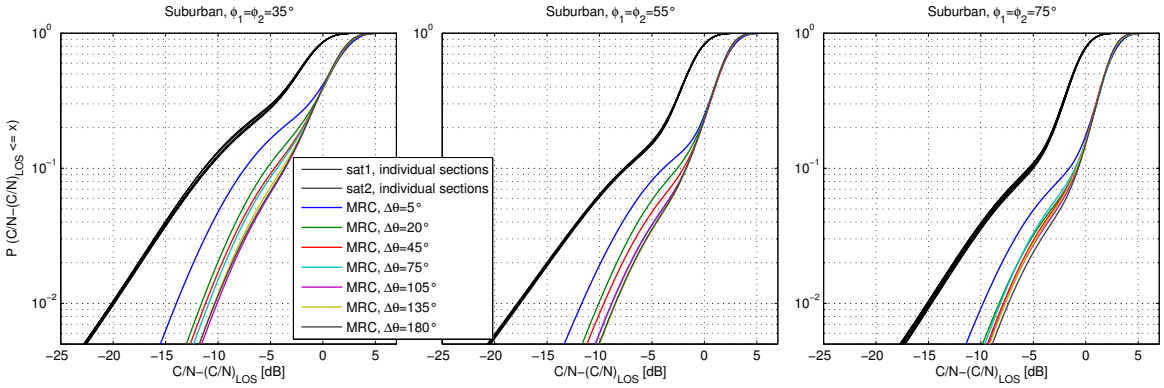

Figure 5.10.: CDFs from the channel model output for single satellite signals and MRC signals considering different elevations ϕ and azimuth angle separations $\Delta\theta$. The *MiLADY SDARS Loo- & GNSS state parameter set* is used for simulation. The driving direction is assumed to be equally distributed.

overlaid CDFs of the single satellites demonstrate that the single satellite channels are not affected by variable correlation coefficients and therefore by variable dual-satellite model parameters.[1] Thus, meaningful and comparable analyses of satellite diversity between different satellite constellations are possible. From the CDFs the required margins for 99% signal availability are derived in Figure 5.11. As expected, the MRC gain has inversely proportional behaviour to the satellites correlation from Figure 5.9. For example, the MRC gain for 99% signal availability in case of $\Delta\theta \approx 100°$ is 4 dB greater than for $\Delta\theta = 5°$, as obtained from Figure 5.11 for the suburban environment at $\phi = 35°$. It corresponds to correlation coefficients of $\rho \approx 0.1$ ($\approx \rho_{\text{states}} \approx \rho_{\text{gg}} \approx \rho_{\text{bb}}$) and $\rho \approx 0.9$, respectively.

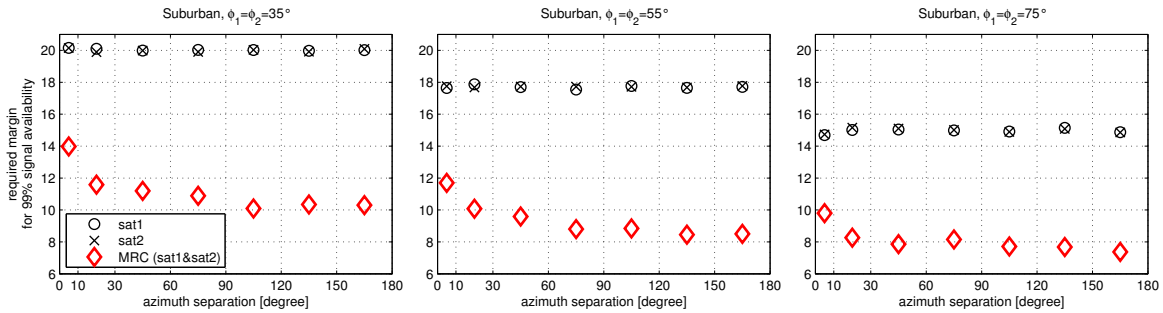

Figure 5.11.: Required margins for 99% signal availability derived from the channel model output for single satellite signals and MRC signals considering different elevations ϕ and azimuth angle separations $\Delta\theta$. The *MiLADY SDARS Loo- & GNSS state parameter set* is used for simulation.

To compare the dual-satellite model output with SDARS measurements, Figure 5.12 shows the CDFs for the selected urban and suburban dual-satellite scenario from Section 5.1 and after re-simulation using the *MiLADY SDARS parameter set* as well as the *MiLADY SDARS Loo- & GNSS state parameter set*.

For single-satellite reception, the *MiLADY SDARS parameter set* provide more optimistic results (i.e. less attenuation) than the exemplary urban and suburban scenario. It is due to the fact that the model parameter set represents the average of all observations in urban or suburban environments from the SDARS measurements within an elevation interval of 10°. Thus, the *MiLADY SDARS parameter set* for single-satellite reception represent a medium dense urban environment and a suburban environment with medium shadowing, respectively. The *MiLADY SDARS Loo- & GNSS state parameter set* more accurately describes the selected scenarios in case of single-satellite reception.

Looking at the MRC statistics in the suburban environment, a high agreement between measurements and re-simulation is seen for the *MiLADY SDARS Loo- & GNSS state parameter set*. From the *MiLADY SDARS parameter set* a deviation between the measured and re-simulated MRC statistics is seen. Nevertheless, this result is acceptable, since the MRC offset is similar to that from satellite 1 and satellite 2.

Looking at the MRC statistics in the urban environment, it is seen that the re-modelled MRC gain from both parameter sets is significantly greater than from the measurements. Different effects contribute to this deviation: Firstly, in Section 5.1.2 it is shown that this

[1] Small differences between the single-satellite statistics are due to limited simulation length.

urban scenario is challenging for diversity modelling, also when model parameters are directly estimated from the corresponding measured sequence. Secondly, the state correlation coefficient in the *GNSS correlation database* is lower ($\rho_{\text{states}} = 0.1894$) than in the current selection ($\rho_{\text{states}} = 0.3316$, cf. Table 5.4). A possible reason for this difference is that ρ_{states} not only depends on the azimuth separation between the satellites, but also on the vehicles driving direction. A corresponding analysis is found in [RAIG13]. In this work, ρ_{states} is derived assuming an equally distributed driving direction of the vehicle.

It can be concluded that the correlation coefficients ρ_{states} in the GNSS correlation database are in general too small for the urban environment. An alternative is to use the empirical model of Robet et al. [REE92] to calculate greater ρ_{states} in urban (cf. also Section 3.4.2), which are $\rho_{\text{states}} = 0.34$ for the *MiLADY SDARS parameter set* and $\rho_{\text{states}} = 0.28$ for the *MiLADY SDARS parameter set* and the given constellation.

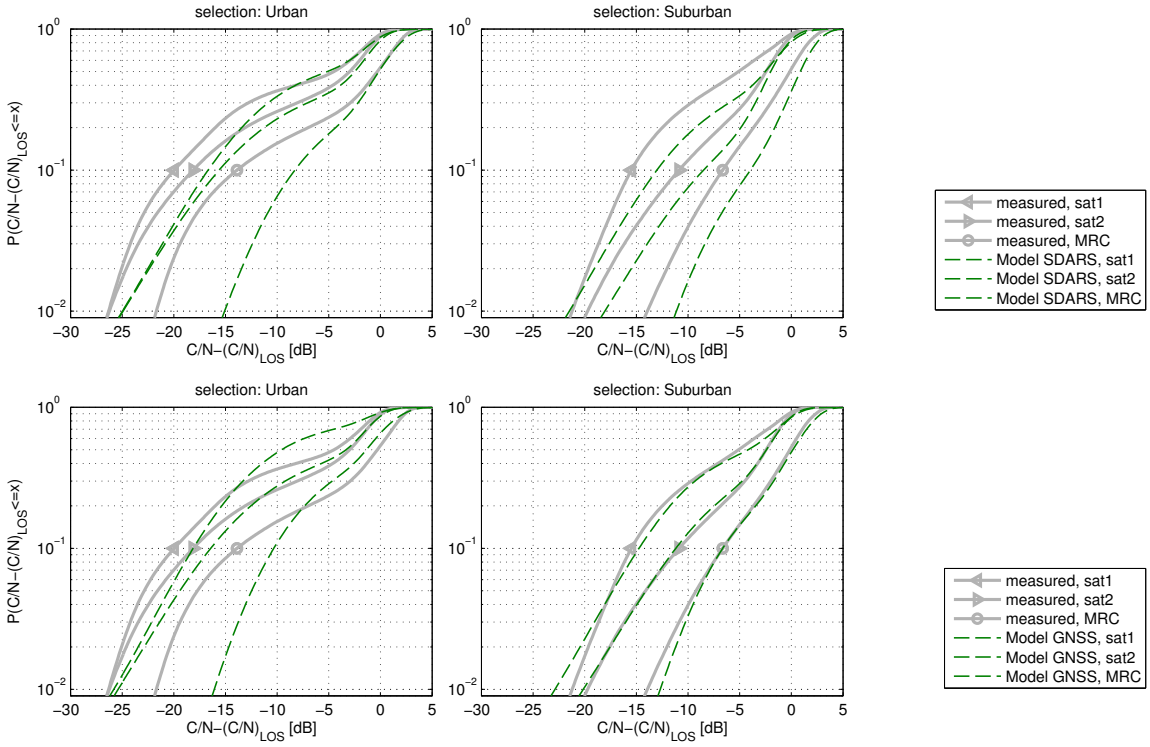

Figure 5.12.: CDFs from the dual-satellite LMS model output using the *MiLADY SDARS parameter set* (Model SDARS) and the *MiLADY SDARS Loo- & GNSS state parameter set* (Model GNSS) in comparison with the exemplary urban and suburban measurements from Section 5.1.

5.3.3. Re-modelling of Time Diversity

By changing only the correlation coefficients between two satellites, the developed dual-satellite model provides different statistics of the combined signal of two satellites, while the first-order statistics of the individual channels remain constant. However, it holds not for the second-order statistics of the individual channels by applying the proposed *semi-Markov, lognormal fit & Lutz, empirical* model for state sequence generation. Figure 5.13 shows

the state duration PDFs of a single satellite at elevation $\phi_1 = 35°$ simulated by the dual-satellite state model with parameters from multiple satellite constellations. In detail, the constellations are all permutations of $\phi_1 = 35°$ and $\phi_2 = \{15, 25, 35, 45, 55, 65, 75, 85\}°$ and $\Delta\theta = \{5, 20, 45, 75, 105, 135, 165\}°$. Two effects are obtained in Figure 5.13: Firstly, by using the dual-satellite *semi-Markov, lognormal fit & Lutz, empirical* model, the state duration statistics of satellite 1 are influenced by the position of satellite 2. Secondly, these SDPDFs are different from the comparable single-satellite semi-Markov model with lognormal fit, whose curve-fit is closer to the measurements. Both limitations are generally valid for semi-Markov models as well as for dynamic Markov models for multi-satellite reception.

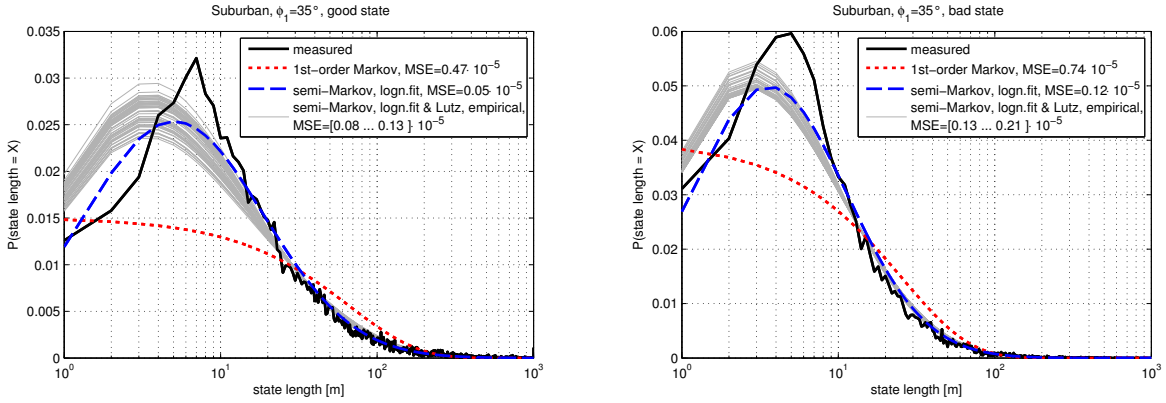

Figure 5.13.: State duration PDFs for good state (left) and bad state (right) for a satellite at $\phi = 35°$ obtained from GNSS measurements and re-simulated by the *semi-Markov, logn.fit & Lutz, empirical* state model using multiple selections from the *MiLADY SDARS Loo- & GNSS state parameter set*. Parameters are taken from $\phi_1 = 35°$ and $\phi_2 = \{15, 25, 35, 45, 55, 65, 75, 85\}°$ and $\Delta\theta = \{5, 20, 45, 75, 105, 135, 165\}°$. For comparison, the simulation results for the single-satellite semi-Markov model (logn. fit) and a first-order Markov model are depicted.

Nevertheless, despite of these limitations of the *semi-Markov, lognormal fit & Lutz, empirical* model, the SDPDFs are more accurately described than the traditionally used *first-order Markov & Lutz* model. It is indicated by the MSE between measured and re-simulated 'bad'-state duration statistic given in Figure 5.13.

To evaluate the consequence of different SDPDF fits from the given state models above, Figure 5.14 presents the required margins for 99% signal availability incorporating different interleaver lengths after LMS channel simulations using the *MiLADY SDARS Loo- & GNSS state parameter set*. To have a reference, the state model with best possible performance is selected for single-satellite case. It is the dynamic Markov model (or alternatively: the semi-Markov model without any approximation), in which the measured state duration statistics are applied as model parameter. Note that this reference is not availalbe for dual-satellite reception due to missing measurement data. Without time interleaving, i.e. 0 m interleaver length, the results are equal, since the selected models provide the same equilibrium state probability. The influence of different state duration approximations (*exponential fit* , *lognormal fit*, *no fit* from Figure 5.13) for single-satellite reception is noticeable for time interleaving over 25 m of travelled distance. For greater interleaver lengths the two semi-Markov models with lognormal fit predict an up to 1 dB lower 99% margin ($\hat{=}$ higher signal availability) than the reference model, whereas the margins for the first-order Markov model

are 3 dB lower. This difference between semi-Markov and first-order Markov is by tendency obtained for MRC combined signals of two satellites as well. It is obtained that the four-state *semi-Markov, lognormal fit & Lutz, empirical* model has quite similar performance on the single-satellite channel as the two-state *semi-Markov model with lognormal fit*, which is the recommended model in literature for single-satellite reception. The difference of the required margins is below 0.5 dB for all interleaver lengths. Thus, the dual-satellite model developed in this work is appropriate to describe single-satellite reception in case of time interleaving. It indicates an appropriate description of satellite diversity in combination with time interleaving.

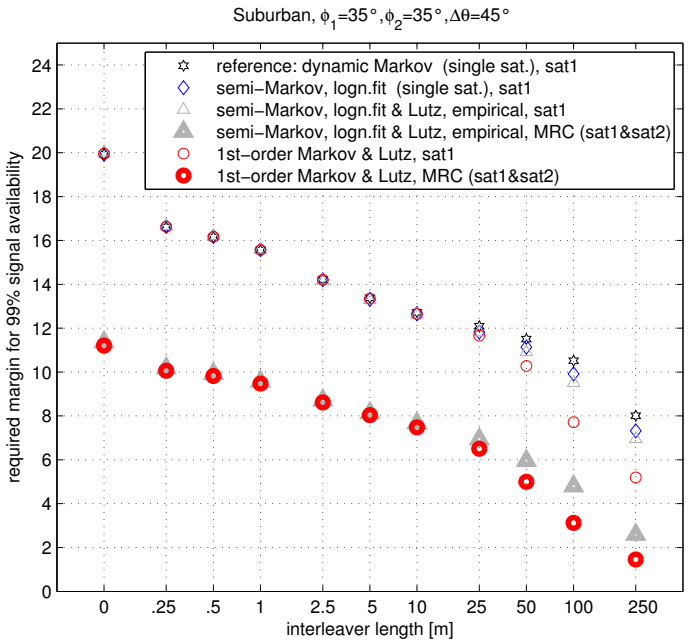

Figure 5.14.: Required margins for 99% signal availability after LMS channel simulation with *MiLADY SDARS Loo- & GNSS state parameter set* and three state models incorporating satellite diversity and different interleaver lengths.

6. Diversity Studies and First Application of the LMS Model

Signal reception of mobile digital satellite broadcasting services is limited by shadowing or blocking objects within the transmission path. To meet availability, continuity and quality of service requirements, commercial broadcasting systems combine angle diversity with time diversity, e.g. the Satellite Digital Audio Radio Services (SDARS) system [Mic02][Akt08]. Using time diversity, the information is spread within a certain time interval by an interleaver and additional redundancy by means of channel coding is added. As time diversity relies on the time variability of the transmission channel, it is effective only for moving receivers. In case of angle (or satellite) diversity, the information is transmitted simultaneously from multiple satellites in different orbital positions. Even though angle diversity is also effective for slow moving or even static receivers, it requires additional effort in the infrastructure.

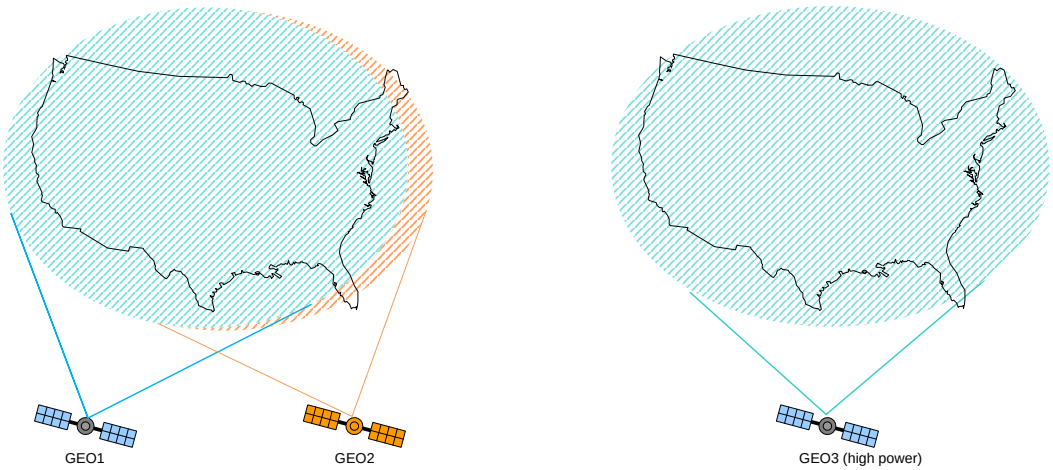

Figure 6.1.: Typical configurations for satellite broadcasting, with and without angle diversity.

The choice of a diversity configuration impacts the service availability and the cost of the satellite network. To facilitate a decision, different satellite configurations are compared in this chapter for broadcasting applications:

- One high power satellite is used to serve the complete coverage area. The required QoS is provided by time interleaving.
- Two satellites at separate orbital positions are used where the coverage area is completely overlapped. The required QoS is provided by angle- and time diversity. To ensure equal transmission power for both satellite configurations, both satellites have 50% of the power of the high power satellite.
- The performance of a dual-satellite system depends on the angular separation between the satellites. Indeed a high angular separation provides a high diversity gain, but lower elevations to the coverage area have to be taken into account. A detailed analysis of this fact is required.

Scope of this chapter is to compare these configurations by statistical analysis of the fading signal and to point out achievable gains of time and/or angle diversity in selected receive scenarios.

6.1. Diversity Analysis Based on Measurement Data

Right before this work in 2008 an LMS measurement campaign in the S-band has been carried out with a quality and resolution that is not previously reported in literature: the power levels of four satellite signals were measured synchronously with a sampling rate of 2.1 kHz along a travelled distance of 3700 km through different environments. These measurements of the SDARS satellites were carried out in the context of the project MiLADY [HEA+10] (cf. Appendix A for details). Based on this data, a joint analysis of satellite- and time diversity is presented in this section. It is also focused in the contributions [AIH+09], [AIH+10] and [AIH+11].

For the subsequent analysis, the signals from two geostationary satellites are selected. The satellites are located over the west coast and east coast of the USA, and are denoted with GEO1 and GEO2 in the following. A corresponding sketch of satellite positions, measurement route and coverage area is given in Figure 6.4.

The characteristics of the signal fading process strongly depends on the satellite positions from the receivers point of view. The elevation angle of GEO1 (located at 115° west) varies between 25° and 40° and GEO2 (located at 85° west) varies between 38° and 54°. As both elevations encompass a rather small interval of 15°, a finer division of elevation angles is out of scope for the diversity analysis in this section (for comparison, the LMS model parameters are derived within elevation intervals of 10°). The azimuth angle separation between GEO1 and GEO2 is $\Delta\theta \approx 40°$. The driving direction is assumed to be uniformly distributed between 0° and 360°.

The characteristics of the signal fading further depends on the environment around the mobile receiver. As a current method, environment classes are defined and each section of the measurement route is assigned to one of these classes. The environment types are 'Urban', 'Suburban', 'Forest', 'Commercial', and 'Highway' and are described in Appendix A.

To determine the performance improvements due to angle diversity and time diversity, Figure 6.2 shows the CDFs of the normalised C/N of the 'GEO' signals in suburban environments. A MRC of two signals is used for the evaluation of angle diversity. The resulting gain consists of a *power combining gain* (due to increased overall signal because of the second satellite) and a *diversity gain* due to fading reduction. For further validation the power combining gain is removed, such that the pure diversity gain is remaining. Thus, two different network configurations from Figure 6.1 can be approximately compared:

1. One 100% power satellite. Since no measurement data is available from a satellite at location GEO3, the satellite GEO1 or GEO2 is assumed to be a high-power satellite.
2. Two satellites, each with 50% power. [1]

[1] It holds $(C/N)_{\mathrm{MRC},50\%} = 0.5 \cdot [(C/N)_1 + (C/N)_2]$ in linear domain.
$\rightarrow (C/N)_{\mathrm{MRC},50\%}[\mathrm{dB}] = (C/N)_{\mathrm{MRC},100\%} - 3\,\mathrm{dB}$

As criterion for the comparison in the subsequent analysis, the required margins for a signal availability of 99% are derived from the CDFs. It can be found as the difference between the C/N at LOS (0 dB) and the C/N, which is exceeded with a probability of 99%. Based on the required margin, the gains using MRC and/or time interleaving are extracted, as indicated in Figure 6.2. The angle diversity gain is related to the single satellite with the higher signal availability. It is clearly GEO2 having a ≈15° higher elevation than GEO1.

For evaluating the influence of time diversity, an interleaver with a fixed length is assumed (i.e. a constant time interleaver with a constant receiver speed). It may be noted that the term 'time diversity' is not correct, since the interleaver size is given in distance. But for simplicity we will continue to refer to the term 'time diversity'. The diversity gain is related to the static reception.

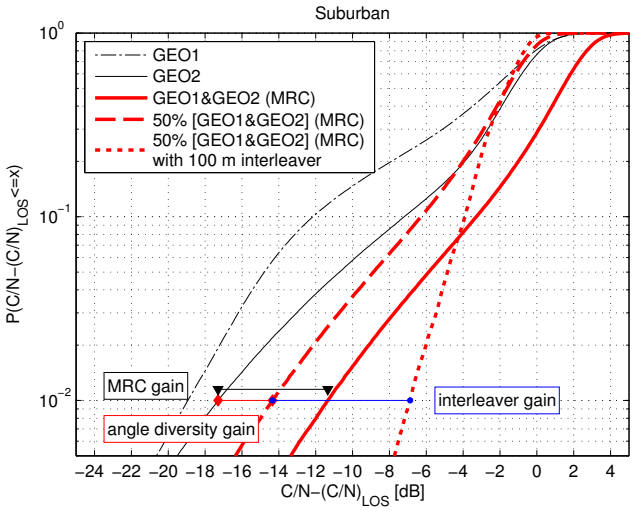

Figure 6.2.: Exemplary CDF of the normalised C/N in a suburban environment. The required margins for 99% signal availability and the diversity gains due to MRC and time interleaving are indicated.

Figure 6.3 presents the required margins for a signal availability of 99% for the 'GEO' configurations in different environments by using different interleaver lengths. The following observations are made:

- The required margins to provide 99% signal availability for GEO1 are greater than for GEO2. It is an expected result, as the probability of obstacles being between the satellite and the receiver reduces with increasing elevation.
- Different environments exhibit varying obstacle density. For example, in urban or suburban environments, the required margins are greater than for open environments like Highway.
- Both angle diversity and time diversity offer significant gain when employed as single means of availability improvement. Consequently, the incremental increase of the diversity gain is smaller for the combination of diversity methods (i.e. for angle diversity *and* time diversity). It can be seen by steeper slope of the required margins from GEO2 with increasing interleaver length in comparison to the slope of the MRC signal.

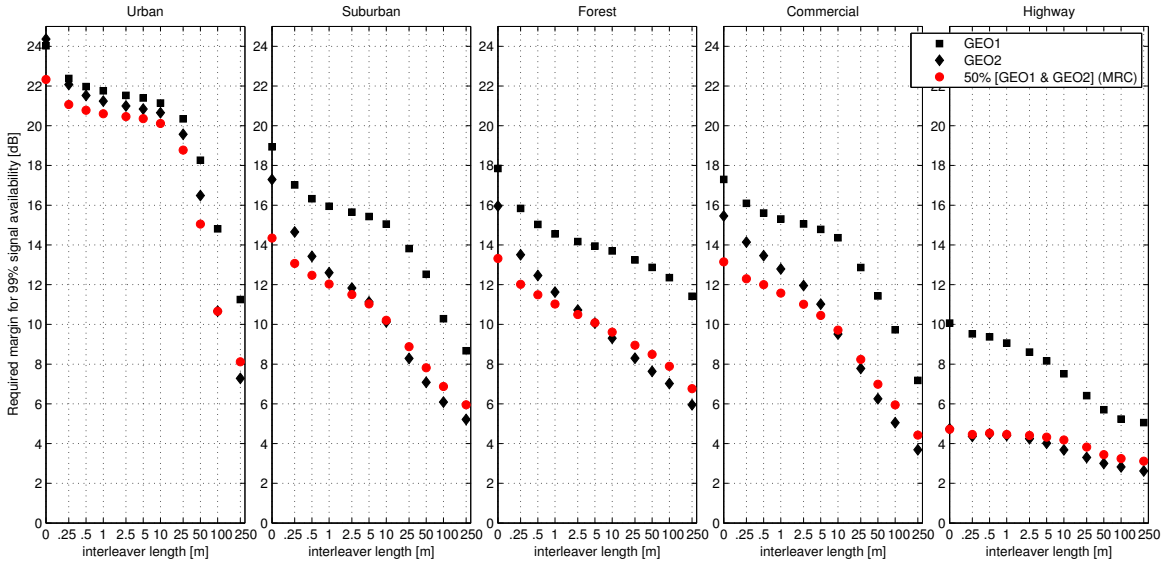

Figure 6.3.: Required margins for 99% signal availability incorporating angle diversity and various interleaver lengths considering two GEO satellites with mean elevations $\bar{\phi}_1 \approx 30°$ and $\bar{\phi}_2 \approx 45°$.

- A long interleaver with GEO2 is more effective than the combined half-power satellite signals with the same interleaver length. This can be mainly obtained for interleaver lengths of 10 m and more.
  Note that MRC of two signals never result in a loss. To point out the diversity effect, the transmission power of both configurations is normalised.

The analysis from measurement data show that angle diversity as well as time diversity are effective methods to increase the signal availability. Angle diversity has significant advantages for short interleavers and for the static reception. In urban environments, where a low receiver speed and stops are common, the required margin can be reduced by 2 dB in comparison to single-satellite reception. In suburban, forest and commercial environments the static reception is improved by ≈ 3 dB with angle diversity of two GEO satellites. However, the effective angle diversity gain decreases for long interleaver lengths when comparing single- and dual-satellite reception.
Time diversity has some gain for short interleavers. With time interleaving over 10 m length, the required margin could be reduced by 3-4 dB for the dual-satellite system and 3-7 dB for single satellites in comparison with the static reception (i.e. no interleaving), as seen in Figure 6.3. To double these interleaver gains an interleaver length of at least 100 m is required.

Results in Figure 6.3 indicate that a single high-power satellite with interleaving over a long distance provides higher signal availability than two (half power) satellites using MRC. Note that the position of the high power satellite (=GEO2) is optimistic regarding a fair comparison with a dual-satellite angle diversity constellation. A real alternative to this angle diversity constellation GEO1&GEO2 would be the high-power satellite positioned between them, which elevation angle and signal availability is consequently lower. This alternative high-power satellite is denoted as GEO3 in Figure 6.4 and a constellation comparison is task of next section.

6.2. Diversity Analysis Based on LMS Model

The new multi-satellite LMS model allows diversity studies for satellite constellations and locations, where measurement data is not available. In this section, three alternative configurations of geostationary satellites are compared to provide the required QoS. To compare the results with SDARS measurements from previous Section 6.1, the USA is selected as coverage area (cf. Figure 6.4).

1. One high power satellite (GEO3) is located at 100° west above the centre of the coverage area.
2. Two satellites (GEO1&GEO2) are located at 85° west and 115° west. It is the constellation used by XM Satellite Radio.
3. Two satellites (GEO4&GEO5) are located at 70° west and 130° west. Although this constellation provides lower elevation angles to the coverage area, a higher satellite diversity gain is expected than constellation 2 due to a higher azimuth separation.

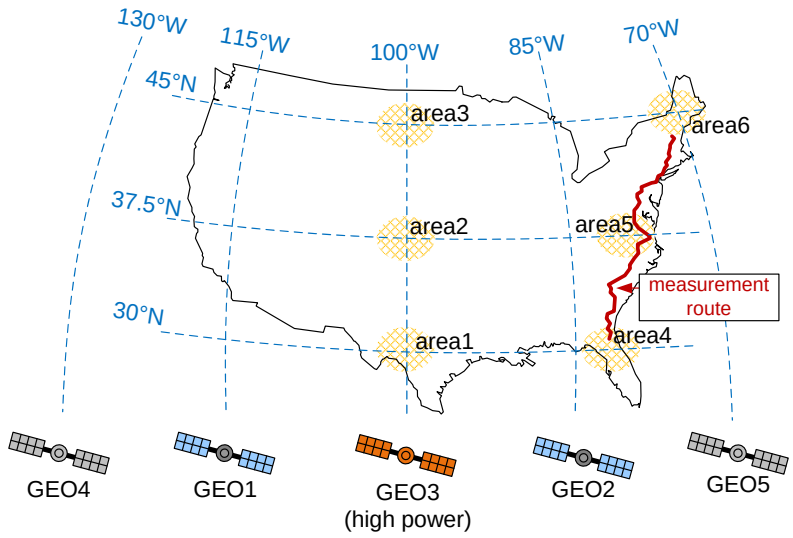

Figure 6.4.: Three alternative satellite configurations (GEO3 vs. GEO1&GEO2 vs. GEO4&GEO5) to serve the coverage area. For comparison, the expected signal availability is evaluated from six selected locations (area1-6).

A performance comparison of the constellations is carried out at six different locations in the USA, as sketched out in Figure 6.4. These locations differ with respect to elevation angles ϕ and azimuth angle separations $\Delta\theta$ of the satellites. The corresponding values are given in Table 6.1. The driving direction of the terminal within the observation areas is assumed to be equally distributed.

For each area and satellite constellation, timeseries of the normalised C/N are generated with the LMS model by taking the *MiLADY SDARS parameter set*. Therefore, Loo parameters for the five satellites GEO1-5 are found in Table C.1, which elevation angles are closest to the values given in Table 6.1. The corresponding state model parameters are derived from Table C.2. By following the guidelines in Section 3.4.4, the state parameters are interpolated

Table 6.1.: Position of satellites from three constellations as seen from different areas.

area	centre position		GEO3	GEO1&GEO2			GEO4&GEO5		
			ϕ_3 [°]	ϕ_1 [°]	ϕ_2 [°]	$\Delta\theta_{(1,2)}$ [°]	ϕ_4 [°]	ϕ_5 [°]	$\Delta\theta_{(4,5)}$ [°]
1	30.0°N	100.0°E	55	51	51	56	42	42	98
2	37.5°N	100.0°E	47	44	44	48	36	36	87
3	45.0°N	100.0°E	38	36	36	42	30	30	78
4	30.0°N	82.5°E	50	40	55	47	28	52	89
5	37.5°N	77.5°E	41	32	46	39	21	46	77
6	45.0°N	70.0°E	30	22	36	34	12	38	68

with respect to the elevation angles given in Table 6.1. Additionally, for the dual-satellite constellations GEO1&GEO2 and GEO4&GEO5, correlation coefficients have to be selected according to the azimuth angle separations from the *GNSS correlation parameter set* in Table C.4 and Table C.5. They are interpolated with respect to the azimuth separations from Table 6.1 as well.

From the timeseries, the required margins for 99% signal availability are derived from the high-power satellite (GEO3) signal and the MRC combined signals of GEO1&GEO2 and GEO4&GEO5 by considering different interleaver lengths. Simulation results for suburban environments and forested roads in areas 1-6 are shown in Figure 6.5.

Comparing single-satellite with dual-satellite reception with results shown in Figure 6.5, leads to the conclusion that:

- for stationary reception as well as for mobile reception with short interleaver lengths, a dual-satellite system with angle diversity clearly provides higher signal availability than one high-power satellite. This even holds for areas 1, 2, 3, where the single satellite GEO3 has a higher elevation than the satellites of the dual-satellite systems. The angle diversity gains for stationary reception are between 2 and 5 dB in suburban environments and up to 6 dB in forested environments for different locations in the coverage area.

- the incremental improvement due to time interleaving is greater for the single satellite than for the dual-satellite configuration (as obtained from the measurement-based diversity analysis). Consequently, when long time interleaving ($\geq$ 100 m) is considered, a single high-power satellite provides similar signal availability to a dual-satellite configuration. However, as a satellite broadcasting system has to be dimensioned for slow and fast moving receivers as well, a dual-satellite configuration is the preferred one.

Comparing the dual-satellite constellations GEO1&GEO2 (small azimuth separation) and GEO4&GEO5 (high azimuth separation) with results shown in Figure 6.5, leads to the conclusion that:

- the required margins for 99% signal availability in case of stationary dual-satellite reception vary between 9 and 14 dB for suburban and 6 and 14 dB for forest environments, depending on the receive area. Time interleaving with, e.g. 100 m length reduces further the required margins by ranges from 6 to 9.5 dB and from 2 to 8 dB in suburban and forested environments, respectively.

- the time interleaver gains with respect to *no interleaving* for GEO1&GEO2 and GEO4&GEO5 are very similar. It is obtained that the constellations have a similar incremental decrease of the required margin with increasing interleaver length.
- the dual-satellite configuration with small azimuth separation (GEO1&GEO2) provides slightly a better performance than the configuration with high azimuth separation (GEO4&GEO5). In seven of ten areas and environments the required margins are smaller with GEO1&GEO2 (area 6 is ignored) for short and for long time interleaving compared to GEO4&GEO5. In three cases the required margins with GEO1&GEO2 are even clearly smaller with $\gtrapprox 2\,\mathrm{dB}$, whereas in other three cases the required margins are only $\approx 1\,\mathrm{dB}$ greater than for GEO4&GEO5.

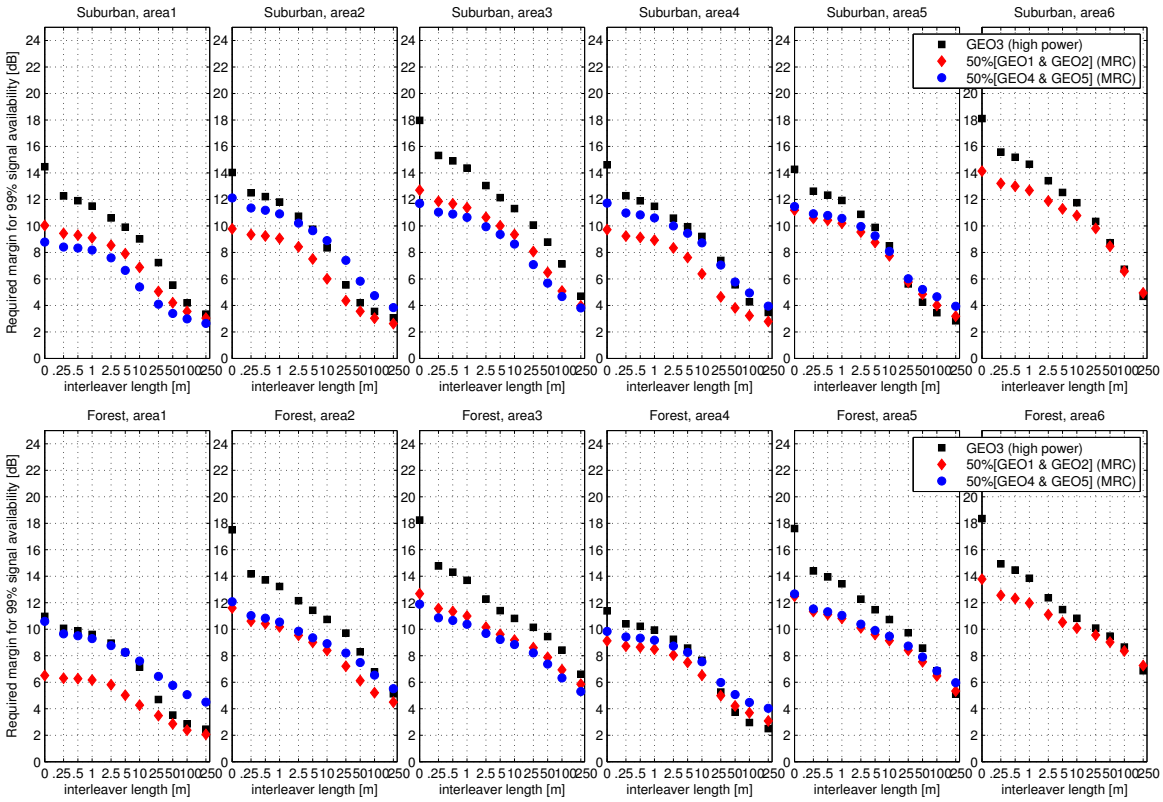

Figure 6.5.: Required margins for 99% signal availability incorporating angle diversity and various interleaver lengths for three satellite constellations. The results are calculated for suburban environments (top) and forest (bottom) located in six different areas of the USA.
Note that GEO4 could not be simulated for area6, since the required model parameters for elevation $\phi = 12°$ (cf. Table 6.1) are not available.

7. Summary and Conclusions

In this work LMS models for single-, dual-, and triple-satellite reception are developed with a special attention on the performance analysis of satellite broadcasting systems using time diversity and satellite diversity. The focus lies on an accurate description of the signals temporal composition, the correlation between the satellites, and the capability to describe fading for multiple environments and variable satellite positions.

In **Chapter 2** basics for satellite radio wave propagation focusing on mobile reception are introduced. In two parts, modelling of single-satellite reception and contributions for multi-satellite LMS models are described. It is found that available multi-satellite models lack the correct description of correlations between satellite signals, since the correlation is implemented only in terms of the two states 'good' and 'bad'. Furthermore, the available multi-satellite models do not include the state duration modelling improvements (semi-Markov and dynamic Markov models), which are already developed for the single-satellite case. These potential weaknesses of describing time diversity and satellite diversity effects motivate this work.

A **comprehensive study of state modelling approaches** and their application **for single-, dual-, and triple-satellite** time series generation are presented in **Chapter 3**. Three basic groups of existing models are distinguished: first-order Markov models, semi-Markov models, and dynamic Markov models. Based on these groups, the following concepts for dual-satellite modelling are derived:

- *Straightforward methods* extend the known Markov models for all permutations of combined states. An exponentially increasing number of model parameters has to be taken into account. A reference state series is required for the parametrisation.
- The *Lutz approach* allows to calculate parameters for a multi-state Markov model, including the permutations of combined states by simply considering the correlation coefficient between two satellites. Parameters and modelling algorithm are similar to the *straightforward method*, but only an application for a first-order Markov model is available in literature. As the *Lutz approach* has great advantages is terms of model parametrisation, a solution is found in this work to combine it with a semi-Markov model.
- A new *Master-Slave* concept is presented, which targets the conditional state sequence modelling of a secondary satellite (slave) based on an existing state sequence (master). In this work the first state modelling approaches are developed, which successfully realise the *Master-Slave* concept. Due to its related complexity, only efficient implementations of conditional first-order Markov chains are considered in the context of this work.

Criteria for the evaluation of *straightforward models*, *Lutz models*, and *Master-Slave models* are state probabilities, correlation coefficients, mean state durations, and state duration distributions, which are compared with measurement data as a reference. For this purpose,

expressions for new state models as well as for existing state models are developed to derive the results analytically. They are given in Appendix B. Depending on the individual parametrisation, it is shown that all modelling concepts are able to accurately re-simulate the measured state probabilities and correlation coefficients. For semi-Markov models and dynamic Markov models with SDPDF approximations, necessary corrections are introduced. In the context of a complete LMS model simulation equal fade probability distributions (first-order statistics) are thus provided for different state models. The best re-simulation of state duration distributions based on reference measurement data is provided by the *straightforward* dynamic Markov model without approximations. However, this method is not feasible to parametrise a multi-satellite model describing multiple receive scenarios, such as different environment types, different elevation angles, and different azimuth separations, as it requires the same variability of dual-satellite measurements. The alternative developed in this work, a **Lutz approach combined with a semi-Markov model**, is able to accurately describe state probabilities and well approximates the state duration distributions by simply relying on the single-satellite parameters and a correlation coefficient. This approach is successfully evaluated in terms of state-based evaluation criteria (Chapter 3) and in the context of the full LMS model (Chapter 5). It introduces an improvement of the state-of-the-art.

Regarding **state modelling with three satellites**, the **Master-Slave approach** is identified as a practicable method and is evaluated in the last part of Chapter 3. Although the Master-Slave approach does not describe the correlation between the slave satellites, an appropriate definition of the master satellite provides an accurate description of the overall system. Implementations in combination with a dual-satellite approach are further developed to improve the state duration modelling for a three-satellite system. The great advantage of the Master-Slave approach is the feasibility of parametrising a three-satellite model.

Chapter 4 focused on the analysis of slow- and fast signal variations within the states. By taking an existent single-satellite LMS model as baseline (the 'versatile Loo' model in [PCPFB+10]), correlation effects between the fading of two satellites are analysed from high-resolution measurement data. As a result, **additional correlation coefficients** between mean values of the direct signal (Loo parameter M_A) and between the lognormal variations of the direct signal are introduced and implemented in the new multi-satellite LMS model.

In **Chapter 5**, simulation results of the newly developed LMS model and of alternative LMS models developed in this work and from literature are compared with measurement data. Dual-satellite reception with diversity is assessed by assuming MRC of two satellite signals. Evaluation criteria are CDFs, average fade durations, level crossing rates, and CDFs under consideration of time interleaving with variable lengths. It is shown that due to the incorporation of additional correlation effects between satellites, the new model describes satellite diversity with higher accuracy than available models from literature.

In the second part of Chapter 5 the model parameter sets for multiple user-scenarios are evaluated. It is shown that the new dual-satellite model allows to simulate representative timeseries for five different environments, each combination of elevation angles between 15° and 85° per satellite in 10° intervals, and different azimuth angle separations between 0° and 180° (7 intervals). By optional interpolation of model parameters, which is applied in the last Chapter 6, a refined resolution of the elevation angle and the azimuth angle separation is possible.

As first application for the new multi-satellite LMS model, a **coverage study for satellite broadcasting applications under consideration of satellite diversity and time diversity** is carried out in **Chapter 6**. As a reference, a joint analysis of satellite- and time diversity for a system with two geostationary satellites is performed based on high-resolution measurement data. This high-resolution data represents the basis for the statistical analyses and the model development in this work and was captured within the MiLADY project [EHH08]. As the diversity study with measurement data is limited by the satellite constellation and the measurement route, the channel model offers to compare alternative satellite constellations for variable coverage areas. A comparison between

- a high-power satellite in geostationary orbit (GEO),
- a dual-satellite GEO constellation with low azimuth separation (Δ(longitude) = 30°),
- and a dual-satellite GEO constellation with high azimuth separation (Δ(longitude) = 60°)

have shown that a dual-satellite constellation has advantages over a single satellite, even if the single satellite has higher power or longer time interleavers. Further it is shown that the dual-satellite GEO constellation with low azimuth separation provides a slightly better signal availability than the dual-satellite GEO constellation with high azimuth separation for coverage areas between 30 and 45 degrees latitude. This first application can be understood as verification of the new LMS model in practice.

A. Satellite Signal Measurements

To derive the parameters for a new multi-satellite LMS model, two measurement campaigns were carried out in the context of the project MiLADY [EHH08][HEA+10]. In this chapter, the measurement campaigns and the preprocessing of measurenment data are described in detail.

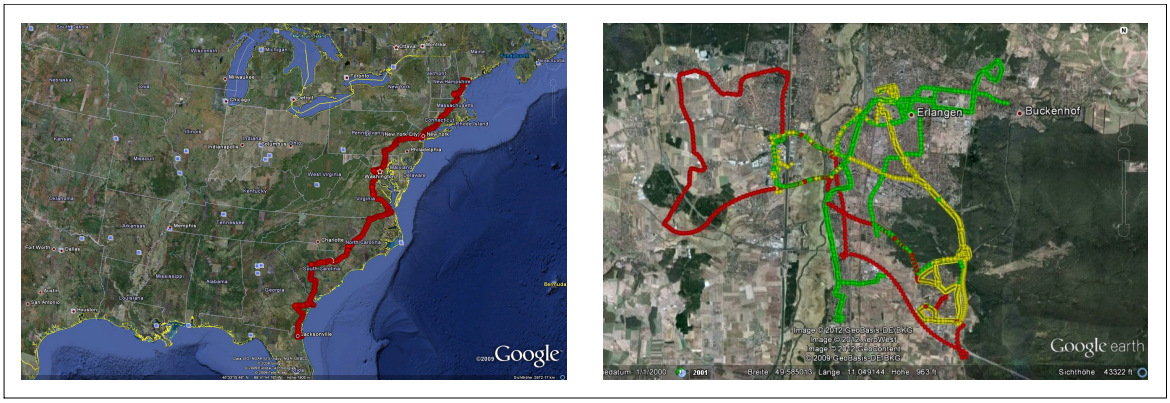

Figure A.1.: Measurement campaigns within the project MiLADY. Left: SDARS measurements along the U.S. east coast. Right: GNSS measurements in area of Erlangen, Germany. The colours indicate three parts of the GNSS measurements with a van (red), and two city buses (green and yellow).

A.1. SDARS Measurements, U.S. East Coast

In a first campaign S-band measurements at 2.3 GHz were carried out in September 2008 along the east coast of the USA. In Figure A.1, the measurement route from Jacksonville (Florida) to Portland (Maine) is indicated. Over a total distance of 3700 km and a measuring time of 75 hours the power levels of four satellites were recorded simultaneously with a sampling rate of 2.1 kHz, specificially, two geostationary (GEO) satellites of XM Satellite Radio [Mic02] and two of three highly elliptical orbit (HEO) satellites of Sirius Satellite Radio [Akt08]. The antenna noise power was measured simultaneously to the signal in a quiet band. Supplementary data about the exact measurement time and vehicle position were captured by two GPS receivers. The GPS location information is further improved by a wheel sensor, producing an impulse every 2 cm of travelled distance. Moreover, two cameras were mounted on the van capturing image material to derive information about the current environment.

Signal Preprocessing

To prepare the data for analysis, the following preprocessing tasks are performed:

1. From the receivers point of view, the **effective C/N is relevant** rather than the measured signal power (C+N). The noise power level depends on the receiver system noise and the temperature of the environment as seen by the antenna. Since an antenna with an omnidirectional characteristic was used for measurements, the noise power is increased close to obstructing objects like buildings or trees. In open environments the noise power is reduced. Variations of the noise power level as large as 2 dB are found in the data. From the signal power and the noise power the effective carrier-to-noise level is calculated.

2. The measurement vehicle travelled from north to south along the U.S. east coast over a linear distance of about 2000 km. Along this route, the line-of-sight (LOS) signal level varies, e.g. according to the satellite antenna footprint. To compare the received signals from different locations over the complete measurement route, the **C/N is normalised to the expected C/N at line-of-sight**.

3. The signal fading speed is determined by the speed of the mobile receiver. During measurements, it cannot be ensured that the speed of the measurement van is typical for the current type of environment. Although representative moving speeds can be assumed for various environments, they involve factors like the daytime, traffic conditions, etc. For a comprehensive treatment studies of user mobility these considerations would have to be incorporated. This is out of scope in this thesis. Therefore, we characterize the fading process independently from the receiver's speed by **resampling it from time domain to travelled distance units**.

Environment Classification

The signal fading process strongly depends on the nature of obstacles between the satellite and the receiver. As a current method, environment classes are defined [GV98][PFVCB+98]. Using the image material from the cameras (cf. Figure A.2), the following six environment types are identified:

- *Urban environments* cover typical city centers with buildings with at least three floors.
- *Suburban environments* cover residential areas of cities and greater villages. The building height is limited to three floors, also foliage on both sides of the roads is usual.
- *Commercial areas* include business parks and industrial parks with wide roads (often four lanes) in the outskirts of a city. The buildings aside the roads are often flat and the foliage is light.
- *Highways*, freeway and interstates are characterized by wide highspeed roads with at least two lanes. Vegetation asides the road is usual.

- *Intermediate tree shadowed rural areas* (ITS) include two-lane roads in the countryside with a mixture of line-of-sight conditions and sections with groups of trees beside the road.
- *Forested rural areas* include two-lane roads in the countryside with forests aside the road.

The amount of data in each environment available for the statistical analysis is given in Table A.1.

Table A.1.: Available data depending on environment.

Environment class	Measurement length
Urban	98 km
Suburban	200 km
Commercial	170 km
Highway	2144 km
Rural (Forest)	238 km
Rural (Intermediate Tree Shadowed)	216 km

(a) Urban (b) Suburban (c) Commercial

(d) Highway (e) Rural (Forest) (f) Rural (Intermediate Tree Shadowed)

Figure A.2.: Example images of the defined six different environment types.

A.2. GNSS Measurements, Erlangen, Germany

A second measurement campaign was carried out around Erlangen (Germany) to record the carrier-to-noise spectral density ratio (C/N_0) from Global Navigation Satellite System

(GNSS) satellites in the L-band. Due to a permanent availability of at least 8 satellites on the hemisphere, a comprehensive analysis of fading effects for a wide range of elevation and azimuth angle combinations of multiple satellites is possible. Because of the low C/N_0 resolution in time (20 Hz) and in amplitude (1 dB quantisation), only parameters for slow variations can be derived.

The GNSS campaign were split in two parts:

- The first part of the campaign has been carried out in July 2008. The GNSS antenna was mounted on a measurement van at a height of 2 m. A measurement round-trip of 38 km length was driven 10 times, covering several environments (suburban, forest, open, commercial) in and around Erlangen (cf. Figure A.1, red line).
- The second part of the measurements was done in late September and early October 2010 by mounting the setup in two city buses, driving on different routes. The GNSS antenna was mounted at a height of 3.1 m. The city buses drove for three days an identical route. The covered environments were urban, suburban and partly open rural areas. The individual routes of the two buses spanned 7 km and 6 km in North-South direction and 6 km and 5 km in West-East direction, respectively. (cf. Figure A.1, green and yellow line)

The trials were carried out in summer and in autumn months, where leaves were on the trees.

For the measurements a professional GNSS receiver (built by Fraunhofer IIS by using a Javad receiver core) was used. Beside information of vehicle speed and positioning data, the GNSS signal includes a C/N_0 estimation of the GPS L1 carrier at 1575.420 MHz. It has a dynamic range of 20 dB and a quantisation of 1 dB. The time resolution of the C/N_0 estimation is 20 Hz. At lower signal levels of a specific satellite (e.g. during deep blockages), the GNSS receiver loses the satellites signal synchronisation and the C/N_0 estimation of this satellite is no more available. In terms of state detection it will be defined as 'bad' state. Additional information of azimuth and elevation of the individual satellites were captured with 1° resolution.

The characteristics of the environments covered by the GNSS measurements are:

- *Urban*: The urban centre of Erlangen is characterized by narrow roads and dense buildings with mainly 4-5 floors.
- *Suburban*: Measurement cars drove through several suburban areas in and around Erlangen. Depending on the area, the separated buildings have between 1 and 2 (family houses) and 2-3 floors (apartment buildings).
- *Forest*: The selected forests for the trials consist of homogeneous dense mixed trees w/o clearances.
- *Commercial areas*: are characterized by wide roads and buildings of various heights aside the road. Usually these roads cross commercial and industrial areas.
- *Open areas* were passed on rural roads along fields and meadows on both sides.

A.3. Summary and Comparison of Measurement Campaigns

For the channel model parametrisation, data from both measurement campaigns are analysed. Table A.2 summarises the main aspects.

Table A.2.: Overview on two measurement campaigns for the parameter extraction of a multi-satellite LMS model.

SDARS measurements (USA, East Coast)	**GNSS measurements (Germany, Erlangen)**
high sample rate (2.1 kHz) → reliable for Loo parameter extraction and state parameter extraction	low sample rate (20 Hz) → reliable for state parameter extraction
4 satellites (2 GEO from XM, 3 HEO from Sirius) → limited combinations of orbital positions	>20 satellites (MEO from GPS, GLONASS) → many combinations of orbital positions
environments: Urban, Suburban, Tree-shadowed, Forest, Commercial, Highway (Open)	environments: Urban, Suburban, Forest, Commercial, Open
model validation for a limited set of orbital positions	preliminary state parameters for many orbital positions which need refinement and validation

A.4. State Identification

The procedures for analysis of both SDARS and GNSS data are similar. First, the signal is normalised to the LOS level [AIH+09]. Afterwards, the timeseries are re-sampled into travelled distance units. As resolution, 1 cm and 10 cm is chosen for the SDARS and GNSS data, respectively. State identification is performed by global thresholding (threshold 5 dB below LOS) of the low-pass filtered signal (sliding window over 5 m), similar to [BT02].

Figure A.3 shows example measurement sequences from GNSS and SDARS trials, which are separated into two states.

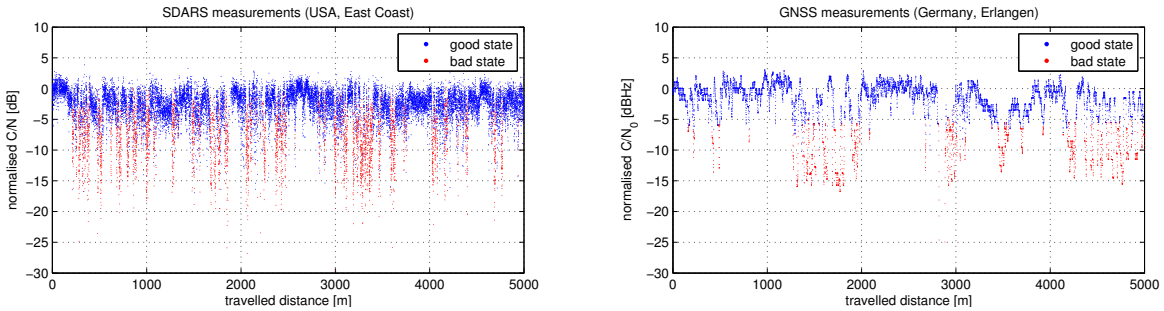

Figure A.3.: Exemplary measurement signals from two campaigns separated into 'good' state and 'bad' state. Left: normalised C/N from SDARS measurements in the USA. Right: normalised C/N_0 estimation at the GNSS receiver from measurements in Germany.

A.5. Loo Parameter Extraction

Once the measurement data is separated into the states, the Loo triplets are derived to characterise the signal behaviour within each state. Loo triplets are found by comparing

the distribution of the measured signal within a state with theoretical Loo distribution functions. Finally, the Loo parameter triplet is selected, where the theoretical statistic fits best the measured one [KAIH12]. As mentioned before, only the SDARS measurements are feasible for Loo parameter extraction.

A.6. Separation of Data into Environments and Satellite Positions

Single-satellite reception depends on the kind of the environment, the elevation angle of the satellite, and the azimuth of the satellite relative to the driving direction. For a detailed analysis of the single-satellite state characteristics, the SDARS- and GNSS measurement data are divided into:

- different environment types 'Urban', 'Suburban', 'Forest', 'Commercial', and 'Open' (Note that the 'Highway' environment from SDARS measurements is assigned to 'Open'). The environment classification for the SDARS measurement data is performed by visual inspection of the image material from two cameras. For the GNSS measurement data the Land-Usage data from the European Corine project [Cor] is used.
- different elevation angles from 10° to 90° in segments of 10°. The mean elevation angles represented by these datasets are therefore 15°, 25°, ... , 85°, respectively.
- four classes of driving directions (for GNSS data, only) with the intervals 0-10°, 10-30°, 30-60°, and 60-90°.

Figure A.5 shows the amount of data from SDARS and GNSS measurements for single-satellite analysis. Due to the limited amount of SDARS data (except open environments), different driving directions are excluded from the analysis.

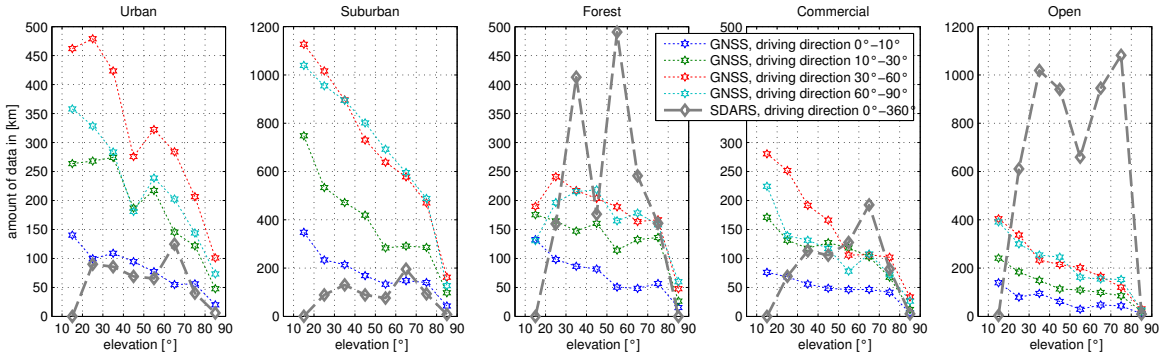

Figure A.4.: Amount of data from SDARS measurements and GNSS measurements for different environments and elevation angles. Please note that the values are connected only for better visibility.

The **dual-satellite (and multi-satellite) reception** depends on the kind of the environment, the elevation angle of each satellite, and the azimuth of each satellite relative to the driving direction. Especially the angular separation of the satellites of elevation and azimuth are crucial, since it affects the correlation of the received signals. For a detailed analysis of state characteristics for dual-satellite reception, the measurement data from SDARS and GNSS measurements are divided into:

- five environments (the same as for single-satellite case).
- combinations of eight elevation angles as used for single-satellite analysis. Thus, the elevation angle separation is included as well.
- seven intervals of the azimuth angle separation between the satellites (0-10°, 10-30°, 30-60°, 60-90°, 90-120°, 0-150°, and 150-180°).

This adds up to a total of $5 \cdot 8 \cdot 8 \cdot 7 = 2240$ segments (further denoted as *receive scenario*) of measurement data. A further division into driving directions is omitted. For a reliable dual-satellite state analysis (especially in terms of state duration analysis) and parametrisation of the Markov models, a minimum number of states is required. For this purpose, we define a receive scenario as 'valid' if each combined state ('good good', 'good bad', 'bad good', 'bad bad') is visited at least 50 times[1]. It corresponds to a state sequence with more than 200 state transitions. Based on this condition, Figure A.5 presents the available receive scenarios for the SDARS and GNSS measurements. The dual-satellite state analysis in this work is based on GNSS data. A dual-satellite analysis of the SDARS data is omitted, since the limited SDARS constellations restricts conclusions for dual-satellite reception in dependence on azimuth angle separation or elevation.

Figure A.6 presents the amount of data within the proposed 2240 receive scenarios sorted by measurement length, and by number of visits of the combined states. From GNSS data, about 2000 scenarios are valid for analysis (with $\geq$50 visits per combined state). In the SDARS data only 200 valid receive scenarios are found. Taking the condition of $\geq$50 visits per combined state, the shortest measurement length is $\approx$4 km for GNSS and SDARS. From GNSS, about 50% of the scenarios include more than 100 km of data. Even 1% of the scenarios have more than 1000 km. It allows to draw reliable statistical conclusions for dual-satellite reception. Note that the available measurement length for analysis does not directly correspond to the driven distance. It rather describes the available length after combining any of the visible satellites.

[1] the state duration statistic of a combined state include $\geq$ 50 elements

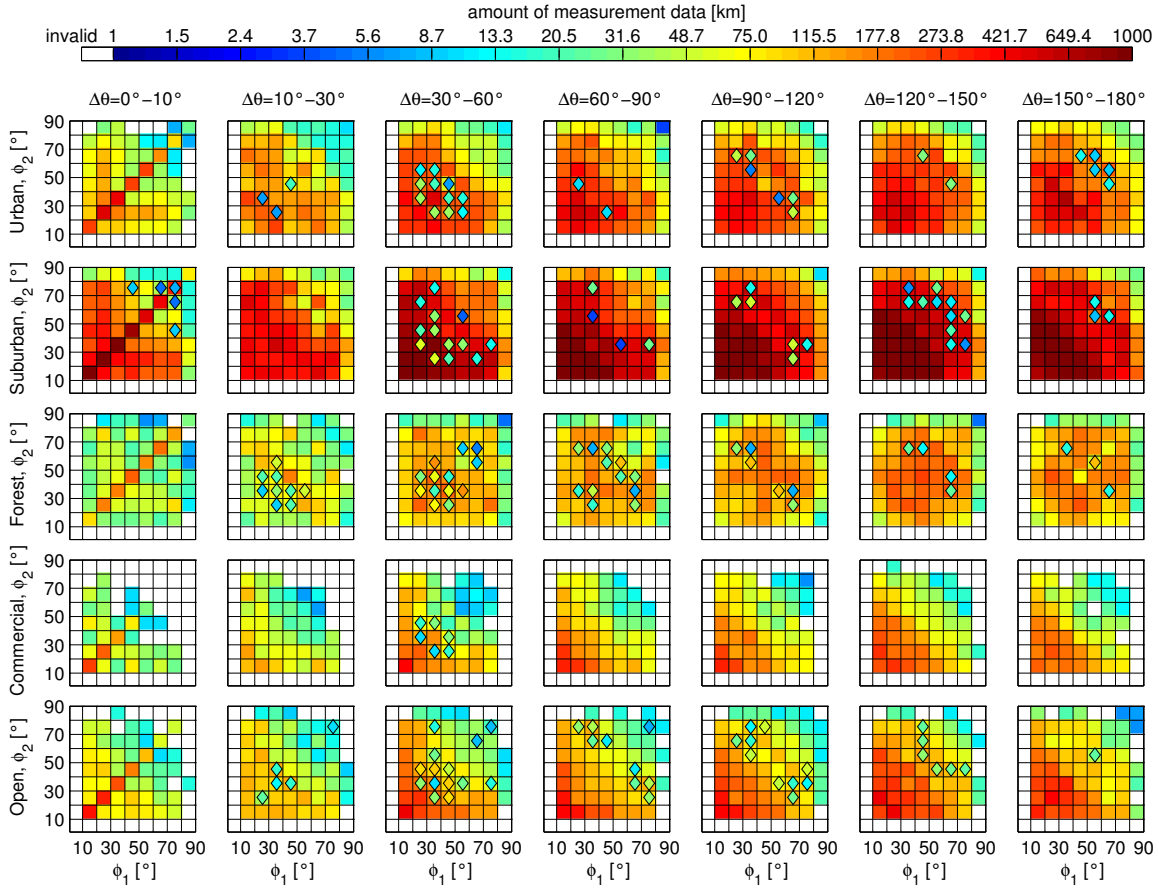

Figure A.5.: Available orbital constellations of two satellites from SDARS measurements (coloured diamonds) and from GNSS measurements (coloured fields) quantised to 7 sections of the azimuth separation angle ($\Delta\theta$), 9 elevation ranges per satellite (ϕ_1, ϕ_2) and 5 environments. The colour indicates the measurement length. The GNSS data is further used for dual-satellite state analysis. A dual-satellite state analysis from SDARS is omitted, since conclusions for dual-satellite reception in dependency on the azimuth angle separation or the elevation are rather limited.

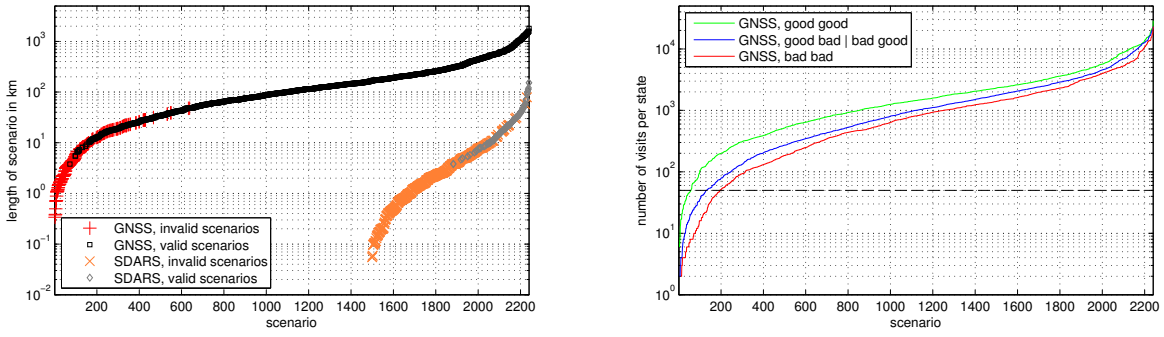

Figure A.6.: Amount of data for dual-satellite analysis within 2240 receive scenarios (5 environments $\cdot$ 8 $\times$ 8 elevation angles $\cdot$ 7 azimuth separations) sorted by measurement length (left) and by number of visits per combined state (right). The criterion for 'valid' scenarios is that $\geq$50 visits for each joint state are achieved.

B. Calculation for State Models

This chapter is a survey on state models for single-, dual-, and multi-satellite reception, arranged in three parts Appendix B.1, Appendix B.2, and Appendix B.3. It targets to improve the readability of Chapter 3, as supplementary formulas are presented to describe and analytically evaluate the state approaches that are investigated in Chapter 3.

B.1. Single-Satellite and Multi-State Modelling

In this section the available Markov approaches for single-satellite state modelling are summarised: first-order Markov, semi-Markov, and dynamic Markov. Expressions for state probabilities, mean state durations, and state duration distribution functions are given for up to N states, which are required for studies in Chapter 3. The expressions are also valid for the multi-satellite 'straightforward' methods, in which all permutations of single-satellite states are considered.

B.1.1. First-Order Markov Model

Concept and Parameters

A Markov model is a random process for generating discrete samples corresponding to channel states s. For a first-order Markov model, each state depends only on the previous state. The conditional probabilities of state $s_{n+1}|s_n$ are described by state transition probabilities p_{ij} $(i, j \in \{1, 2, 3, ..., N\})$, which are elements in a state transition probability matrix $\mathbf{P}_{\text{trans}}$.

$$\mathbf{P}_{\text{trans}} = \begin{bmatrix} p_{11} & \cdots & p_{1N} \\ \vdots & \ddots & \vdots \\ p_{N1} & \cdots & p_{NN} \end{bmatrix} \tag{B.1}$$

N denotes the number of states.

For a first-order Markov model further holds:

$$\mathbf{p} \cdot [\mathbf{P}_{\text{trans}} - \mathbf{I}] = \mathbf{0} \tag{B.2}$$

with $\mathbf{p}$ is the row vector of the equilibrium state probabilities, the identity matrix $\mathbf{I}$, and the zero vector $\mathbf{0}$.

State Probability

The equilibrium state probability (row) vector $\mathbf{p}$ is calculated by

$$\mathbf{p} = \mathbf{1}(\mathbf{I} - \mathbf{P}_{\text{trans}} + \mathbf{U})^{-1} \tag{B.3}$$

where $\mathbf{1}$ is a row vector with ones, and $\mathbf{U}$ is a matrix with all elements are ones. Alternatively, the state probabilities can be derived by

$$\lim_{k\to\infty} (\mu \cdot \mathbf{P}_{\text{trans}}^{(k)}) = \mathbf{p} \tag{B.4}$$

where $\boldsymbol{\mu}$ is an arbitrary probability vector with $\sum_i \mu_i = 1$. The latter method is only valid for aperiodic, irreducible, and homogeneous Markov chains [Rab89].

State Duration Probability Density Function

The probability that the Markov chain stays in state i for n consecutive samples is given by

$$P_i(D = n\Delta d) = p_{ii}^{n-1} \cdot (1 - p_{ii}), \quad n \in \mathbb{N}, \tag{B.5}$$

where p_{ii} is the state transition probability between two equal states, and Δd denotes the sampling distance (frame length). The SDPDF $P(D)$ follows an exponential distribution.

Mean State Duration

The mean duration $\bar{D}$ of state i is calculated by

$$\bar{D}_i = \frac{1}{1 - p_{ii}} \cdot \frac{1}{\Delta d}, \tag{B.6}$$

B.1.2. Semi-Markov Model

Concept and Parameters

A semi-Markov model generates a random sequence of N states. In contrast to the first-order Markov model, the state transitions do not occur at constant time intervals. In fact, the time interval of the model staying in state i follows a certain state duration probability $P(D_i)$. Therefore, the model parameters are N SDPDFs. State transitions are described by state transition probabilities p_{ij}, but with $i \neq j$.

$$\mathbf{P}_{\text{trans}}^{semiM} = \begin{bmatrix} 0 & p_{12} & \dots & p_{1N} \\ p_{21} & 0 & \dots & p_{2N} \\ \vdots & & \ddots & \vdots \\ p_{N1} & \dots & & 0 \end{bmatrix} \tag{B.7}$$

State Duration Probability Density Function and Mean State Duration

The semi-Markov model allows some options to describe the SDPDF of each state. From the SDPDF, the mean duration is further derived.

- The SDPDF is arbitrary and could be, e.g. the SDPDF of the reference data or the measurements.

$$P(D) = P(D_{\text{reference}}) \tag{B.8}$$

The corresponding mean duration of state i is

$$\bar{D} = \int_0^\infty D \cdot P(D) \mathrm{d}D \tag{B.9}$$

If the SDPDF is described with discrete values q, the mean state duration is

$$\bar{D} = \sum_{q=1}^{q_{\max}} q \cdot P(D = q), \tag{B.10}$$

where $q_{\max}$ corresponds to the maximum state length.

- The SDPDF is described by a lognormal PDF

$$P(D) = \frac{K}{D\sigma_{\text{Dur}}\sqrt{2\pi}} \exp\left[-\frac{(20\log(D) - \mu_{\text{Dur}})^2}{2\sigma_{\text{Dur}}^2}\right], \tag{B.11}$$

where μ_{Dur} and σ_{Dur} are respectively the mean value and the standard deviation of $20\log(D)$, and $K = 20\log\mathrm{e} \approx 8.686$. The mean state duration $\bar{D}$ can be calculated with

$$\bar{D} = \exp\left[\frac{\mu_{\text{Dur}}}{K} + 0.5\left(\frac{\sigma_{\text{Dur}}}{K}\right)^2\right]. \tag{B.12}$$

State Probability

The equilibrium probability P_i of the state i is calculated as the product of the normalised mean state duration $\bar{D}_{i,norm}$ and the probability of entering a state P_i':

$$P_i = P_i' \cdot \bar{D}_{i,norm} \tag{B.13}$$

$$\bar{D}_{i,norm} = \frac{\bar{D}_i}{\sum_k \bar{D}_k} \tag{B.14}$$

P_i' is element of the state probability vector $\mathbf{p}^{semiM}$ and is calculated analogously to Equation (B.4):

$$\lim_{k\to\infty} (\mu \cdot \mathbf{P}_{\text{trans}}^{semiM(k)}) = \mathbf{p}^{semiM} \tag{B.15}$$

B.1.3. Dynamic Markov Model

Concept and Parameters

The dynamic Markov model was introduced from Milojevic et al. in [MHEH09]. It is a random process for generating discrete samples corresponding to channel states s. In contrast to first-order Markov chains, the state transition probability depends additionally on the current state duration q.

$$p_{ij} = f(q)\,. \tag{B.16}$$

The model parameter is a three-dimensional STPT $\mathcal{P}_{\text{trans}} \in \mathbb{R}_{0+}^{N\times N\times q_{\max}}$, where $q_{\max}$ corresponds to the maximum state duration obtained from the measurements with $D_{\max} = q_{\max}\Delta d$.

$$\mathcal{P}_{\text{trans}} = \begin{bmatrix} p_{11}(q) & \dots & p_{1N}(q) \\ \vdots & \ddots & \vdots \\ p_{N1}(q) & \dots & p_{NN}(q) \end{bmatrix} \qquad q \in \{1, 2, ..., q_{\max}\} \tag{B.17}$$

State duration PDF

The probability that the duration of state i is equal to D is

$$P_i(D = q\Delta d) = (1 - p_{ii}(q\Delta d)) \cdot \prod_{r=1}^{q-1} p_{ii}(r\Delta d), \quad q \in \mathbb{N}\,. \tag{B.18}$$

The corresponding state duration CDF is given by

$$P_i(D < q\Delta d) = 1 - \prod_{r=1}^{q-1} p_{ii}(r\Delta d), \quad q \in \mathbb{N}\,. \tag{B.19}$$

State Probability and Mean State Duration

The state probability and the mean state duration are crucial factors to evaluate the performance of state models. Expressions to calculate these factors from a dynamic Markov model are missing in the contributions from Milojevic et al. [MHEH09][MHEH08]. Therefore, in context of this thesis the calculation of state probability and mean state duration from a dynamic Markov model is worked out.

To calculate the equilibrium state probabilities, first the equivalent of the state transition probability matrix according to the first-order Markov model $\mathbf{P}'_{\text{trans}}$ is derived from the state transition tensor $\mathcal{P}_{\text{trans}}$. The elements p'_{ij} of $\mathbf{P}'_{\text{trans}}$ are calculated with:

$$\mathbf{P}'_{\text{trans}}: \quad p'_{ij} = \sum_{q=1}^{q_{\max}} p_{ij}(q) \cdot K_i(q) \tag{B.20}$$

$p_{ij}(q)$ are elements of $\mathcal{P}_{\text{trans}}$. The factor $K_i(q)$ is related to the complementary CDF of the state durations $P_i(D \geq q)$. The complementary state duration CDF is given by

$$P_i(D \geq q) = \prod_{r=1}^{q} p_{ii}(r\Delta d) \tag{B.21}$$

The sum of all elements of $P_i(D \geq q)$ equals the **mean state duration** $\bar{D}_i$. $K_i(q)$ is the normalised CCDF:

$$K_i(q) = \frac{P_i(D \geq q)}{\sum_1^{q_{\max}} P_i(D \geq q)} = \frac{P_i(D \geq q)}{\bar{D}_i} \tag{B.22}$$

The **equilibrium state probabilities** (and again the mean state durations) can be derived from $\mathbf{P}'_{\text{trans}}$ according to Equation (B.3) or Equation (B.4).

B.2. Dual-Satellite Modelling

In this section the state modelling approaches for dual-satellite case are described: straightforward approach, Lutz approach, Master-Slave approach. Expressions for correlation coefficients, state probabilities, mean state durations, and state duration distribution functions for the combined states and for the states from individual satellites are given.

B.2.1. Correlation Coefficient Between Two Satellites

The Pearson's correlation coefficient between two channels is given by

$$\rho = \frac{E\left[(c_1(t) - \bar{c})(c_2(t) - \bar{c})\right]}{\sigma_1 \sigma_2}\,. \tag{B.23}$$

When only two states per satellite are assumed, the phi coefficient ϕ [Cra46] can be used to describe the correlation coefficient of the state sequence from two satellites. The phi coefficient is defined as

$$\phi = \frac{n_{11} \cdot n_{22} - n_{12} \cdot n_{21}}{\sqrt{(n_{1X})(n_{2X})(n_{X1})(n_{X2})}}\,, \tag{B.24}$$

where n_{ij} is the number of samples where sequence 1 has state i and sequence 2 has state j. For state modelling this formula can be adapted by using the single- and joint state probabilities of two satellites

$$\rho_{\text{states}} = \frac{P_{\text{gg}} \cdot P_{\text{bb}} - P_{\text{gb}} \cdot P_{\text{bg}}}{\sqrt{P_{\text{g1}} P_{\text{b1}} P_{\text{g2}} P_{\text{b2}}}}, \tag{B.25}$$

where g stands for 'good'-state, b for 'bad'-state, bb for 'bad bad' etc.

Taking the condition that each single state probability is the addition of two combined states (e.g. $P_{\mathrm{g1}} = P_{\mathrm{gg}} + P_{\mathrm{gb}}$), the combined states can be also expressed as a function of single satellite probabilities and the correlation coefficient:

$$\mathbf{p}^{joint(sat1,sat2)} = \begin{bmatrix} P_{\mathrm{gg}} \\ P_{\mathrm{gb}} \\ P_{\mathrm{bg}} \\ P_{\mathrm{bb}} \end{bmatrix} = \begin{bmatrix} +v + P_{\mathrm{b1}}P_{\mathrm{b2}} + P_{\mathrm{g2}} - P_{\mathrm{b1}} \\ -v - P_{\mathrm{b1}}P_{\mathrm{b2}} + P_{\mathrm{b2}} \\ -v - P_{\mathrm{b1}}P_{\mathrm{b2}} + P_{\mathrm{b1}} \\ +v + P_{\mathrm{b1}}P_{\mathrm{b2}} \end{bmatrix} \tag{B.26}$$

with

$$v = \rho \cdot \sqrt{P_{\mathrm{g1}}P_{\mathrm{b1}}P_{\mathrm{g2}}P_{\mathrm{b2}}} \tag{B.27}$$

B.2.2. Lutz Approach

In [Lut96] a method is introduced to realise correlated state sequences of two satellites with a first-order Markov model. It is valid for two states per satellite. Based on the state transition probabilities of two satellites ($\mathbf{P}^{sat1}_{\mathrm{trans}}, \mathbf{P}^{sat2}_{\mathrm{trans}}$) and one correlation coefficient (ρ), a correlated joint STPM $\mathbf{P}^{joint}_{\mathrm{trans}}$ is calculated without influencing the transition probabilities of the individual satellites. For purpose of completion, it is described here in detail.

The STPMs of two single satellites are given. By exchanging the notation of the state transitions to $p_{\mathrm{bg}} = g$, $p_{\mathrm{gb}} = b$, $p_{\mathrm{bb}} = (1-g)$, $p_{\mathrm{gg}} = (1-b)$, the STPMs are:

$$\mathbf{P}^{sat1}_{\mathrm{trans}} = \begin{bmatrix} 1-b_1 & b_1 \\ g_1 & 1-g_1 \end{bmatrix} \qquad \mathbf{P}^{sat2}_{\mathrm{trans}} = \begin{bmatrix} 1-b_2 & b_2 \\ g_2 & 1-g_2 \end{bmatrix} \tag{B.28}$$

In case that two satellites are uncorrelated (i.e. $\rho = 0$), the joint STPM of these two satellites can be estimated by the product of each of two state transition probabilities from the single satellites:

$$\mathbf{P}^{joint,uncorrelated}_{\mathrm{trans}} = \begin{bmatrix} (1-b_1)(1-b_2) & (1-b_1)b_2 & b_1(1-b_2) & b_1b_2 \\ (1-b_1)g_2 & (1-b_1)(1-g_2) & b_1g_2 & b_1(1-g_2) \\ g_1(1-b_2) & g_1b_2 & (1-g_1)(1-b_2) & (1-g_1)b_2 \\ g_1g_2 & g_1(1-g_2) & (1-g_1)g_2 & (1-g_1)(1-g_2) \end{bmatrix} \tag{B.29}$$

An important fact is that $\mathbf{P}^{joint,uncorrelated}_{\mathrm{trans}}$ include all characteristics of the two individual satellites (state probability, mean state duration, SDPDF).

Concept of the Lutz approach is to add values to $\mathbf{P}^{joint,uncorrelated}_{\mathrm{trans}}$ such that a certain correlation coefficient is achieved and the characteristics of single satellites remain unaltered. Thus, the following modification is proposed:

$$\mathbf{P}^{joint}_{\mathrm{trans}} = \mathbf{P}^{joint,uncorrelated}_{\mathrm{trans}} + \begin{bmatrix} x & -x & -x & x \\ y & -y & -y & y \\ v & -v & -v & v \\ w & -w & -w & w \end{bmatrix} \tag{B.30}$$

With the requirement $0 \leq p_{ij} \leq 1$ for the elements of $\mathbf{P}_{\text{trans}}^{joint}$, and the reasonable assumption that $g_1, b_1, g_2, b_2 \leq 0.5$, the possible ranges of the variables x, y, v, and w are:

$$\begin{aligned} x_{\min} &= -b_1 b_2 \\ x_{\max} &= \min\{b_1; b_2\} - b_1 b_2 \\ y_{\min} &= b_1 g_2 - \min\{b_1; g_2\} \\ y_{\max} &= b_1 g_2 \\ v_{\min} &= g_1 b_2 - \min\{g_1; b_2\} \\ v_{\max} &= g_1 b_2 \\ w_{\min} &= -g_1 g_2 \\ w_{\max} &= \min\{g_1; g_2\} - g_1 g_2 \end{aligned} \tag{B.31}$$

The variables x, y, v, and w can be chosen freely within their possible ranges. To have one final variable, Lutz propose to couple these variables by a scaling coefficient c.

$$\begin{aligned} x &= c x_0 \\ y &= c y_0 \\ v &= c v_0 \\ w &= c w_0 \end{aligned} \tag{B.32}$$

with

$$x_0, y_0, v_0, w_0 = \begin{cases} x_{\max}, y_{\max}, v_{\max}, w_{\max}\,, & \rho \geq 0 \\ x_{\min}, y_{\min}, v_{\min}, w_{\min}\,, & \rho < 0 \end{cases} \tag{B.33}$$

In the context of this work also alternatives without this scaling coefficient c are analysed. It has the advantage that additional information, such as the mean duration of the combined states, can be taken into account (cf. Section 3.2.3).

Finding the scaling coefficient c

By using the relation for first-order Markov chains ($\mathbf{p} = \mathbf{p} \cdot \mathbf{P}_{\text{trans}}$, cf. Equation (B.2)), the following expression can be adapted from Equation (B.30).

$$P_4 = P_1(p'_{14} + c x_0) + P_2(p'_{24} + c y_0) + P_3(p'_{34} + c v_0) + P_4(p'_{44} + c w_0) \tag{B.34}$$

with P_i are the equilibrium state probabilities of the correlated matrix $\mathbf{P}_{\text{trans}}^{joint}$ and p'_{ij} are the elements of the uncorrelated matrix $\mathbf{P}_{\text{trans}}^{joint,uncorrelated}$ with

$$\begin{aligned} p'_{14} &= b_1 b_2 \\ p'_{24} &= b_1(1 - g_2) \\ p'_{34} &= (1 - g_1) b_2 \\ p'_{44} &= (1 - g_1)(1 - g_2) \end{aligned} \tag{B.35}$$

By solving Equation (B.34) for the parameter c, it holds

$$c = \frac{-P_1(b_1 b_2) - P_2(b_1(1 - g_2)) - P_3((1 - g_1) b_2) - P_4((1 - g_1)(1 - g_2) - 1)}{P_1 x_0 + P_2 y_0 + P_3 v_0 + P_4 w_0}\,. \tag{B.36}$$

The joint state probabilities have to be substituted by known values g_1, b_1, g_2, b_2, and ρ.

Introducing the correlation coefficient

In Equation (B.26) in previous Section B.2.1 it is already shown that the joint state probabilities are a function of the correlation coefficient ρ and the state probabilities from single satellites. By expressing the single satellite probabilities with parameters b and g

$$P_{\mathrm{g1}} = \frac{g_1}{g_1 + b_1}, \qquad P_{\mathrm{b1}} = \frac{b_1}{g_1 + b_1}, \qquad P_{\mathrm{g2}} = \frac{g_1}{g_2 + b_2}, \qquad P_{\mathrm{b2}} = \frac{b_1}{g_2 + b_2}, \tag{B.37}$$

the (correlated) joint state probabilities can be written as

$$\begin{array}{rcl} P_1 & = & [g_1 g_2 + \rho Q]/[(g_1 + b_1)(g_2 + b_2)] \\ P_2 & = & [g_1 b_2 - \rho Q]/[(g_1 + b_1)(g_2 + b_2)] \\ P_3 & = & [b_1 g_2 - \rho Q]/[(g_1 + b_1)(g_2 + b_2)] \\ P_4 & = & [b_1 b_2 + \rho Q]/[(g_1 + b_1)(g_2 + b_2)] \end{array} \tag{B.38}$$

with

$$Q = \sqrt{g_1 g_2 b_1 b_2} \tag{B.39}$$

Inserting the state probabilities from Equation (B.38) to Equation (B.36) result in

$$c = \frac{\rho Q(1 - (1 - g_1 - b_1)(1 - g_2 - b_2))}{(g_1 g_2 x_0 + g_1 g_2 y_0 + b_1 g_2 v_0 + b_1 b_2 w_0) - \rho Q(-x_0 + y_0 + v_0 - w_0)} \tag{B.40}$$

The parameter c is used to calculate x, y, v, w according to Equation (B.32) and to achieve finally the correlation matrix from Equation (B.30).

B.2.3. First-Order Markov Model for Two Satellites: Single-Satellite Characteristics

A first-order Markov chain for two satellites is described by a joint state transition probability matrix $\mathbf{P}_{\mathrm{trans}}^{joint}$. Assuming two states ('good' and 'bad') per satellite, it is denoted with

$$\mathbf{P}_{\mathrm{trans}}^{joint} = \begin{bmatrix} p_{11} & p_{12} & p_{13} & p_{14} \\ p_{21} & p_{22} & p_{23} & p_{24} \\ p_{31} & p_{32} & p_{33} & p_{34} \\ p_{41} & p_{42} & p_{43} & p_{44} \end{bmatrix} \tag{B.41}$$

The equilibrium state probabilities are

$$\mathbf{p}^{joint} = [P_1 P_2 P_3 P_4]^T \tag{B.42}$$

According to Equation (B.5), the diagonal elements of $\mathbf{P}_{\mathrm{trans}}^{joint}$ give information on the SDPDF of the four joint states, which follows an exponential distribution.

The joint STPM include characteristics of the individual satellites as well. Therefore, the STPMs of satellite 1 and satellite 2 ($\mathbf{P}_{\text{trans}}^{sat1}$, $\mathbf{P}_{\text{trans}}^{sat2}$) are derived from the joint STPM.

$$\mathbf{P}_{\text{trans}}^{sat1} = \begin{bmatrix} p_{\text{gg},1} & (1-p_{\text{gg},1}) \\ p_{\text{bg},1} & (1-p_{\text{bg},1}) \end{bmatrix} \qquad \mathbf{P}_{\text{trans}}^{sat2} = \begin{bmatrix} p_{\text{gg},2} & (1-p_{\text{gg},2}) \\ p_{\text{bg},2} & (1-p_{\text{bb},2}) \end{bmatrix} \tag{B.43}$$

The state transitions for satellite 1 are:

$$p_{\text{gg},1} = \frac{P_1}{P_1+P_2}(p_{11}+p_{12}) + \frac{P_2}{P_1+P_2}(p_{21}+p_{22}) \tag{B.44}$$

$$p_{\text{bg},1} = \frac{P_3}{P_3+P_4}(p_{31}+p_{32}) + \frac{P_4}{P_3+P_4}(p_{41}+p_{42}) \tag{B.45}$$

The state transitions for satellite 2 are:

$$p_{\text{gg},2} = \frac{P_1}{P_1+P_3}(p_{11}+p_{13}) + \frac{P_3}{P_1+P_3}(p_{31}+p_{33}) \tag{B.46}$$

$$p_{\text{bg},2} = \frac{P_2}{P_2+P_4}(p_{21}+p_{23}) + \frac{P_4}{P_2+P_4}(p_{41}+p_{43}) \tag{B.47}$$

From the resulting state transition matrices the equilibrium state probabilities and the **mean state durations for the single satellites** can be calculated according to Equation (B.4) and Equation (B.5), respectively.

Although the transition probabilities in $\mathbf{P}_{\text{trans}}^{sat1}$ and $\mathbf{P}_{\text{trans}}^{sat2}$ are valid, the actual SDPDFs for satellite 1 and satellite 2 **are not exactly exponentially distributed** as expected for first-order Markov models (c.f. Equation (B.5)) in any case. Therefore, a method to calculate the single-satellite SDPDFs from semi-Markov chains is given in next section and can be adapted for first-order Markov models as well.

B.2.4. Semi-Markov Model for Two Satellites: Single-Satellite Characteristics

A semi-Markov model is mainly described by SDPDFs for each state. For a single-satellite semi-Markov model, the SDPDFs of the 'good' and 'bad' state are parameters of the model. For a dual-satellite semi-Markov model, the SDPDFs of the joint states ('good good', 'good bad', 'bad good', 'bad bad') and a STPM are the parameters. However, the SDPDFs of the single satellites (i.e. 'good' and 'bad' for satellite 1 and satellite 2) have to be determined in case of a dual-satellite model. In this section, a calculation of single-satellite SDPDFs is introduced. To the best knowledge of the author, this calculation has not been considered in the literature, so far.

Assuming a semi-Markov model for two satellites, which is described by four SDPDFs $P(D)$ for combined states 'good good', 'good bad', 'bad good', 'bad bad', and a joint STPM $\mathbf{P}_{\text{trans}}^{semiM}$ with diagonal elements are zero. In the following, the calculation of the single-satellite SDPDFs is exemplarily presented for the 'good' state of satellite 1.

The SDPDF of state 'good' for satellite 1 ($P(D_{\mathrm{g}}^{Sat1})$) depends on the SDPDFs for 'good good' and 'good bad', the transition probabilities $p_{12} = p_{\mathrm{gg}\to\mathrm{gb}}$ and $p_{21} = p_{\mathrm{gb}\to\mathrm{gg}}$ and the probability of entering the combined states P_1' and P_2'.

$$P(D_{\mathrm{g}}^{Sat1}) = f(P(D_{\mathrm{gg}}), P(D_{\mathrm{gb}}), p_{12}, p_{21}, P_1', P_2') \tag{B.48}$$

In the following expressions it is assumed that the SDPDFs of single and combined states are given by probabilities of durations with discrete sample length: $P(D = k)$ with $k \in \{1, 2, 3, ..., q_{\max}\}$.

Starting with the probability of the 'good'-state having duration $D = 1$: This case is valid if one of the combined states (gg or gb) have a duration of $D = 1$ and there is no state transition between gg and gb. The exact expression is:

$$\begin{aligned} P(D_{\mathrm{g}}^{sat1} = 1) &= P_1' \cdot P(D_{\mathrm{gg}} = 1) \cdot (1 - p_{12}) \\ &+ P_2' \cdot P(D_{\mathrm{gb}} = 1) \cdot (1 - p_{21}) \end{aligned} \tag{B.49}$$

A 'good' state duration of $D = 2$ is achieved, if whether one of the joint durations is $D = 2$ and there is no transition between gg and gb **or** the joint durations are $D = 1$ and there is a transition between gg and gb.

$$\begin{aligned} P(D_{\mathrm{g}}^{sat1} = 2) &= P_1' \cdot P(D_{\mathrm{gg}} = 2) \cdot (1 - p_{12}) \\ &+ P_1' \cdot P(D_{\mathrm{gg}} = 1) \cdot p_{12} \cdot P(D_{\mathrm{gb}} = 1) \cdot (1 - p_{21}) \\ &+ P_2' \cdot P(D_{\mathrm{gb}} = 2) \cdot (1 - p_{21}) \\ &+ P_2' \cdot P(D_{\mathrm{gb}} = 1) \cdot p_{21} \cdot P(D_{\mathrm{gg}} = 1) \cdot (1 - p_{12}) \end{aligned} \tag{B.50}$$

A 'good'-state duration of $D = 3$ is calculated with:

$$\begin{aligned} P(D_{\mathrm{g}}^{sat1} = 3) &= P_1' \cdot P(D_1 = 3) \cdot (1 - p_{12}) \\ &+ P_1' \cdot P(D_1 = 2) \cdot p_{12} \cdot P(D_2 = 1) \cdot (1 - p_{21}) \\ &+ P_1' \cdot P(D_1 = 1) \cdot p_{12} \cdot P(D_2 = 2) \cdot (1 - p_{21}) \\ &+ P_1' \cdot P(D_1 = 1) \cdot p_{12} \cdot P(D_2 = 1) \cdot (p_{21}) \cdot P(D_1 = 1) \cdot (1 - p_{12}) \\ &+ P_2' \cdot P(D_2 = 3) \cdot (1 - p_{21}) \\ &+ P_2' \cdot P(D_2 = 2) \cdot p_{21} \cdot P(D_1 = 1) \cdot (1 - p_{12}) \\ &+ P_2' \cdot P(D_2 = 1) \cdot p_{21} \cdot P(D_1 = 2) \cdot (1 - p_{12}) \\ &+ P_2' \cdot P(D_2 = 1) \cdot p_{21} \cdot P(D_1 = 1) \cdot (p_{12}) \cdot P(D_2 = 1) \cdot (1 - p_{21}) \end{aligned} \tag{B.51}$$

The three examples demonstrate that the alternative paths to achieve a certain 'good'-state duration grow with increasing state length. However, parts of Equation (B.51) are found in Equation (B.50) and parts of Equation (B.50) are found in Equation (B.49). Thus, the remaining probabilities of 'good'-state durations can be calculated by an iterative algorithm.

$$P(D_{\mathrm{g}}^{sat1} = 1) = P_1' \cdot A(1) + P_2' \cdot B(1) \tag{B.52}$$

with

$$\begin{aligned} A(1) &= P(D_{\mathrm{gg}} = 1) \cdot (1 - p_{12}) \\ B(1) &= P(D_{\mathrm{gb}} = 1) \cdot (1 - p_{21}) \end{aligned} \tag{B.53}$$

The remaining elements are calculated with:

$$P(D_{\mathrm{g}}^{sat1} = k) = P_1' \cdot A(k) + P_2' \cdot B(k) \tag{B.54}$$

with

$$\begin{aligned} A(k) &= P(D_{\mathrm{gg}} = k) \cdot (1 - p_{12}) + \sum_{q=1}^{k-1} (P(D_{\mathrm{gg}} = k - q) \cdot p_{12} \cdot B(q)) \\ B(k) &= P(D_{\mathrm{gb}} = k) \cdot (1 - p_{21}) + \sum_{q=1}^{k-1} (P(D_{\mathrm{gb}} = k - q) \cdot p_{21} \cdot A(q)) \end{aligned} \tag{B.55}$$

P_1' and P_2' (with $P_1' + P_2' = 1$) are the probabilities of starting the iteration with the combined states gg and gb, respectively. In other words, P_1' and P_2' are the effective transition probabilities from one of the other states (i.e. bb and bg) to the states of interest (gg or gb). Therefore, the joint transitions $p_{\mathrm{bg}\to\mathrm{gg}}$, $p_{\mathrm{bb}\to\mathrm{gg}}$, $p_{\mathrm{bg}\to\mathrm{gb}}$, $p_{\mathrm{bb}\to\mathrm{gb}}$ are important:

$$P_1' = \frac{p_{31} + p_{41}}{p_{31} + p_{41} + p_{32} + p_{42}} \qquad P_2' = \frac{p_{32} + p_{42}}{p_{31} + p_{41} + p_{32} + p_{42}} \tag{B.56}$$

The SDPDFs $P(D_{\mathrm{b}}^{sat1})$, $P(D_{\mathrm{g}}^{sat2})$, and $P(D_{\mathrm{b}}^{sat2})$ are calculated analogously to the given example. From the SDPDFs the mean state durations for the individual satellites are derived according to Equation (B.10). The results are valid for semi-Markov models with arbitrary joint SDPDFs.

With a small modification the calculation method above can be used for dual-satellite first-order Markov chains. Therefore, all diagonal elements of $\mathbf{P}_{\mathrm{trans}}^{joint}$ must be set to zero and the remaining transitions have to be normalised such that the sum of each row equals 1. Knowing the SDPDFs for joint states (Equation (B.5)), the SDPDFs for single satellite states are derived.

B.2.5. Dynamic Markov Model for Two Satellites: Single-Satellite Characteristics

Similarly to the dual-satellite semi-Markov model from previous section, the calculation of single-satellite SDPDFs on the basis of a dual-satellite dynamic Markov model is introduced in this section.

A dynamic Markov model for two satellites is described by a three-dimensional state transition probability tensor. Assuming the joint states for 'good' and 'bad', the STPT is of dimension $\mathcal{P}_{\mathrm{trans}}^{joint} \in \mathbb{R}_{0+}^{4\times4\times q_{\max}}$, where $q_{\max}$ corresponds to the maximum joint state duration. The SDPDFs of the joint states are estimated with Equation (B.18), which is found also in [MHEH09]. In the context of this work analytic expressions are developed to derive

the SDPDFs of the two individual satellites. An iterative algorithm is used similar to the approach for semi-Markov models from previous section. The calculation of the 'good'-SDPDF for satellite 1 is taken as example again.

Required parameters to derive the 'good'-SDPDF for satellite 1 are:

1. the SDPDFs of the combined states 'good good' and 'good bad' $P(D_{\mathrm{gg}})$ and $P(D_{\mathrm{gb}})$
2. a modified STPT which is similar to a semi-Markov model. Therefore, the diagonal elements of $\mathcal{P}_{\mathrm{trans}}^{joint}$ must be set to zero for each value of the current state duration q. Afterwards, the STPT have to be normalised such that the sum of each row equals 1.

$$\mathcal{P}_{\mathrm{trans}}^{joint} \quad \rightarrow \quad \mathcal{P}_{\mathrm{trans}}^{joint'} = \begin{bmatrix} 0 & p'_{12}(q) & p'_{13}(q) & p'_{14}(q) \\ p'_{21}(q) & 0 & p'_{23}(q) & p'_{24}(q) \\ p'_{31}(q) & p'_{32}(q) & 0 & p'_{34}(q) \\ p'_{41}(q) & p'_{42}(q) & p'_{43}(q) & 0 \end{bmatrix} \qquad q \in \{1, 2, ..., q_{\max}\} \tag{B.57}$$

   Important vectors to get $P(D_{\mathrm{g}}^{sat1})$ are $p'_{12}(q)$ and $p'_{21}(q)$.

3. the probabilities (P'_1 and P'_2) of entering the states of interest (gg or gb) after beeing in one of the other states (bg or bb). For this purpose, first the equivalent of the STPM according to the first-order Markov model $\mathbf{P}'_{\mathrm{trans}}$ must be derived from the state transition tensor $\mathcal{P}_{\mathrm{trans}}^{joint}$ as described in Section B.1.3. Then, the diagonal elements of $\mathbf{P}'_{\mathrm{trans}}$ must be set to zero and the remaining transitions are normalised ($\mathbf{P}'_{\mathrm{trans}} \rightarrow \mathbf{P}''_{\mathrm{trans}}$). P'_1 and P'_2 are calculated with

$$P'_1 = \frac{p''_{31} + p''_{41}}{p''_{31} + p''_{41} + p''_{32} + p''_{42}} \qquad P'_2 = \frac{p''_{32} + p''_{42}}{p''_{31} + p''_{41} + p''_{32} + p''_{42}} \tag{B.58}$$

The probability of a 'good'-state duration of $D = 1$ is given by

$$P(D_{\mathrm{g}}^{sat1} = 1) = P'_1 \cdot A(1) + P'_2 \cdot B(1) \tag{B.59}$$

with

$$\begin{aligned} A(1) &= P(D_{\mathrm{gg}} = 1) \cdot (1 - p'_{12}(1)) \\ B(1) &= P(D_{\mathrm{gb}} = 1) \cdot (1 - p'_{21}(1)) \end{aligned} \tag{B.60}$$

The probabilities for durations $D > 1$ are calculated iteratively with:

$$P(D_{\mathrm{g}}^{sat1} = k) = P'_1 \cdot A(k) + P'_2 \cdot B(k) \tag{B.61}$$

with

$$\begin{aligned} A(k) &= P(D_{\mathrm{gg}} = k) \cdot (1 - p'_{12}(k)) + \sum_{q=1}^{k-1} \left(P(D_{\mathrm{gg}} = k - q) \cdot p'_{12}(k - q) \cdot B(q) \right) \\ B(k) &= P(D_{\mathrm{gb}} = k) \cdot (1 - p'_{21}(k)) + \sum_{q=1}^{k-1} \left(P(D_{\mathrm{gb}} = k - q) \cdot p'_{21}(k - q) \cdot A(q) \right) \end{aligned} \tag{B.62}$$

The main difference to the algorithm for semi-Markov chains from previous section is that the transition probabilities are a function of the state duration. The SDPDFs $P(D_{\mathrm{b}}^{sat1})$, $P(D_{\mathrm{g}}^{sat2})$, and $P(D_{\mathrm{b}}^{sat2})$ are calculated analogously to the given example. From the SDPDFs the mean state durations for the individual satellites are derived according to Equation (B.10).

B.3. Multi-Satellite Modelling

This section describes two Master-Slave approaches including the state probability calculation for two- and three satellites, as well as the calculation of state probabilities in a three-satellite system, which is taken as reference in Section 3.5. All expressions from this section are developed in the context of this thesis. (cf. also Section 3.2.5 and Section 3.5)

B.3.1. Master-Slave with Conditional Assembling Method

The Conditional Assembling Method developed in this work is one possible realisation for the Master-Slave concept. In this section the calculation of joint state probabilities and correlation coefficients for two and more satellites are given. They are derived from the equilibrium state probabilities of the master ($\mathbf{p}^M$), of the conditional slave states when master is in good state ($\mathbf{p}^{S|M=good}$) and the conditional slave states when master is in bad state ($\mathbf{p}^{S|M=bad}$).

$$\mathbf{p}^M = \begin{bmatrix} P^M_{\mathrm{g}} & P^M_{\mathrm{b}} \end{bmatrix}^T, \qquad \mathbf{p}^{S|M=good} = \begin{bmatrix} P^S_{\mathrm{g|g}} & P^S_{\mathrm{b|g}} \end{bmatrix}^T, \qquad \mathbf{p}^{S|M=bad} = \begin{bmatrix} P^S_{\mathrm{g|b}} & P^S_{\mathrm{b|b}} \end{bmatrix}^T \tag{B.63}$$

$P^S_{i|j}$ defines the probability of the slave state i in case of the master state is j.

Calculation of State Probabilities (one Master, one Slave)

From the master probabilities and conditional slave probabilities the combined probability vector $\mathbf{p}^{joint}$ is calculated:

$$\mathbf{p}^{joint} = \begin{bmatrix} P_{\mathrm{gg}} \\ P_{\mathrm{gb}} \\ P_{\mathrm{bg}} \\ P_{\mathrm{bb}} \end{bmatrix} = \begin{bmatrix} P^M_{\mathrm{g}} \cdot P^S_{\mathrm{g|g}} \\ P^M_{\mathrm{g}} \cdot P^S_{\mathrm{b|g}} \\ P^M_{\mathrm{b}} \cdot P^S_{\mathrm{g|b}} \\ P^M_{\mathrm{b}} \cdot P^S_{\mathrm{b|b}} \end{bmatrix} \tag{B.64}$$

The state probabilities of the slave are:

$$\mathbf{p}^S = \begin{bmatrix} P^S_{\mathrm{g}} \\ P^S_{\mathrm{b}} \end{bmatrix} = \begin{bmatrix} P_{\mathrm{gg}} + P_{\mathrm{bg}} \\ P_{\mathrm{gb}} + P_{\mathrm{bb}} \end{bmatrix} \tag{B.65}$$

Calculation of State Probabilities with one Master and Multiple Slaves

Analogously to the two-satellite case, the combined probability vector $\mathbf{p}^{joint}$ for multiple satellites (with k satellites) is the product of master probabilities and multiple conditional slave probabilities.

$$\mathbf{p}^{joint} = \begin{bmatrix} P_{\text{ggg..g}} \\ P_{\text{ggg..b}} \\ \dots \\ P_{\text{gbg..b}} \\ P_{\text{gbb..g}} \\ \dots \\ P_{\text{bbb..b}} \end{bmatrix} = \begin{bmatrix} P_{\text{g}}^{M} \cdot P_{\text{g|g}}^{S2} \cdot P_{\text{g|g}}^{S3} \cdot , \dots, \cdot P_{\text{g|g}}^{Sk} \\ P_{\text{g}}^{M} \cdot P_{\text{g|g}}^{S2} \cdot P_{\text{g|g}}^{S3} \cdot , \dots, \cdot P_{\text{b|g}}^{Sk} \\ \dots \\ P_{\text{g}}^{M} \cdot P_{\text{b|g}}^{S2} \cdot P_{\text{g|g}}^{S3} \cdot , \dots, \cdot P_{\text{b|g}}^{Sk} \\ P_{\text{g}}^{M} \cdot P_{\text{b|g}}^{S2} \cdot P_{\text{b|g}}^{S3} \cdot , \dots, \cdot P_{\text{g|g}}^{Sk} \\ \dots \\ P_{\text{b}}^{M} \cdot P_{\text{b|b}}^{S2} \cdot P_{\text{b|b}}^{S3} \cdot , \dots, \cdot P_{\text{g|b}}^{Sk} \end{bmatrix} \tag{B.66}$$

Correlation coefficient between Master and Slave

Based on combined probabilities of master and slave, the correlation coefficient $\rho_{\text{Master\&Slave}}$ is found with Equation (B.25).

Correlation coefficient between two Slaves

The correlation coefficient between two slaves depends on the combined state probabilities P'_{ij} of the slaves:

$$\rho_{\text{states, Slaves}} = \frac{P'_{\text{gg}} \cdot P'_{\text{bb}} - P'_{\text{gb}} \cdot P'_{\text{bg}}}{\sqrt{(P'_{\text{gg}} + P'_{\text{gb}})(P'_{\text{bb}} + P'_{\text{bg}})(P'_{\text{gg}} + P'_{\text{bg}})(P'_{\text{bb}} + P'_{\text{gb}})}} \tag{B.67}$$

The combined state probabilities P'_{ij} of the slaves can be calculated from the joint state probabilities of the whole system Master(1)-Slave(2)-Slave(3). According to Equation (B.66) it holds:

$$\mathbf{p}^{joint(Slave2\&Slave3)} = \begin{bmatrix} P'_{\text{gg}} \\ P'_{\text{gb}} \\ P'_{\text{bg}} \\ P'_{\text{bb}} \end{bmatrix} = \begin{bmatrix} P_{\text{ggg}} + P_{\text{bgg}} \\ P_{\text{ggb}} + P_{\text{bgb}} \\ P_{\text{gbg}} + P_{\text{bbg}} \\ P_{\text{gbb}} + P_{\text{bbb}} \end{bmatrix} = \begin{bmatrix} P_{\text{g}}^{M} \cdot P_{\text{g|g}}^{S2} \cdot P_{\text{g|g}}^{S3} + P_{\text{b}}^{M} \cdot P_{\text{g|b}}^{S2} \cdot P_{\text{g|b}}^{S3} \\ P_{\text{g}}^{M} \cdot P_{\text{g|g}}^{S2} \cdot P_{\text{b|g}}^{S3} + P_{\text{b}}^{M} \cdot P_{\text{g|b}}^{S2} \cdot P_{\text{b|b}}^{S3} \\ P_{\text{g}}^{M} \cdot P_{\text{b|g}}^{S2} \cdot P_{\text{g|g}}^{S3} + P_{\text{b}}^{M} \cdot P_{\text{b|b}}^{S2} \cdot P_{\text{g|b}}^{S3} \\ P_{\text{g}}^{M} \cdot P_{\text{b|g}}^{S2} \cdot P_{\text{b|g}}^{S3} + P_{\text{b}}^{M} \cdot P_{\text{b|b}}^{S2} \cdot P_{\text{b|b}}^{S3} \end{bmatrix} \tag{B.68}$$

By inserting Equation (B.68) in Equation (B.67) the correlation coefficient between the slaves $\rho_{\text{states, Slaves}}$ can be described as a function of the correlation coefficients between master and slave(2), and master and slave(3):

$$\rho_{\text{states, Slaves}} = \rho_{\text{states, Master\&Slave2}} \cdot \rho_{\text{states, Master\&Slave3}} \tag{B.69}$$

B.3.2. Master-Slave with Adaptive Slave Transition Matrix based on Master Transitions (ASTM-MT)

A further realisation of the Master-Slave concept is denoted as Adaptive Slave Transition Matrix. It means in general that state model parameters of the slave depend on one or more state model parameters of the master. A relevant approach is found in this work, when the

state transitions probability matrix of the slave ($\mathbf{P}_{\text{trans}}^{Slave}$) is a function of the master state transition probabilities:

$$\mathbf{P}_{\text{trans}}^{Slave} = f(p_{ij}^{Master}), \qquad i,j \in \{\text{g,b}\} \tag{B.70}$$

If the master satellite is described by a **first-order Markov model**, then the joint STPM of master and slave is the product of the master transition probabilities with the corresponding STPM of the slave:

$$\mathbf{P}_{\text{trans}}^{joint} = \begin{bmatrix} p_{\text{gg}}^{Master} \cdot \mathbf{P}_{\text{trans}}^{Slave|\text{gg}} & p_{\text{gb}}^{Master} \cdot \mathbf{P}_{\text{trans}}^{Slave|\text{gb}} \\ p_{\text{bg}}^{Master} \cdot \mathbf{P}_{\text{trans}}^{Slave|\text{bg}} & p_{\text{bb}}^{Master} \cdot \mathbf{P}_{\text{trans}}^{Slave|\text{bb}} \end{bmatrix} \tag{B.71}$$

$\mathbf{P}_{\text{trans}}^{joint}$ include all information for equilibrium state probabilities, mean state durations, and SDPDFs for single satellite states and combined states. The information can be estimated as described in Section B.1.1 for first-order Markov chains.

If the master satellite is described by a semi-Markov or a dynamic Markov model, Equation (B.71) is approximately valid.

State Transition Probability Matrix with Three Satellites

The joint STPM for a three-satellite constellation using the ASTM-MT approach is determined by the product of transition probabilities from master(1), the conditional transition probabilities of slave(2), and the conditional transition probabilities of slave(3).

$$\mathbf{P}_{\text{trans}}^{M1\&S2\&S3} =$$

$$\begin{bmatrix} p_{\text{gg}}^{M} \cdot \begin{bmatrix} p_{\text{gg|gg}}^{S2} \cdot \mathbf{P}_{\text{trans}}^{S3|\text{gg}} & p_{\text{gb|gg}}^{S2} \cdot \mathbf{P}_{\text{trans}}^{S3|\text{gg}} \\ p_{\text{bg|gg}}^{S2} \cdot \mathbf{P}_{\text{trans}}^{S3|\text{gg}} & p_{\text{bb|gg}}^{S2} \cdot \mathbf{P}_{\text{trans}}^{S3|\text{gg}} \end{bmatrix} & p_{\text{gb}}^{M} \cdot \begin{bmatrix} p_{\text{gg|gb}}^{S2} \cdot \mathbf{P}_{\text{trans}}^{S3|\text{gb}} & p_{\text{gb|gb}}^{S2} \cdot \mathbf{P}_{\text{trans}}^{S3|\text{gb}} \\ p_{\text{bg|gb}}^{S2} \cdot \mathbf{P}_{\text{trans}}^{S3|\text{gb}} & p_{\text{bb|gb}}^{S2} \cdot \mathbf{P}_{\text{trans}}^{S3|\text{gb}} \end{bmatrix} \\ p_{\text{bg}}^{M} \cdot \begin{bmatrix} p_{\text{gg|bg}}^{S2} \cdot \mathbf{P}_{\text{trans}}^{S3|\text{bg}} & p_{\text{gb|bg}}^{S2} \cdot \mathbf{P}_{\text{trans}}^{S3|\text{bg}} \\ p_{\text{bg|bg}}^{S2} \cdot \mathbf{P}_{\text{trans}}^{S3|\text{bg}} & p_{\text{bb|bg}}^{S2} \cdot \mathbf{P}_{\text{trans}}^{S3|\text{bg}} \end{bmatrix} & p_{\text{bb}}^{M} \cdot \begin{bmatrix} p_{\text{gg|bb}}^{S2} \cdot \mathbf{P}_{\text{trans}}^{S3|\text{bb}} & p_{\text{gb|bb}}^{S2} \cdot \mathbf{P}_{\text{trans}}^{S3|\text{bb}} \\ p_{\text{bg|bb}}^{S2} \cdot \mathbf{P}_{\text{trans}}^{S3|\text{bb}} & p_{\text{bb|bb}}^{S2} \cdot \mathbf{P}_{\text{trans}}^{S3|\text{bb}} \end{bmatrix} \end{bmatrix} \tag{B.72}$$

p_{ij}^{M} $(i,j \in \{\text{g,b}\})$ are state transition probabilities of the master, $p_{kl|ij}^{S2}$ are transition probabilities of slave(2) from state k to l $(k,l \in \{\text{g,b}\})$ under the condition of master goes from state i to j, and $\mathbf{P}_{\text{trans}}^{S3|ij}$ is the STPM of slave(3) under the condition of master goes from i to j.

From $\mathbf{P}_{\text{trans}}^{M1\&S2\&S3}$ the **joint state probabilities** can be derived according to Equation (B.3), and the **mean joint state durations** are calculated according to Equation (B.6), respectively.

The **correlation coefficient between the slaves** $\rho_{\text{states, Slaves}}$ can be calculated from the joint state probabilities with

$$\rho_{\text{states, Slaves}} = \frac{P'_{\text{bb}} - A_1 A_2}{\sqrt{(1-A_1)(1-A_2)A_1 A_2}}\,, \tag{B.73}$$

where

$$\begin{aligned} P'_{\text{bb}} &= P_{\text{gbb}} + P_{\text{bbb}}\,, \\ A_1 &= P_{\text{gbg}} + P_{\text{gbb}} + P_{\text{bbg}} + P_{\text{bbb}}\,, \text{and} \\ A_2 &= P_{\text{gbg}} + P_{\text{gbb}} + P_{\text{bgb}} + P_{\text{bbb}}\,. \end{aligned}$$

By evaluating $\rho_{\text{states, Slaves}}$ for a number of constellations with three satellites it is found that

$$\rho_{\text{states, Slaves}} \approx \rho_{\text{states, Master\&Slave2}} \cdot \rho_{\text{states, Master\&Slave3}} \tag{B.74}$$

B.3.3. State Probabilities of a Three-Satellite System

The joint state probabilities of a three-satellite system are given by:

$$\mathbf{p}^{joint(sat1\&sat2\&sat3)} = \begin{bmatrix} P_{\text{ggg}} \\ P_{\text{ggb}} \\ P_{\text{gbg}} \\ P_{\text{gbb}} \\ P_{\text{bgg}} \\ P_{\text{bgb}} \\ P_{\text{bbg}} \\ P_{\text{bbb}} \end{bmatrix} = \begin{bmatrix} P_1 \\ P_2 \\ P_3 \\ P_4 \\ P_5 \\ P_6 \\ P_7 \\ P_8 \end{bmatrix} \tag{B.75}$$

To analytically derive the combined state probabilities from dual-satellite measurement data, we consider the state probabilities of the individual satellites, and the correlation coefficients between the satellites:

$$\mathbf{p}^{sat1} = \begin{bmatrix} P_{\text{g1}} \\ P_{\text{b1}} \end{bmatrix}, \quad \mathbf{p}^{sat2} = \begin{bmatrix} P_{\text{g2}} \\ P_{\text{b2}} \end{bmatrix}, \quad \mathbf{p}^{sat3} = \begin{bmatrix} P_{\text{g3}} \\ P_{\text{b3}} \end{bmatrix}, \quad \rho = \begin{bmatrix} \rho_{11} & \rho_{12} & \rho_{13} \\ \rho_{21} & \rho_{22} & \rho_{23} \\ \rho_{31} & \rho_{32} & \rho_{33} \end{bmatrix}, \tag{B.76}$$

with $\rho_{xx} = 1$, and $\rho_{xy} = \rho_{yx}$.

The sum of two combined probabilities from $\mathbf{p}^{joint(sat1\&sat2\&sat3)}$ equals the combined probabilities of two satellites:

$$\mathbf{p}^{joint(sat1\&sat2)} = \begin{bmatrix} P_{\text{gg}X} \\ P_{\text{gb}X} \\ P_{\text{bg}X} \\ P_{\text{bb}X} \end{bmatrix} = \begin{bmatrix} P_{\text{ggg}} + P_{\text{ggb}} \\ P_{\text{gbg}} + P_{\text{gbb}} \\ P_{\text{bgg}} + P_{\text{bgb}} \\ P_{\text{bbg}} + P_{\text{bbb}} \end{bmatrix} \tag{B.77}$$

$$\mathbf{p}^{joint(sat1\&sat3)} = \begin{bmatrix} P_{\mathrm{g}X\mathrm{g}} \\ P_{\mathrm{g}X\mathrm{b}} \\ P_{\mathrm{b}X\mathrm{g}} \\ P_{\mathrm{b}X\mathrm{b}} \end{bmatrix} = \begin{bmatrix} P_{\mathrm{ggg}} + P_{\mathrm{gbg}} \\ P_{\mathrm{ggb}} + P_{\mathrm{gbb}} \\ P_{\mathrm{bgg}} + P_{\mathrm{bbg}} \\ P_{\mathrm{bgb}} + P_{\mathrm{bbb}} \end{bmatrix} \tag{B.78}$$

$$\mathbf{p}^{joint(sat2\&sat3)} = \begin{bmatrix} P_{X\mathrm{gg}} \\ P_{X\mathrm{gb}} \\ P_{X\mathrm{bg}} \\ P_{X\mathrm{bb}} \end{bmatrix} = \begin{bmatrix} P_{\mathrm{ggg}} + P_{\mathrm{bgb}} \\ P_{\mathrm{ggb}} + P_{\mathrm{bgb}} \\ P_{\mathrm{gbg}} + P_{\mathrm{bbg}} \\ P_{\mathrm{gbb}} + P_{\mathrm{bbb}} \end{bmatrix} \tag{B.79}$$

It is assumed that the combined probabilities $\mathbf{p}^{joint(sat1\&sat2)}$, $\mathbf{p}^{joint(sat1\&sat3)}$, and $\mathbf{p}^{joint(sat2\&sat3)}$ include already the single satellite probabilities and the correlation coefficients according to Equation (B.26).

By denoting $\mathbf{p}^{joint(sat1\&sat2)} = \mathbf{a}$, $\mathbf{p}^{joint(sat1\&sat3)} = \mathbf{b}$, $\mathbf{p}^{joint(sat2\&sat3)} = \mathbf{c}$, the Equations (B.77), (B.78), (B.79) are written in matrix form:

$$\begin{bmatrix} A_1 \\ A_2 \\ A_3 \\ A_4 \\ B_1 \\ B_2 \\ B_3 \\ B_4 \\ C_1 \\ C_2 \\ C_3 \\ C_4 \end{bmatrix} = \begin{bmatrix} 1 & 1 & 0 & 0 & 0 & 0 & 0 & 0 \\ 0 & 0 & 1 & 1 & 0 & 0 & 0 & 0 \\ 0 & 0 & 0 & 0 & 1 & 1 & 0 & 0 \\ 0 & 0 & 0 & 0 & 0 & 0 & 1 & 1 \\ 1 & 0 & 1 & 0 & 0 & 0 & 0 & 0 \\ 0 & 1 & 0 & 1 & 0 & 0 & 0 & 0 \\ 0 & 0 & 0 & 0 & 1 & 0 & 1 & 0 \\ 0 & 0 & 0 & 0 & 0 & 1 & 0 & 1 \\ 1 & 0 & 0 & 0 & 1 & 0 & 0 & 0 \\ 0 & 1 & 0 & 0 & 0 & 1 & 0 & 0 \\ 0 & 0 & 1 & 0 & 0 & 0 & 1 & 0 \\ 0 & 0 & 0 & 1 & 0 & 0 & 0 & 1 \end{bmatrix} \cdot \begin{bmatrix} P_1 \\ P_2 \\ P_3 \\ P_4 \\ P_5 \\ P_6 \\ P_7 \\ P_8 \end{bmatrix} \tag{B.80}$$

Equation (B.80) has an infinite number of solutions for P_i. With assumption $P_8 = n$ it holds:

$$\begin{aligned} P_8 &= n \\ P_7 &= A_4 - n \\ P_6 &= B_4 - n \\ P_5 &= B_3 - A_4 + n \\ P_4 &= C_4 - n \\ P_3 &= C_3 - A_4 + n \\ P_2 &= C_2 - B_4 + n \\ P_1 &= C_1 - B_3 + A_4 - n \end{aligned} \tag{B.81}$$

All solutions of Equation (B.81) provide the state probabilities of the individual satellites as well as the correlation coefficients between two pairs of satellites. By considering $0 \leq P_i \leq 1$, the range of valid probabilities is found with

$$
\begin{array}{ll}
n \leq 1 & n \geq 0 \\
n \leq A_4 & n \geq A_4 - 1 \\
n \leq B_4 & n \geq B_4 - 1 \\
n \leq 1 - B_3 + A_4 & n \geq A_4 - B_3 \\
n \leq C_4 & n \geq C_4 - 1 \\
n \leq 1 - C_4 + A_4 & n \geq A_4 - C_3 \\
n \leq 1 - C_2 + B_4 & n \geq B_4 - C_2 \\
n \leq C_1 - B_3 + A_4 & n \geq C_1 - B_3 + A_4 - 1
\end{array}
\tag{B.82}
$$

It can be further reduced to

$$
\begin{array}{rcl}
n_{\max} & = & \min\{\ A_4;\ B_4;\ C_4;\ (A_4 - B_3 + C_1)\ \} \\
n_{\min} & = & \max\{\ 0;\ (A_4 - B_3);\ (A_4 - C_3);\ (B_4 - C_2)\ \}
\end{array}
\tag{B.83}
$$

To evaluate the probability error of Master-Slave approaches with three satellites in Chapter 3.5, the mean probability of P_{bbb} is taken as reference: $P_{\text{bbb,ref}} = 1/2(P_{\text{bbb,min}} + P_{\text{bbb,max}}) = 1/2(n_{\min} + n_{\max})$

C. LMS Model Parameters

In this chapter the LMS model parameters for single- and dual-satellite reception for multiple receive scenarios (including different environments, elevation angles, azimuth angles) are listed. The model parameters are derived from SDARS measurements as well as from GNSS measurements in the context of the project MiLADY, which are described in Appendix A. The meaning and application of LMS model parameters are described in Chapter 4.

Table C.1.: Two-state model parameters for S-band derived from MiLADY SDARS measurements for different environments *env* (Urban (U), Suburban (S), Forest (F), Commercial (C), Open/Highway (O), intermediate tree-shadowed (T)), elevation angles ϕ, and states (1...good, 2...bad). The parameters are representative for a uniformly distributed driving direction within $[0; 2\pi\}$.

			M_A		$\Sigma_A(\mu_2)$			$\Sigma_A(\sigma_2)$			MP	
env	ϕ [°]	State	μ_1	σ_1	a_1	a_2	a_3	b_1	b_2	b_3	μ_3	σ_3
U	15	1										
		2										
U	25	1	-1.25	1.53	0.03	-0.09	0.60	0.02	-0.04	0.49	-16.04	4.62
		2	-12.92	3.88	-0.01	-0.41	0.18	0.00	0.07	1.83	-24.78	8.39
U	35	1	-1.30	1.21	0.00	-0.21	0.48	0.03	-0.01	0.43	-15.69	3.71
		2	-13.18	4.30	-0.01	-0.42	0.20	0.00	0.07	1.75	-22.84	9.06
U	45	1	-1.39	1.34	0.00	-0.13	0.61	0.03	-0.05	0.44	-16.28	4.59
		2	-13.42	4.36	-0.02	-0.72	-1.83	0.00	0.02	1.73	-20.03	8.45
U	55	1	-1.15	1.21	0.03	-0.01	0.55	0.04	-0.06	0.19	-18.89	4.92
		2	-13.15	4.85	-0.02	-0.67	-2.03	0.00	0.06	1.91	-20.93	8.53
U	65	1	-0.78	1.04	0.02	-0.07	0.52	0.05	-0.06	0.16	-22.52	5.91
		2	-13.41	5.05	-0.02	-0.62	-1.54	-0.00	-0.09	1.02	-22.90	8.05
U	75	1	-0.87	0.88	0.00	-0.11	0.48	0.02	-0.19	0.02	-23.19	4.72
		2	-14.30	6.12	0.00	-0.07	0.91	0.01	0.21	2.68	-23.44	8.79
U	85	1										
		2										
S	15	1										
		2										
S	25	1	-1.23	1.53	0.00	-0.18	0.57	-0.01	-0.12	0.47	-16.08	4.42
		2	-11.34	3.48	0.00	-0.04	2.03	0.01	0.17	2.11	-22.38	8.20
S	35	1	-1.60	1.32	-0.00	-0.17	0.53	0.02	-0.07	0.33	-16.64	3.97
		2	-10.26	3.06	-0.00	-0.26	0.94	0.01	0.05	1.22	-18.21	7.13
S	45	1	-1.34	1.18	0.01	-0.14	0.52	0.01	-0.08	0.39	-16.84	4.03
		2	-10.79	3.26	-0.01	-0.53	-0.98	-0.01	-0.20	0.34	-15.94	6.42
S	55	1	-1.30	1.25	0.03	-0.02	0.53	0.03	-0.02	0.28	-19.44	5.04
		2	-10.18	2.68	0.00	-0.23	0.52	-0.01	-0.30	-0.39	-14.70	4.74
S	65	1	-0.88	1.12	0.02	-0.05	0.45	0.01	-0.16	0.13	-20.51	5.02
		2	-9.65	3.06	-0.00	-0.32	0.12	-0.01	-0.33	-0.60	-16.30	6.44
S	75	1	-1.04	1.25	0.03	-0.03	0.38	0.02	-0.19	0.06	-21.07	6.13
		2	-8.95	2.85	0.01	0.07	2.36	-0.01	-0.28	-0.43	-15.93	5.19
S	85	1										
		2										
F	15	1										

Continued on next page

Table C.1 – continued from previous page

			M_A		$\Sigma_A(\mu_2)$			$\Sigma_A(\sigma_2)$			MP	
env	ϕ [°]	State	μ_1	σ_1	a_1	a_2	a_3	b_1	b_2	b_3	μ_3	σ_3
		2										
F	25	1	-2.77	1.38	0.01	-0.13	0.63	0.00	-0.07	0.59	-16.74	5.47
		2	-10.13	2.20	-0.01	-0.45	-0.64	-0.00	-0.10	0.45	-19.20	6.90
F	35	1	-2.92	1.29	-0.00	-0.21	0.63	-0.00	-0.15	0.47	-15.34	5.16
		2	-9.60	1.92	-0.00	-0.29	0.15	-0.00	-0.17	0.19	-17.51	6.53
F	45	1	-2.76	1.33	-0.00	-0.25	0.39	0.00	-0.17	0.38	-15.24	5.20
		2	-10.38	2.53	-0.00	-0.30	-0.04	-0.01	-0.36	-0.63	-15.43	5.77
F	55	1	-0.90	0.91	0.00	-0.15	0.59	-0.00	-0.08	0.35	-19.41	5.51
		2	-9.60	2.22	0.01	-0.11	0.78	-0.01	-0.38	-0.84	-16.39	6.18
F	65	1	-0.89	0.78	-0.00	-0.23	0.44	-0.01	-0.07	0.30	-20.75	5.25
		2	-11.51	2.82	-0.02	-0.54	-1.10	-0.02	-0.43	-0.90	-16.92	7.36
F	75	1	-0.66	0.54	0.03	-0.19	0.37	-0.06	-0.20	0.20	-22.71	4.45
		2	-6.19	7.74	-0.00	-0.41	-0.40	-0.01	-0.51	-0.72	-17.19	7.78
F	85	1										
		2										
C	15	1										
		2										
C	25	1	-1.31	1.30	-0.01	-0.17	0.49	0.00	-0.05	0.37	-18.56	5.76
		2	-11.47	4.10	-0.01	-0.54	-1.36	0.01	0.10	1.54	-23.08	8.52
C	35	1	-1.37	1.30	0.01	-0.03	0.58	0.00	-0.04	0.36	-18.48	4.67
		2	-10.70	4.17	-0.02	-0.65	-1.76	0.00	0.02	1.14	-21.16	7.86
C	45	1	-1.06	1.30	0.03	-0.01	0.54	0.01	-0.10	0.29	-18.14	4.61
		2	-10.89	4.42	-0.02	-0.74	-2.47	-0.01	-0.32	-0.55	-17.83	7.92
C	55	1	-0.62	0.60	0.00	-0.00	0.52	-0.02	-0.22	0.11	-20.87	3.09
		2	-12.28	4.95	-0.02	-0.82	-2.90	-0.02	-0.54	-1.54	-19.65	9.39
C	65	1	-0.59	0.89	-0.03	-0.20	0.40	0.04	0.02	0.12	-23.71	3.85
		2	-13.53	5.56	-0.02	-0.73	-2.74	0.00	0.14	2.70	-24.59	9.53
C	75	1										
		2										
C	85	1										
		2										
O	15	1										
		2										
O	25	1	-1.70	1.50	0.00	-0.10	0.56	0.01	-0.03	0.40	-20.14	6.13
		2	-10.30	4.40	-0.00	-0.36	-0.24	0.00	-0.05	0.57	-20.42	7.54
O	35	1	-1.22	1.08	0.00	-0.12	0.57	0.02	0.01	0.39	-20.88	6.74
		2	-7.50	4.78	-0.00	-0.33	0.06	0.00	-0.09	0.47	-20.54	8.34
O	45	1	-1.17	1.14	-0.00	-0.19	0.50	0.00	-0.08	0.40	-18.98	6.25
		2	-9.31	5.47	-0.00	-0.38	-0.17	0.00	-0.09	0.73	-18.05	8.40
O	55	1	-1.04	1.05	-0.03	-0.17	0.46	-0.00	-0.01	0.32	-23.92	7.47
		2	-6.51	6.15	-0.00	-0.35	-0.05	-0.01	-0.30	-0.12	-20.59	10.15
O	65	1	-0.52	0.75	0.00	-0.14	0.34	0.00	-0.08	0.20	-25.52	6.19
		2	-12.52	7.99	-0.00	-0.33	0.48	-0.01	-0.34	0.16	-20.79	9.85
O	75	1	-0.61	1.05	0.01	-0.12	0.30	-0.00	-0.04	0.17	-26.68	5.65
		2	-10.56	9.43	-0.00	-0.36	0.27	-0.01	-0.38	0.09	-21.64	10.12
O	85	1										
		2										
T	15	1										
		2										
T	25	1	-1.02	1.50	0.04	-0.02	0.51	-0.01	-0.15	0.30	-17.62	4.31
		2	-11.09	2.81	-0.01	-0.40	-0.35	0.01	0.24	2.28	-22.83	7.77
T	35	1	-1.32	1.27	0.04	-0.02	0.49	0.03	-0.00	0.38	-17.68	4.61
		2	-10.24	2.85	-0.00	-0.37	-0.06	0.00	0.01	1.17	-18.15	7.17

Continued on next page

Table C.1 – continued from previous page

			M_A		$\Sigma_A(\mu_2)$			$\Sigma_A(\sigma_2)$			MP	
env	ϕ [°]	State	μ_1	σ_1	a_1	a_2	a_3	b_1	b_2	b_3	μ_3	σ_3
T	45	1	-0.81	1.42	0.02	-0.08	0.49	0.03	-0.11	0.30	-18.37	6.56
		2	-10.40	2.77	-0.00	-0.26	0.86	0.00	0.06	1.39	-14.74	4.92
T	55	1	-0.93	1.21	-0.00	-0.12	0.46	-0.01	-0.19	0.13	-21.60	6.35
		2	-10.03	2.54	-0.01	-0.52	-0.85	0.01	0.24	2.20	-15.43	4.99
T	65	1	-0.90	0.93	0.02	-0.07	0.46	-0.00	-0.29	-0.00	-21.16	4.66
		2	-9.84	2.71	-0.01	-0.60	-1.65	-0.00	-0.14	0.42	-15.72	5.48
T	75	1										
		2										
T	85	1										
		2										

Table C.2.: Semi-Markov parameters for state sequence modelling derived from Milady SDARS measurements for different environments (Urban (U), Suburban (S), Forest (F), Commercial (C), Open/Highway (O), intermediate tree-shadowed (T)) and elevation angles. The driving direction is assumed to be uniformly distributed, but it is given anyway to equalise the format with next table. The parameters are mean and standard deviation of the lognormal distribution for 'good' state ($\mu_{\mathrm{Dur},1}, \sigma_{\mathrm{Dur},1}$) and for 'bad' state ($\mu_{\mathrm{Dur},2}, \sigma_{\mathrm{Dur},2}$) given in dB.

Environment	Elevation [°]	Driving Dir.	$\mu_{\mathrm{Dur},1}$	$\sigma_{\mathrm{Dur},1}$	$\mu_{\mathrm{Dur},2}$	$\sigma_{\mathrm{Dur},2}$
U	15	all				
	25	all	25.92	27.13	11.78	11.13
	35	all	27.51	23.58	12.70	11.38
	45	all	28.28	21.59	12.65	10.89
	55	all	29.98	19.19	13.58	10.22
	65	all	35.53	16.86	14.42	9.88
	75	all	33.56	16.19	17.28	10.36
	85	all				
S	15	all				
	25	all	26.18	22.58	12.28	10.05
	35	all	27.70	18.96	13.10	9.57
	45	all	30.08	14.13	14.19	8.12
	55	all	30.01	16.84	14.69	8.33
	65	all	33.48	12.74	14.40	7.45
	75	all	32.53	12.03	14.66	7.87
	85	all				
F	15	all				
	25	all	26.26	27.01	14.33	12.79
	35	all	26.48	21.77	13.90	11.33
	45	all	28.16	18.45	14.26	9.88
	55	all	32.45	15.78	16.35	8.45
	65	all	32.98	18.22	17.83	9.10
	75	all	42.15	15.07	20.02	7.14
	85	all				
C	15	all				
	25	all	30.81	22.12	15.64	10.72
	35	all	30.29	18.70	16.00	10.21
	45	all	32.53	18.16	16.40	9.60
	55	all	37.19	19.85	20.11	10.13
	65	all	37.38	16.97	19.46	8.32
	75	all				

Continued on next page

Table C.2 – continued from previous page

Environment	Elevation [°]	Driving Dir.	$\mu_{\mathrm{Dur},1}$	$\sigma_{\mathrm{Dur},1}$	$\mu_{\mathrm{Dur},2}$	$\sigma_{\mathrm{Dur},2}$
	85	all				
O	15	all				
	25	all	31.52	25.16	17.83	12.00
	35	all	30.11	21.84	20.44	11.10
	45	all	30.69	21.11	19.69	10.58
	55	all	29.30	21.06	22.88	9.98
	65	all	48.48	25.05	17.50	8.02
	75	all	57.25	22.96	13.09	7.35
	85	all				
T	15	all				
	25	all	27.24	26.38	14.98	12.38
	35	all	28.35	21.66	15.46	11.34
	45	all	27.58	20.71	15.10	10.40
	55	all	32.37	16.97	19.78	10.09
	65	all	31.51	17.17	18.60	8.80
	75	all				
	85	all				

Table C.3.: Semi-Markov parameters for state sequence modelling derived from Milady GNSS measurements for different environments (Urban (U), Suburban (S), Forest (F), Commercial (C), Open (O)), elevation angles, and driving directions. The special case 'uniformly distributed driving direction' is indicated with 'all'. The parameters are mean and standard deviation of the lognormal distribution for 'good' state ($\mu_{\mathrm{Dur},1}, \sigma_{\mathrm{Dur},1}$) and for 'bad' state ($\mu_{\mathrm{Dur},2}, \sigma_{\mathrm{Dur},2}$) given in dB.

Environment	Elevation [°]	Driving Dir.[°]	$\mu_{\mathrm{Dur},1}$	$\sigma_{\mathrm{Dur},1}$	$\mu_{\mathrm{Dur},2}$	$\sigma_{\mathrm{Dur},2}$
U	15	5	35.13	25.56	10.72	12.23
	15	20	30.18	29.99	8.65	14.45
	15	45	25.69	31.19	8.23	15.10
	15	75	21.59	33.34	7.98	14.25
	15	all	27.78	31.27	9.42	14.64
U	25	5	32.92	20.42	11.38	10.82
	25	20	30.36	24.31	10.51	11.88
	25	45	26.36	26.97	8.76	13.45
	25	75	23.71	28.42	8.66	13.03
	25	all	27.64	26.75	9.73	13.06
U	35	5	36.59	15.91	12.37	9.06
	35	20	30.82	20.42	11.59	9.85
	35	45	27.40	23.41	10.48	11.45
	35	75	24.88	23.94	9.82	12.05
	35	all	28.23	23.05	11.11	11.40
U	45	5	35.22	16.30	13.12	7.86
	45	20	32.66	17.02	12.17	9.11
	45	45	28.15	21.46	11.52	10.26
	45	75	25.58	22.47	10.76	10.95
	45	all	28.78	21.06	11.98	10.38
U	55	5	34.99	12.22	13.67	7.40
	55	20	33.80	14.87	13.63	7.59
	55	45	29.61	19.36	12.84	9.04
	55	75	28.17	20.68	12.36	9.97
	55	all	30.07	19.14	13.28	9.31
U	65	5	35.64	15.10	13.58	8.33

Continued on next page

Table C.3 – continued from previous page

Environment	Elevation [°]	Driving Dir.[°]	$\mu_{\mathrm{Dur},1}$	$\sigma_{\mathrm{Dur},1}$	$\mu_{\mathrm{Dur},2}$	$\sigma_{\mathrm{Dur},2}$
	65	20	34.01	16.30	14.60	8.14
	65	45	31.26	17.44	13.52	8.63
	65	75	29.30	18.55	14.19	8.70
	65	all	31.19	17.55	14.13	8.60
U	75	5	35.23	16.60	14.38	9.44
	75	20	34.49	16.73	14.64	8.66
	75	45	31.79	17.50	14.26	7.73
	75	75	31.71	17.48	13.75	7.72
	75	all	32.45	17.17	14.29	7.93
U	85	5	33.16	15.67	16.00	7.09
	85	20	32.67	17.67	14.95	7.74
	85	45	32.89	17.16	15.75	7.79
	85	75	33.35	17.49	15.51	8.56
	85	all	33.05	17.17	15.53	7.97
S	15	5	35.54	26.55	10.65	12.34
	15	20	33.06	28.93	9.26	12.82
	15	45	27.36	29.71	8.21	13.30
	15	75	25.18	30.92	8.00	13.63
	15	all	29.17	29.91	9.28	13.32
S	25	5	33.86	22.92	11.61	11.23
	25	20	33.13	24.61	10.72	11.13
	25	45	29.34	25.54	9.47	11.45
	25	75	26.44	26.13	8.64	11.75
	25	all	29.31	25.65	9.87	11.56
S	35	5	33.97	19.64	12.98	9.16
	35	20	32.67	21.52	12.23	9.96
	35	45	29.18	22.87	11.39	9.88
	35	75	26.93	22.74	10.35	10.10
	35	all	29.07	22.59	11.42	9.99
S	45	5	31.11	20.33	13.85	9.70
	45	20	30.82	20.64	13.50	9.53
	45	45	29.21	21.20	12.09	9.17
	45	75	27.65	21.91	11.36	9.49
	45	all	29.07	21.41	12.16	9.38
S	55	5	31.76	18.90	14.81	9.36
	55	20	30.72	19.04	13.87	8.45
	55	45	30.47	20.01	13.13	8.77
	55	75	28.54	21.00	12.93	9.13
	55	all	29.72	20.34	13.33	8.95
S	65	5	32.06	18.75	13.80	8.63
	65	20	30.63	19.18	13.51	8.84
	65	45	29.99	19.44	14.18	8.77
	65	75	29.06	20.01	13.38	8.95
	65	all	29.87	19.60	13.78	8.87
S	75	5	31.45	19.07	14.12	8.55
	75	20	29.37	19.96	14.45	8.56
	75	45	29.29	20.09	14.57	8.70
	75	75	30.00	18.35	13.68	8.93
	75	all	29.83	19.32	14.20	8.79
S	85	5	29.82	18.40	14.73	8.23
	85	20	29.47	18.43	14.41	8.36
	85	45	30.39	18.51	14.69	8.29
	85	75	30.00	19.17	13.79	8.41
	85	all	30.12	18.67	14.34	8.32
F	15	5	35.77	31.08	9.41	11.37

Continued on next page

Table C.3 – continued from previous page

Environment	Elevation [°]	Driving Dir.[°]	$\mu_{\mathrm{Dur},1}$	$\sigma_{\mathrm{Dur},1}$	$\mu_{\mathrm{Dur},2}$	$\sigma_{\mathrm{Dur},2}$
	15	20	33.01	35.92	8.45	13.30
	15	45	27.37	36.92	7.95	15.07
	15	75	25.94	42.45	8.02	12.92
	15	all	31.93	35.79	9.18	14.06
F	25	5	34.93	27.07	10.82	9.94
	25	20	31.53	29.64	9.22	11.84
	25	45	27.61	30.75	8.03	12.75
	25	75	24.14	30.19	7.41	13.54
	25	all	29.02	30.23	9.23	12.62
F	35	5	32.37	21.40	12.95	9.36
	35	20	29.30	24.45	11.66	9.92
	35	45	27.44	27.85	9.15	10.80
	35	75	24.03	28.42	7.88	11.58
	35	all	27.91	27.29	10.09	10.94
F	45	5	31.58	22.52	11.91	8.80
	45	20	28.73	24.46	11.25	8.62
	45	45	27.15	26.63	10.03	9.97
	45	75	24.99	26.72	9.04	11.01
	45	all	27.53	26.14	10.39	10.05
F	55	5	30.23	19.22	13.41	8.30
	55	20	29.18	21.61	12.41	8.73
	55	45	28.86	23.46	11.42	9.06
	55	75	26.30	24.23	10.02	9.26
	55	all	28.36	23.20	11.35	9.14
F	65	5	31.07	19.46	13.16	8.59
	65	20	29.75	20.62	12.60	8.68
	65	45	29.01	21.89	12.07	8.52
	65	75	26.89	22.01	11.33	8.72
	65	all	28.50	21.57	12.14	8.67
F	75	5	29.18	21.56	12.69	8.64
	75	20	30.00	21.38	12.40	8.85
	75	45	30.00	21.43	12.49	8.80
	75	75	29.28	22.46	12.32	8.16
	75	all	29.69	21.75	12.45	8.63
F	85	5	31.43	17.86	12.12	8.18
	85	20	29.60	20.86	13.05	8.59
	85	45	31.30	19.83	13.66	9.13
	85	75	30.82	22.09	12.73	9.34
	85	all	30.98	20.85	13.00	9.10
C	15	5	25.76	12.78	16.65	17.16
	15	20	33.06	22.19	10.59	13.59
	15	45	29.53	23.82	9.11	13.93
	15	75	26.98	19.30	9.22	17.75
	15	all	29.59	20.09	10.45	16.29
C	25	5	40.84	19.43	12.22	13.33
	25	20	34.72	19.51	12.24	10.72
	25	45	30.79	21.67	10.42	10.44
	25	75	28.66	23.01	10.63	11.49
	25	all	31.38	21.88	11.37	10.94
C	35	5				
	35	20	38.56	13.60	12.40	9.26
	35	45	31.19	18.49	12.57	9.47
	35	75	28.67	19.60	11.50	9.95
	35	all	31.40	18.59	12.99	9.74
C	45	5	42.37	17.20	12.14	12.27

Continued on next page

Table C.3 – continued from previous page

Environment	Elevation [°]	Driving Dir.[°]	$\mu_{\mathrm{Dur},1}$	$\sigma_{\mathrm{Dur},1}$	$\mu_{\mathrm{Dur},2}$	$\sigma_{\mathrm{Dur},2}$
	45	20	40.27	13.62	12.60	10.23
	45	45	32.89	17.53	13.48	9.45
	45	75	30.96	18.12	11.87	9.37
	45	all	33.15	17.26	13.54	9.68
C	55	5				
	55	20	40.05	14.33	13.54	11.52
	55	45	34.32	15.58	14.30	12.84
	55	75	29.31	13.71	15.19	12.77
	55	all	33.76	13.63	15.11	13.15
C	65	5				
	65	20	32.44	12.99	17.99	11.73
	65	45	35.03	16.63	14.89	10.46
	65	75	32.33	14.05	15.92	9.26
	65	all	34.06	14.87	16.04	10.22
C	75	5	27.10	11.05	19.74	10.23
	75	20	32.13	14.69	18.81	14.87
	75	45	33.85	10.88	16.60	10.17
	75	75	18.10	15.03	22.24	10.83
	75	all	26.19	11.18	19.95	13.19
C	85	5				
	85	20	19.70	18.67	20.97	11.77
	85	45				
	85	75				
	85	all	25.97	10.57	19.86	12.25
O	15	5	38.79	21.90	11.83	11.45
	15	20	35.52	28.90	10.97	11.56
	15	45	32.31	29.63	10.60	12.25
	15	75	30.10	29.60	10.35	12.18
	15	all	32.89	29.30	11.07	12.08
O	25	5	38.47	20.32	11.92	10.75
	25	20	36.15	24.67	12.00	11.48
	25	45	31.33	25.86	11.24	11.47
	25	75	29.96	25.14	11.41	11.79
	25	all	31.94	25.29	11.86	11.60
O	35	5	37.91	14.14	12.97	10.25
	35	20	34.36	20.72	12.53	9.75
	35	45	32.11	22.68	12.37	10.56
	35	75	29.40	21.61	12.07	10.75
	35	all	31.59	21.50	12.71	10.59
O	45	5	36.50	17.49	12.58	10.06
	45	20	35.74	17.96	13.40	9.18
	45	45	30.82	20.03	12.75	9.35
	45	75	29.31	22.25	12.42	10.32
	45	all	31.03	20.86	13.00	9.94
O	55	5	36.26	19.72	12.08	10.69
	55	20	36.36	15.78	13.48	8.59
	55	45	31.62	18.62	13.39	8.90
	55	75	30.04	19.41	13.25	9.51
	55	all	31.78	18.68	13.60	9.19
O	65	5	33.52	16.66	13.61	8.54
	65	20	34.90	14.52	14.15	8.22
	65	45	33.59	15.66	13.65	9.09
	65	75	31.90	16.94	13.58	9.43
	65	all	33.13	16.22	13.82	9.09
O	75	5	34.82	16.57	14.35	8.02

Continued on next page

Table C.3 – continued from previous page

Environment	Elevation [°]	Driving Dir.[°]	$\mu_{\mathrm{Dur},1}$	$\sigma_{\mathrm{Dur},1}$	$\mu_{\mathrm{Dur},2}$	$\sigma_{\mathrm{Dur},2}$
	75	20	36.06	19.34	13.57	8.20
	75	45	33.44	13.81	13.99	8.13
	75	75	34.64	15.75	12.97	8.59
	75	all	34.51	16.12	13.60	8.44
O	85	5				
	85	20	35.70	13.37	12.74	8.16
	85	45	32.06	13.26	13.69	8.68
	85	75				
	85	all	34.24	14.60	13.59	8.41

Table C.4.: State correlation coefficients ρ_{states} between two satellites for multi-satellite LMS modelling derived from Milady GNSS measurements. The values are given for different environments *env*, elevation angle of satellite 1 (ϕ_1) and satellite 2 (ϕ_2), and azimuth separation $\Delta\theta$ between the satellites.

			ρ_{states} for $\Delta\theta =$						
env	ϕ_1 [°]	ϕ_2 [°]	5°	20°	45°	75°	105°	135°	165°
U	15	15	0.89	0.28	0.02	-0.02	-0.00	0.02	0.10
	15	25	0.41	0.31	0.06	0.00	-0.02	-0.00	0.12
	15	35	0.35	0.25	0.03	0.02	-0.02	0.06	0.15
	15	45	0.25	0.21	0.02	0.06	-0.00	0.03	0.09
	15	55	0.12	0.10	0.07	0.04	0.07	0.02	0.14
	15	65	0.12	0.08	0.07	0.02	0.05	-0.02	0.05
	15	75	0.09	0.05	0.05	0.05	-0.03	0.05	0.05
	15	85		0.01	-0.03	-0.02	0.04	0.06	0.07
U	25	25	0.89	0.40	0.07	0.11	-0.02	0.09	0.21
	25	35	0.51	0.35	0.09	0.13	0.15	0.08	0.21
	25	45	0.45	0.34	0.15	0.09	0.06	0.13	0.21
	25	55	0.25	0.23	0.10	0.06	0.05	0.10	0.14
	25	65	0.17	0.14	0.10	0.07	0.05	0.07	0.10
	25	75	0.10	0.11	0.09	0.09	0.05	0.06	0.09
	25	85	0.07	0.12	0.06	0.14	0.10	0.04	0.08
U	35	35	0.91	0.49	0.20	0.01	0.14	0.10	0.17
	35	45	0.60	0.41	0.22	0.13	0.19	0.13	0.18
	35	55	0.32	0.33	0.27	0.06	0.15	0.06	0.17
	35	65	0.29	0.23	0.15	0.05	0.11	0.04	0.09
	35	75	0.10	0.12	0.14	0.11	0.10	0.08	0.08
	35	85	0.08	0.09	0.02	0.16	0.14	0.10	0.11
U	45	45	0.92	0.45	0.26	-0.00	0.11	0.09	0.14
	45	55	0.57	0.36	0.31	0.09	0.10	0.13	0.20
	45	65	0.41	0.39	0.21	0.21	0.14	0.12	0.10
	45	75	0.27	0.21	0.21	0.27	0.13	0.18	0.16
	45	85		0.15	0.13	0.15	0.20	0.20	0.18
U	55	55	0.92	0.39	0.32	0.14	0.08	0.15	0.25
	55	65	0.40	0.37	0.32	0.18	0.12	0.17	0.25
	55	75	0.36	0.26	0.27	0.16	0.28	0.17	0.29
	55	85		0.23	0.16	0.24	0.26	0.13	0.12
U	65	65	0.92	0.43	0.28	0.33	0.28	0.21	0.21
	65	75	0.56	0.52	0.44	0.39	0.21	0.23	0.22
	65	85		0.19	0.26	0.28	0.18	0.17	0.33
U	75	75	0.96	0.59	0.45	0.22	0.21	0.37	0.25

Continued on next page

Table C.4 – continued from previous page

			ρ_{states} for $\Delta\theta =$						
env	ϕ_1 [°]	ϕ_2 [°]	5°	20°	45°	75°	105°	135°	165°
	75	85	0.30	0.38	0.38	0.35	0.40	0.37	0.24
U	85	85	0.90	0.15	0.50	0.73			
S	15	15	0.86	0.38	0.21	0.02	0.03	0.13	0.22
	15	25	0.44	0.36	0.23	0.06	0.03	0.11	0.19
	15	35	0.33	0.28	0.21	0.15	0.08	0.11	0.20
	15	45	0.24	0.24	0.16	0.13	0.08	0.14	0.15
	15	55	0.22	0.19	0.14	0.14	0.10	0.11	0.11
	15	65	0.16	0.18	0.16	0.16	0.10	0.11	0.13
	15	75	0.15	0.18	0.13	0.14	0.14	0.14	0.16
	15	85	0.18	0.15	0.13	0.14	0.12	0.12	0.10
S	25	25	0.87	0.43	0.31	0.14	0.12	0.18	0.19
	25	35	0.52	0.45	0.34	0.21	0.09	0.20	0.21
	25	45	0.46	0.40	0.33	0.25	0.16	0.19	0.17
	25	55	0.35	0.35	0.26	0.21	0.17	0.16	0.18
	25	65	0.31	0.30	0.24	0.24	0.22	0.22	0.22
	25	75	0.27	0.24	0.21	0.20	0.21	0.22	0.21
	25	85	0.08	0.18	0.23	0.15	0.24	0.18	0.23
S	35	35	0.90	0.52	0.40	0.32	0.15	0.19	0.15
	35	45	0.61	0.50	0.41	0.33	0.21	0.20	0.27
	35	55	0.48	0.52	0.40	0.35	0.23	0.23	0.23
	35	65	0.41	0.36	0.39	0.31	0.30	0.27	0.27
	35	75	0.32	0.33	0.34	0.32	0.32	0.32	0.30
	35	85	0.34	0.36	0.32	0.27	0.30	0.33	0.26
S	45	45	0.93	0.54	0.52	0.43	0.33	0.32	0.21
	45	55	0.60	0.58	0.49	0.40	0.41	0.28	0.27
	45	65	0.48	0.57	0.55	0.46	0.34	0.30	0.36
	45	75	0.53	0.42	0.40	0.43	0.42	0.39	0.29
	45	85	0.49	0.41	0.41	0.36	0.44	0.43	0.35
S	55	55	0.94	0.63	0.50	0.37	0.37	0.32	0.32
	55	65	0.72	0.68	0.57	0.41	0.41	0.38	0.34
	55	75	0.49	0.55	0.46	0.48	0.42	0.36	0.47
	55	85	0.44	0.44	0.52	0.47	0.47	0.51	0.48
S	65	65	0.93	0.75	0.62	0.58	0.45	0.32	0.28
	65	75	0.70	0.57	0.63	0.58	0.49	0.42	0.45
	65	85	0.52	0.56	0.58	0.47	0.50	0.51	0.51
S	75	75	0.95	0.56	0.50	0.61	0.51	0.47	0.42
	75	85	0.55	0.52	0.62	0.58	0.62	0.62	0.60
S	85	85	0.98	0.75	0.63	0.48	0.39	0.34	0.48
F	15	15	0.87	0.16	0.19	0.03	0.16	0.13	0.21
	15	25	0.46	0.36	0.13	0.09	0.07	0.08	0.30
	15	35	0.41	0.36	0.12	0.00	0.06	0.11	0.26
	15	45	0.39	0.31	0.13	0.07	0.12	0.16	0.29
	15	55	0.30	0.11	0.16	0.09	0.10	0.18	0.21
	15	65	0.09	0.13	0.12	0.02	-0.03	0.18	0.17
	15	75	0.23	0.13	0.17	0.13	0.04	0.12	0.17
	15	85		0.09	0.02	0.15	0.19		
F	25	25	0.87	0.41	0.10	0.07	0.08	0.11	0.25
	25	35	0.49	0.52	0.14	0.09	0.08	0.11	0.29
	25	45	0.36	0.31	0.15	0.15	0.08	0.17	0.30
	25	55	0.30	0.31	0.18	0.15	0.13	0.13	0.17
	25	65	0.22	0.20	0.17	0.05	0.14	0.11	0.18
	25	75	0.13	0.20	0.17	0.14	0.10	0.10	0.14
	25	85	-0.03	0.10	0.05	0.04	0.09	-0.03	0.09

Continued on next page

Table C.4 – continued from previous page

			ρ_{states} for $\Delta\theta =$						
env	ϕ_1 [°]	ϕ_2 [°]	5°	20°	45°	75°	105°	135°	165°
F	35	35	0.93	0.51	0.13	0.11	-0.06	0.11	0.25
	35	45	0.62	0.50	0.21	0.09	0.12	0.18	0.25
	35	55	0.45	0.43	0.27	0.13	0.08	0.23	0.27
	35	65	0.31	0.36	0.24	0.15	0.15	0.20	0.24
	35	75	0.39	0.24	0.26	0.19	0.23	0.23	0.23
	35	85	0.19	0.23	0.09	0.13	0.17	0.25	0.23
F	45	45	0.96	0.51	0.32	-0.05	0.21	0.19	0.26
	45	55	0.47	0.52	0.30	0.28	0.21	0.23	0.28
	45	65	0.48	0.40	0.34	0.33	0.12	0.17	0.21
	45	75	0.36	0.25	0.20	0.27	0.23	0.28	0.23
	45	85	0.14		0.21		0.25	0.14	0.14
F	55	55	0.96	0.38	0.43	0.48	0.23	0.31	0.35
	55	65	0.59	0.51	0.35	0.28	0.24	0.28	0.27
	55	75	0.39	0.43	0.31	0.40	0.29	0.28	0.29
	55	85	0.41	0.27	0.27	0.31	0.37	0.32	0.21
F	65	65	0.86	0.55	0.39	0.43	0.28	0.37	0.17
	65	75	0.64	0.50	0.55	0.50	0.28	0.34	0.29
	65	85	0.47	0.35	0.52	0.07	0.23	0.28	0.31
F	75	75	0.98	0.55	0.31	0.35	0.08	0.39	0.35
	75	85		0.39	0.14	0.50	0.51	0.36	0.31
F	85	85	0.97		0.72		0.06	0.56	
C	15	15	0.86	0.41	0.14	0.15	-0.00	0.10	0.11
	15	25	0.33	0.31	0.09	0.09	0.02	0.02	0.12
	15	35	0.30	0.27	0.16	0.12	-0.03	-0.01	0.07
	15	45	0.17	0.16	0.18	0.05	0.06	0.01	0.07
	15	55	0.20	0.27	0.15	0.10	0.15	0.05	0.09
	15	65	0.14	0.14	0.13	0.08	0.10	0.08	0.12
	15	75		0.04	0.03	0.02	0.11	0.09	0.12
	15	85							
C	25	25	0.83	0.37	0.11	0.11	0.06	0.12	0.16
	25	35	0.45	0.38	0.26	0.20	0.14	0.14	0.16
	25	45	0.43	0.28	0.33	0.28	0.10	0.09	0.13
	25	55	0.20	0.28	0.22	0.07	0.24	0.05	0.07
	25	65	0.23	0.31	0.25	0.15	0.10	0.28	0.27
	25	75	0.08	0.30	0.17	0.18	0.13	0.28	0.19
	25	85						0.20	
C	35	35	0.86	0.69	0.46	0.25	0.15	0.22	0.24
	35	45	0.55	0.53	0.46	0.26	0.16	0.30	0.38
	35	55		0.30	0.49	0.40	0.21	0.09	0.08
	35	65		0.53	0.41	0.33	0.37	0.51	0.41
	35	75		0.38	0.40	0.42	0.48	0.47	
	35	85							
C	45	45	0.93	0.57	0.18	0.29	0.25	0.28	0.41
	45	55	0.38	0.71	0.54	0.50	0.36	0.35	0.17
	45	65	0.88	0.56	0.74	0.51	0.25	0.37	0.42
	45	75				0.40		0.56	0.31
	45	85							
C	55	55	0.93	0.63	0.43	0.81	0.63	0.17	
	55	65		0.77	0.86	0.16	0.69	0.74	0.41
	55	75			0.18	0.68	0.75	0.75	0.65
	55	85							
C	65	65		0.73	0.77	0.81	0.71	0.70	0.66
	65	75			0.61		0.86	0.60	0.77

Continued on next page

Table C.4 – continued from previous page

			ρ_{states} for $\Delta\theta =$						
env	ϕ_1 [°]	ϕ_2 [°]	5°	20°	45°	75°	105°	135°	165°
	65	85							
C	75	75					0.32		
	75	85							
C	85	85							
O	15	15	0.88	0.37	0.36	0.30	0.22	0.17	0.22
	15	25	0.48	0.55	0.39	0.29	0.22	0.16	0.22
	15	35	0.44	0.39	0.38	0.24	0.14	0.23	0.25
	15	45	0.38	0.37	0.31	0.27	0.22	0.17	0.27
	15	55	0.31	0.28	0.19	0.21	0.18	0.20	0.24
	15	65	0.22	0.20	0.21	0.17	0.15	0.16	0.18
	15	75	0.18	0.16	0.14	0.15	0.14	0.15	0.15
	15	85							0.08
O	25	25	0.85	0.54	0.41	0.33	0.25	0.23	0.25
	25	35	0.57	0.48	0.46	0.36	0.26	0.27	0.30
	25	45	0.47	0.47	0.40	0.34	0.24	0.26	0.29
	25	55	0.34	0.35	0.29	0.22	0.24	0.15	0.26
	25	65	0.29	0.30	0.27	0.25	0.19	0.20	0.16
	25	75	0.17	0.26	0.22	0.23	0.17	0.17	0.07
	25	85		0.04	0.12		0.12	0.25	
O	35	35	0.86	0.63	0.48	0.27	0.29	0.38	0.35
	35	45	0.62	0.58	0.49	0.40	0.26	0.29	0.40
	35	55	0.44	0.48	0.40	0.36	0.29	0.23	0.23
	35	65	0.46	0.31	0.29	0.32	0.31	0.21	0.26
	35	75	0.00	0.31	0.35	0.28	0.24	0.22	0.26
	35	85	0.26	0.28	0.15	0.07	0.12	0.17	0.15
O	45	45	0.93	0.64	0.54	0.40	0.26	0.34	0.32
	45	55	0.61	0.62	0.54	0.30	0.21	0.29	0.30
	45	65	0.47	0.49	0.49	0.37	0.28	0.23	0.21
	45	75	0.21	0.33	0.30	0.35	0.26	0.26	0.25
	45	85	0.00	0.29	0.39	0.00	0.24	0.00	0.27
O	55	55	0.93	0.60	0.49	0.31	0.29	0.20	0.14
	55	65	0.61	0.60	0.46	0.37	0.39	0.17	0.19
	55	75	0.30	0.51	0.37	0.38	0.23	0.21	0.20
	55	85	0.00	0.00	0.24	0.15	0.36	0.00	0.00
O	65	65	0.99	0.80	0.69	0.41	0.31	0.17	0.05
	65	75	0.00	0.47	0.51	0.47	0.33	0.23	0.28
	65	85	0.00	0.00	0.00	0.00	0.45	0.51	0.00
O	75	75	0.93	0.47	0.32	0.47	0.33	0.53	0.38
	75	85	0.00	0.00	0.00	0.57	0.57	0.00	0.22
O	85	85	0.00	0.00	0.00	0.00	0.00	0.00	0.47

Table C.5.: Correlation coefficients between two satellites for fading within the combined states derived from Milady GNSS measurements. They are applied as correlation coefficients for Loo parameter M_A (ρ_{M_A}) as well as correlation coefficients for lognormal fading samples (ρ_{logn}) in the dual-satellite LMS model (cf. Chapter 4.4.3). The parameters ρ_{gg} ($= \rho_{M_A,\text{gg}} = \rho_{\text{logn,gg}}$) and ρ_{bb} ($= \rho_{M_A,\text{bb}} = \rho_{\text{logn,bb}}$) are fading correlation coefficients for joint state 'good good' and 'bad bad', respectively. The values are given for different elevation angles of satellite 1 (ϕ_1) and satellite 2 (ϕ_2), and azimuth separations ($\Delta\theta$) between the satellites, and are valid for all environment types.

			azimuth separation $\Delta\theta =$						
parameter	ϕ_1 [°]	ϕ_2 [°]	5°	20°	45°	75°	105°	135°	165°
ρ_{gg}	15	15	0.81	0.09	0.12	0.02	0.04	0.06	0.08
ρ_{bb}	15	15	0.84	0.10	0.07	0.03	-0.06	-0.03	-0.04
ρ_{gg}	15	25	0.16	0.11	0.12	0.07	0.04	0.10	0.09
ρ_{bb}	15	25	0.11	0.09	0.06	0.06	0.04	0.09	0.04
ρ_{gg}	15	35	0.15	0.12	0.10	0.06	0.06	0.09	0.11
ρ_{bb}	15	35	0.18	0.05	0.08	0.05	-0.04	0.03	0.07
ρ_{gg}	15	45	0.14	0.17	0.07	0.08	0.07	0.07	0.10
ρ_{bb}	15	45	0.18	0.15	0.01	0.05	0.02	0.03	0.05
ρ_{gg}	15	55	0.09	0.10	0.10	0.11	0.07	0.08	0.08
ρ_{bb}	15	55	0.09	0.05	-0.10	0.00	-0.04	-0.02	0.07
ρ_{gg}	15	65	0.12	0.10	0.08	0.06	0.10	0.05	0.06
ρ_{bb}	15	65	-0.06	-0.02	-0.04	-0.00	-0.10	-0.16	0.12
ρ_{gg}	15	75	0.09	0.11	0.06	0.10	0.01	0.06	0.05
ρ_{bb}	15	75	0.42	0.08	-0.01	0.03	-0.06	0.10	-0.01
ρ_{gg}	15	85	0.06	0.04	0.06	0.12	0.10	0.04	0.05
ρ_{bb}	15	85	0.26	0.17	-0.04	0.15	0.23	-0.12	0.05
ρ_{gg}	25	25	0.79	0.21	0.18	0.13	0.11	0.11	0.13
ρ_{bb}	25	25	0.88	0.08	0.06	0.08	0.02	0.05	0.02
ρ_{gg}	25	35	0.25	0.20	0.14	0.15	0.15	0.14	0.14
ρ_{bb}	25	35	0.21	0.17	0.03	0.04	0.02	0.01	0.02
ρ_{gg}	25	45	0.21	0.22	0.19	0.18	0.11	0.14	0.14
ρ_{bb}	25	45	0.13	0.04	0.06	0.06	0.01	0.04	0.03
ρ_{gg}	25	55	0.22	0.17	0.13	0.16	0.15	0.12	0.12
ρ_{bb}	25	55	0.09	0.06	0.00	0.04	-0.04	-0.06	0.05
ρ_{gg}	25	65	0.19	0.18	0.18	0.12	0.12	0.14	0.13
ρ_{bb}	25	65	0.03	0.03	-0.02	0.01	-0.05	0.06	0.05
ρ_{gg}	25	75	0.17	0.15	0.14	0.18	0.16	0.13	0.11
ρ_{bb}	25	75	0.12	0.02	0.05	0.01	0.05	-0.01	-0.01
ρ_{gg}	25	85	0.14	0.11	0.15	0.12	0.13	0.12	0.06
ρ_{bb}	25	85	0.05	0.01	-0.07	0.01	0.01	-0.15	0.03
ρ_{gg}	35	35	0.87	0.25	0.21	0.11	0.12	0.14	0.14
ρ_{bb}	35	35	0.84	0.17	0.06	0.13	-0.00	0.01	0.01
ρ_{gg}	35	45	0.27	0.23	0.21	0.20	0.20	0.18	0.15
ρ_{bb}	35	45	0.18	0.09	0.11	0.06	0.08	-0.00	0.03
ρ_{gg}	35	55	0.25	0.24	0.19	0.18	0.19	0.13	0.17
ρ_{bb}	35	55	0.14	0.09	0.11	-0.00	-0.01	-0.02	-0.05
ρ_{gg}	35	65	0.24	0.23	0.21	0.19	0.16	0.16	0.17
ρ_{bb}	35	65	-0.03	0.13	0.01	0.05	-0.08	-0.09	-0.13
ρ_{gg}	35	75	0.23	0.18	0.17	0.18	0.20	0.15	0.13
ρ_{bb}	35	75	-0.10	-0.01	0.00	0.02	-0.04	-0.03	-0.10
ρ_{gg}	35	85	0.18	0.17	0.17	0.17	0.17	0.16	0.18
ρ_{bb}	35	85	0.01	-0.03	-0.32	-0.09	0.02	0.04	0.04
ρ_{gg}	45	45	0.84	0.27	0.26	0.16	0.20	0.17	0.17
ρ_{bb}	45	45	0.86	0.20	0.15	0.13	0.03	0.09	-0.02
ρ_{gg}	45	55	0.34	0.31	0.27	0.22	0.19	0.21	0.20
ρ_{bb}	45	55	0.28	0.24	0.10	-0.00	-0.02	0.05	-0.02

Continued on next page

Table C.5 – continued from previous page

			azimuth separation $\Delta\theta$ =						
parameter	ϕ_1 [°]	ϕ_2 [°]	5°	20°	45°	75°	105°	135°	165°
ρ_{gg}	45	65	0.25	0.30	0.25	0.23	0.22	0.23	0.17
ρ_{bb}	45	65	0.17	0.21	0.07	0.13	0.02	-0.14	-0.05
ρ_{gg}	45	75	0.23	0.23	0.27	0.24	0.22	0.22	0.18
ρ_{bb}	45	75	0.19	0.11	0.11	0.12	-0.01	0.01	-0.05
ρ_{gg}	45	85	0.27	0.14	0.24	0.23	0.23	0.25	0.22
ρ_{bb}	45	85	0.49	-0.12	0.02	0.22	0.13	0.18	0.03
ρ_{gg}	55	55	0.86	0.33	0.23	0.23	0.19	0.19	0.19
ρ_{bb}	55	55	0.85	0.15	0.13	-0.04	0.05	-0.08	-0.14
ρ_{gg}	55	65	0.30	0.33	0.27	0.25	0.25	0.22	0.22
ρ_{bb}	55	65	0.01	0.08	0.22	0.10	0.02	-0.07	-0.09
ρ_{gg}	55	75	0.35	0.28	0.29	0.27	0.27	0.25	0.24
ρ_{bb}	55	75	0.24	0.13	0.24	-0.02	-0.09	-0.02	0.05
ρ_{gg}	55	85	0.31	0.33	0.27	0.25	0.23	0.24	0.25
ρ_{bb}	55	85	0.30	0.17	-0.01	0.36	0.29	0.14	0.16
ρ_{gg}	65	65	0.90	0.35	0.30	0.28	0.27	0.25	0.26
ρ_{bb}	65	65	0.81	0.23	0.27	0.12	0.08	0.13	-0.04
ρ_{gg}	65	75	0.44	0.40	0.29	0.32	0.29	0.29	0.26
ρ_{bb}	65	75	0.25	0.30	0.19	0.20	-0.03	0.08	0.10
ρ_{gg}	65	85	0.31	0.33	0.29	0.30	0.28	0.29	0.28
ρ_{bb}	65	85	0.12	0.02	0.10	-0.06	-0.07	-0.07	-0.04
ρ_{gg}	75	75	0.90	0.40	0.35	0.26	0.28	0.31	0.29
ρ_{bb}	75	75	0.87	0.47	0.21	0.06	0.11	0.17	0.11
ρ_{gg}	75	85	0.41	0.36	0.33	0.33	0.30	0.30	0.30
ρ_{bb}	75	85	0.16	0.17	0.20	0.20	0.23	-0.07	0.14
ρ_{gg}	85	85	0.96	0.45	0.29	0.44	0.35	0.30	0.24
ρ_{bb}	85	85	0.82	0.58	0.20	0.44		0.08	

Glossary of Abbreviations, Symbols and Notation

Abbreviations

AFD	average fade duration
ASTM	adaptive slave transition matrix
ASTM-MT	adaptive slave transition matrix based on master transitions
C/N	carrier-to-noise ratio
C/N_0	carrier-to-noise spectral density ratio
CDF	cumulative distribution function
CCDF	complementary cumulative distribution function
DVB-SH	digital video broadcasting - service handheld
GEO	geostationary orbit
EIRP	equivalent isotropic radiated power
EGC	equal gain combining
GNSS	global navigation satellite system
GPS	global positioning system
HEO	high-elliptical orbit
LCR	level crossing rate
LEO	low earth orbit
LMS	land mobile satellite
LOS	line-of-sight
MEO	medium earth orbit
MIMO	Multiple Input Multiple Output
MKA	masking angle
MRC	maximal-ratio combining
MSE	mean squared error
PDF	probability density function
PDP	power delay profile
PPG	propagation parameter generator
PSD	power spectral density
QoS	Quality-of-Service
RF	radio frequency
RLN	Rice-lognormal
RMS	root mean square
SC	selection combining
SDARS	Satellite Digital Audio Radio Services
SDPDF	state duration probability density function
SDCDF	state duration cumulative distribution function
SNR	signal-to-noise ratio
SSG	state sequence generator
SSFG	small-scale fading generator

STPM	state transition probability matrix
STPT	state transition probability tensor
UHF	ultra-high frequency

Operators

$\delta(.)$	Dirac delta function
$\mathrm{E}\{\cdot\}$	expectation value
${}_1F_1$	confluent hypergeometric function
$I_0\{\cdot\}$	modified Bessel function of first kind and order zero
$\Gamma\{\cdot\}$	Gamma function
$\ln\{\cdot\}$	logarithmus to base e
$\min\{\cdot\}$	minimum
$\max\{\cdot\}$	maximum
$\mathcal{N}$	Gaussian distribution
$\mathcal{F}\{\cdot\}$	Fourier transform
$\mathrm{Re}\{\cdot\}$	real part
$\mathrm{Im}\{\cdot\}$	imaginary part

Units

Hz	hertz
MHz	megahertz
dB	decibel
m	metre
km	kilometre
s	second

Constants

e	Euler's number $e = 2.71828...$
c	light speed $c = 3 \cdot 10^8$ m/s
j	imaginary unit
π	$\pi = 3.141592653...$
∞	infinity

Variables

a	amplitude
α	amplitude
B_c	coherence bandwidth
B_d	Doppler spread
D	state duration
$\bar{D}_i$	mean duration of state i
f	frequency
f_c	carrier frequency
f_D	Doppler shift
$f_{D\max}$	maximum Doppler shift
$f_{D\mathrm{dir}}$	Doppler shift of the direct signal component
$H(f, v)$	output Doppler spread function
$h(t)$	time-variant complex fading coefficient
$h(t, \tau)$	time-variant impulse response
k	Rice factor
λ_c	carrier wavelength
L_{corr}	correlation distance
l_i	interleaver length
M_A	Loo parameter: mean value of lognormal fading component
MP	Loo parameter: multipath power
P	state probability
P_{g1}, P_{b1}, P_{bb}	'good'-state probability of satellite 1, 'bad'-state probability of satellite 1, 'bad bad'-state probability

$\mathbf{p}$	state probability vector
$\mathbf{P}_{\text{trans}}$	state transition probability matrix
$P(D)$	state duration probability density function
$\mathcal{P}_{\text{trans}}$	state transition probability tensor
q	discrete state duration in samples
$r = \|h(t)\|$	envelope of the received signal
s	state
$S(\tau, v)$	delay Doppler spread function
t	time
T_m	delay spread
T_c	coherence time
$T(f, t)$	time-variant transfer function
v	Doppler shift
v_{mobile}	vehicle speed
$v_{\text{rel,sat}}$	satellite speed relative to a fixed observation point on earth
$\Delta\theta$	azimuth angle separation between two satellites
$\Delta\phi$	elevation angle separation between two satellites
ΔP_{bbb}	state modelling error for state 'bad bad bad': difference between measured and re-simulated 'bad bad bad'-probability
μ	mean value of a random variable
ϕ	elevation angle of the satellite
$\phi(t)$	time-variant phase of fading
ρ	correlation coefficient
ρ_{States}	correlation coefficient of the state sequences between two satellites
σ	standard deviation of a random variable
σ^2	variance of a random variable
Σ_A	Loo parameter: standard deviation of lognormal fading component
τ	delay time
τ_{RMS}	RMS delay spread
θ	azimuth angle of the satellite with respect to the vehicle's driving direction

Bibliography

[AADH98] Irfan Ali, Naofal Al-Dhahir, and John E. Hershey. Doppler characterization for leo satellites. *IEEE Transactions on Communications*, 46(3):309–313, 1998.

[AHH+12] Daniel Arndt, Thomas Heyn, Albert Heuberger, Roberto Prieto-Cerdeira, and Ernst Eberlein. State modeling of the land mobile satellite channel with angle diversity. In *6th European Conference on Antennas and Propagation*, Prag, Czech, April 2012.

[AHK+12] Daniel Arndt, Thomas Heyn, Jonas König, Alexander Ihlow, Albert Heuberger, Roberto Prieto-Cerdeira, and Ernst Eberlein. Extended two-state narrowband lms propagation model for s-band. In *IEEE International Symposium on Broadband Multimedia Systems and Broadcasting (BMSB)*, pages 1–6, 2012.

[AIH+] Daniel Arndt, Alexander Ihlow, Thomas Heyn, Albert Heuberger, Roberto Prieto-Cerdeira, and Ernst Eberlein. State modelling of the land mobile propagation channel for dual-satellite systems. *EURASIP Journal on Wireless Communications and Networking*.

[AIH+09] Daniel Arndt, Alexander Ihlow, Albert Heuberger, Thomas Heyn, and Ernst Eberlein. Land mobile satellite channel characteristics from the MiLADY project. In *Proceedings of the 10th Workshop Digital Broadcasting*, pages 49–55, Ilmenau, Germany, September 2009.

[AIH+10] Daniel Arndt, Alexander Ihlow, Albert Heuberger, Thomas Heyn, Ernst Eberlein, and Roberto Prieto-Cerdeira. Mobile satellite broadcasting with angle diversity – performance evaluation based on measurements. In *IEEE International Symposium on Broadband Multimedia Systems and Broadcasting (BMSB)*, 2010.

[AIH+11] Daniel Arndt, Alexander Ihlow, Albert Heuberger, Thomas Heyn, and Ernst Eberlein. Qos prediction for mobile satellite broadcasting with angle diversity based on measurements. In *IEEE International Symposium on Broadband Multimedia Systems and Broadcasting (BMSB)*, pages 1 –8, june 2011.

[AIHE11a] Daniel Arndt, Alexander Ihlow, Albert Heuberger, and Ernst Eberlein. Antenna diversity for mobile satellite applications: Performance evaluation based on measurements. In *Proceedings of the 5th European Conference on Antennas and Propagation (EUCAP)*, pages 3729–3733, 2011.

[AIHE11b] Daniel Arndt, Alexander Ihlow, Albert Heuberger, and Ernst Eberlein. Measurement-based evaluation of antenna- and time diversity for mobile

satellite systems. In *Proceedings of the 11th International Conference on Telecommunications (ConTEL)*, pages 457–464, 2011.

[AIHE12] Daniel Arndt, Alexander Ihlow, Albert Heuberger, and Ernst Eberlein. State modelling of the land mobile propagation channel with multiple satellites. *International Journal of Antennas and Propagation*, 2012:15, 2012.

[Akt08] Riza Akturan. An overview of the Sirius Satellite Radio system. *International Journal of Satellite Communications and Networking*, 26(5):349–358, 2008.

[ALAK03] Ali Abdi, Wing C. Lau, Mohamed-Slim Alouini, and Mostafa Kaveh. A new simple model for land mobile satellite channels: first- and second-order statistics. *Transactions on Vehicular Technology*, 2(3):519–528, May 2003.

[AP95] Fulvio Ananasso and Francesco Delli Priscoli. The role of satellites in personal communication services. *IEEE Journal on Selected Areas in Communications*, 13(2):180–196, 1995.

[AS03] Mohamed-Slim Alouini and Marvin K. Simon. Postdetection switched combining - a simple diversity scheme with improved ber performance. *IEEE Transactions on Communications*, 51(9):1591–1602, 2003.

[ASHE08] Clémence Alasseur, Sandro Scalise, Lionel Husson, and Harald Ernst. A novel approach to model the land mobile satellite channel through reversible jump markov chain monte carlo technique. *IEEE Transactions on Wireless Communications*, 7(2):532 –542, february 2008.

[AV95] Riza Akturan and Wolfhard J. Vogel. Optically derived elevation angle dependence of fading for satellite PCS. In *19th NASA Propagation Experimenters Meeting (NAPEX 19)*, pages 127–132, August 1995.

[AV97] Riza Akturan and Wolfhard J. Vogel. Path diversity for leo satellite-pcs in the urban environment. *IEEE Transactions on Antennas and Propagation*, 45(7):1107 –1116, jul 1997.

[Bel63] Philip A. Bello. Characterization of randomly time-variant linear channels. *IEEE Transactions on Communications Systems*, 11(4):360–393, 1963.

[Ber94] Peter Berlin. Inmarsat-p the world in your hand. In *Proceedings of International Conference on Satellite Communications, ICSC'94*, volume 1, pages 106–111 vol.1, 1994.

[Bre59] Donald G. Brennan. Linear diversity combining techniques. *Proc. IRE*, 47(1):1075–1102, 1959.

[BS92] R. Michael Barts and Warren L. Stutzman. Modeling and simulation of mobile satellite propagation. *IEEE Transactions on Antennas and Propagation*, 40(4):375 –382, apr 1992.

[BT02] Lars Erling Bråten and Terje Tjelta. Semi-markov multistate modeling of the land mobile propagation channel for geostationary satellites. *IEEE Transactions on Antennas and Propagation*, 50(12):1795 – 1802, dec 2002.

[BWL96] Hermann Bischl, Markus Werner, and Erich Lutz. Elevation-dependent channel model and satellite diversity for ngso s-pcns. In *Vehicular Technology Conference, 1996. 'Mobile Technology for the Human Race'., IEEE 46th*, volume 2, pages 1038–1042 vol.2, Apr-1 May 1996.

[Cor] Corine Land cover - Technical guide. Office for official publications of the European Communities. Luxembourg. 1994.

[Cou01] Olivier Courseille. Role of satellites in mobile systems. *Alcatel Telecommunications Review*, 2001.

[Cra46] Harald Cramer. *Mathematical Methods of Statistics.* Princeton University Press, Princeton, 1946.

[CV94] Giovanni E. Corazza and Francesco Vatalaro. A statistical model for land mobile satellite channels and its application to nongeostationary orbit systems. *IEEE Transactions on Vehicular Technology*, 43(3):738–742, 1994.

[Dav87] Faramaz Davarian. Channel simulation to facilitate mobile-satellite communications research. *Communications, IEEE Transactions on*, 35(1):47–56, 1987.

[Die97] Dr. Fred J. Dietrich. The globalstar satellite cellular communication system: design and status. In *Wescon/97. Conference Proceedings*, pages 180–186, 1997.

[DJDW01] Martin Döttling, Axel Jahn, Dirk Didascalou, and Werner Wiesbeck. Two- and three-dimensional ray tracing applied to the land mobile satellite (lms) propagation channel. *Antennas and Propagation Magazine, IEEE*, 43(6):27–37, 2001.

[DJY+05] Shen Dongya, Rong Jian, Yang Yihuai, Quo Yong, Cao Hongliang, and Fu Shigang. The six-state markov model for land mobile satellite channels. In *IEEE International Symposium on Microwave, Antenna, Propagation and EMC Technologies for Wireless Communications, 2005. MAPE 2005.*, volume 2, pages 1619 – 1622 Vol. 2, aug. 2005.

[DVB] DVB BlueBook A120 (2008-05). DVB-SH Implementation Guidelines. `http://www.dvb-h.org/technology.htm`.

[DVB07] Etsi ts 102 585 v1.1.2, digital video broadcasting (dvb); system specifications for satellite services to handheld devices (sh) below 3 ghz,. Tech. Rep., ETSI, Jul. 2007., July 2007.

[EAH+10] Ernst Eberlein, Daniel Arndt, Albert Heuberger, Joachim Oschek, and Simon Sudler. Diversity reception in S-band: Field trials and analysis results. In *Proceedings of the 11th Workshop Digital Broadcasting*, pages 47–53, Erlangen, Germany, September 2010.

[EBW+11] Ernst Eberlein, Frank Burkhardt, Carmen Wagner, Albert Heuberger, Daniel Arndt, and Roberto Prieto-Cerdeira. Statistical evaluation of the mimo gain for lms channels. In *Proceedings of the 5th European Conference on Antennas and Propagation (EUCAP)*, pages 2695–2699, 2011.

[EHH08] Ernst Eberlein, Albert Heuberger, and Thomas Heyn. Channel models for systems with angle diversity – The MiLADY project. In *ESA Workshop on Radiowave Propagation Models, Tools and Data for Space Systems*, Noordwijk, the Netherlands, December 2008.

[Eva97] John V. Evans. Satellite systems for personal communications. *Antennas and Propagation Magazine, IEEE*, 39(3):7 –20, jun 1997.

[FHS00] Antonie Franchi, Alan Howell, and Jay R. Sengupta. Broadband mobile via satellite: inmarsat bgan. In *IEE Seminar on Broadband Satellite: The Critical Success Factors - Technology, Services and Markets (Ref. No. 2000/067)*, pages 23/1–23/7, 2000.

[GV98] Julius Goldhirsh and Wolfgang J. Vogel. *Handbook of Propagation Effects for Vehicular and Personal Mobile Satellite Systems*. John Hopkins University: University of Texas at Austin, Austin, TX, U.S.A., 1998.

[HEA+10] Thomas Heyn, Ernst Eberlein, Daniel Arndt, Albert Heuberger, Balazs Matuz, Francisco Lázaro Blasco, and Roberto Prieto-Cerdeira. Mobile satellite channel with angle diversity: the MiLADY project. In *European Conference on Antennas and Propagation*, Barcelona, 12-16 April 2010.

[Heu06] Albert Heuberger. Diversity concepts in mobile satellite broadcasting. In *Proceedings of the 7th Workshop on Digital Broadcasting Systems*, Erlangen, Germany, 2006.

[Heu08] Albert Heuberger. Fade correlation and diversity effects in satellite broadcasting to mobile users in S-band. *International Journal of Satellite Communications and Networking*, 26:359–379, 2008.

[HKAW97] Seung-Hoon Hwang, Ki-Jun Kim, Jae-Young Ahn, and Keum-Chan Whang. A channel model for nongeostationary orbiting satellite system. In *Vehicular Technology Conference, 1997, IEEE 47th*, volume 1, pages 41 –45 vol.1, may 1997.

[HYZ04] Yi Huang, Na Yi, and Xu Zhu. Investigation of using passive repeaters for indoor radio coverage improvement. In *Antennas and Propagation Society International Symposium, 2004. IEEE*, volume 2, pages 1623 – 1626 Vol.2, june 2004.

[IAT+11] Alexander Ihlow, Daniel Arndt, Felix Topf, Christoph Rothaug, Thomas Wittenberg, and Albert Heuberger. Photogrammetric satellite service prediction – correlation of RF measurements and image data. In *IEEE International Symposium on Broadband Multimedia Systems and Broadcasting*, Nuremberg, June 2011.

[Inm09] *Inmarsat Maritime Handbook - issue 4*. Inmarsat Organisation London, 2009.

[ITU00] Itu-r v.431-7, nomenclature of the frequency and wavelength bands used in telecommunications, 2000.

[ITU03a] Itu-r p.618-8, propagation data and prediction methods required for the design of earth-space telecommunication systems, 2003.

[ITU03b] Itu-r p.681-6, propagation data required for the design of earth space land mobile telecommunication systems, 2003.

[ITU09] Itu-r p.676-8, attenuation by atmospheric gases, 2009.

[ITU12] Itu-r p.531-11, ionospheric propagation data and prediction methods required for the design of satellite services and systems, 2012.

[Jah99] Axel Jahn. Propagation characteristics for land mobile satellite systems from l-band to ehf-band, 1999.

[Jak74] William C. Jakes. *Microwave Mobile Communications*. Wiley, 1974.

[JBH96] Axel Jahn, Hermann Bischl, and Günter Heiss. Channel characterisation for spread spectrum satellite communications. In *IEEE 4th International Symposium on Spread Spectrum Techniques and Applications Proceedings, 1996*, volume 3, pages 1221 –1226 vol.3, sep 1996.

[J.D00] Parsons J.D. *The Mobile Radio Propagation Channel*. New York, 2000.

[JL94] Axel Jahn and Erich Lutz. Dlr channel measurement programme for low earth orbit satellite systems. In *Third Annual International Conference on Universal Personal Communications. Record., 1994*, pages 423 –429, sep-1 oct 1994.

[KAIH12] Jonas König, Daniel Arndt, Alexander Ihlow, and Albert Heuberger. Estimation of fading parameter correlation for modeling the land mobile satellite channel. In *IEEE International Symposium on Broadband Multimedia Systems and Broadcasting (BMSB)*, pages 1–5, 2012.

[KC96] Athanasios G. Kanatas and Philip Constantinou. Narrowband characterisation of the land mobile satellite channel: A comparison of empirical models. *European Transactions on Telecommunications*, 7(4):315–321, 1996.

[KC00] Athanasios G. Kanatas and Philip Constantinou. A narrowband land mobile satellite channel software simulator for urban environments. *International Journal of Satellite Communications*, 18(1):17–45, 2000.

[KKM97] Yoshio Karasawa, Kazuhiro Kimura, and Kenichi Minamisono. Analysis of availability improvement in lmss by means of satellite diversity based on three-state propagation channel model. *IEEE Transactions on Vehicular Technology*, 46(4):1047 –1056, nov 1997.

[KMM95] Yoshio Karasawa, Kenichi Minamisono, and Takashi Matsudo. A propagation channel model for personal mobile-satellite services. In *Proceedings of Progress of Electromagnetic Research Symposium of the European Space Agency (ESA)*, pages 11–15, Noordwijk, The Netherlands, July 1995.

[KP99] Merkouris S. Karaliopoulos and Fotini-Niovi Pavlidou. Modelling the land mobile satellite channel: a review. *Electronics Communication Engineering Journal*, 11(5):235 –248, oct 1999.

[Las75] Edward M. Lassiter. Navstar global positioning system: A satellite based microwave navigation system. In *Microwave Symposium, 1975 IEEE-MTT-S International*, pages 334–334, 1975.

[LCD+91] Erich Lutz, Daniel Cygan, Michael Dippold, Frank Dolainsky, and Wolfgang Papke. The land mobile satellite communication channel - recording, statistics, and channel model. *IEEE Transactions on Vehicular Technology*, 40:375–386, May 1991.

[Leo91] Raymond J. Leopold. Low-earth orbit global cellular communications network. In *IEEE International Conference on Communications, 1991. ICC '91, Conference Record.*, pages 1108–1111 vol.2, 1991.

[Loo84] Chun Loo. A statistical model for a land mobile satellite link. In *ICC '84 - Links for the future: Science, systems and services for communications, Proceedings of the International Conference on Communications*, volume 2, pages 588–594, May 14-17 1984.

[Lut96] Erich Lutz. A Markov model for correlated land mobile satellite channels. *International Journal of Satellite Communications*, 14:333–339, 1996.

[MDY+08] Hui Ming, Shen Dongya, Cui Yanni, Xu Jie, Yuan Dong, Chen Jie, and Lu Anxian. A new five-state markov model for land mobile satellite channels. In *8th International Symposium on Antennas, Propagation and EM Theory, 2008. ISAPE 2008.*, pages 1512 –1515, nov. 2008.

[MH99] Alireza Mehrnia and Homayoun Hashemi. Mobile satellite propagation channel. part ii-a new model and its performance. In *Vehicular Technology Conference, 1999. VTC 1999 - Fall. IEEE VTS 50th*, volume 5, pages 2780 –2784 vol.5, 1999.

[MHEH08] Marko Milojević, Martin Haardt, Ernst Eberlein, and Albert Heuberger. Channel state modeling for single and multiple satellite broadcasting systems. In *IWSSC*, 2008.

[MHEH09] Marko Milojević, Martin Haardt, Ernst Eberlein, and Albert Heuberger. Channel modeling for multiple satellite broadcasting systems. *IEEE Transactions on Broadcasting*, 55(4):705 –718, dec. 2009.

[Mic02] Richard A. Michalski. An overview of the XM satellite radio system. In *20th AIAA International Communication Satellite Systems Conference and Exhibit*, May 2002.

[mil] MiLADY project web page. `http://telecom.esa.int/telecom/www/object/index.cfm?fobjectid=29020`.

[MNG+02] David W. Matolak, Anthony R. Noerpel, Rupert LA Goodings, D.V. Staay, and José Maria Baldasano. Recent progress in deployment and standardization of geostationary mobile satellite systems. In *MILCOM 2002. Proceedings*, volume 1, pages 173–177 vol.1, 2002.

[MPTE98] C. Meenan, M. Parks, Rahim Tafazolli, and Barry Evans. Availability of 1st generation satellite personal communication network service in urban environments. In *Vehicular Technology Conference, 1998. VTC 98. 48th IEEE*, volume 2, pages 1471 –1475 vol.2, may 1998.

[MSL+09] Jan Mietzner, Robert Schober, Lutz Lampe, Wolfgang H. Gerstacker, and Peter A. Hoeher. Multiple-antenna techniques for wireless communications - a comprehensive literature survey. *Communications Surveys Tutorials, IEEE*, 11(2):87 –105, quarter 2009.

[MTTK02] Lorenzo Mucchi, Raffaello Tesi, Djordje Tujković, and Esa Kunnari. Space-time coded transmit diversity in multi-satellite umts. In *The 5th International Symposium on Wireless Personal Multimedia Communications*, volume 2, pages 696–700 vol.2, 2002.

[Nak60] M. Nakagami. The m-distribution, a general formula of intensity of rapid fading. In *reprint from Statistical Methods in Radio Wave Propagation.* Pergamon Press, 1960.

[Nor90] Gary K. Noreen. Mobile satellite broadcast system design. In *Vehicular Technology Conference, 1990 IEEE 40th*, pages 233–236, 1990.

[PCPFB+10] Roberto Prieto-Cerdeira, Fernando Pérez-Fontán, Paolo Burzigotti, Ana Bolea-Alamañac, and Iria Sanchez-Lago. Versatile two-state land mobile satellite channel model with first application to DVB-SH analysis. *International Journal of Satellite Communications and Networking*, 28:291–315, 2010.

[PFBA+08] Fernando Pérez-Fontán, Antía Mayo Bazarra, David Marote Alvarez, Roberto Prieto Cerdeira, Perfecto Mari no, Fernando Machado, and Núria Riera Diaz. Review of generative models for the narrowband land mobile satellite propagation channel. 26(4):291–316, 2008.

[PFGF+97] Fernando Pérez-Fontán, Jorge Pereda González, Maria Jose Sedes Ferreiro, Maryan Vázquez-Castro, Sergio Buonomo, and Jose Pedro Poiares-Baptista. Complex envelope three-state markov model based simulator for the narrow-band lms channel. *International Journal of Satellite Communications*, 15(1):1–15, 1997.

[PFSLCn07] Fernando Pérez-Fontán, Iria Sanchez-Lago, Roberto Prieto Cerdeira, and Ana Bolea-Alama nac. Consolidation of a multi-state narrowband land mobile satellite channel model. In *The Second European Conference on Antennas and Propagation, EuCAP 2007.*, pages 1 –6, nov. 2007.

[PFVCB+98] Fernando Pérez-Fontán, Maryan Vázquez-Castro, Sergio Buonomo, Jose Pedro Poiares-Baptista, and Bertram R. Arbesser-Rastburg. S-band LMS propagation channel behaviour for different environments, degrees of shadowing and elevation angles. *IEEE Transactions on Broadcasting*, 44(1):40–76, March 1998.

[PFVCC+01] Fernando Pérez-Fontán, Maryan Vázquez-Castro, Cristina Enjamio Cabado, Jorge Pita Garcia, and Erwin Cubista. Statistical modeling of the lms channel. *IEEE Transactions on Vehicular Technology*, 50(6):1549–1567, november 2001.

[PKL98] Matthias Pätzold, Ulrich Killat, and Frank Laue. An extended suzuki model for land mobile satellite channels and its statistical properties. *IEEE Transactions on Vehicular Technology*, 47(2):617 –630, may 1998.

[PNIS+11] Ana Isabel Pérez-Neira, Christian Ibars, Jordi Serra, Aitor del Coso, Jesús Gómez-Vilardebó, Márius Caus, and Konstantinos P. Liolis. Mimo channel modeling and transmission techniques for multi-satellite and hybrid satellite-terrestrial mobile networks. *Elsevier Physical Communication (PHYCOM) Journal*, 4(2):127–139, jun 2011.

[Pos98] Peter Poskett. The ico system for personal communications by satellite. In *IEE Colloquium on Communication Opportunities Offered by Advanced Satellite Systems - Day 1 (Ref. No. 1998/484)*, pages 2/1–2/6, 1998.

[Pro95] John G. Proakis. *Digital Communications*. New York, 1995.

[Pro00] John G. Proakis. *Digital Communications 4th edition*. New York, 2000.

[PSE97] M. A N Parks, S.R. Saunders, and B.G. Evans. Wideband characterisation and modelling of the mobile satellite propagation channel at l- and s-bands. In *Tenth International Conference on Antennas and Propagation (Conf. Publ. No. 436)*, volume 2, pages 39–43 vol.2, 1997.

[Pun02] Milton B. Punnett. The building of the telstar antennas and radomes. *Antennas and Propagation Magazine, IEEE*, 44(2):80–90, 2002.

[Rab89] Lawrence R. Rabiner. A tutorial on hidden markov models and selected applications in speech recognition. *Proceedings of the IEEE*, 77(2):257–286, 1989.

[RAIG13] Marie Rieche, Daniel Arndt, Alexander Ihlow, and Giovanni Del Galdo. Influence of driving direction on land mobile satellite channels. In *Broadband Multimedia Systems and Broadcasting (BMSB), 2013 IEEE International Symposium on*, pages 1–5, June 2013.

[REE92] P. P. Robet, B. G. Evans, and A. Ekman. Land mobile satellite communication channel model for simultaneous transmission from a land mobile terminal via two separate satellites. *International Journal of Satellite Communications*, 10(3):139–154, 1992.

[RH97] Michael Rice and Brian Humpherys. Statistical models for the acts k-band land mobile satellite channel. In *Vehicular Technology Conference, 1997, IEEE 47th*, volume 1, pages 46 –50 vol.1, may 1997.

[Ric48] Stephen O. Rice. Mathematical analysis of a sine wave plus random noise. *Bell System Technical Journal*, 27 (1):pp. 109–117, 1948.

[SAHE] Sandro Scalise, Clémence Alasseur, Lionel Husson, and Harald Ernst. Accurate and novel modeling of the land mobile satellite channel using reversible jump markov chain monte carlo technique.

[SANS08] Hussein Sallam, Tarek Abdel-Nabi, and J'/erome Soumagne. A geo satellite system for broadcast audio and multimedia services targeting mobile users in europe. In *Advanced Satellite Mobile Systems, 2008. ASMS 2008. 4th*, pages 134–139, 2008.

[SAZ07] Simon R. Saunders and Alejandro Aragon-Zavala. *Antennas and Propagation for Wireless Communication Systems: 2nd Edition*. New York, 2007.

[SE96] Simon R. Saunders and B.G. Evans. Physical model of shadowing probability for land mobile satellite propagation. *Electronics Letters*, 32(17):1548 –1549, aug 1996.

[SM99] Hae-Won Son and Noh-Hoon Myung. A deterministic ray tube method for microcellular wave propagation prediction model. *IEEE Transactions on Antennas and Propagation*, 47(8):1344–1350, 1999.

[SP05] Masashi Suenaga and Robert J. Prevaux. {MBSAT} a direct broadcast satellite for mobile users in japan and korea. *Acta Astronautica*, 57:215 – 223, 2005. Infinite Possibilities Global Realities, Selected Proceedings of the 55th International Astronautical Federation Congress, Vancouver, Canada, 4-8 October 2004.

[Spi94] Vladimir V. Spiridonov. Inmarsat systems and services. In *Proceedings of International Conference on Satellite Communications, 1994. ICSC'94*, volume 1, pages 45–52 vol.1, 1994.

[SUM00] Final report s-umts: Preparation of next generation universal mobile satellite telecommunications systems. Technical report, ESA, ESTEC, 2000.

[Suz77] Hirofumi Suzuki. A statistical model for urban radio propagation. *IEEE Transactions on Communications*, 25(7):673 – 680, jul 1977.

[SWT92] Yoshizumi Serizawa, Yoshihiro Watanabe, and Shinya Takeshita. Multipath propagation effects on digital radio equipped with a plane reflector repeater. *Communications, Speech and Vision, IEE Proceedings I*, 139(2):176 –180, april 1992.

[TSE98] Constantinos Tzaras, Simon R. Saunders, and B.G. Evans. A physical-statistical propagation model for diversity in mobile satellite pcn. In *Vehicular Technology Conference, 1998. VTC 98. 48th IEEE*, volume 1, pages 525 –529 vol.1, may 1998.

[Vat95] Francesco Vatalaro. Generalised rice-lognormal channel model for wireless communications. *Electronics Letters*, 31(22):1899 –1900, oct 1995.

[VCPFISBF01] Maryan Vázquez-Castro, Fernando Pérez-Fontán, H. Iglesias-Salgueiro, and M.A. Barcia-Fernandez. A simple three-segment model for shadowing cross correlation in multisatellite systems in street canyons. *Microwave and Optical Technology Letters*, 28(3):160–164, 2001.

[VCPFS02] Maryan Vázquez-Castro, Fernando Pérez-Fontán, and Simon R. Saunders. Shadowing correlation assessment and modeling for satellite diversity in urban environments. *International Journal of Satellite Communications*, 20(2):151–166, 2002.

[VGH92] Wolfgang J. Vogel, Julius Goldhirsh, and Yoshihiro Hase. Land-mobile satellite fade measurements in australia. *J. Spacecraft Rockets*, 29:123–128, Januar 1992.

[Wak91] Hiromitsu Wakana. A propagation model for land mobile satellite communications. In *Antennas and Propagation Society International Symposium, 1991. AP-S. Digest*, pages 1526 –1529 vol.3, jun 1991.

[WP93] Yiu-Fai Wong and Edward C. Posner. A new clustering algorithm applicable to multispectral and polarimetric sar images. *IEEE Transactions on Geoscience and Remote Sensing*, 31(3):634–644, 1993.

[WV93] Robert A. Wiedeman and Andrew J. Viterbi. The Globalstar mobile satellite system for worldwide personal communications. In *3rd International Mobile Satellite Conference*, pages 291–296, 1993.

[XF00] Yongjun Xie and Yuguang Fang. A general statistical channel model for mobile satellite systems. *IEEE Transactions on Vehicular Technology*, 49(3):744 –752, may 2000.

[Yan57] Richard F. H. Yang. Passive repeater using double flat reflectors. In *IRE International Convention Record*, volume 5, pages 36 – 41, mar 1957.